



The  
University  
Of  
Sheffield.

**Biophysical studies on dinuclear DNA metallo-  
intercalators containing the ruthenium (II)  
tris(1-pyrazolyl)methane unit**

**By:**

Hiwa Karim Saeed

Supervisor: Prof Jim Thomas

A thesis submitted for the degree of Doctor of Philosophy

The University of Sheffield

Department of Chemistry

May 2016

## Abstract

This thesis discusses the construction and DNA-binding properties of homo- and heterometallic, oligonuclear complexes containing the  $[\text{Ru}(\text{tpm})(\text{dppz})]^{2+}$  moiety. Specifically it explores how the nature of the tether affects the binding properties of these systems. Towards these goals, four new connecting ligands that possess potential DNA recognition sites in themselves have been prepared. The ligands have also been chosen to investigate the effects of changes in connectivity and linker rigidity on the binding properties of these metallo-intercalators. A series of mononuclear complexes incorporating the new tether ligands  $N,N'$ -bis(4-pyridylmethyl)-1,6-hexanediamine ( $\text{pyX}_a\text{py}$ ),  $N,N'$ -bis(3-pyridylmethyl)-1,6-hexanediamine ( $\text{pyX}_b\text{py}$ ),  $\text{pyY}_a\text{py} = N,N'$ -bis(4-pyridylmethyl)-1,4-benzenedimethyleneamine, and  $(\text{pyY}_b\text{py}) = N,N'$ -bis(3-pyridylmethyl)-1,4-benzenedimethyleneamine were first synthesized. These mononuclear complexes were then used to synthesize analogous dinuclear systems **Figure 1**. The DNA-binding properties of the mono- and dinuclear complexes were then explored and compared.

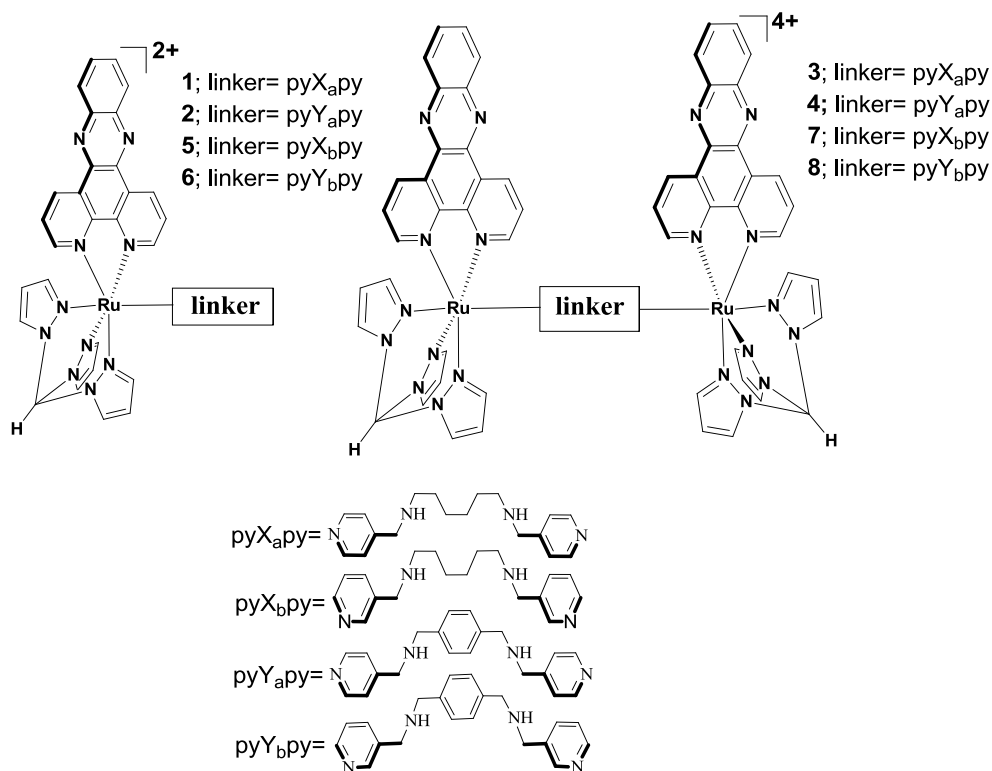


**Figure 1:** New mono- and dinuclear Ru(dppz) complexes

A combination of techniques indicates that all the complexes bind to CT-DNA through intercalation. These studies have also shown that whilst complexes [1-4] clearly bind to CT-DNA, complexes [5-8] bind with higher affinities. Furthermore, it seems binding can also be enhanced through the use of more rigid ligands pyY<sub>a</sub>py and pyY<sub>b</sub>py.

This thesis also reports the DNA binding and cleavage properties of heterobimetallic Ru<sup>II</sup>-Re<sup>I</sup> and homoleptic (dppn/dppn) and heteroleptic (dppz/dppn) Ru<sup>II</sup>-Ru<sup>II</sup> complexes - **Figure 2**. The cellular response of cisplatin sensitive and resistant A2780/A2780cis human ovarian carcinoma lines towards these complexes was then studied. The heterobimetallic Ru<sup>II</sup>-Re<sup>I</sup> system complex binds to duplex DNA by intercalation with good affinity and displays a DNA light switch effect but does not cleave DNA. The complex-DNA interaction is enthalpically unfavourable and entropically favoured. Moreover, although the molecule does not display significant phototoxicity (PI = 2), it displays significant dark cytotoxicity.

On the other hand, the Ru<sup>II</sup>-Ru<sup>II</sup> polypyridyl complexes with the dppn ligand produce a higher <sup>1</sup>O<sub>2</sub> quantum yield. This is due to long-lived ππ\* triplet state centred on the dppn ligand. Thus these dppn complexes show high phototoxicity indices.

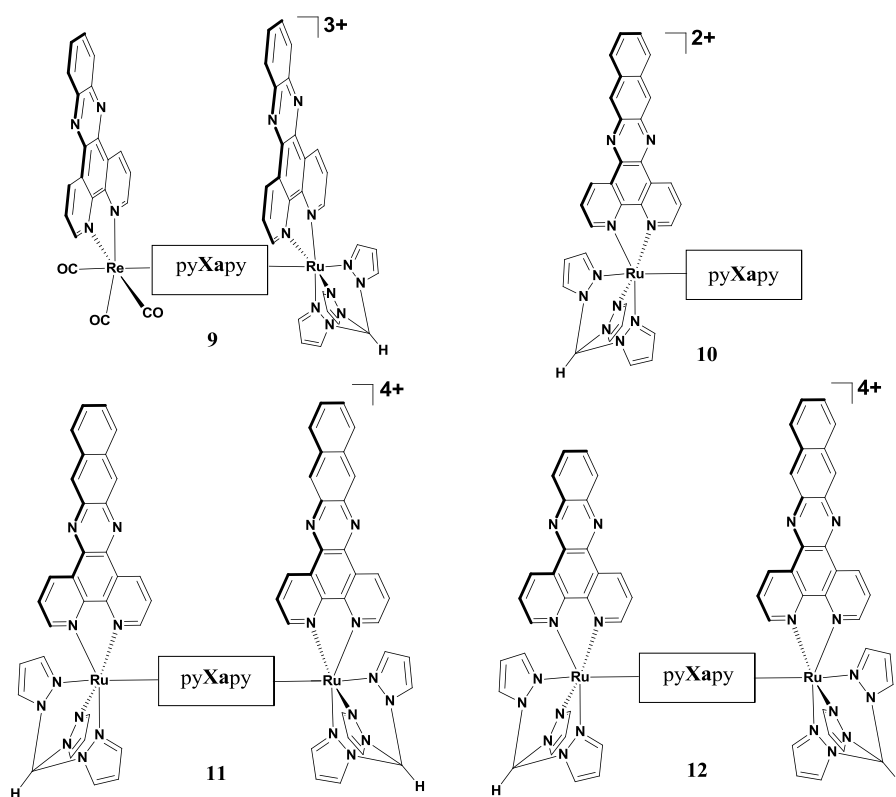


**Figure 2:** Structures of bisintercalator Ru<sup>II</sup>Re<sup>I</sup>, mono- and dinuclear Ru<sup>II</sup>Ru<sup>II</sup> complexes.

## **Declaration**

*The work in this thesis is the original work of the author except where specific references have been made to other sources. It has not been submitted, in whole or in part, for any other degree. Some results have already been submitted to peer-reviewed journals and will be published subject to acceptance.*

**Hiwa Karim Saeed**

**May 2016**

## Acknowledgments

*Undertaking this PhD has been a truly life-changing experience for me and it would not have been possible to do without the support and guidance that I received from many people.*

*I would like to express my special appreciation and thanks to my supervisor Professor Jim Thomas- you have been a tremendous mentor for me. I would like to thank you for encouraging my research and for allowing me to grow as a research scientist. Your advice on both my research and my career has been priceless.*

*I am grateful for the support and guidance given to me by Dr. Niek Buurma for his help and patience in understanding ITC and also for allowing me to work in his research facility in Cardiff University. Also I would like to acknowledge the help of Dr. Andrea and Dr Jenny in the Staniland group for allowing me to do DNA photocleavage experiments in their lab'.*

*A special thank you to all the technical staff at the University for their continued help and support. In the Chemistry department itself, my thanks go out to Sue and Dr Sandra van Meurs in NMR, Sharon and Simon in Mass spec., Jenny in Elemental, Harry in X-Ray and for the technical support of Keith and Stephen Atkin. Thank you to Dan in the glass workshop for constantly creating works of art to be used for scientific purposes in our lab. I would like to thank the gents in stores, Pete and Nick, as well as the ladies in accounts, Denise, Rachel and Louise. You all make the department a nice place to be around.*

*My deep appreciation goes out to all the members of the Thomas group. The beautiful ladies - Caroline, Sasha, and Rachel, as well as the gents- Mike, Stuart, Tom, Sree, Sam, Shahryar, and Simon. I would like to thank them all for their friendship and the warmth they extended to me during my PhD, and for always being there and bearing with me during the ups and downs of life over the last 4 years. I could not have asked for more than I got from them. To Paul Jarman- from the day I began my PhD, you have become one of my best friends. We have seen and helped each other through both good times and bad. I will always remember the great conversations we had about premier league football, feeding birds in Western Park, and playing pool in the common room etc. I know that we will break bread together many more times. Jack and Claire's encouragement and love have made this journey bearable, and no amount of thanks will ever be enough to return that joy.*

*John Lennon said it best: “I get by with a little help from my friends”*

*From my time in Sheffield, I want to thank my remarkable friends Ashley, David, Mark, Esther, Hannah, Ian, Craig, Adel, William, Lee, Zayed, Mar Cardellach, Sana, Luke, who have been incredible friends to me over the years. Wednesday football has been an important part of the weekly routine and thanks must go to PJ, Matt, Joe, Nathan, Scott, Methers, Jonny, Tim and all the rest. Their moral support has made all the difference. Thank you to all of the Exeter Gently team, past and present, for many great summer tournaments.*

*My very sincere thanks to ‘Dler & Shno’, ‘Omed & Kwestan’, ‘Atheer & Anona’, and Sardar & Zryan’ for their parent-like support, generous care, and the feeling of home whenever I was in need during my PhD. I will miss you all very much.*

*A special thanks to my family. Words cannot express how grateful I am to my mom, dad, my brothers and sisters for all of the sacrifices that you’ve made on my behalf. Your prayer for me was what sustained me thus far. I consider myself the luckiest in the world to have such a supportive family, standing behind me with their love and support.*

*Last but not least; I gratefully acknowledge the funding received towards my PhD from the Kurdistan Regional Government (KRG)-Human Capacity Development program Scholarship.*

*There are inevitably people I have missed out. If you are not mentioned, it is not because you didn’t contribute. Thank you.*

## Abbreviations

*L1: N,N'-bis(4-pyridylmethyl)-1,6-hexanediamine*

*L2: N,N'-bis(4-pyridylmethyl)-1,4-benzenedimethyleneamine*

*L'1: N,N'-bis(3-pyridylmethyl)-1,6-hexanediamine*

*L'2: N,N'-bis(3-pyridylmethyl)-1,4-benzenedimethyleneamine*

*Tpm: Tris(1-pyrazolyl)methane*

*Dppn: Benzo[i]dipyrido[3,2-a:2',3'-c]phenazine*

*Dpq: 1,10-phenanthroline-5,6-dione*

*Dppz: Dipyrido [3,2-a:2',3'-c] phenazine*

*Phen: 1,10-phenanthroline*

*Bpy: 2,2-bipyridine*

*NN: Bidentate ligand*

*AgNO<sub>3</sub>: Silver nitrate*

*AgCF<sub>3</sub>SO<sub>3</sub>: Silver trifluoromethanesulfonate*

*<sup>n</sup>Bu<sub>4</sub>NCl: Tetra-n-butyl ammonium chloride*

*Na<sub>2</sub>CO<sub>3</sub>: Sodium carbonate*

*NH<sub>4</sub>PF<sub>6</sub>: Ammonium hexafluorophosphate*

*NaBH<sub>4</sub>: Sodium tetrahydridoborate*

*DCM: Dichloromethane*

*DMF: Dimethylformamide*

*TFA: Trifluoroacetic acid*

*THF: Tetrahydrofuran*

*EtBr: Ethidium bromide*

*H33258: Hoechst 33258*

*DNA: Deoxyribonucleic Acid*

***CT-DNA:*** *Calf thymus DNA*

***RNA:*** *Ribonucleic Acid*

***TAE:*** *Tris-acetate-EDTA*

***Tris:*** *Tris(hydroxymethyl)aminomethane*

***IL:*** *Intraligand*

***ISC:*** *Intersystem crossing*

***CT:*** *Charge transfer*

***LLCT:*** *Ligand to ligand charge transfer*

***MC:*** *Metal centred*

***MLCT:*** *Metal to ligand charge transfer*

***K<sub>b</sub>:*** *Intrinsic binding constant*

***IC<sub>50</sub>:*** *Half maximal inhibitory concentration*

***ICP-MS:*** *Inductively coupled plasma mass spectrometry*

***PDT:*** *Photodynamic therapy*

***PI:*** *Phototoxic index*

***LISA:*** *Light Irradiation Source Apparatus*

***ITC:*** *Isothermal Titration Calorimetry*

***COSY:*** *Correlation spectroscopy*

***HPLC:*** *High-performance liquid chromatography*

***UV:*** *Ultraviolet*

## Contents

### **Chapter 1 Introduction**

1.1 Nucleic acid (DNA) - The molecule of life .....	1
1.2 The DNA structure.....	2
1.3 The major and minor grooves .....	4
1.4 DNA Binding .....	7
1.4.1 Irreversible Binding.....	7
1.4.2 Reversible Binding.....	8
1.4.2.1 Electrostatic binding .....	8
1.4.2.2 Groove binding .....	9
1.4.3 Intercalation.....	12
1.4.3.1 Organic intercalators.....	14
1.4.3.2 Metallo-intercalators.....	17
1.5 Mono- and bimetallic complexes.....	18
1.5.1 Monometallic Complexes .....	18
• Tris(phenanthroline) Complexes.....	18
1.5.1.1 The molecular light switch effect .....	20
1.5.2 Bimetallic Complexes .....	33
1.6 Project Aims.....	41
References.....	42

### **Chapter 2 Bimetallic DNA Metallo-intercalators containing the ruthenium (II) tris(1-pyrazolyl)methane Unit**

2.1 Introduction.....	48
2.2 Syntheses.....	49
2.2.1 Linker syntheses .....	49
2.2.2 Synthesis of complexes .....	50
2.2.2.1 Monometallic complexes.....	50
2.2.2.2 Bimetallic complexes .....	51
2.3 Characterization .....	52
2.3.2 Mass spectrometry data.....	52
2.3.3 Photophysical studies .....	52
2.3.4 DNA Binding Studies.....	57
2.3.5 UV-Visible titrations .....	61

2.3.6 Luminescence emission titrations .....	65
2.3.7 Viscosity.....	72
References.....	75

***Chapter 3 The effect of the nature and positioning of the functional group on the binding mode and affinity of Ruthenium polypyridyl complexes***

3.1 Introduction.....	77
3.2 Syntheses.....	78
3.3.1 Linker syntheses .....	78
3.3.2 Synthesis of complexes.....	79
3.3.2.1 Monometallic complexes .....	79
3.3.2.2 Bimetallic complexes .....	80
3.3 Characterization .....	81
3.3.1 <sup>1</sup> H NMR spectroscopy studies .....	81
3.3.1.1 [Ru(tpm)(dppz)(μ-L' <sup>2</sup> )][(PF <sub>6</sub> ) <sub>2</sub> ].....	81
3.3.2 Photophysical studies .....	84
3.4 DNA Binding Studies .....	88
3.4.1 Absorption titration .....	88
3.4.2 Luminescence titration .....	90
3.4.3. Luminescence lifetimes.....	96
3.4.4. Viscosity Measurements .....	96
References.....	100

***Chapter 4 Isothermal Titration Calorimetry***

4.1 Introduction.....	101
4.2 General principles of the ITC experimental setup .....	101
4.3 Titration curve and binding constant .....	105
4.4 ITC calibration .....	107
4.5 Heat of dilution .....	108
4.6 Data analysis .....	108
4.7 ITC studies .....	109
4.7.1 Set one: Complexes [1]Cl <sub>2</sub> , [2]Cl <sub>2</sub> , [3]Cl <sub>4</sub> and [4]Cl <sub>4</sub> titrated into CT-DNA solution. .....	109
4.7.2 Set two: Complexes [5]Cl <sub>2</sub> , [6]Cl <sub>2</sub> , [7]Cl <sub>4</sub> and [8]Cl <sub>4</sub> titrated into CT-DNA solution. .....	117
References.....	122

**Chapter 5 DNA Binding and Cleavage Properties of a heterobimetallic Ru<sup>II</sup>-Re<sup>I</sup> system and Ru<sup>II</sup>-Ru<sup>II</sup> Polypyridyl complex with mixed-bis-intercalating ligands (dppz-dppn)**

5.0 Introduction.....	123
5.1.1 DNA Binding and Cleavage Properties of a heterobimetallic Ru <sup>II</sup> -Re <sup>I</sup> system .....	123
5.1.2 Synthetic Studies.....	124
5.1.3 Characterization .....	126
5.1.3.1 Absorption spectrum of ruthenium-rhenium complex.....	126
5.1.4 DNA Binding Studies .....	128
5.1.4.1 Absorption titration .....	128
5.1.4.2 Luminescence titration .....	131
5.1.4.3 Isothermal Titration Calorimetry (ITC) .....	132
5.1.5 RuRe Phototoxicity .....	134
5.1.6 DNA Photocleavage.....	136
5.1.6.1 Phototoxicity of RuRe bis-intercalator towards A2780 and A2780cis cell lines... 138	
5.2 Ru <sup>II</sup> -Ru <sup>II</sup> Polypyridyl complex with mixed-bis-intercalating ligands (dppz-dppn).....	143
5.2.1 Introduction.....	143
5.2.2 Synthetic Studies.....	143
5.2.2.1 Ligand synthesis.....	143
5.2.2.2 Synthesis of complexes .....	144
5.2.3 Characterization .....	146
5.2.3.1 Absorption spectra.....	146
5.2.4 Transient Absorption Studies.....	151
5.2.5 DNA binding studies.....	153
5.2.5.1 UV-Vis titrations .....	153
5.2.5.2 Luminescence titrations.....	157
5.2.6 Singlet oxygen quantum yield .....	160
5.2.7 DNA photocleavage and Singlet Oxygen Production .....	162
5.2.8 Phototoxicity.....	163
5.2.8.1 Inductively coupled plasma mass spectrometry (ICP-MS).....	168
References.....	171

**Chapter 6 Conclusions**

6.0 Conclusions.....	175
6.1 Chapter 2: Bimetallic DNA Metallo-intercalators containing the ruthenium (II) tris(1-pyrazolyl)methane Unit.....	175
6.2 Chapter 3: The effect of the nature and positioning of the functional group on the binding mode and affinity of Ruthenium polypyridyl complexes. ....	175

6.3 Chapter 4: Isothermal Titration Calorimetry (ITC).....	176
6.4 Chapter 5.1: DNA Binding and Cleavage Properties of a heterobimetallic RuII-ReI system.....	176
6.5 Chapter 5.2: RuII-RuII Polypyridyl complex with mixed-bis-intercalating ligands (dppz-dppn).....	177
<b>Chapter 7 Experimental</b>	
7.0 Experimental.....	178
7.1 Materials and Equipment.....	178
7.1.1 Chemicals.....	178
7.1.2 Nuclear Magnetic Resonance (NMR) Spectra.....	178
7.1.3 Mass Spectrometry.....	178
7.1.4 UV-Visible Absorption Spectroscopy.....	178
7.1.5 Luminescence Spectroscopy.....	179
7.2 DNA Binding Studies.....	179
7.2.1 Buffer Preparation.....	179
7.2.2 Sample Preparation.....	179
7.2.3 DNA Preparation.....	180
7.2.4 Viscometry.....	180
7.2.5 UV-Visible Titrations.....	181
7.2.6 Luminescence Titrations.....	181
7.2.7 Isothermal Titration Calorimetry.....	181
7.2.8 Agarose Gel Electrophoresis of DNA.....	182
7.2.9 Transient Absorption Spectroscopy.....	182
7.3 Cellular phototoxicity Studies.....	183
7.3.1 Light Irradiation Source Apparatus (LISA).....	183
7.3.2 Photocytotoxicity (phototoxicity).....	184
7.3.3 Intracellular metal content (ICP-MS).....	184
7.4 Synthesis.....	186
7.4.1 Preparation of Tris(1-pyrazolyl)methane (tpm) <sub>2</sub> .....	186
7.4.2 Preparation of 1, 10-phenanthroline-5,6-dione (dpq) <sup>3</sup> .....	187
7.4.3 Preparation of dipyrido [3,2-a:2',3'-c] Phenazine (dppz) <sup>4</sup> .....	188
7.4.4 Preparation of N,N'-bis(4-pyridylmethyl)-1,6-hexanediamine (L1).....	188
7.4.5 Preparation of N,N'-bis(4-pyridylmethyl)-1,4-benzene dimethyleneamine (L2)..	189
7.4.6 Preparation of (tpm)RuCl <sub>3</sub> .3H <sub>2</sub> O.....	190
7.4.7 Preparation of [(tpm)RuCl(dppz)][(PF <sub>6</sub> )] <sub>2</sub> .....	191

7.4.8 Preparation of [(tpm)Ru(dppz)( $\mu$ -L1)][Cl <sub>2</sub> ] .....	192
7.4.9 Preparation of [(tpm)Ru(dppz)( $\mu$ -L2)][Cl <sub>2</sub> ] .....	193
7.4.10 Preparation of [{(tpm)Ru(dppz)} <sub>2</sub> ( $\mu$ -L1)][(PF <sub>6</sub> ) <sub>4</sub> ] .....	194
7.4.11 Preparation of [{(tpm)Ru(dppz)} <sub>2</sub> ( $\mu$ -L2)][(PF <sub>6</sub> ) <sub>4</sub> ] .....	195
7.4.12 Preparation of N,N'-bis(3-pyridylmethyl)-1,6-hexanediamine (L'1) .....	196
7.4.13 Preparation of N,N'-bis(3-pyridylmethyl)-1,4-benzene dimethyleneamine (L'2) .....	197
7.4.14 Preparation of [(tpm)Ru(dppz)( $\mu$ -L'1)][Cl <sub>2</sub> ] .....	198
7.4.15 Preparation of [(tpm)Ru(dppz)( $\mu$ -L'2)][Cl <sub>2</sub> ] .....	199
7.4.16 Preparation of [{(tpm)Ru(dppz)} <sub>2</sub> ( $\mu$ -L'1)][(PF <sub>6</sub> ) <sub>4</sub> ] .....	200
7.4.17 Preparation of [{(tpm)Ru(dppz)} <sub>2</sub> ( $\mu$ -L'2)][(PF <sub>6</sub> ) <sub>4</sub> ] .....	201
7.4.18 Preparation of [Re(CO) <sub>3</sub> dppzCl] .....	202
7.4.19 Preparation of [Ru(tpm)dppz-L1-Re(CO) <sub>3</sub> dppz][Cl <sub>3</sub> ] .....	203
7.4.20 Preparation of Benzo[i]dipyrido[3,2-a:2',3'-c]phenazine (dppn) <sup>5</sup> .....	204
7.4.21 Preparation of [Ru(tpm)dppnCl][PF <sub>6</sub> ] .....	205
7.4.22 Preparation of [Ru(tpm)dppn( $\mu$ -L1)][(PF <sub>6</sub> ) <sub>2</sub> ] .....	206
7.4.23 Preparation of [Ru(tpm)dppn-L1-Ru(tpm)dppn][(PF <sub>6</sub> ) <sub>4</sub> ] .....	207
7.4.24 Preparation of [Ru(tpm)dppz-L1-Ru(tpm)dppn][(PF <sub>6</sub> ) <sub>4</sub> ] .....	208
References .....	209

# Chapter 1

## Introduction

---

1.1 Nucleic acid (DNA) - The molecule of life .....	1
1.2 The DNA structure.....	2
1.3 The major and minor grooves .....	4
1.4 DNA Binding .....	7
1.4.1 Irreversible Binding.....	7
1.4.2 Reversible Binding.....	8
1.4.2.1 Electrostatic binding .....	8
1.4.2.2 Groove binding .....	9
1.4.3 Intercalation.....	12
1.4.3.1 Organic intercalators.....	14
1.4.3.2 Metallo-intercalators.....	17
1.5 Mono- and bimetallic complexes.....	18
1.5.1 Monometallic Complexes .....	18
1.5.1.1 The molecular light switch effect .....	20
1.5.2 Bimetallic Complexes .....	33
1.6 Project Aims.....	41
References.....	42

## 1.1 Nucleic acid (DNA) - The molecule of life

For more than 50 years, deoxyribose nucleic acid (DNA) has thrilled and inspired the scientific world, largely because its study is essential to the understanding of life. DNA is a chemical repository for the genetic information of an organism. The genetic information stored within DNA, in the form of four distinct building blocks, governs characteristics of every living species on earth. In recent years, the detailed mechanisms of DNA, and its function in the cell cycle, have been fully investigated.<sup>1,2</sup>

The processes of transcription, translation and replication, which all involve nucleic acids, are known as the “central dogma of molecular biology”<sup>3</sup> and are shown in **(Figure 1.1)**. Through these processes, DNA can be simply copied, and important information can be passed on from generation to generation. This genetic information is sometimes changed, either as a result of reproduction - where the individual genetic characteristic is mixed from the parents - or as a result of a physical modification such as miscopying. These modifications are known as mutations and frequently trigger a cascade of events that can lead to the organism developing a disease state. One of the aims of genetic science is to gain control of DNA function at the molecular scale. In this context, an important goal is ‘gene modulation’ which is a process of selectively switching a gene on or off by using DNA binding agents. If this occurs in a gene which has a marked negative effect on an organism, it would be inestimable contribution to the combat against disease.<sup>2</sup>

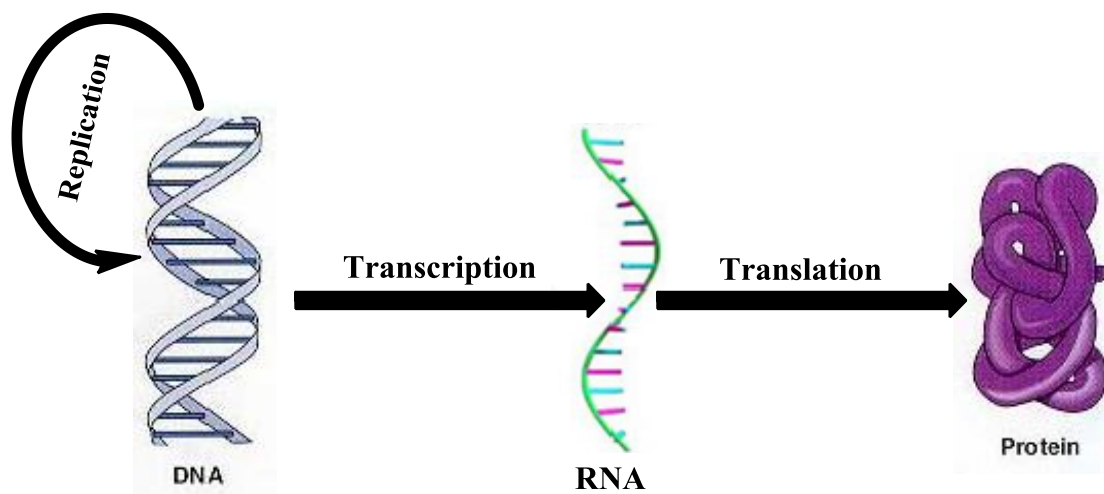


**Figure 1.1:** The central dogma of molecular genetics, DNA replication, RNA transcription and Protein translation.

## 1.2 The DNA structure

In 1953, James Watson and Francis Crick first described the structure of DNA<sup>4</sup> as a linear polymer consisting of repeating nucleotide building blocks. Each nucleotide consists of a pentose sugar and a phosphate residue linked to a nitrogen heterocyclic base.<sup>5,6</sup> There are four nitrogen heterocyclic bases in DNA; two of these bases are the purine derivatives adenine (A) and guanine (G), whilst cytosine (C) and thymine (T) are pyrimidine derivatives. The bases are linked to the sugar with a glycosidic bond, through N9 of a purine bases and N1 of a pyrimidine bases (**Figure 1.2**).

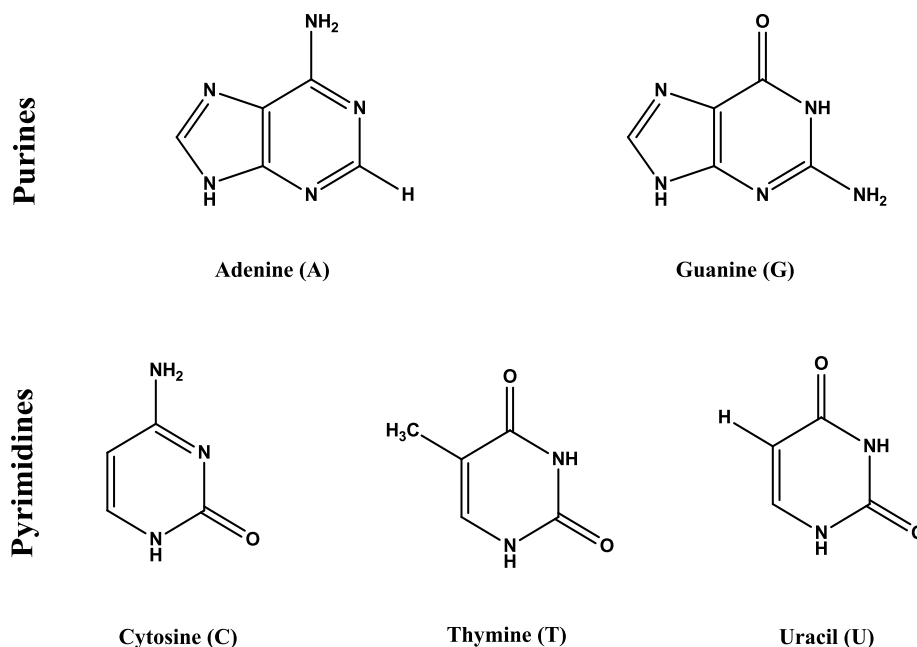


**Figure 1.2:** Nitrogenous base of DNA

The polynucleotide chain is made by phosphodiester linkages between the 3'-position of one nucleotide and the 5'-position of the next nucleotide.<sup>3</sup> Specifically the 3'-hydroxyl group of one nucleotide, esterified to a phosphate group, is joined to the 5'-hydroxyl group of the next nucleotide. A schematic of this arrangement is shown in (**Figure 1.3**).

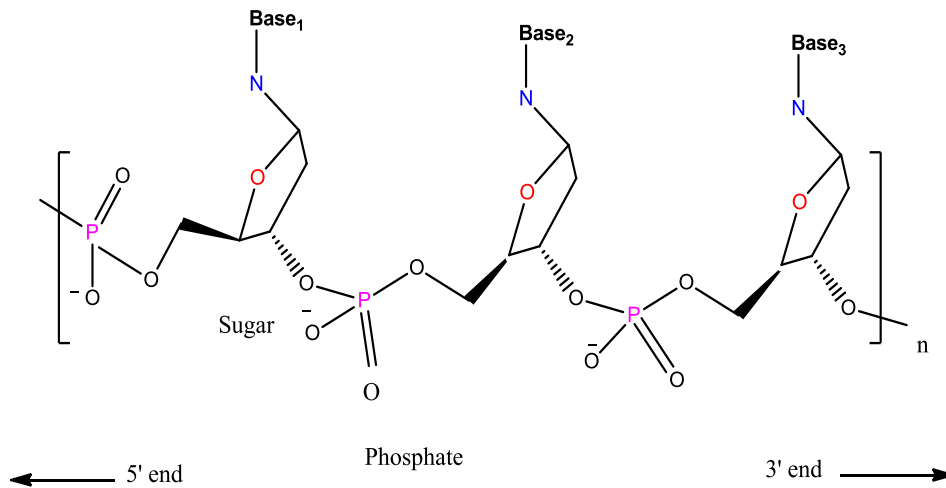


**Figure 1.3:** The covalent structure of DNA

When Watson and Crick described the structure of DNA in 1953, they made a proposal for its secondary structure, suggesting that wherever an A appeared it was always paired with T. Similarly G always seemed to be paired to C. This led them to suggest the idea of complementary strands held together by hydrogen bonds (**Figure 1.4**).

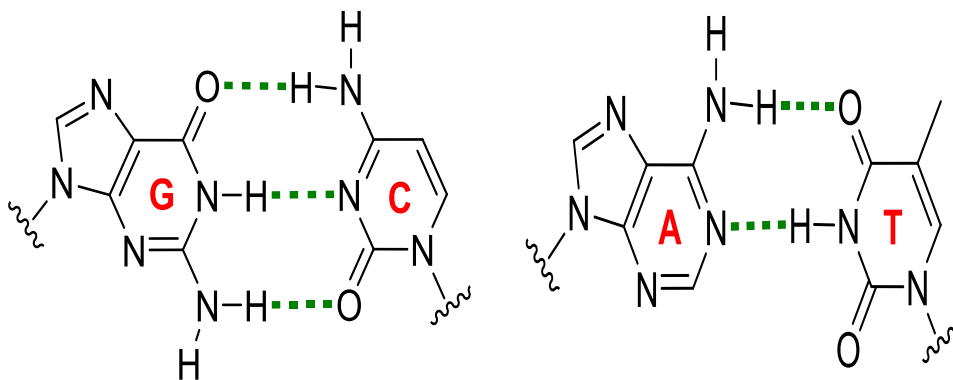


**Figure 1.4:** Complementary base pairs (GC and AT) with hydrogen bonds shown in green

As a result the structure has a degree of flexibility, as hydrogen bonds are much weaker than the covalent bonds that define the structures of the bases themselves. To biochemical systems these weak bonds are crucial; they are weak enough to be reversibly broken, but when many form simultaneously, strong enough to help stabilize the DNA double helix.<sup>7</sup> The complementary pairing of bases clarifies why A and T are always found in equal amounts, as

C and G. Two helical chains form from these complementary strands, running anti-parallel to one another and to create a double helix twisted around a common axis.

The purine and pyrimidine bases are on the inside of the helix, and the negatively charged backbone (deoxyribose and phosphate) is on the outside (**Figure 1.5**). Stability between the adjacent purines and pyrimidines is created through  $\pi$ - $\pi$  stacking interactions. Likewise, the polar sugar phosphate backbone forms favourable polar interactions with water molecules and cations.<sup>8</sup> All these forces contribute to maintain the two-stranded double helical structure, which contains a major and minor groove.

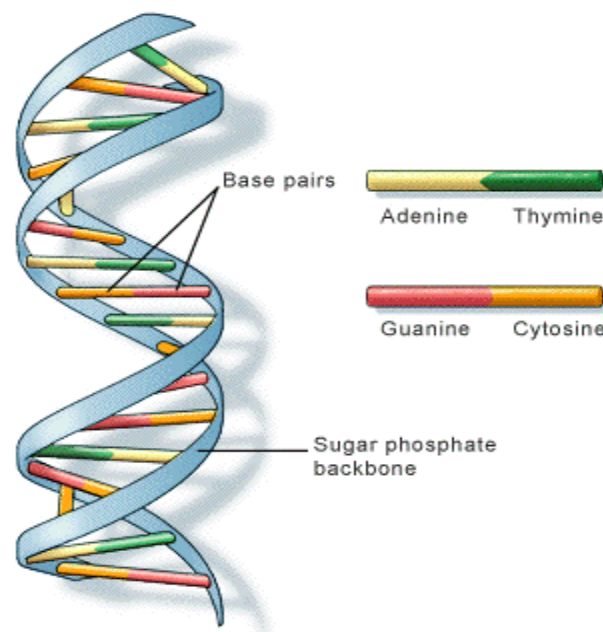


**Figure 1.5:** B-form structure of DNA. Showing the inside and outside double helix

### 1.3 The major and minor grooves

A consequence of the DNA helical structure is that there are two helical grooves running the entire length of the DNA molecule called the major and the minor groove (**Figure 1.6**). The sizes of the grooves are different, with the major groove being wider (12 Å) than the minor groove (6 Å). In these grooves, edges of bases are exposed at the surface of the DNA and provide sites where proteins or other small molecules can interact with DNA or read its

code.<sup>9</sup> The major and minor grooves differ in hydrogen bonding characteristics, steric effect, hydration and electrostatic potential.

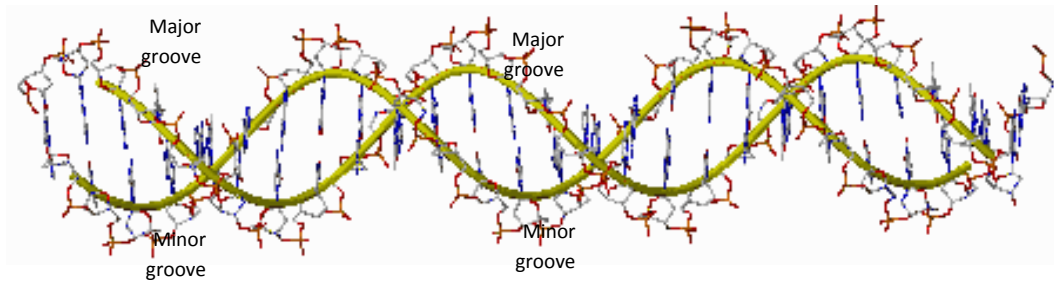


**Figure 1.6:** Picture of DNA showing the major and minor grooves

X-ray diffraction studies on heterogeneous DNA backbones carried out by Rosalind Franklin<sup>10</sup> were essential in providing more understanding on DNA structure. There are three main possible duplex conformations of DNA observed in organisms, A-DNA, B-DNA and Z-DNA (**Figure 1.7**). The first two conformations are right handed helices whilst the latter is a left-handed helix.<sup>12</sup> It is known that under physiological conditions most DNA is found in the Watson and Crick B form.<sup>11</sup> There are some obvious differences between these three major conformations of DNA in diameter, size, helical orientation and shape of the grooves. These different properties are summarised in (**Table 1.1**).<sup>7,13</sup>

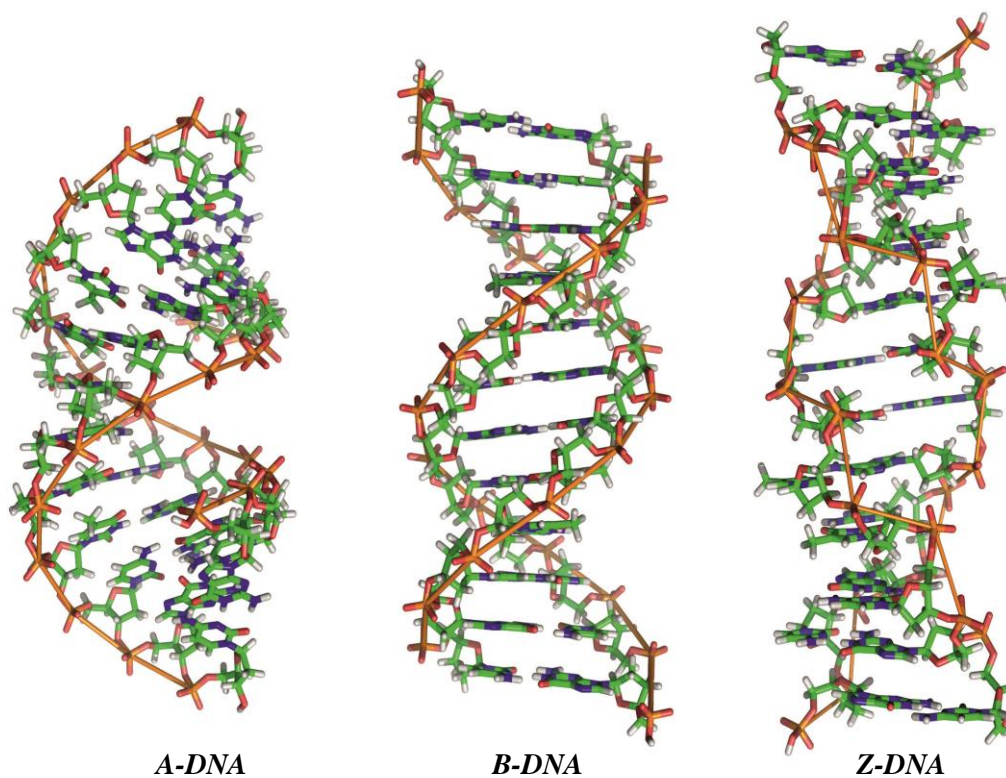


**Figure 1.7:** The main nucleic acid conformations

**Table 1.1:** Main structural features of A-, B- and Z-DNA.<sup>1, 12</sup>

Property	A-DNA	B-DNA	Z-DNA
Helix handedness	Right	Right	Left
Repeating unit	1 base pair	1 base pair	2 base pair
Diameter	~23 Å	~20 Å	~ 18 Å
Rotation per base pair	33°	36°	30°
Base pairs per turn	11	10.5	11.6
Helix rise per base pair	2.6 Å	3.4 Å	3.7 Å
Sugar pucker	C3' endo	C2' endo	C2' endo at C C3' endo at G
Major groove	Narrow and deep	Wide and deep	Narrow and deep
Minor groove	Wide and shallow	Narrow and deep	Narrow and deep

## 1.4 DNA Binding

There are several different mechanisms that allow small molecules to bind to DNA, and because DNA is fundamental to cellular processes it is an attractive target for therapeutics. These mechanisms will be described in this section.

### 1.4.1 Irreversible Binding

Non-specific covalent binding can occur by the formation of coordination bonds with either the phosphodiester backbone or sugar residues of the DNA helices. Irreversible binding can affect transcription processes, which usually ultimately causes cell death or alters gene expression.<sup>14</sup> Drug molecules that bind to DNA in this way can bind to sites either in the same strand (intrastrand) or crosslink from a base on one strand to base on the complementary strand.<sup>15</sup> Cis-diamminedichloroplatinum (II) is an example of an irreversible binding molecule, and is one of the most common anticancer drugs in the world (**Figure 1.8**). Cisplatin is used to treat testicular, ovarian, bladder, lung and stomach cancer. This drug forms intrastrand bonds to the DNA helix, through the N7 atom of either guanine or adenine base is binding to DNA. The trans-isomer of cisplatin is not an effective chemotherapeutic agent, indicating that not every irreversibly bound molecule can have this effect.<sup>16</sup>

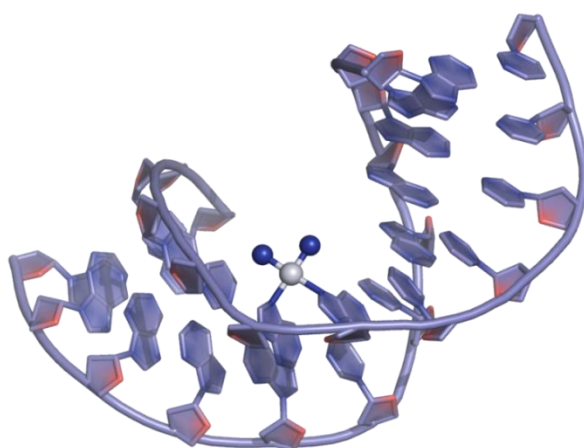


**Figure 1.8:** Cisplatin DNA binding structure. Shown platinum atom as a white sphere and NH<sub>3</sub> ligands shown as a blue spheres.

## 1.4.2 Reversible Binding

A broad range of chemical species that includes water, metal ions and their complexes, proteins, and also small molecules, can reversibly bind to DNA.<sup>8</sup> This includes many antibiotic, anticancer and antiviral drugs, which utilize their primary biological effects with nucleic acids by reversible interactions. These interactions can occur through three main modes; electrostatic interactions, groove binding interactions, and intercalation<sup>17,18</sup> (**Figure 1.9**).

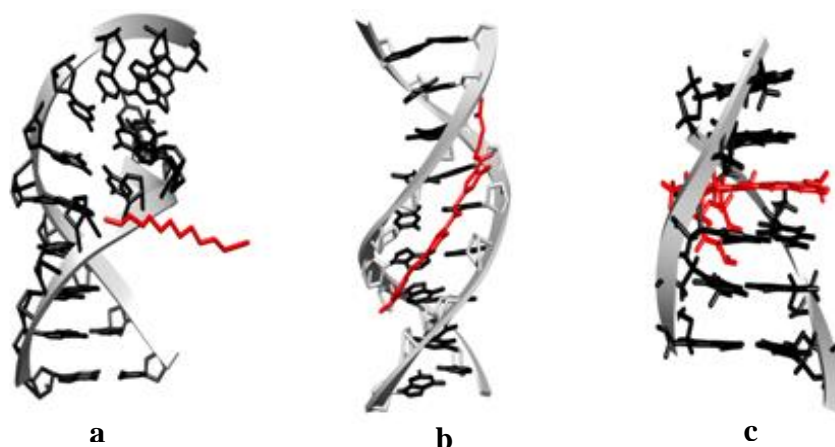


**Figure 1.9:** The three main modes of reversible binding of molecules to DNA. Showing a) spermine, b) distamycin and c) daunomycin as examples of each type. (From left to right PDB ID: 100D, 2DND and 1AL9).

### 1.4.2.1 Electrostatic binding

The DNA molecule exists as a polyanion under physiological conditions, due to the negatively charged phosphate groups that run along the backbone of the structure.<sup>5</sup> This means that cationic molecules are able to interact with the biopolymer. The stability of the DNA conformation is increased as a result of this interaction. The cations size can range from small ions (eg.  $\text{Na}^+$  or  $\text{Mg}^{2+}$ ) to larger cationic polyamines, spermidine and spermine are typical biomolecules that employ this type of interaction<sup>19,20</sup> (**Figure 1.10**).

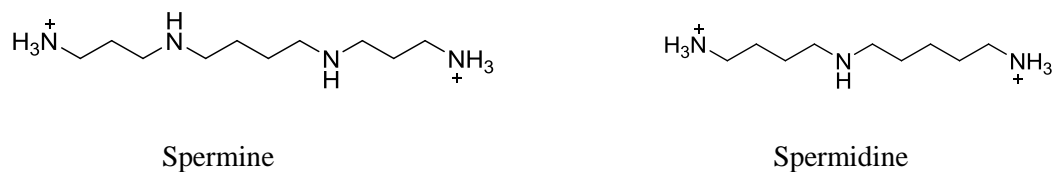


**Figure 1.10:** Chemical structures of spermine and spermidine

The counter-ion condensation effect caused by polyamines, such as spermine, reduces the nucleic acids effective charge and affects the solution properties, binding interactions, and stability of the biopolymer.<sup>8</sup>

### 1.4.2.2 Groove binding

In B-DNA the major and minor groove afford appropriate binding sites through reversible van der Waals, hydrophobic and hydrogen bonding interactions. Unlike other binding forms, groove binding can extend over many base pairs and therefore very high levels of DNA sequence can be specifically recognised. **(Figure 1.11)** shows the hydrogen bonding sites of A-T and G-C base pairs that are available in the major and minor grooves.<sup>21</sup>

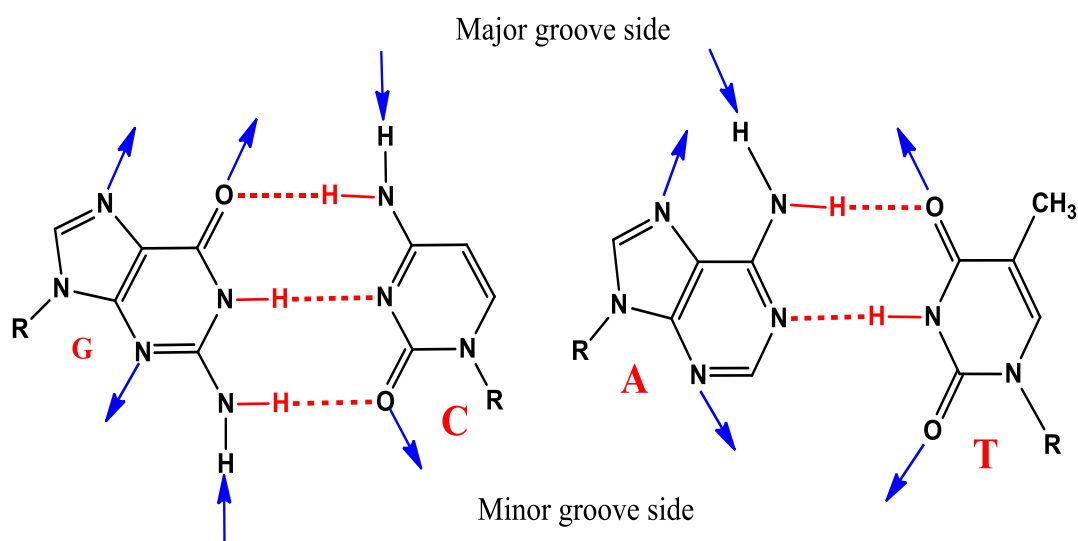


**Figure 1.11:** Hydrogen bonding sites reachable from the grooves of DNA

Many proteins have evolved to display explicit groove binding interactions. Some proteins and many small molecules will interact with DNA through the minor groove as this provides better van der Waals contacts. Typically, groove binding molecules are polyamides with aromatic rings linked by bonds with torsional freedom so that they can twist and become isohelical with the curve of the DNA groove. The majority of these compounds bind selectively to A-T rather than G-C rich sequences because the groove is narrower in these sequences and therefore facilitate van der Waals contacts with the walls of the groove. Lower affinity binding to G-C rich sequence is due to the N2 amine group of guanine, which sterically inhibits the penetration of molecules into these groove regions. Furthermore, negative electrostatic potentials in A-T minor grooves are greater than in G-C minor grooves.<sup>22,23</sup> As a consequence cationic molecules have a higher affinity for A-T sequences. To enhance G-C minor groove binding, ligands have to form hydrogen bonds with the guanine amine group. Groove binders are frequently positively charged, as binding will decrease the charge density of the DNA helix and thus condensed counter ion ions will be released.<sup>24</sup> These effects are illustrated by the interaction of netropsin and distamycin with DNA.

#### ***1.4.2.2.1 Netropsin and Distamycin***

Netropsin and its close relative distamycin have been extensively studied as typical examples of minor groove binders that favour A-T rich sites over sterically blocked G-C rich sequences<sup>22,25,26</sup> (**Figure 1.12**). Probably as a result of their affinity for DNA, both pyrrole-amidine structures are antibiotics that have antiviral, antibacterial and antitumor activity.<sup>25</sup> Netropsin and distamycin have more potential for recognising defined base sequences than do typical intercalators, which insert horizontal organic rings between base pairs adjacent to them. This is because intercalators basically detect only the base pair adjacent to them, while the groove binding drugs can extend for many steps along the level of the groove<sup>27</sup>, *vide infra*.

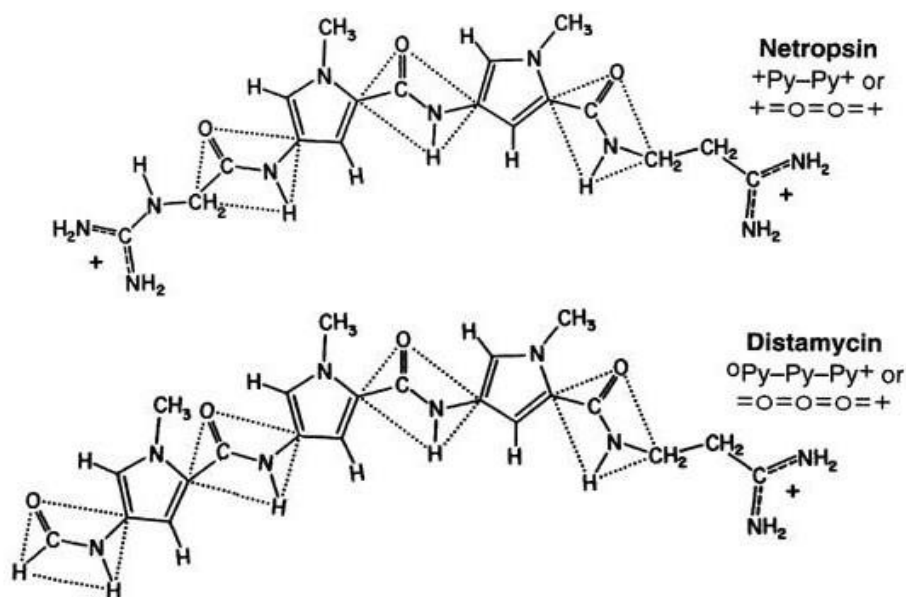


**Figure 1.12:** Molecular structures of Netropsin and Distamycin

An X-ray structure of netropsin with C-G-C-G-A-A-A-T-T-C-G-C-G showed the basis for the AT-specificity of a groove-binding drug complexed to DNA.<sup>27, 28, 22</sup> Firstly, AT-base pair reading is accomplished under the aegis of non-bonded contacts between the C2 hydrogen on adenine and CH of the netropsin pyrrole or methylene groups. Secondly, AT base pairs can twist like propellers more than GC pairs with three hydrogen bonds, because an AT base pair has only two such bonds. This propeller twisting narrows the groove<sup>29</sup>, and as a result the narrow groove strongly binds to a planar drug molecule. Thirdly, an absence of N2 amine group on adenine makes the groove deeper. Finally, in AT regions of the minor groove the electrostatic potential is deeper than GC regions, perhaps because of the absence of the same amine group<sup>30,31</sup> (**Figure1.13**, taken from references 25 and 33). Therefore like most groove binders these cationic drugs are more strongly attracted to AT regions. Both netropsin and distamycin can be seen as polypeptide chains in which every alpha carbon has been substituted by a five membered ring pyrrole ring. In such an augmented polypeptide chain the distance between pyrroles is approximately the same as the distance from one base pair to the next along the surface of a B-DNA minor groove.<sup>32</sup>

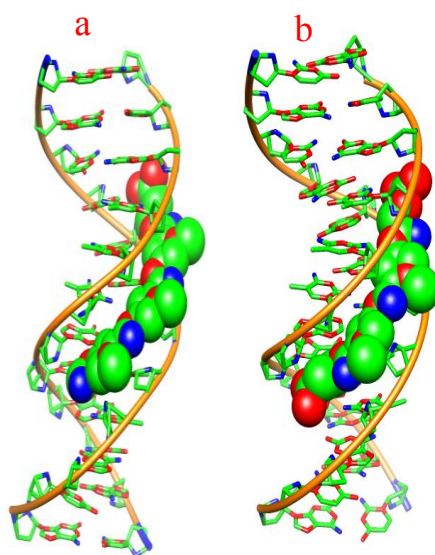


**Figure 1.13:** X-ray crystal structures of netropsin (a) bound to d(CGCGAATTCGCG)<sub>2</sub>, (PDB ID: 101D)<sup>33</sup> and distamycin A (b) bound to d(CGCAAATTTGCG)<sub>2</sub>, (PDB ID: 2DND).<sup>25</sup>

As a consequence of these interactions, both netropsin and distamycin have a high binding affinities ( $K_b=10^9 M^{-1}$ ) and high selectivity which is credited to the local short-range ligand DNA interactions rather than from any entropy driven process resulting from the displacement of ordered water from the minor groove and desolvation of the ligand itself.

### 1.4.3 Intercalation

In the early 1960s, DNA intercalation of ligands was first suggested by Leonard Lerman.<sup>34,35</sup> Intercalation is the process in which planar aromatic compounds insert and stack between two adjacent base pairs in the DNA double helix. This interaction includes significant  $\pi$  system overlap between the intercalated molecule and DNA bases, in addition to van der Waals and electrostatic interactions. Intercalation has the effect of unfastening and lengthening the DNA double helix. The binding affinity and selectivity of the intercalating ligand is extremely affected by the energetic cost of distorting the helix and disrupting the existing base pair stacks.<sup>36</sup> Ethidium bromide is a typical example of a simple “pure” intercalator that shows little selectivity in binding, displaying only a slight preference for G-C rich sequences of

DNA (**Figure 1.14**). In fact, most intercalators bind well to mixed sequences of alternating purine pyrimidine bases. Due to the principle of neighbour exclusion, in which the intercalative site narrows the gap between base pair “ladder rungs” on either side of it, binding site sizes are usually at least three base pairs.<sup>17</sup>

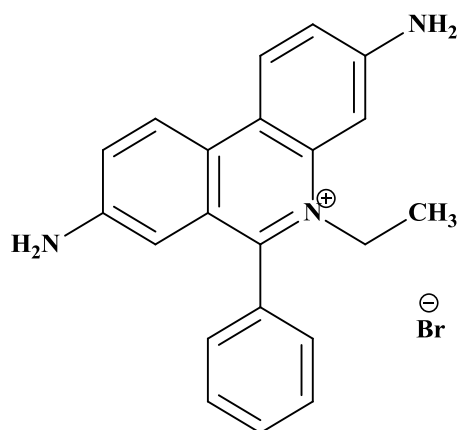


**Figure 1.14:** Structure of ethidium bromide

Intercalation and groove binding have very different effects on DNA structure. Whereas groove binders such as netropsin and distamycin only result in slight changes in structure, with DNA remaining basically unperturbed; substantial changes such as lengthening, stiffening and unwinding of DNA structure result from intercalation, producing definite effects on hydrodynamic properties. This allows intercalators and groove binders to be experimentally differentiated.<sup>36,37</sup> For example, viscosity measurements and Scanning Probe Microscopes (SPMs) provide a means of determining DNA binding modes, as they allow the length of plasmid DNA in both the presence and absence of DNA binding agents to be directly measured.<sup>10</sup> Since the orientation of the ligand and its closeness to DNA bases can be investigated through dichroism and fluorescence energy transfer, these measurements can also possibly differentiate between groove binding and intercalation.<sup>37</sup> The inhibition of polymerase activity by intercalators is often observed as the duplex is stabilized and therefore harder to unwind. Enzymes are also unable to bind to the disrupted regions of DNA, which in turn results in the inhibition of replication, transcription, or endonuclease activity. Many commercial anti-tumour drugs like amsacrine act by inhibiting topoisomerase II - which is

involved in twisting and untwisting (super coiling) of DNA during transcription and replication (**Figure 1.15**) - intercalate into alternating purine-pyrimidine sequences.<sup>17</sup>

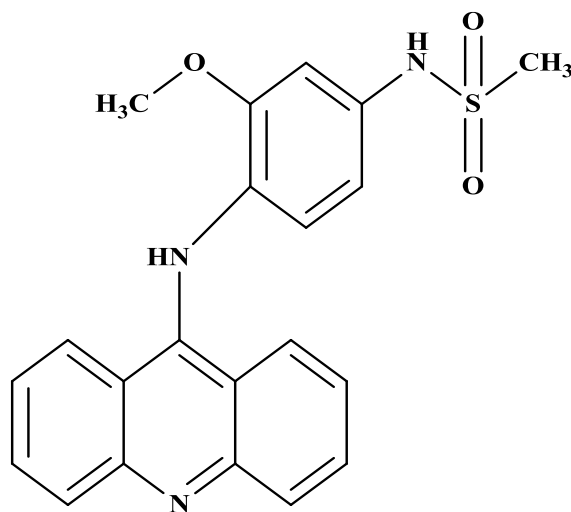


**Figure 1.15:** Amsacrine structure

#### 1.4.3.1 Organic intercalators

A number of studies have indicated that the minimal requirement for intercalative binding is a fused two-ring system. Through NMR experiments, Sartorius, *et al.*<sup>38</sup> have shown that there is no evidence for intercalation of isolated benzene rings and also that two condensed rings can only interact with DNA if assisted by positive charges in the side chains.

Such ligands can intercalate without the assistance of side chains when they are three ring systems. In addition, Sartorius proved that the strength of intercalation is not influenced by the presence of hetero elements within the  $\pi$ -system. These effects are illustrated by the observation made on the quinolinium derivatives shown in (**Figure 1.16**). It was shown to bind in the minor groove of an oligonucleotide when the substituent R1 is attached.<sup>39</sup> However the corresponding acridinium analogue with R2 attached was shown to be an intercalator.<sup>40</sup>

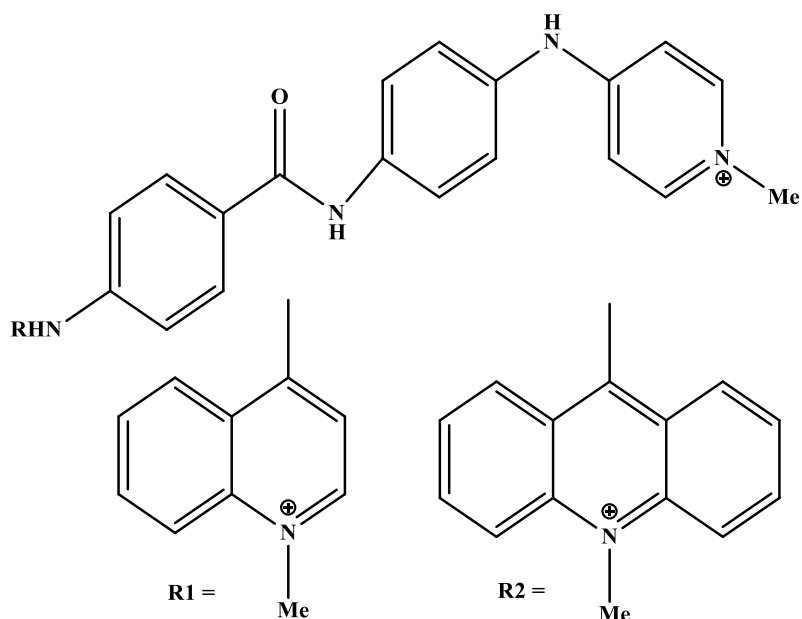


**Figure 1.16:** Quinolinim derivatives structure, with different R groups

The activity relationship noticed between high DNA binding affinity and biological efficacy has resulted in compounds with more than one DNA intercalating group or cationic side chain to obtain higher affinity binding complexes. Daunomycin is a characteristic example of such an organic intercalator. In cancer chemotherapy daunomycin is mainly used as an antibiotic for acute leukaemia<sup>41</sup> (**Figure 1.17**).

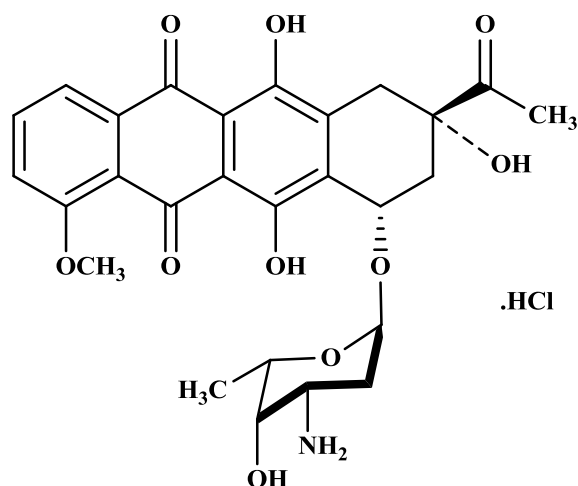


**Figure 1.17:** Daunomycin structure

The lack of activity against resistant cancer cells is one of the most important problems connected with the main clinical anticancer drugs. In an attempt to overcome this problem, two of these drug molecules have been bound together.<sup>42,43</sup> It was found from the original crystal structures of daunomycin binding to CGTACG<sup>41</sup> that the drug binds to DNA in a 2:1 ratio. The drug is intercalated at either end of the nucleotide with the amine moieties pointing towards one another. This arrangement brings the reactive NH<sub>2</sub> substituent of each drug molecule closer than 7 Å. In an attempt to produce more powerful chemotherapeutics from this information a bisanthracycline molecule with the potential to bis-intercalate into DNA was designed.<sup>42</sup> The connector had to be of suitable length and without steric hindrance so as to fit into the minor groove. To do this a para-xylene connector was used and the molecule given the code name WP631 was synthesised (**Figure 1.18**, taken from reference 44).

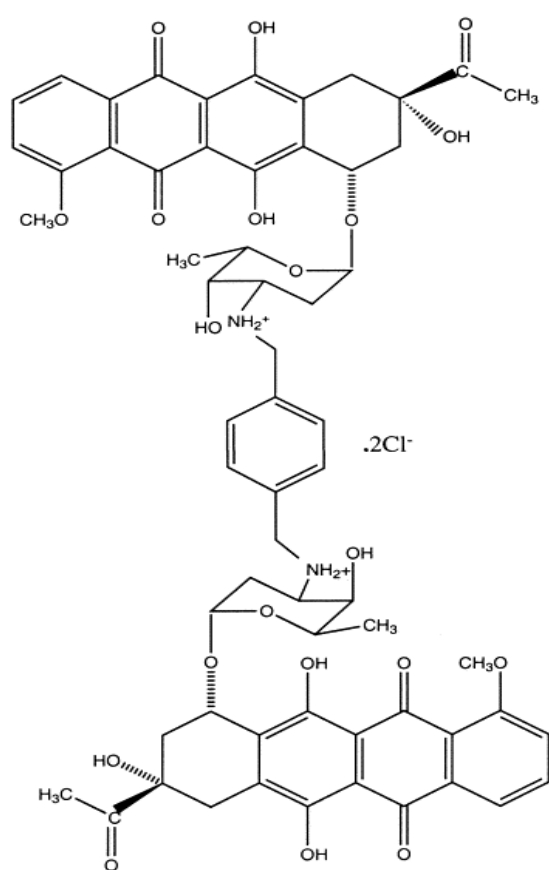


**Figure 1.18:** Chemical structure of WP631<sup>44</sup>

Generally, the binding affinity of bis-intercalators compared to the monomer should increase. Specifically, since the bis-intercalator's binding free energy should be approximately the sum

of the two free energies of mono-intercalator binding, the binding constant of a bisintercalator ought to be nearly the square of those of the monomer.<sup>42, 45</sup>

The X-ray crystal structures of the WP631-DNA complex confirmed that the drug binds to DNA almost exactly as planned<sup>43</sup>; with the planar aromatic groups intercalating inside the helix and the linker lying along the minor groove. The binding affinity of WP631 is also considerably improved, as shown by Chaires *et al.*<sup>42</sup> The site size of bisintercalators is much bigger than their monointercalator counterpart, which should lead to improved selectivity. Since daunomycin binding site fills three base pairs, the newer molecule should occupy twice as many base pairs. The greater site size should also impart a binding specificity similar to enzymes<sup>42</sup>. Experimentally, it was found that favoured binding sites usually contained the general sequence (G/C)(G/C)(A/T)(A/T)(G/C)(G/C). This molecule appears to address specific forms of multidrug resistance as initial biological studies in cultured cell lines revealed that it was more active than the original compound.

### 1.4.3.2 Metallo-intercalators

The study of transition metal complexes that reversibly bind to DNA is a growing research area. Complexes that bind to DNA through intercalation have become known as metallo-intercalators (**Figure 1.19**, taken from reference 47). This growth of interest is due to the useful properties of transition metal complexes, which possess rich photophysical and electrochemical properties, allowing for extensive possible applications from luminescent labels to DNA foot-printing agents and electrochemical probes.<sup>46</sup> The large choice of metal ions and ligands offers the possibility of tuning DNA binding and recognition properties. An important factor for stability in cellular conditions is that the interacting complexes need to be kinetically inert. Therefore the complexes that are most used are  $d^6$  octahedral and  $d^8$  square-planar which provide a rigid three dimensional structure.

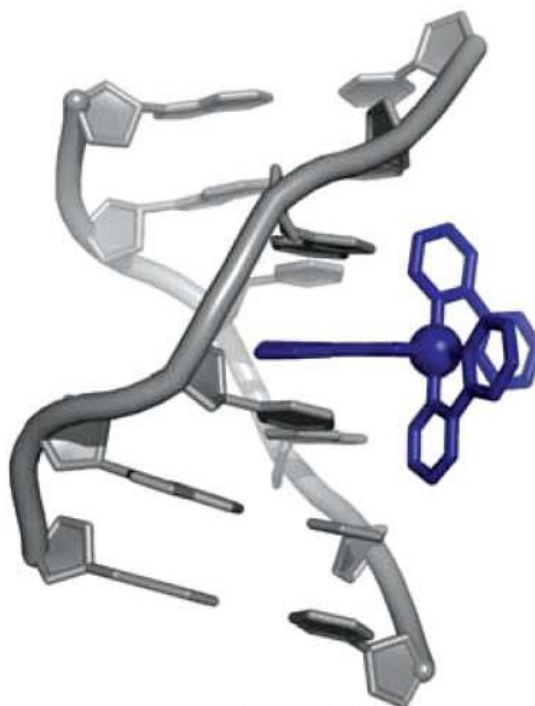


**Figure 1.19:** Intercalation binding mode of metal complex with DNA (metallo-intercalator)<sup>47</sup>

## 1.5 Mono- and bimetallic complexes

### 1.5.1 Monometallic Complexes

From the early 1970s onwards, many examples of monometallic complexes that bind to DNA through intercalation have been described. For example, it was established by Lippard<sup>48,49</sup> and Nordén<sup>50</sup> that square planar complexes of platinum with 2,2':6'2,2" terpyridine (tpy) or 2,2'dipyridine could bind to DNA via intercalation, whereas the non-planar  $[\text{Cu}(\text{dipy})_2]^{2+}$  (dipy = 2,2'-dipyridyl) behaves differently and binds via the minor groove, a fact that was later confirmed by X-ray studies.<sup>51</sup>

#### • *Tris(phenanthroline) Complexes*

In the early 1980s Barton *et al.* began to investigate octahedral metal complexes as DNA binding agents. Initially, these studies focused on the binding of tris-(phenanthroline) complexes of chromium<sup>52</sup>, zinc<sup>53</sup> and ruthenium to DNA. It was first suggested that

tris(phenanthroline) complexes of Zn(II) reversibly unwind the DNA duplex and partially insert between the base pairs. This suggestion was based on the different behaviour of closed circular DNA in the presence and absence of the metal complex during electrophoresis. From steric arguments, it was proposed that the  $\Delta$  enantiomer preferentially bound to right handed DNA.  $^1\text{H}$  NMR studies on  $\Delta$ - and  $\Lambda$ - $[\text{Ni}(\text{phen})_3]^{2+}$ ,  $\Delta$ - and  $\Lambda$ - $[\text{Cr}(\text{phen})_3]^{3+}$  bound to oligonucleotides described different behaviours depending on the isomer, with  $\Lambda$ -isomers preferring surface binding and the  $\Delta$ -isomers apparently intercalating<sup>54</sup> (**Figure 1.20**).

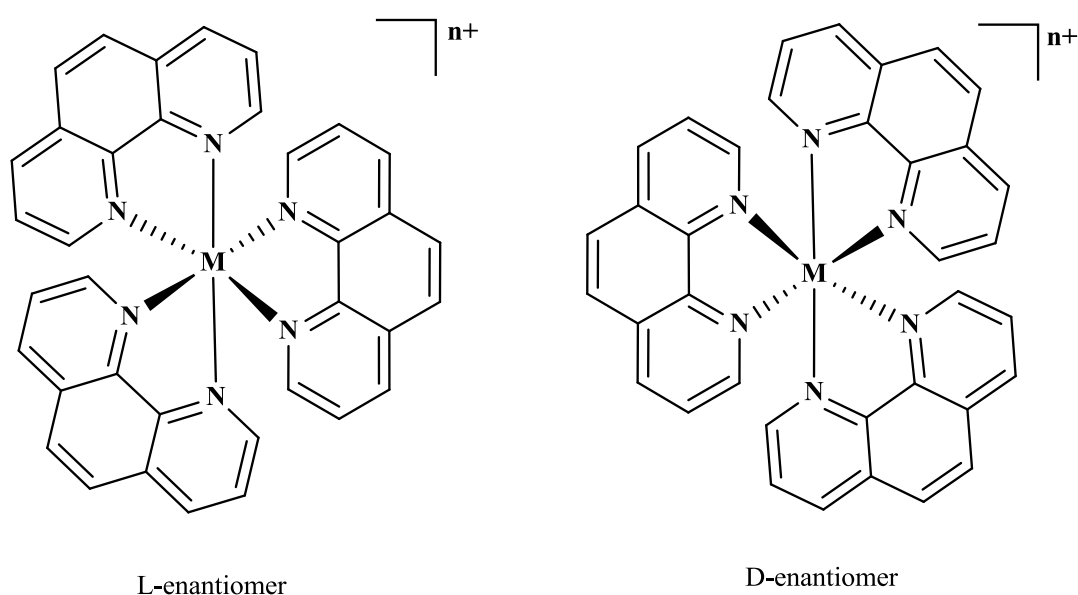


**Figure 1.20:** Structure of different enantiomers of a  $[\text{M}(\text{phen})_3]^{n+}$ , where **M** = central metal and **n** = represents the charge on the metal complex

As a result of the kinetically inert characteristics of low spin  $d^6$  systems and also because of their metal to ligand charge transfer (MLCT) band in the visible region, ruthenium systems were later investigated and  $[\text{Ru}(\text{phen})_3]^{2+}$  gave similar evidence for stereospecific binding to DNA.<sup>55</sup> Although it was later established by Chaires that these ligands could not intercalate as the phen ligand is not extended enough to insert between base pairs.<sup>56</sup>

## • Dipyridophenazine Complexes

One important feature of metallo-intercalators is that they have rich photochemistry and photophysical properties, which can be influenced by their interaction with DNA. This is illustrated by the molecular light switch intercalators first reported by Barton *et al.*<sup>57</sup>. They understood that an increase in the surface of an extended ligand is important in creating a true intercalating agent. Subsequently, the interaction of  $[\text{Ru}(\text{bpy})_2(\text{dppz})]^{2+}$  and  $[\text{Ru}(\text{phen})_2(\text{dppz})]^{2+}$  with DNA have been widely studied<sup>57,58</sup> (**Figure 1.21**).

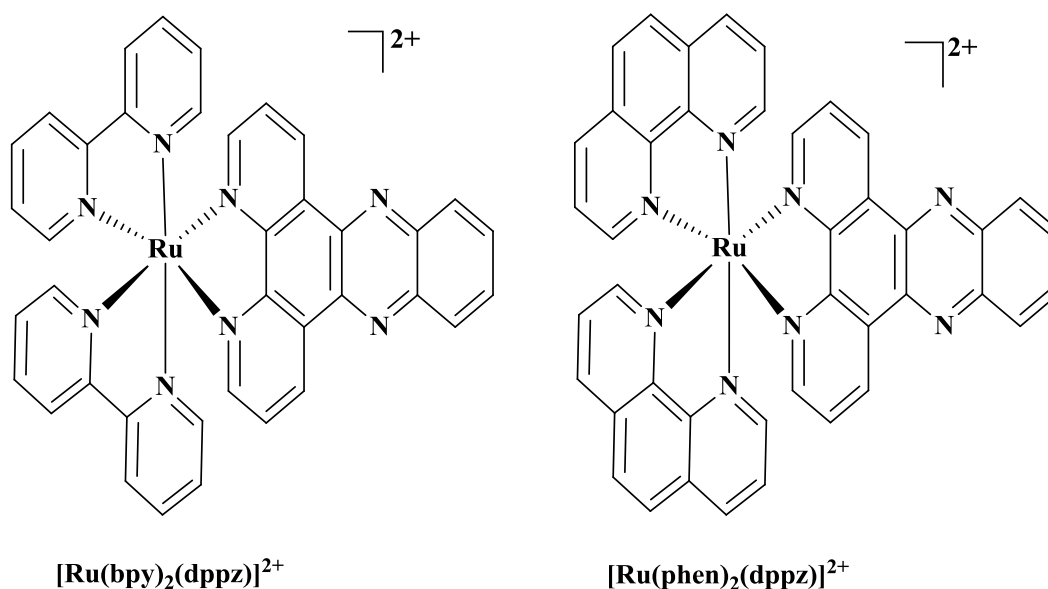


**Figure 1.21:** Chemical structures of  $[\text{Ru}(\text{bpy})_2(\text{dppz})]^{2+}$  and  $[\text{Ru}(\text{phen})_2(\text{dppz})]^{2+}$  complexes

### 1.5.1.1 The molecular light switch effect

Complexes such as  $[\text{Ru}(\text{bpy})_2(\text{dppz})]^{2+}$  (**Figure 1.22**, taken from reference 57) not only demonstrate enhanced DNA binding ( $K_b \sim 10^6 \text{ M}^{-1}$ ) but also display a photophysical phenomenon known as the ‘light switch effect’.<sup>57</sup>

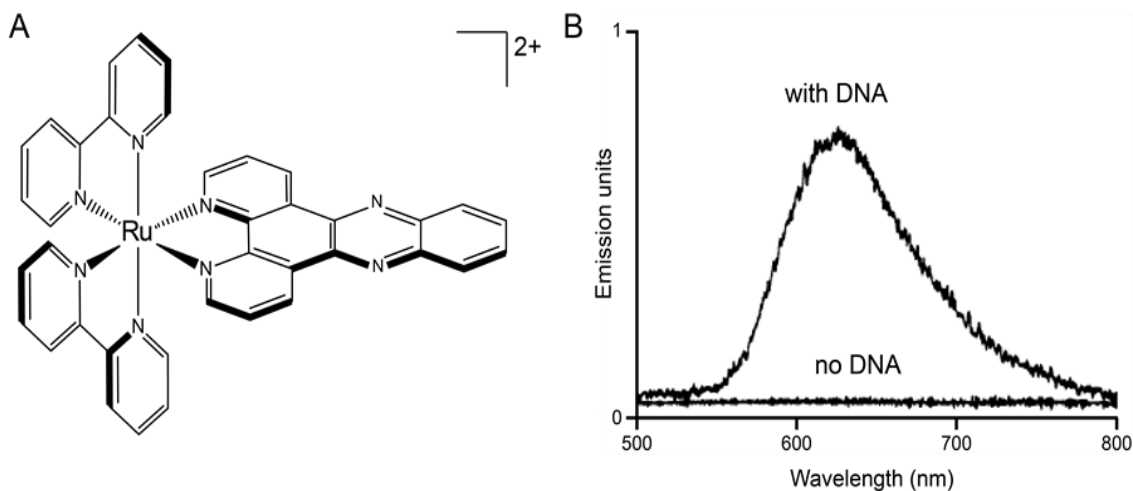


**Figure 1.22:** A) Metallo-intercalator  $[\text{Ru}(\text{bpy})_2(\text{dppz})]^{2+}$ , B) emission spectra of  $[\text{Ru}(\text{bpy})_2(\text{dppz})]^{2+}$  in the presence and absence of DNA.<sup>57</sup>

The ability of a chemical substance to change emission colour as a result of change in solvent polarity is known as solvatochromic luminescence. A molecular light switch deviates from this in the sense that upon moving from one environment into another a transition from no luminescence to intense luminescence is seen. In one environment the complex is basically “switched off” (with little to no luminescence), and then “switched on” in the other, thus the often made comparison with switching on a light. This feature is useful because it can be used to detect changes in micro-environment.<sup>59</sup> The emission of the  $[\text{Ru}(\text{bpy})_2\text{dppz}]^{2+}$  complex in aqueous condition is off because the excited state of the phenazine nitrogen atoms are quenched through the hydrogen bonding of water molecules<sup>60</sup> but the luminescence is activated when interacting with DNA as the dppz is shielded from water. The light switch effect was first reported by Barton *et al.* and is shown in **(Figure 1.22)**.

The characterisation of MLCT luminescence was reported by Sauvage *et al.* and they assumed that the light induced charge transfer (CT) is directed from the ruthenium atom to a  $\pi^*$  orbital mainly located on the dppz ligand.<sup>61</sup> This  $^1\text{MLCT}$  excited state then decays rapidly via intersystem crossing (ISC) to a  $^3\text{MLCT}$  excited state primarily localised on the phenazine nitrogen atoms **(Figure 1.23)**.

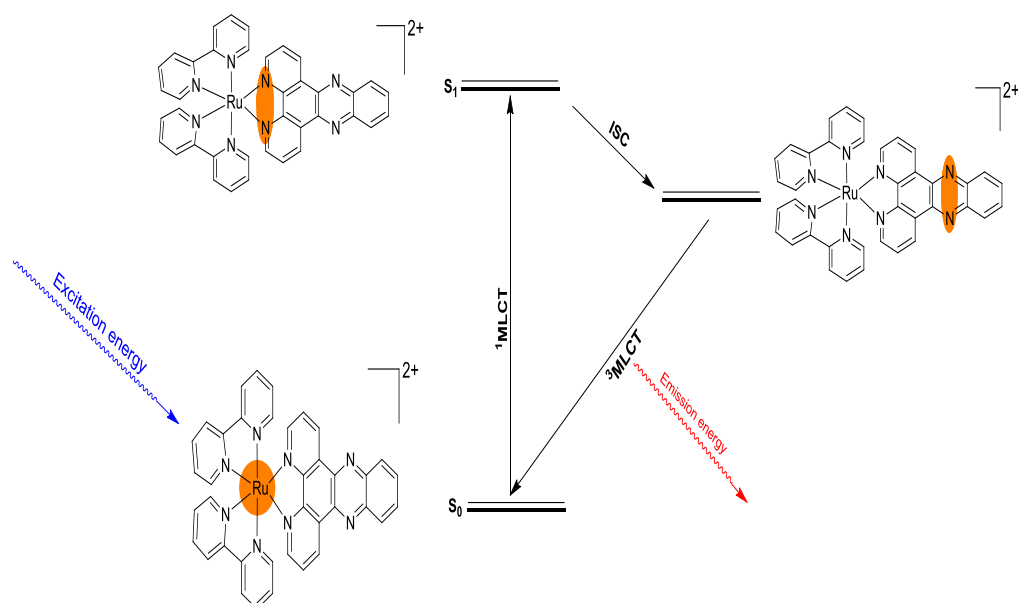


**Figure 1.23:** Jablonski diagram illustrating excited states involved in the DNA light switch effect.

From steady state emission spectra it was established that distinct discrimination in this effect could be observed between A-,B- and Z-DNA.<sup>57</sup> In spite of the high affinity of these complexes for DNA ( $10^6$ - $10^7$  M<sup>-1</sup>), there has been much discussion over the binding orientation of [Ru(phen)<sub>2</sub>(dppz)]<sup>2+</sup>. Photophysical studies show that both enantiomers of [Ru(phen)<sub>2</sub>(dppz)]<sup>2+</sup> exhibit bi-exponential decay of luminescence lifetime when bound to DNA.<sup>62</sup> It has been suggested that in one mode the dppz ligand intercalates from the major groove, with the metal-dppz axis perpendicular to the base pair, while in the other mode the dppz ligand is side-on, with the metal-dppz axis situated along the long axis of the base pair (**Figure 1.24**). In this binding mode, one of the nitrogen atoms in phenazine is still reachable by water as it points out into the major groove, resulting in quenching of the excited state, although much more slowly than if it was free in solution. However, both of the nitrogen atoms in the perpendicular mode are completely intercalated inside the base pair stack, rendering them inaccessible to external solvents, which results in a significantly improved and longer lived excited state.

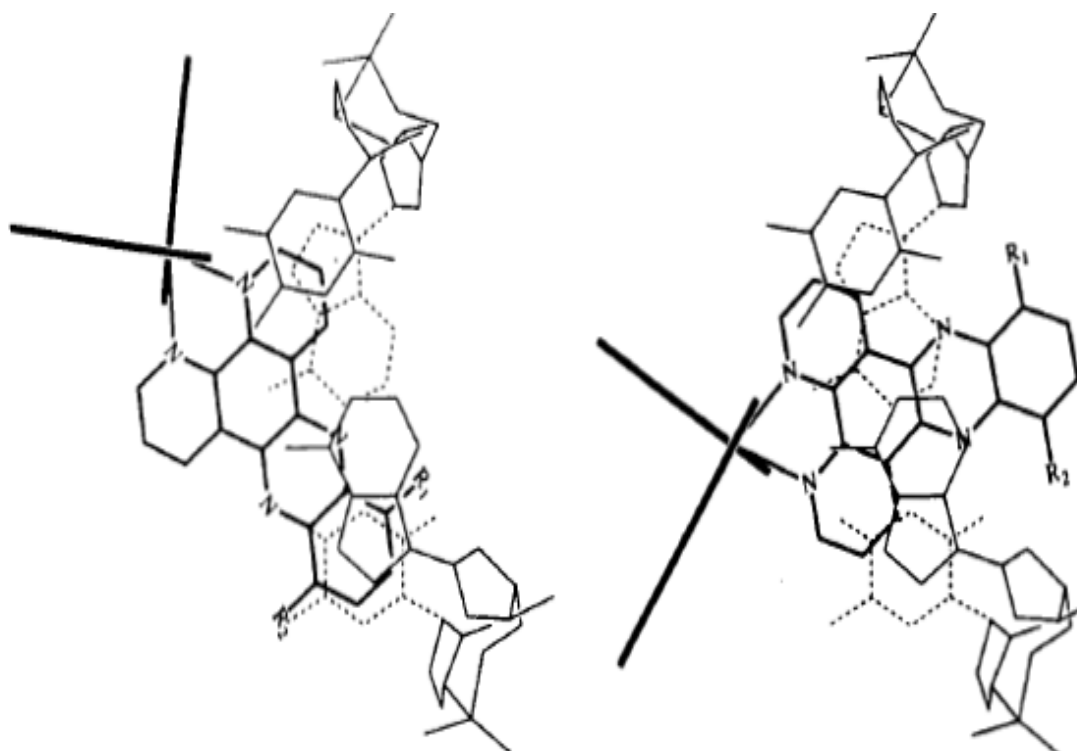


**Figure 1.24:** Side on (**left**) and perpendicular (**right**) modes of intercalation of dppz into B-form DNA

In 1998, the competition binding interaction of  $[\text{Ru}(\text{phen})_2(\text{dppz})]^{2+}$  with a known major groove intercalator ( $\Delta\text{-}\alpha\text{-}[\text{Rh}[(R,R)\text{-Me}_2\text{trien}]\text{phi}]^{3+}$ ) and a minor (distamycin) groove binding agents was investigated by Holmlin *et al.*<sup>63</sup> It was found that  $[\text{Ru}(\text{phen})_2(\text{dppz})]^{2+}$  was displaced upon titration of the rhodium complex, while addition of the minor groove binder distamycin produces an increase in ruthenium emission, consistent with the double helix being able to accommodate major and minor groove binders at the same time. Distamycin has no effect on the emission of  $[\text{Ru}(\text{phen})_2(\text{dppz})]^{2+}$  emission bound to poly d(GC). These photophysical results provide support for intercalation through major groove side of the duplex DNA. Later crystallographic work has suggested that this hypothesis is incorrect – see later.

The binding mode of  $[\text{Ru}(\text{phen})_2(\text{dppz})]^{2+}$  with DNA have investigated by Biver *et al.*<sup>64</sup> using stop-flow and spectrophotometric methods and they identified a second non-intercalative binding mode in their studies. They supposed that the phen moieties reside in the grooves allowing the dppz ligand to partially intercalate between the base pair. Therefore, this results

in partial unwinding of the helix and when sufficient unwinding has been realised, the  $[\text{Ru}(\text{phen})_2(\text{dppz})]^{2+}$  inserts between base pairs through a more typical intercalation mode.

In 2012, Niyazi *et al.*<sup>65</sup> described the crystal structures of the light switch ruthenium complex  $[\text{Ru}(\text{phen})_2(\text{dppz})]^{2+}$  bound to two oligonucleotide duplexes (**Figure 1.25**, taken from reference 65).

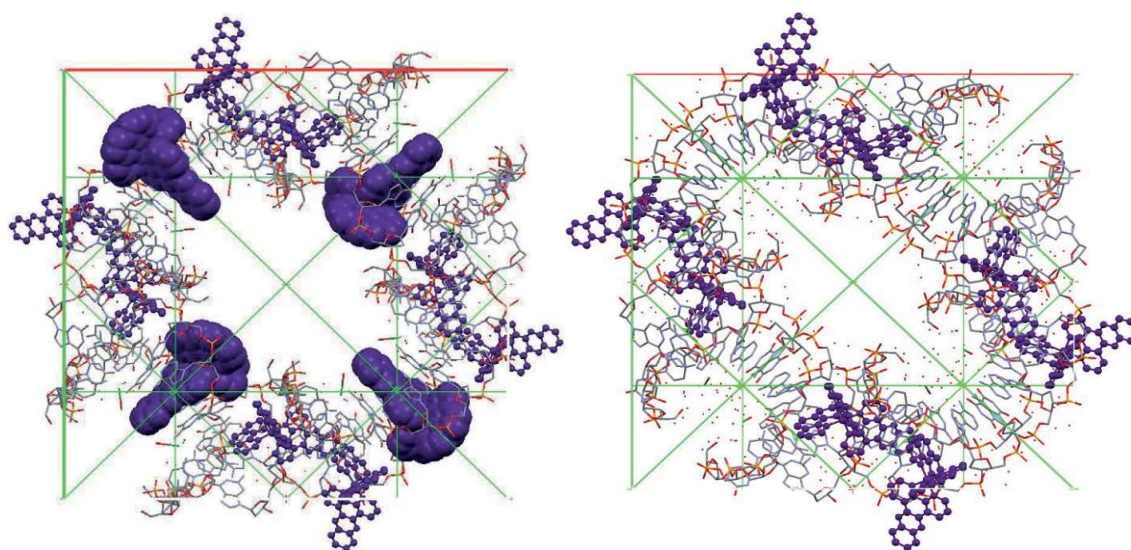


**Figure 1.25:** Crystal structures of ruthenium cation  $\Lambda$ - $[\text{Ru}(\text{phen})_2(\text{dppz})]^{2+}$  and oligonucleotides  $\text{d}(\text{CCGGTACCGG})_2$  duplex (**left**) and  $\text{d}(\text{CCGGATCCGG})_2$  duplex (**right**), Ru2, space-filling in purple; Ru1, ball-and-stick in purple.<sup>65</sup>

This study reported that the ruthenium complex  $[\text{Ru}(\text{phen})_2(\text{dppz})]^{2+}$  binds to an oligonucleotide by two distinct modes of intercalation; symmetrical and angled intercalation, and in each case intercalation is through the minor groove of B-DNA. Semi-intercalation of one phen ligand is also seen in the symmetrical mode of dppz intercalation seen at the central TA/TA step of the oligonucleotide duplex (**Figure 1.26**, taken from reference 65). The structure also shows changes in DNA conformation at the intercalation point that are similar to those found in the crystal structure of certain classical DNA intercalators such as daunomycin, but not others like actinomycin D.

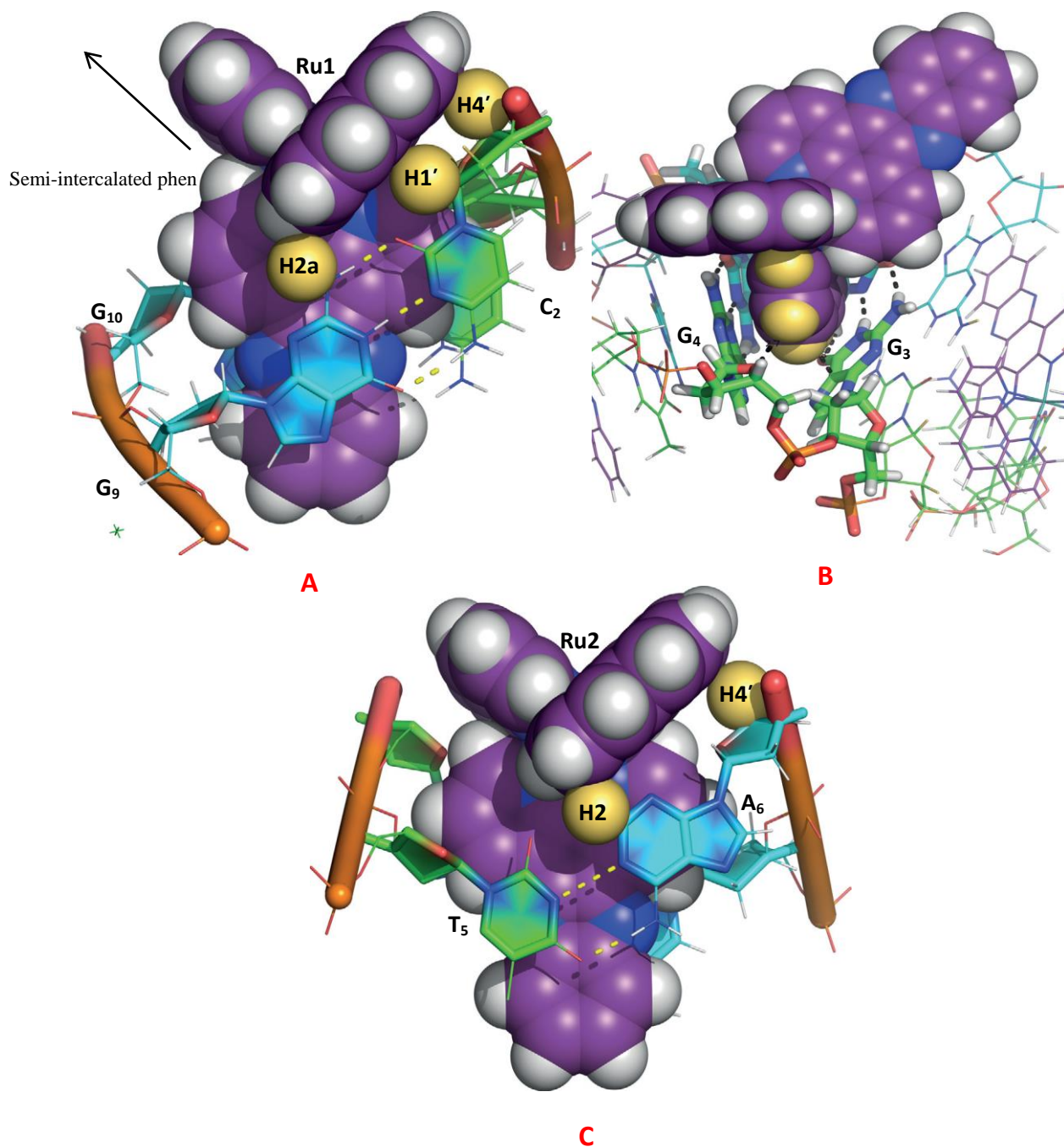


**Figure 1.26:** Geometry of intercalation modes of  $\Lambda$ -[Ru(phen)<sub>2</sub>(dppz)]<sup>2+</sup> complex with oligonucleotides<sup>65</sup>. (A) Angled intercalation; (B) Semi-intercalation of one phenanthroline ligand and (C) Symmetrical intercalation

Metal complexes bearing more bulky intercalating ligands serve as probes for DNA mismatches. In the developing of diagnostics and therapeutics for cancer DNA mismatches represent a unique target, because lacks in DNA mismatch repair are implicated in cancers, and cells that are repair-deficient display a high frequency of mismatches. Song *et al.*<sup>66</sup>

reported the crystal structure of  $\Delta$ -[Ru(bpy)<sub>2</sub>(dppz)]<sup>2+</sup> bound to both mismatched and well-matched sites in the oligonucleotide 5'-(dCGGAAATTACCG)<sub>2</sub>-3' (**Figure 1.27**, taken from reference 66). The results also reveal that the binding of  $\Delta$ -[Ru(bpy)<sub>2</sub>(dppz)]<sup>2+</sup> complex to mismatches DNA occurs via metalloinsertion, while additional ruthenium complexes classically intercalated at well-matched sites.

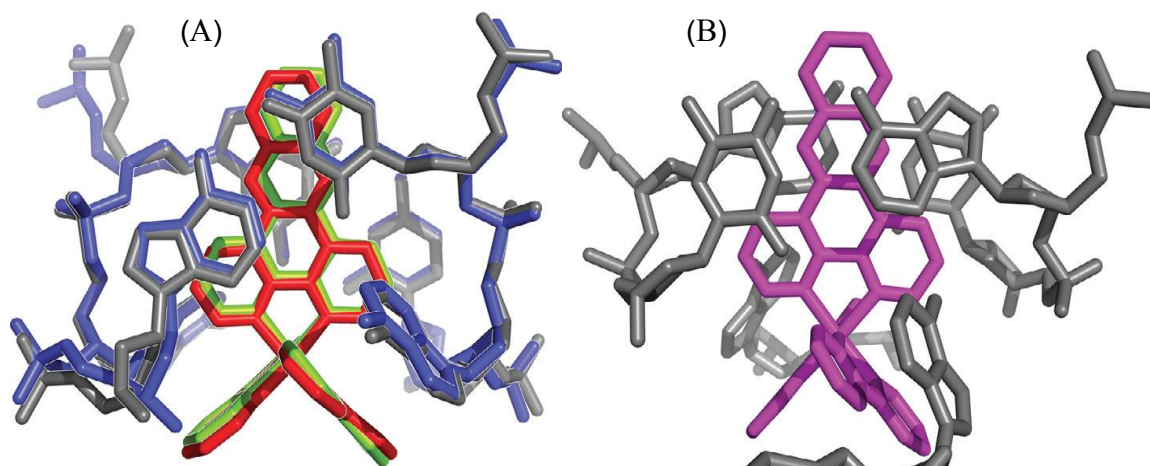


**Figure 1.27:** Two independent views of (A) metalloinsertion at the mismatched sites and (B) metallointercalation at well-matched sites.<sup>66</sup>

In the case of metalloinsertion, through the dppz ligand, the complex inserts tightly from the minor groove and completely ejects the mispaired adenosines. Again intercalation at well-matched base pairs occurs from the minor groove side<sup>67</sup> (**Figure 1.28**, taken from reference 66). These observations highlight the dominance of metalloinsertion at destabilized regions of DNA.

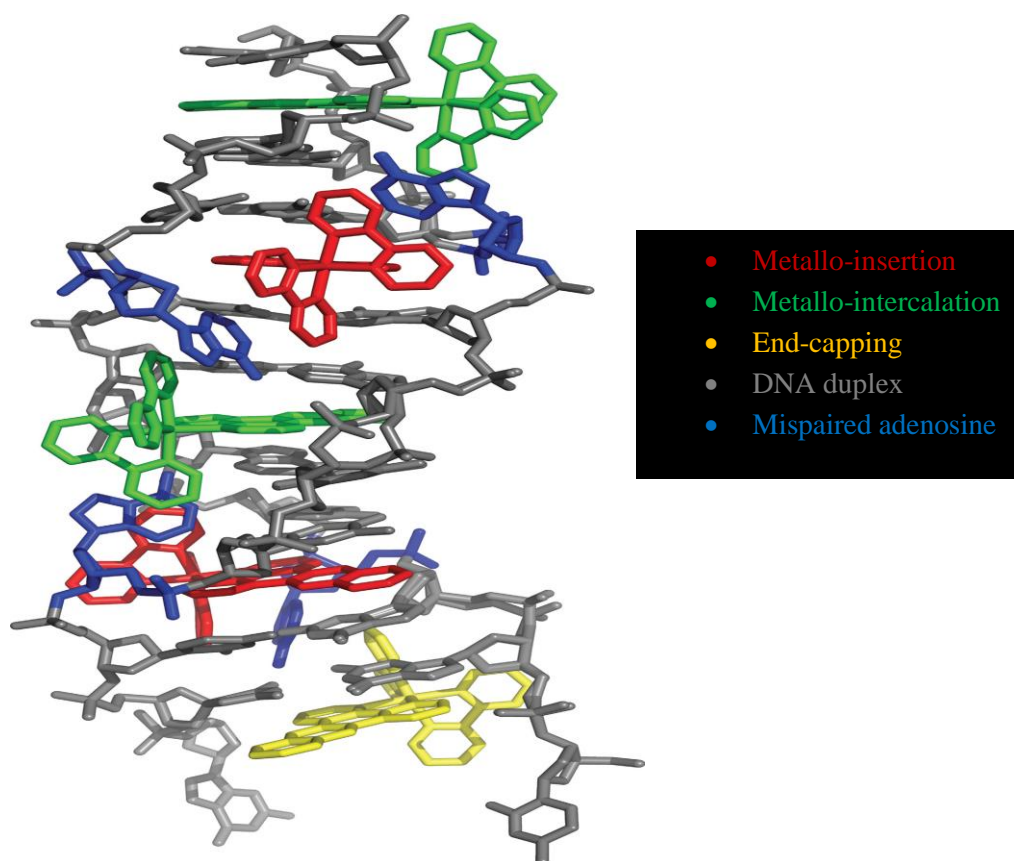


**Figure 1.28:** Structure of  $\Delta$ -  $[\text{Ru}(\text{bpy})_2\text{dppz}]^{2+}$  and three DNA binding modes highlighted for clarifications. (Metalloinsertion, Metallointercalation, End-capping, DNA duplex and Mispaired adenosine).<sup>66</sup>

### • *Benzo-dipyridophenazine Complexes*

In order to explore how the structure and nature of an extended dppz ligand with an extra aromatic ring affected the luminescence properties in the absence and presence of DNA of such systems, a benzo-dipyridophenazine (dppn) complex in the form of  $[\text{Ru}(\text{phen})_2(\text{dppn})]^{2+}$  was first reported by Barton *et al.* (**Figure 1.29**)<sup>58</sup> Compared to the parent complex  $[\text{Ru}(\text{phen})_2(\text{dppz})]^{2+}$ , the dppn complex did not show a light switch effect. Later research revealed that the rhenium (I) complex of dppn has very different excited properties and displays photocleavage activity with plasmid DNA through the generation of reactive singlet oxygen species.<sup>68</sup>

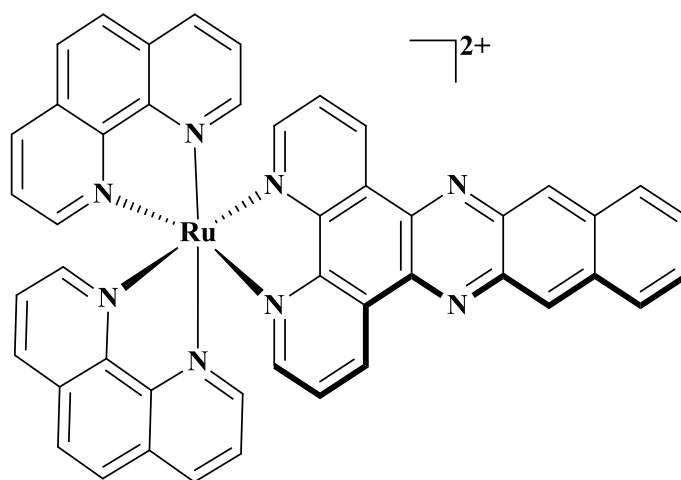


**Figure 1.29:** Chemical structure of [Ru(phen)<sub>2</sub>(dppn)]<sup>2+</sup>

Unlike Ru<sup>II</sup>(dppz) systems, which display an MLCT-based lowest excited state, transient absorption studies on Ru<sup>II</sup>(dppn) complexes revealed that the lowest excited state of these complexes is a <sup>3</sup>π-π\* state centred on the dppn ligand, which was confirmed by DFT calculations on the [Ru(tpm)Cl(dppn)]<sup>+</sup>, [Ru(tpm)MeCN(dppn)]<sup>2+</sup> and [Ru(tpm)py(dppn)]<sup>2+</sup> complexes (tpm = tris(1-pyrazolyl)methane) reported by Foxon *et al.*<sup>69</sup> This metallo-intercalator system may find potential applications in therapeutic systems such as photodynamic therapy (PDT). In this application, targeted tissue is exposed to specific light radiation that induces the production of reactive chemical species, causing adverse effects in and around the surrounding tissue.

In 2014, Yin *et al.*<sup>70</sup> prepared a series of Ru(II)-based transition metal complexes derived from this π-expansive ligand (**Figure 1.30**) and showed that the low-energy and long-lived <sup>3</sup>IL excited states photocleaved DNA with blue, green, red, and near-IR light. The aim of their investigation was to discover whether <sup>3</sup>IL excited states with microsecond lifetimes are generally effective for photodynamic applications, and if these long-lived states are better than their <sup>3</sup>MLCT counterparts as *in vitro* PDT agents. They showed that related Ru(II) complexes having lowest-lying <sup>3</sup>MLCT with much shorter lifetimes did not produce DNA photodamage or *in vitro* PDT effects with red or near-IR light. They concluded that complexes that utilise photosensitizing <sup>3</sup>IL excited states, with long lifetimes are excellent

candidates for multiwavelength PDT even where their molar extinction coefficients are quite small.

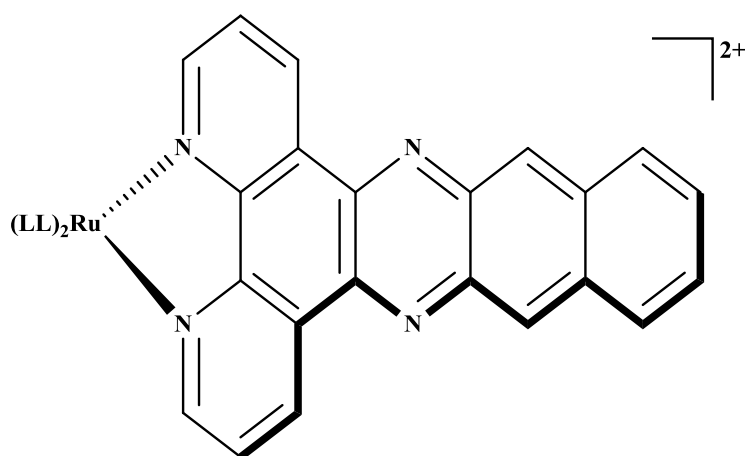


**Figure 1.30:** Chemical structure of  $[\text{Ru}(\text{LL})_2(\text{dppn})]^{2+}$  (where LL = 4,4'-dimethyl-2,2'-bipyridine (**dmb**), 4,4'-di-*t*-butyl-2,2'-bipyridine (**dtbb**) and 1,10-phenanthroline (**phen**))

#### • Tetraazophenanthrene ligand and its complex

The ability of ruthenium-dppz complexes to photo-oxidize nucleic acid<sup>71,72</sup> within living cells is one of the inspirations for this study. Incorporating electron deficient ligands like 1,4,5,8-tetraazophenanthrene(TAP) into octahedral ruthenium complexes greatly affects its excited states causing direct oxidation of guanine moieties; it also leads to covalent adduct formation with nucleic acids.<sup>73</sup> Since the  $[\text{Ru}(\text{TAP})_2(\text{dppz})]^{2+}$  complex is structurally close to  $[\text{Ru}(\text{phen})_2(\text{dppz})]^{2+}$ , it also binds to a wide range of double-stranded DNA sequences. In the presence of guanine, the excited state of  $[\text{Ru}(\text{TAP})_2(\text{dppz})]^{2+}$  is quenched and the oxidation of guanine appears to proceed by proton coupled electron transfer as suggested by picosecond transient absorption experiments.<sup>74</sup>

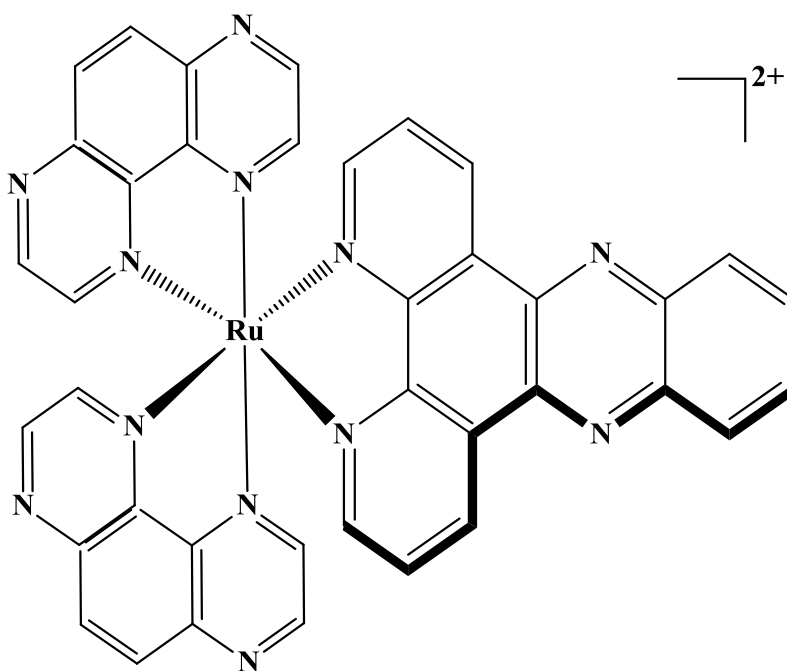


**Figure 1.31:** Chemical formula of  $\Lambda$ -  $[\text{Ru}(\text{TAP})_2(\text{dppz})]^{2+}$  complex

### X-ray structure of the $[\text{Ru}(\text{TAP})_2(\text{dppz})]^{2+}$ complex

The crystal structure of this complex bound to DNA showed that the ruthenium polypyridyl complex sits in duplex DNA with one ligand acting as a wedge in the minor groove, resulting in kinking of the double helix. In the presence of barium ions, the  $\Lambda$ - $[\text{Ru}(\text{TAP})_2(\text{dppz})]^{2+}$  cation crystallizes with the oligonucleotide d(TCGGCGCCGA) in a 1:1 ratio. In each complex the dipyridophenazine ligand binds to one duplex by intercalation and one of the orthogonal TAP ligands binds into a second symmetrically equivalent duplex through semi-intercalation. Non-covalent cross linking and marked kinking of DNA is the result of this binding (**Figure 1.32**, taken from reference 75).<sup>75</sup>

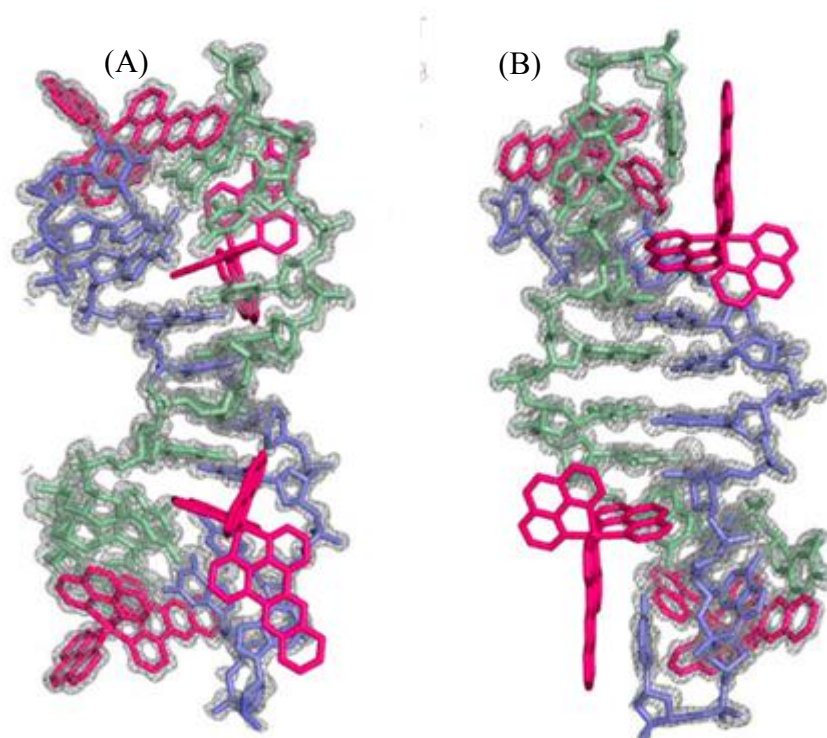


**Figure 1.32:** Structure of the complex cation  $[\text{Ru}(\text{TAP})_2(\text{dppz})]^{2+}$  with oligonucleotide  $\text{d}(\text{TCGGCGCCGA})$ . (A) Shows the ruthenium complex with two symmetry connected strands and (B) shows inside the minor groove of the assembly.<sup>75</sup>

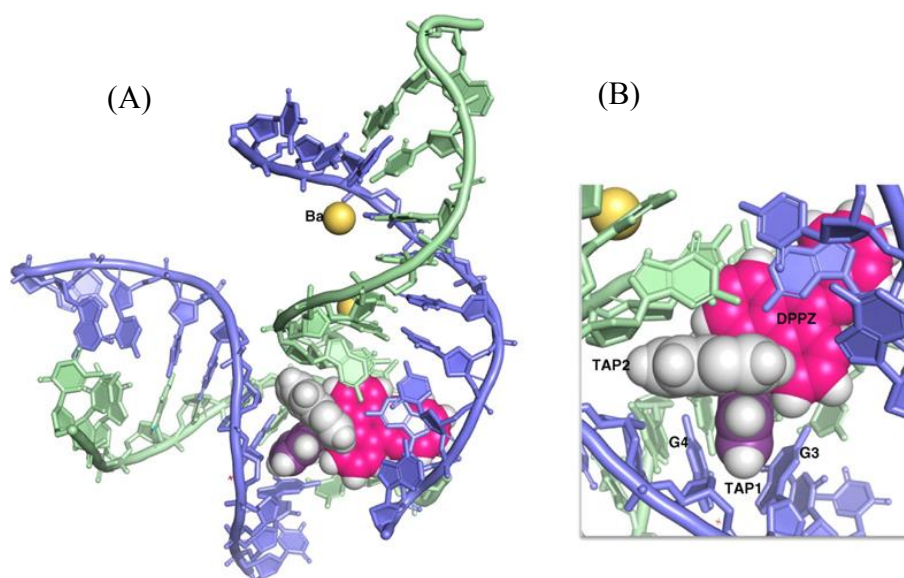


**Figure 1.33:** Binding modes of the ruthenium complex  $[\text{Ru}(\text{TAP})_2(\text{dppz})]^{2+}$  with oligonucleotide. (A) Barium ions and the intercalated ruthenium complex cation showed by one  $\text{d}(\text{TCGGCGGA})_2$  (dppz, pink; TAP1, purple; TAP2, white) (B) Semi-intercalated of TAP1 between G3-G4 step.<sup>75</sup>

### • Different binding modes of the TAP and dppz ligands

Most noticeably, the two chemically identical TAP ligands (differentiated as TAP1 and TAP2) possess very different roles within the structure caused by the intercalation geometry of  $[\text{Ru}(\text{TAP})_2(\text{dppz})]^{2+}$  which also leads to enantiomeric specificity (**Figure 1.33**). At the G3-G4 step the TAP1 ligand semi-intercalates from the minor groove, only interacting with the guanine component of the base pair but not the corresponding C7-C8. TAP2 lies between the minor grooves of two duplexes and remains inert in terms of the overall supramolecular structure. Together, the TAP1 semi-intercalation inside the G3-G4 step and the flipped out T1-A10 base pair, link symmetry equivalent duplexes. TAP1 also makes a series of close contacts with the six-membered purine rings of G3 and G4.<sup>76</sup> Furthermore, semi-intercalation makes a binding site for a barium ion fairly different from that seen in the absence of  $\Lambda$ - $[\text{Ru}(\text{TAP})_2(\text{dppz})]^{2+}$ , with straight coordination to the N7 positions of G3 and O6 and N7 of G4 (**Figure 1.34**, taken from reference 75).

The structure confirms that the dppz ligand of this complex does intercalate into the DNA duplex as suggested by spectroscopic and hydrodynamic data.<sup>58, 77,61-63,78,79</sup>

As with the TAP semi-intercalation, and like the previously described structures, intercalation of the dppz ligand takes place from the minor groove. The interaction between the pyrazine ring of the dppz ligand and the six-membered purine rings of G9 and A10 is the principle stacking interaction, so that the distance of the ruthenium atom is almost 6.5 Å from the helical axis of the duplex. The dppz does not make contact with any of the surrounding water molecules.

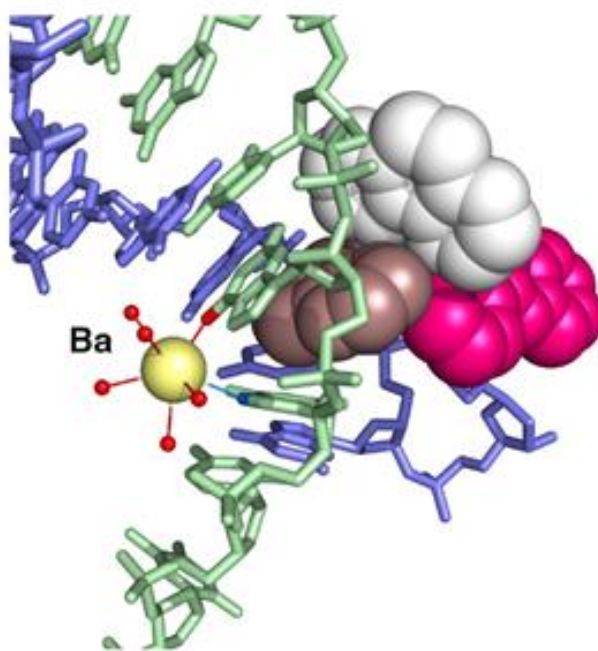


**Figure 1.34:** The hydration and coordination of barium ion to N7 of guanine G3 and O6 of guanine G4 in the major groove.<sup>75</sup>

## 1.5.2 Bimetallic Complexes

As outlined in a previous section, polyfunctional intercalating agents can improve the affinity and selectivity of DNA.<sup>80</sup> The preparation of covalently linked bifunctional compounds designed to improve DNA interaction has been investigated by some research groups. For example, in 1996, Kelly *et al.* tethered relatively weak binding systems such as mononuclear  $[\text{Ru}(\text{bpy})_3]^{2+}$  and  $[\text{Ru}(\text{phen})_3]^{2+}$  into bimetallic systems<sup>81,82</sup> (**Figure 1.35**). They reported that the length of the linker chain ( $n$ ) is a crucial factor in determining the binding efficiency and to show a DNA stacking interaction at high binding concentrations.



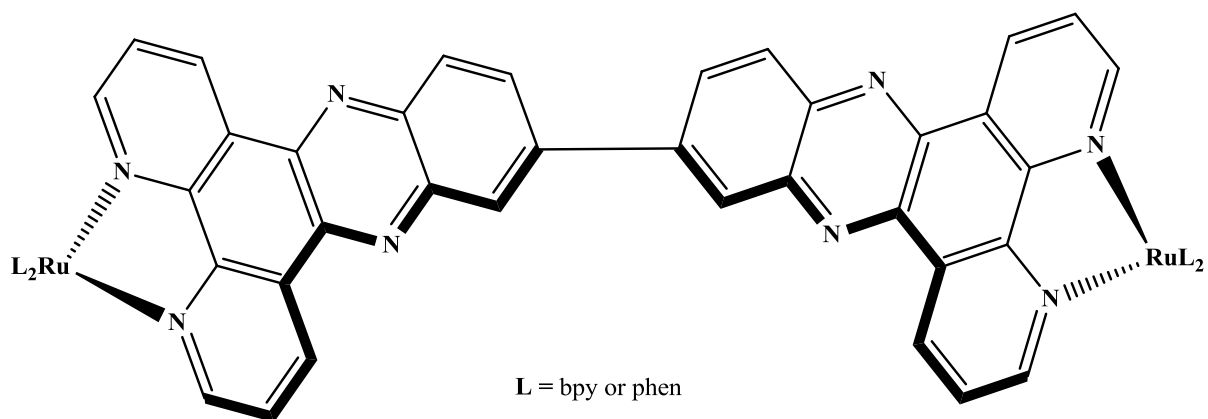


**Figure 1.36:** Structure of  $[L_2Ru\{dppz(11-11')dppz\}RuL_2]^{4+}$

The crystal structure of one of the phen versions of the above binuclear ruthenium complex ( $\Delta,\Delta[\mu-(11,11'\text{-bidppz})(1,10\text{-phenanthroline})_4Ru_2]^{4+}$ ) bound to the oligonucleotide d(CGTACG) was reported by Boer *et al.*<sup>85</sup> (**Figure 1.37**, taken from reference 85). It shows that an AT base pair is extruded when one dppz ligand of the binuclear ruthenium complex inserts into the DNA stack, while the second dppz moiety recruits an adjacent DNA molecule, and by bridging their major grooves the complex cross-links two neighbouring duplexes. This structure is the first example of two DNA duplexes being adjoined at their major grooves.

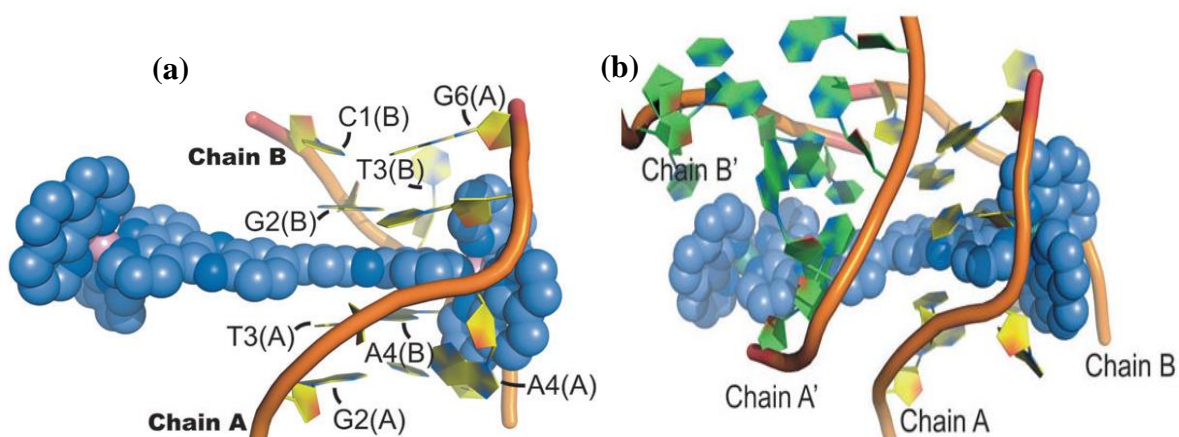


**Figure 1.37:** Structure of the ruthenium complex and the oligonucleotide (a) shows a single molecule binds to a single DNA duplex and (b) shows the stacking interactions of two adjacent strands with one molecule of complex.<sup>85</sup>

In 2015, Almaqwashi *et al.* utilise the  $(\Delta, \Delta[\mu-(11,11'\text{-bidppz})(1,10\text{-phenanthroline})_4\text{Ru}_2]^{4+})$  binuclear ruthenium complex to measure its binding properties (**Figure 1.36**). They used optical tweezers to measure elongation of the DNA at a range of constant stretching forces and characterized the kinetics of intercalation as well as the extent of intercalation at equilibrium. This study revealed that the zero force intercalation of the binuclear ruthenium complex is 25-fold stronger than the analogous mononuclear complex. Moreover, a mechanism that requires DNA elongation for association, relaxation and an additional elongation for dissociation from the equilibrium state was revealed by the force dependent kinetics analysis.<sup>86</sup>

The phenomenon of DNA threading has also been studied in dppz tethered units with a longer and more flexible linker. The three enantiomers of  $[\mu\text{-c}_4(\text{cpdppz})_2\text{-(phen)}_4\text{Ru}_2]^{4+}$  have been synthesised and their binding to DNA characterized by Nordén *et al.* (**Figure 1.38**).<sup>87,88</sup> Linear dichroism (LD) measurement, luminescence spectroscopy and other studies confirmed intercalation of all the complexes between base pair of DNA, with the intercalating ligands separated by two base pairs. Due to the binding mode this complex exhibits, it is known as a DNA staple (**Figure 1.39**).

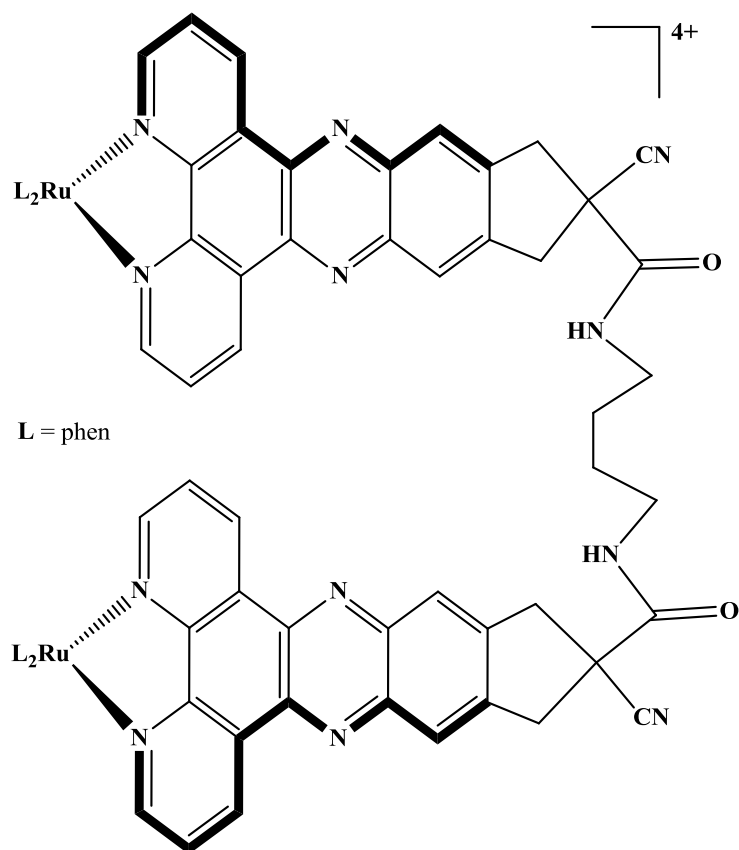


**Figure 1.38:** Dimer structure of the threading  $[\mu\text{-c}_4(\text{cpdppz})_2\text{-(phen)}_4\text{Ru}_2]^{4+}$

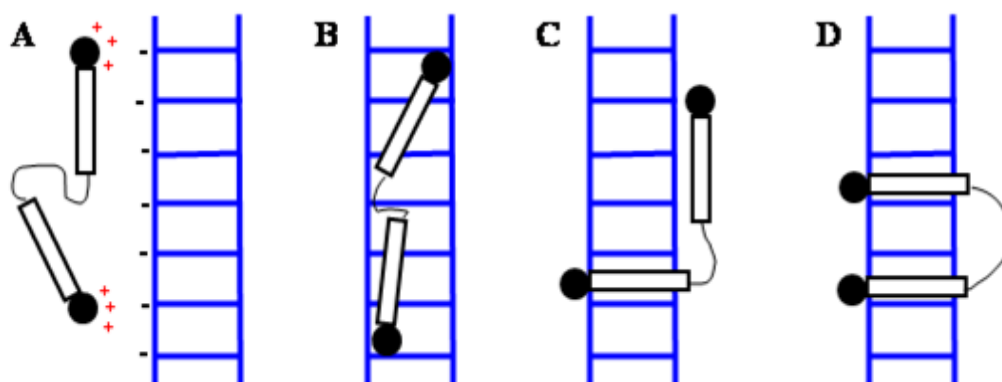


**Figure 1.39:** Schematic DNA interaction modes of Nordén's dimer: A) External binding, B) Groove binding, C) Mono-intercalation, D) Bis-intercalation.

Recent work focused on the influence of the DNA binding properties of  $[\mu\text{-c}_4(\text{cpdppz})_2\text{-(phen)}_4\text{Ru}_2]^{4+}$  system (**Figure 1.38**) for therapeutic use. To quantify ligand binding, a study using optical tweezers was carried out. This study described ligand association by a two-step

process; the first step shows fast bimolecular intercalation of the first dppz moiety followed by almost 10-fold slower intercalation of the second dppz moiety and the second step is the rate that allows the flexible linker to pass through the DNA duplex. Based on the force dependent binding rates and ligand-induced DNA elongation measurements, at zero force the complete binding route involves fast association, slow dissociation and very high affinity.<sup>89</sup> Metcalfe *et al.* have developed a facile route to the synthesis of non-threading bimetallic Re(I) complexes containing two dppz intercalating ligands.<sup>90</sup> Studies showed that the propane tether is not long enough to allow binding of both  $[(\text{CO})_3\text{Re}(\text{dppz})]^+$  units (**Figure 1.40**) with DNA, so the second Re(I) centre interacts with another duplex via interstrand binding.

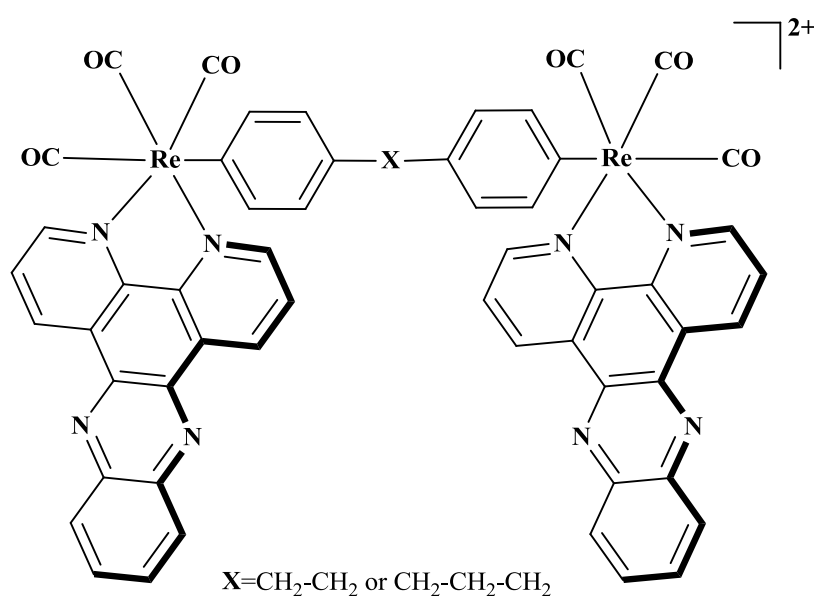


**Figure 1.40:** Structures of Re(I)dppz complexes

Studies on tpm-Ru(II)-dppz binding systems connected together by 4,4'-dipyridyl-1,5-pentane (dpp) (**Figure 1.41**) with DNA were described.<sup>91</sup> Similar affinities for both complexes with DNA ( $K_b \approx 10^5 \text{ M}^{-1}$ ) were shown using luminescence and ITC titrations. However, compared with other simple monometallic systems these interactions are significantly weaker. In the monomer complex the bulky ancillary ligand produced a loss in the selectivity for GC sequences seen for other mononuclear tpm-Ru(II)-dppz system.<sup>92</sup> However, the binding constant of the monomeric analogues was expected to be greatly enhanced in the bis-intercalator, though such behaviour was not seen. This result was

explained through a consideration of the length and rigidity of the connector employed in the complex.

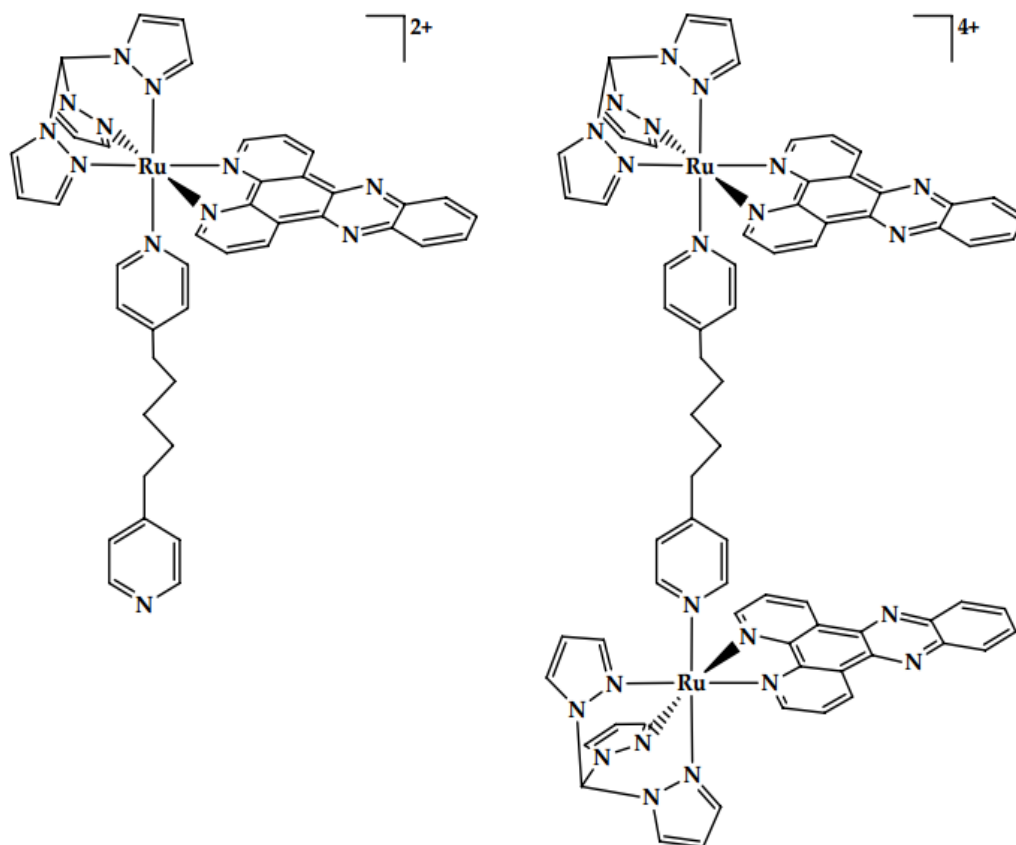


**Figure 1.41:** Structure of mono and bimetallic complexes of tpm-Ru(II)-dppz

In contrast, the mixed Ru-Re system  $[(\text{Ru}(\text{tpm})(\text{dppz}))(\mu\text{-dpp})(\text{fac}(\text{CO})_3\text{Re}(\text{dppz}))]^{3+}$  (**Figure 1.42**)<sup>93</sup> established an order of magnitude increase in the binding affinity compared to the monomeric analogue (containing pyridine instead of the dpp linker); along with a much enhanced light switch effect, which is relatively weak in the  $\text{Re}^{\text{I}}$  complex. In addition to that, the Ru-Re system also causes direct cleavage of DNA and as such is the first example of a complex that possesses this property along with that of the light switches effect.

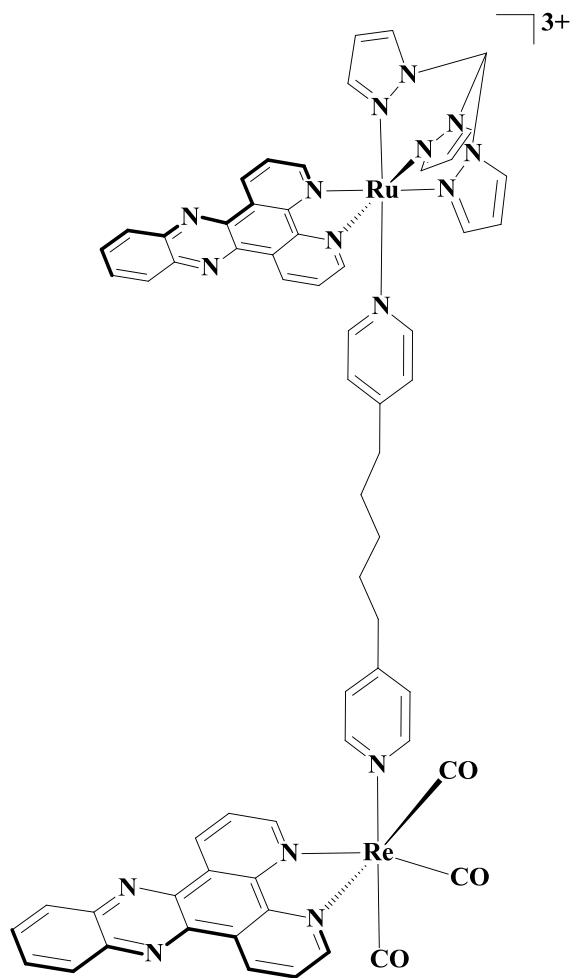


**Figure 1.42:** Structure of bis-intercalator  $[(\text{Ru}(\text{tpm})(\text{dppz}))(\mu\text{-dpp})(\text{fac}(\text{CO})_3\text{Re}(\text{dppz}))]^{3+}$

## 1.6 Project Aims

The aim of this project is to prepare a series of bimetallic complexes of tpm-Ru(II)-dppz linked with new organic tethers designed to enhance the binding affinity, the DNA sequence recognition property, and the photophysical properties of these systems. This will be accomplished by either changing the position of pyridine nitrogen atoms in the organic linker, or by using different substituents within the organic linker. Furthermore, in these complexes the linker contains hydrogen bonding ammine groups capable of interacting within the grooves of DNA.

## References

- (1) Voet, D.; Voet, J. G.: *Biochemistry*; John Wiley and Sons: New York, 1995.
- (2) McMurry, J.: *Organic Chemistry*; 3rd edition ed.; Brooks/Cole, 1992.
- (3) Mainwaring, W. I. P.; Parish, J. H.; Pickering, J. D.; Mann, N. H.: *Nucleic acid Biochemistry and Molecular Biology*; Blackwell Scientific Oxford, 1982.
- (4) Watson, J. D.; Crick, F. H.: *Nature* **1953**, *171*, 737-738.
- (5) Stryer, L.: *Biochemistry*; W.H. Freeman, 1999.
- (6) Moran, L.A.; Scrimgeour, K. G.; Horton, H. R.; Ochs, R. S.; Rawn, J. D.: *Biochemistry*; Neil Patterson: New York, 1994.
- (7) Berg, J. M.; Tymoczko, J. L.; Stryer, L. and Stryer, L.B.: *Biochemistry*; W.H. Freeman ; Basingstoke : Palgrave [distributor]: New York, 2007.
- (8) Blackburn, G. M.; Gait, M. J.; Loakes, D.; Williams, D. M.: *Nucleic Acids in Chemistry and Biology*; Royal Society of Chemistry: Cambridge, 2006.
- (9) Alberts, B.; Johnson, A.; Walter, P.; Lewis, J.; Raff, M. and Roberts, K.: *Molecular Biology of the Cell. Reference edition*; Abingdon: Garland Science, New York, N.Y, 2008.
- (10) Franklin, R. E.; Gosling, R. G.: *Nature* **1953**, *171*, 740-741.
- (11) Leslie, A. G. W.; Arnott, S.; Chandrasekaran, R. and Ratliff, R. L.: *Journal of Molecular Biology* **1980**, *143*, 49-72.
- (12) Dickerson, R. E.; Drew, H. R.; Conner, B. N.; Wing, R. M.; Fratini, A. V.; Kopka, M. L.: *Science* **1982**, *216*, 475-485.
- (13) Belmont, P.; Constant, J. F.; Demeunynck, M.: *Chemical Society Reviews* **2001**, *30*, 70-81.
- (14) Kastan, M. B.; Bartek, J.: *Nature* **2004**, *432*, 316-323.
- (15) Roat-Malone, R.M., John Wiley and Sons,: *Bioinorganic Chemistry* **2002**.
- (16) Takahara, P. M.; Rosenzweig, A. C.; Frederick, C. A.; Lippard, S. J.: *Nature* **1995**, *377*, 649.

- (17) Johnson, D. S.; Boger, D. L.: *Chapter 3 In Comprehensive Supramolecular Chemistry*; .M. Lehn, Y. Murakami, Ed., Pergamon Press: Oxford, 1996.
- (18) Erkkila, K. E.; Odom, D. T.; Barton, J. K.: *Chemical Reviews* **1999**, *99*, 2777-2796.
- (19) Thomas, T.; Gunnia, U.; Thomas, T.: *Journal of Biological Chemistry* **1991**, *266*, 6137-6141.
- (20) Basu, H. S.; Marton, L. J.: *Biochemistry*, **1987**, 243-6.
- (21) Pages, B. J.; Ang, D. L.; Wright, E. P.; Aldrich-Wright, J. R.: *Dalton Transactions* **2015**, *44*, 3505-3526.
- (22) Goodsell, D. S.; Kopka, M. L.; Dickerson, R. E.: *Biochemistry* **1995**, *34*, 4983-4993.
- (23) Pullman, A.; Pullman, B.: *Quarterly Reviews of Biophysics* **1981**, *14*, 289-380.
- (24) Chaires, J. B.: *Archives of Biochemistry and Biophysics* **2006**, *453*, 26-31.
- (25) Kopka, M. L.; Yoon, C.; Goodsell, D.; Pjura, P.; Dickerson, R. E.: *Proceedings of the National Academy of Sciences* **1985**, *82*, 1376-1380.
- (26) Hasanzadeh, M.; Shadjou, N.: *Materials Science and Engineering: C* **2016**, *61*, 1002-1017.
- (27) Coll, M.; Frederick, C. A.; Wang, A. H. J.; Rich, A.: *Proceedings of the National Academy of Sciences of the United States of America* **1987**, *84*, 8385-8389.
- (28) Kopka, M. L.; Yoon, C.; Goodsell, D.; Pjura, P.; Dickerson, R. E.: *Journal of Molecular Biology* **1985**, *183*, 553-563.
- (29) Fratini, A.; Kopka, M. L.; Drew, H. R.; Dickerson, R. E.: *Journal of Biological Chemistry* **1982**, *257*, 14686-14707.
- (30) Pullman, B.: *Journal of Biomolecular Structure and Dynamics* **1983**, *1*, 773-794.
- (31) Zakrzewska, K.; Randrianarivelo, M.; Pullman, B.: *Journal of Biomolecular Structure and Dynamics* **1988**, *6*, 331-344.

- (32) Goodsell, D.S.; Dickerson, R. E.: *Journal of Medicinal Chemistry* **1986**, *29*, 727-733.
- (33) Patel, D. J.: *Proceedings of the National Academy of Sciences* **1982**, *79*, 6424-6428.
- (34) Lerman, L.: *Journal of Molecular Biology* **1961**, *3*, 18-IN14.
- (35) Lerman, L. S.: *Proceedings of the National Academy of Sciences of the United States of America* **1963**, *49*, 94-102.
- (36) Long, E. C.; Barton, J. K.: *Accounts of Chemical Research* **1990**, *23*, 271-273.
- (37) Suh, D.; Chaires, J. B.: *Bioorganic & Medicinal Chemistry* **1995**, *3*, 723-728.
- (38) Sartorius, J.; Schneider, H. J.: *Journal of the Chemical Society, Perkin Transactions 2* **1997**, 2319-2328.
- (39) Leupin, W.; Chazin, W. J.; Hyberts, S.; Denny, W. A.; Wuethrich, K.: *Biochemistry* **1986**, *25*, 5902-5910.
- (40) Braithwaite, A. W.; Baguley, B. C.: *Biochemistry* **1980**, *19*, 1101-1106.
- (41) Wang, A. H.; Ughetto, G.; Quigley, G. J.; Rich, A.: *Biochemistry* **1987**, *26*, 1152-1163.
- (42) Chaires, J. B.; Leng, F.; Przewloka, T.; Fokt, I.; Ling, Y. H.; Perez-Soler, R.; Priebe, W.: *Journal of Medicinal Chemistry* **1997**, *40*, 261-266.
- (43) Hu, G. G.; Shui, X.; Leng, F.; Priebe, W.; Chaires, J. B.; Williams, L. D.: *Biochemistry* **1997**, *36*, 5940-5946.
- (44) Marczak, A.; Bukowska, B.; Rogalska, A.: *Environmental Toxicology and Pharmacology* **2014**, *37*, 256-266.
- (45) Leng, F.; Priebe, W.; Chaires, J. B.: *Biochemistry* **1998**, *37*, 1743-1753.
- (46) Phillips, T.; Haq, I.; Meijer, A. J. H.; Adams, H.; Soutar, I.; Swanson, L.; Sykes, M. J.; Thomas, J. A.: *Biochemistry* **2004**, *43*, 13657-13665.
- (47) Wei, M. Y.; Guo, L. H.; Famouri, P.: *Microchimica Acta* **2011**, *172*, 247-260.
- (48) Jennette, K. W.; Lippard, S. J.; Vassiliades, G. A.; Bauer, W. R.: *Proceedings of the National Academy of Sciences of the United States of America* **1974**, *71*, 3839-3843.
- (49) Howe-Grant, M.; Lippard, S. J.: *Biochemistry* **1979**, *18*, 5762-5769.

- (50) Nordtin, B.: *Inorganica Chimica Acta* **1978**, *31*, 83-95.
- (51) Bond, P.; Langridge, R.; Jennette, K.; Lippard, S.: *Proceedings of the National Academy of Sciences* **1975**, *72*, 4825-4829.
- (52) Barton, J. K.; Raphael, A. L.: *Proceedings of the National Academy of Sciences* **1985**, *82*, 6460-6464.
- (53) Barton, J. K.; Dannenberg, J.; Raphael, A. L.: *Journal of the American Chemical Society* **1982**, *104*, 4967-4969.
- (54) Rehmann, J. P.; Barton, J. K.: *Biochemistry* **1990**, *29*, 1701-1709.
- (55) Barton, J. K.; Danishefsky, A. T.; Goldberg, J. M.: *Journal of the American Chemical Society* **1984**, *106*, 2172-2176.
- (56) Ren, J.; Jenkins, T. C.; Chaires, J. B.: *Biochemistry* **2000**, *39*, 8439-8447.
- (57) Friedman, A. E.; Chambron, J. C.; Sauvage, J. P.; Turro, N. J.; Barton, J. K.: *Journal of the American Chemical Society* **1990**, *112*, 4960-4962.
- (58) Zhu, B. Z.; Chao, X. J.; Huang, C. H.; Li, Y.: *Chemical Science* **2016**.
- (59) Higgs, P.; McKinley, A.; Tuite, E.: *Chemical Communications* **2016**, *52*, 1883-1886.
- (60) Turro, C.; Bossmann, S. H.; Jenkins, Y.; Barton, J. K.; Turro, N. J.: *Journal of the American Chemical Society* **1995**, *117*, 9026-9032.
- (61) Jenkins, Y.; Friedman, A. E.; Turro, N. J.; Barton, J. K.: *Biochemistry* **1992**, *31*, 10809-10816.
- (62) Hiort, C.; Lincoln, P.; Norden, B.: *Journal of the American Chemical Society* **1993**, *115*, 3448-3454.
- (63) Holmlin, R. E.; Stemp, E. D.; Barton, J. K.: *Inorganic Chemistry* **1998**, *37*, 29-34.
- (64) Biver, T.; Cavazza, C.; Secco, F.; Venturini, M.: *Journal of Inorganic Biochemistry* **2007**, *101*, 461-469.
- (65) Niyazi, H.; Hall, J. P.; O'Sullivan, K.; Winter, G.; Sorensen, T.; Kelly, J. M.; Cardin, C. J.: *Nature Chemistry* **2012**, *4*, 621-628.
- (66) Song, H.; Kaiser, J. T.; Barton, J. K.: *Nature Chemistry* **2012**, *4*, 615-620.

- (67) Boynton, A. N.; Marcélis, L.; Barton, J. K.: *Journal of the American Chemical Society* **2016**.
- (68) Yam, V. W. W.; Lo, K. K. W.; Cheung, K. K.; Kong, R. Y. C.: *Journal of the Chemical Society, Chemical Communications* **1995**, 1191-1193.
- (69) Foxon, S. P.; Metcalfe, C.; Adams, H.; Webb, M.; Thomas, J. A.: *Inorganic Chemistry* **2007**, *46*, 409-416.
- (70) Yin, H.; Stephenson, M.; Gibson, J.; Sampson, E.; Shi, G.; Sainuddin, T.; Monro, S.; McFarland, S. A.: *Inorganic Chemistry* **2014**, *53*, 4548-4559.
- (71) Elias, B.; Mesmaeker, A. K. D.: *Coordination Chemistry Reviews* **2006**, *250*, 1627-1641.
- (72) Smith, J. A.; George, M. W. ; Kelly, J. M.: *Coordination Chemistry Reviews* **2011**, *253*, 2021-2035.
- (73) Jacquet, L.; Davies, R. J. H.; Mesmaeker, A. K. D.; Kelly, J. M.: *Journal of the American Chemical Society* **1997**, *119*, 11763-11768.
- (74) Elias, B.; Creely, C.; Doorley, G. W.; Feeney, M. M.; Moucheron, C.; Mesmaeker, A. K. D.; Dyer, J.; Grills, D. C.; George, M. W.; Matousek, P.; Parker, A. W.; Towrie, M.; Kelly, J. M.: *Chemistry- A European Journal* **2008**, *14*, 369-375.
- (75) Hall, J. P.; O'Sullivan, K.; Naseer, A.; Smith, J. A.; Kelly, J. M.; Cardin, C. J.: *Proceedings of the National Academy of Sciences* **2011**, *108*, 17610-17614.
- (76) Parkinson, G.; Wilson, C.; Gunasekera, A.; Ebright, Y. W.; Ebright, R. E.; Berman, H. M.: *Journal of Molecular Biology* **1996**, *260*, 395-408.
- (77) Zeglis, B. M.; Pierre, V. C.; Barton, J. K.: *Chemical Communications* **2007**, 4565.
- (78) Haq, I.; Lincoln, P.; Suh, D.; Norden, B.; Chowdhry, B. Z.; Chaires, J. B.: *Journal of the American Chemical Society* **1995**, *117*, 4788-4796.
- (79) Dupureur, C. M.; Barton, J. K.: *Inorganic Chemistry* **1997**, *36*, 33-43.
- (80) Wakelin, L. P.: *Medicinal Research Reviews* **1986**, *6*, 275-340.
- (81) O'Reilly, F. M.; Kelly, J. M.; Mesmaeker, A. K. D.: *Chemical Communications* **1996**, 1013-1014.

- (82) O'Reilly, F. M.; Kelly, J. M.: *New Journal of Chemistry* **1998**, 22, 215-217.
- (83) Lincoln, P.; Nordén, B.: *Chemical Communications* **1996**, 2145.
- (84) Wilhelmsson, L. M.; Westerlund, F.; Lincoln, P.; Nordén, B.: *Journal of the American Chemical Society* **2002**, 124, 12092-12093.
- (85) Boer, D. R.; Wu, L.; Lincoln, P.; Coll, M.: *Angewandte Chemie International Edition* **2014**, 53, 1949-1952.
- (86) Almaqwashi, A. A.; Paramanathan, T.; Lincoln, P.; Rouzina, I.; Westerlund, F.; Williams, M. C.: *Nucleic Acids Research* **2014**, 42, 11634-11641.
- (87) Oenfelt, B.; Lincoln, P.; Norden, B.: *Journal of the American Chemical Society* **1999**, 121, 10846-10847.
- (88) Önfelt, B.; Lincoln, P.; Nordén, B.: *Journal of the American Chemical Society* **2001**, 123, 3630-3637.
- (89) Bahira, M.; McCauley, M. J.; Almaqwashi, A. A.; Lincoln, P.; Westerlund, F.; Rouzina, I.; Williams, M. C.: *Nucleic Acids Research* **2015**, gkv864.
- (90) Metcalfe, C.; Webb, M.; Thomas, J. A.: *Chemical Communications* **2002**, 2026-2027.
- (91) Metcalfe, C.; Haq, I.; Thomas, J. A.: *Inorganic Chemistry* **2004**, 43, 317-323.
- (92) Metcalfe, C.; Adams, H.; Haq, I.; Thomas, J. A.: *Chemical Communications* **2003**, 1152-1153.
- (93) Foxon, S. P.; Phillips, T.; Gill, M. R.; Towrie, M.; Parker, A. W.; Webb, M.; Thomas, J. A.: *Angewandte Chemie International Edition* **2007**, 46, 3686-3688.

## *Chapter 2*

### *Bimetallic DNA Metallo-intercalators containing the ruthenium (II) tris(1-pyrazolyl)methane Unit*

---

2.1 Introduction.....	48
2.2 Syntheses.....	49
2.2.1 Linker syntheses.....	49
2.2.2 Synthesis of complexes.....	50
2.2.2.1 Monometallic complexes.....	50
2.2.2.2 Bimetallic complexes.....	51
2.3 Characterization.....	52
2.3.2 Mass spectrometry data.....	52
2.3.3 Photophysical studies.....	52
2.3.4 DNA Binding Studies.....	57
2.3.5 UV-Visible titrations.....	61
2.3.6 Luminescence emission titrations.....	65
2.3.7 Viscosity.....	72
References.....	75

## 2.1 Introduction

In recent times a large amount of research has concerned ruthenium polypyridyl complexes system as DNA binding agents, particularly developing systems that show a ‘light switch’ effect or form photo-adducts. The use of complexes with extended aromatic ligands has been a particular focus as this improves non-covalent binding through intercalation.<sup>1,2</sup> More recently, in an attempt to increase the binding affinity and DNA sequence recognition properties of such complexes bimetallic systems have been investigated by Nordén and Kelly. However, the multi-step syntheses, starting from coordinatively saturated, classically resolved chiral metal complexes, are not trivial. In this chapter we describe the synthesis and characterisation of a number of bimetallic complexes using achiral  $[\text{Ru}(\text{tpm})(\text{L})(\text{dppz})]^{n+}$  complexes (tpm = tris(1-pyrazolyl)methane, L = chloride or *N*-donor ligand, dppz = dipyrido[3,2-*a*:2',3'-*c*]phenazine), which contain an easily modulated coordination site (2–4) (**Figure 2.1**).<sup>3-5</sup> To ascertain how the nature of the linker affects DNA-binding properties, we have prepared four new complexes<sup>6,7</sup>:  $[\text{Ru}(\text{tpm})(\text{dppz})(\mu\text{-L1})]^{2+}$  [1],  $[\text{Ru}(\text{tpm})(\text{dppz})(\mu\text{-L2})]^{2+}$  [2],  $[\{\text{Ru}(\text{tpm})(\text{dppz})\}_2(\mu\text{-L1})]^{4+}$  [3] and  $[\{\text{Ru}(\text{tpm})(\text{dppz})\}_2(\mu\text{-L2})]^{4+}$  [4] (where L1 = *N,N'*-bis(4-pyridylmethyl)-1,6-hexanediamine and L2 = *N,N'*-bis(4-pyridylmethyl)-1,4-benzenedimethyleamine).

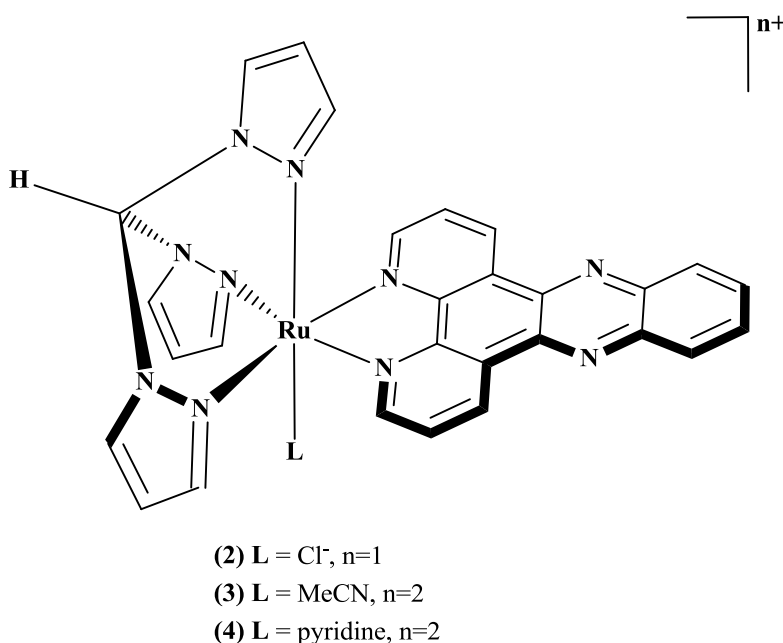


**Figure 2.1:** Ruthenium (II) tris(1-pyrazolyl)methane monomeric complexes.

## 2.2 Syntheses

### 2.2.1 Linker syntheses

**N,N'-bis(4-pyridylmethyl)-1,6-hexanediamine (L1)** was synthesized by refluxing a solution of 4-pyridinecarboxaldehyde and 1,6-hexanediamine in ethanol. Addition of NaBH<sub>4</sub> in small portions and extracting the aqueous solution with CH<sub>2</sub>Cl<sub>2</sub>, followed by evaporation yielded a cream colored solid precipitate.

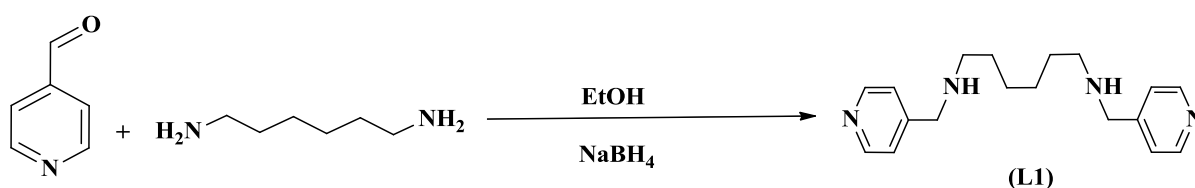


Figure 2.2: Synthesis of L1

**N,N'-bis(4-pyridylmethyl)-1,4-benzenedimethyleneamine (L2)** was prepared by stirring the mixture of benzene-1,4-dicarboxaldehyde and 4-(aminomethyl)pyridine in CH<sub>2</sub>Cl<sub>2</sub> (100 ml) with anhydrous MgSO<sub>4</sub> (at room temperature for 24 h). Addition of NaBH<sub>4</sub> in small portions and extracting the aqueous solution with CH<sub>2</sub>Cl<sub>2</sub> yielded a golden coloured viscous oil product on evaporation of solvent.

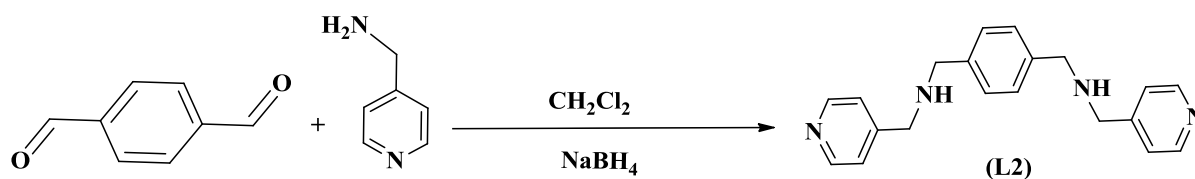


Figure 2.3: Synthesis of L2

## 2.2.2 Synthesis of complexes

### 2.2.2.1 Monometallic complexes

$[\text{Ru}(\text{tpm})(\text{dppz})(\mu\text{-L1})](\text{PF}_6)_2$  [1] and  $[\text{Ru}(\text{tpm})(\text{dppz})(\mu\text{-L2})](\text{PF}_6)_2$  [2].

Complexes [1] and [2] were prepared by refluxing  $[\text{Ru}(\text{tpm})(\text{dppz})\text{Cl}]^+$  and  $\text{AgNO}_3$  in ethanol:water followed by the addition of the L1 or L2 ligand, respectively.  $\text{AgNO}_3$  was added to remove the axial chloride ligand, which precipitated as  $\text{AgCl}$  and was then removed by filtering through celite. After reflux, the desired complex was precipitated as a  $\text{PF}_6^-$  salt by reducing the solvent volume and adding excess  $\text{NH}_4\text{PF}_6$  (Figure 2.4). Both ruthenium complexes were further purified on alumina using column chromatography (acetonitrile: toluene).

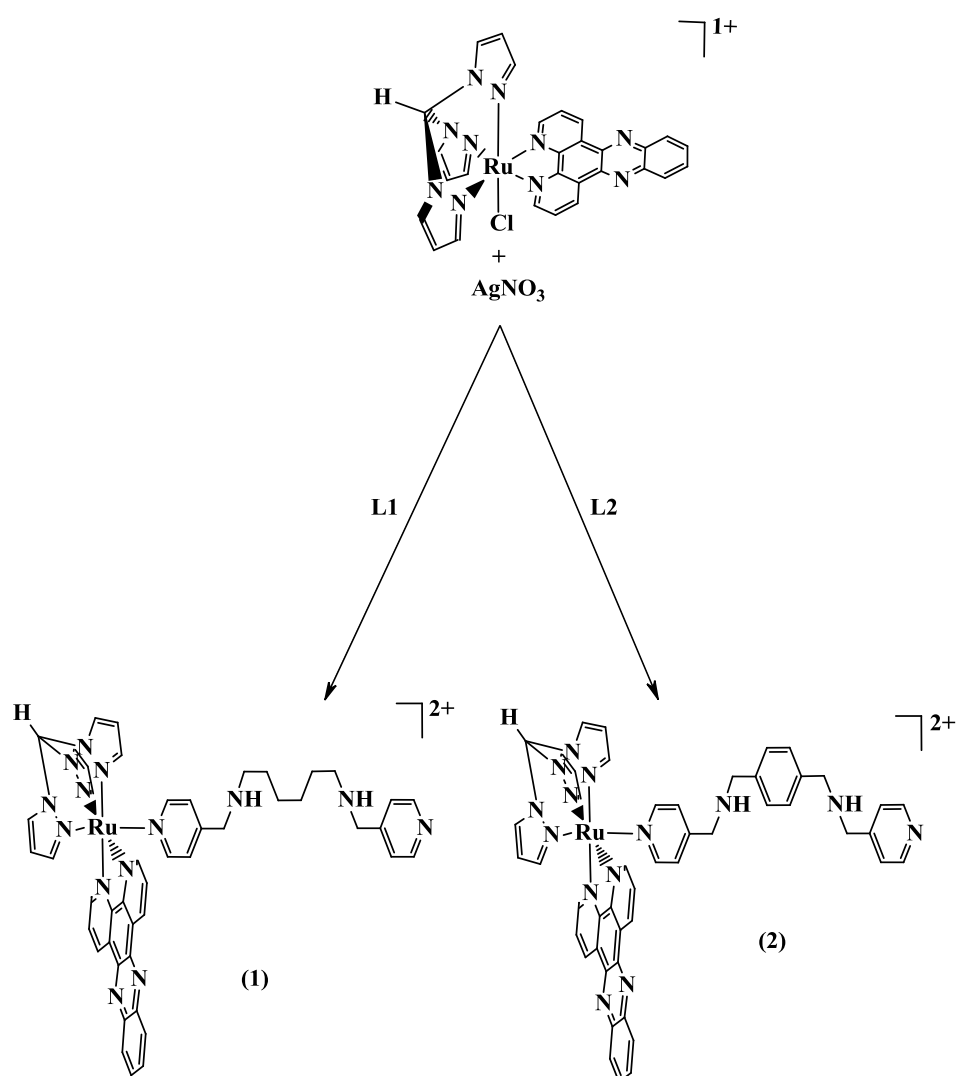


**Figure 2.4:** Synthesis of complexes [1] and [2]

### 2.2.2.2 Bimetallic complexes

$\{[\text{Ru}(\text{tpm})(\text{dppz})]_2(\mu\text{-L1})\}(\text{PF}_6)_4$  [3],  $\{[\text{Ru}(\text{tpm})(\text{dppz})]_2(\mu\text{-L2})\}(\text{PF}_6)_4$  [4]. Both complexes [3] and [4] were synthesized in an identical procedure starting by refluxing  $[\text{Ru}(\text{tpm})(\text{dppz})\text{Cl}]^+$  in ethanol:water. Again,  $\text{AgNO}_3$  was added to remove the chlorido ligand. The filtered solution was then added to  $[(\text{tpm})\text{Ru}(\text{dppz})(\text{L1})](\text{PF}_6)_2$  or  $[(\text{tpm})\text{Ru}(\text{dppz})(\text{L2})](\text{PF}_6)_2$  in acetone and was refluxed for 3 days. The solution was then concentrated and purification was achieved via ion-exchange chromatography on Sephadex CM-25 resin eluting with water acetone mixtures (5:3) with increasing concentrations of  $\text{NaCl}$ . The fractions containing the product were concentrated and the product was precipitated by addition of  $\text{NH}_4\text{PF}_6$ .

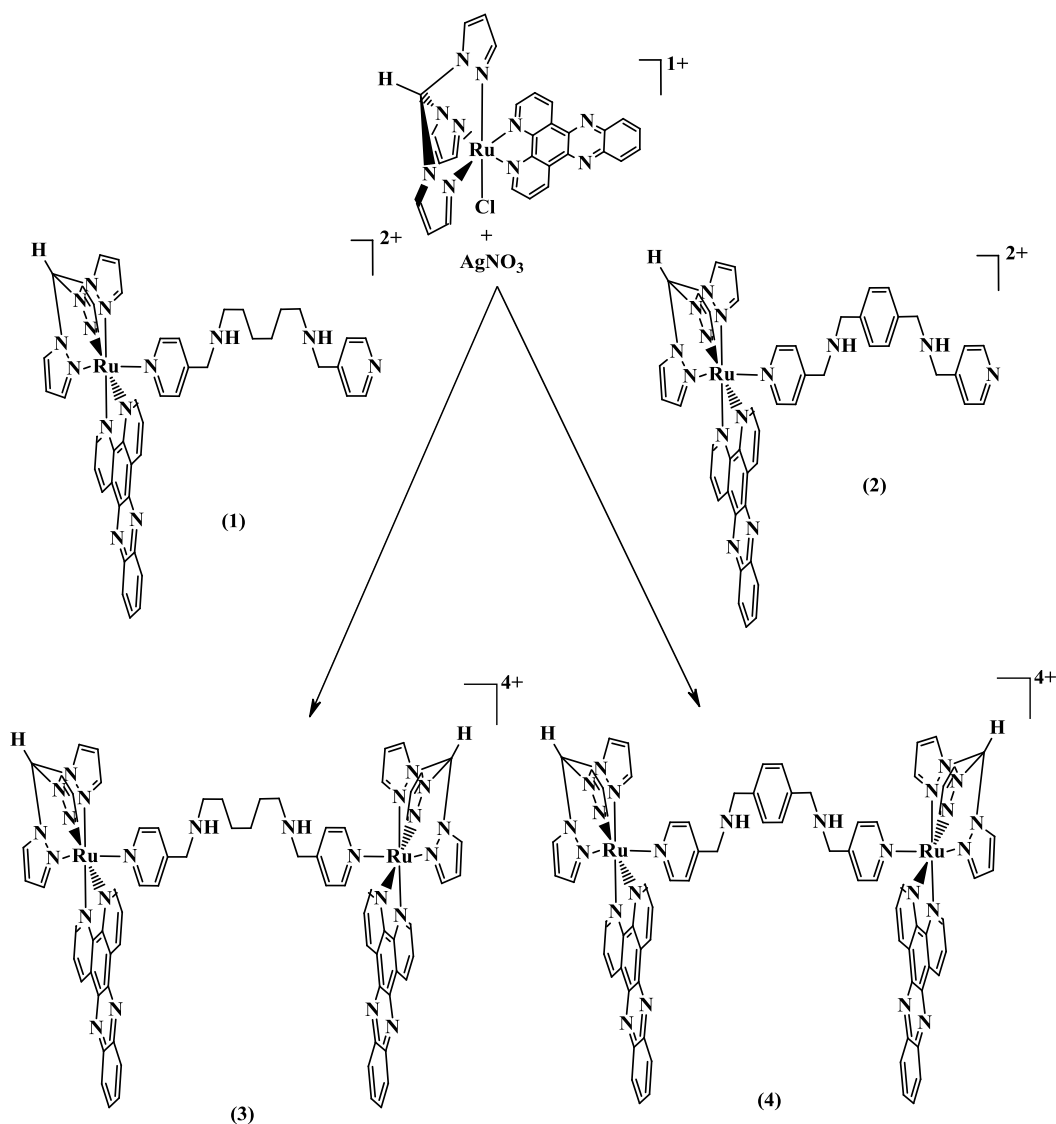


**Figure 2.5:** Synthesis of bimetallic complexes [3] and [4]

## 2.3 Characterization

### 2.3.2 Mass spectrometry data

Electrospray data recorded on an ES-TOF spectrometer for the complexes [1], [2], [3] and [4] are summarised in the table below. All of the complexes showed fragments in their mass spectrum that correspond to their proposed structures, commonly peaks were found that represented sequential loss of counter ions.

Compound	m/z	%	Assignment
(1) [Ru(tpm)(dppz)( $\mu$ -L1)][PF <sub>6</sub> ] <sub>2</sub>	1041.2716	100	[Ru(tpm)(dppz)( $\mu$ -L1)] <sup>+</sup> [PF <sub>6</sub> ]
(2) [Ru(tpm)(dppz)( $\mu$ -L2)][PF <sub>6</sub> ] <sub>2</sub>	1061.2435	100	[Ru(tpm)(dppz)( $\mu$ -L2)] <sup>+</sup> [PF <sub>6</sub> ]
(3) [{(tpm)Ru(dppz)} <sub>2</sub> ( $\mu$ -L1)][(PF <sub>6</sub> ) <sub>4</sub> ]	892.1607	100	[{(tpm)Ru(dppz)} <sub>2</sub> ( $\mu$ -L1)] <sup>2+</sup> [(PF <sub>6</sub> ) <sub>2</sub> ]
(4) [{(tpm)Ru(dppz)} <sub>2</sub> ( $\mu$ -L2)][(PF <sub>6</sub> ) <sub>4</sub> ]	901.76	100	[{(tpm)Ru(dppz)} <sub>2</sub> ( $\mu$ -L2)] <sup>2+</sup> [(PF <sub>6</sub> ) <sub>2</sub> ]

**Table 2.1:** Mass spectrum data for the complexes [1], [2], [3] and [4] as PF<sub>6</sub> salts.

### 2.3.3 Photophysical studies

UV-visible absorption spectra of [1-4] were recorded at room temperature in water (as chloride salts) and acetonitrile (as hexafluorophosphate salts). The UV-visible absorption spectra of [1-4] in acetonitrile are shown in **Figure 2.6** and the data is summarised in **Table 2.3**.

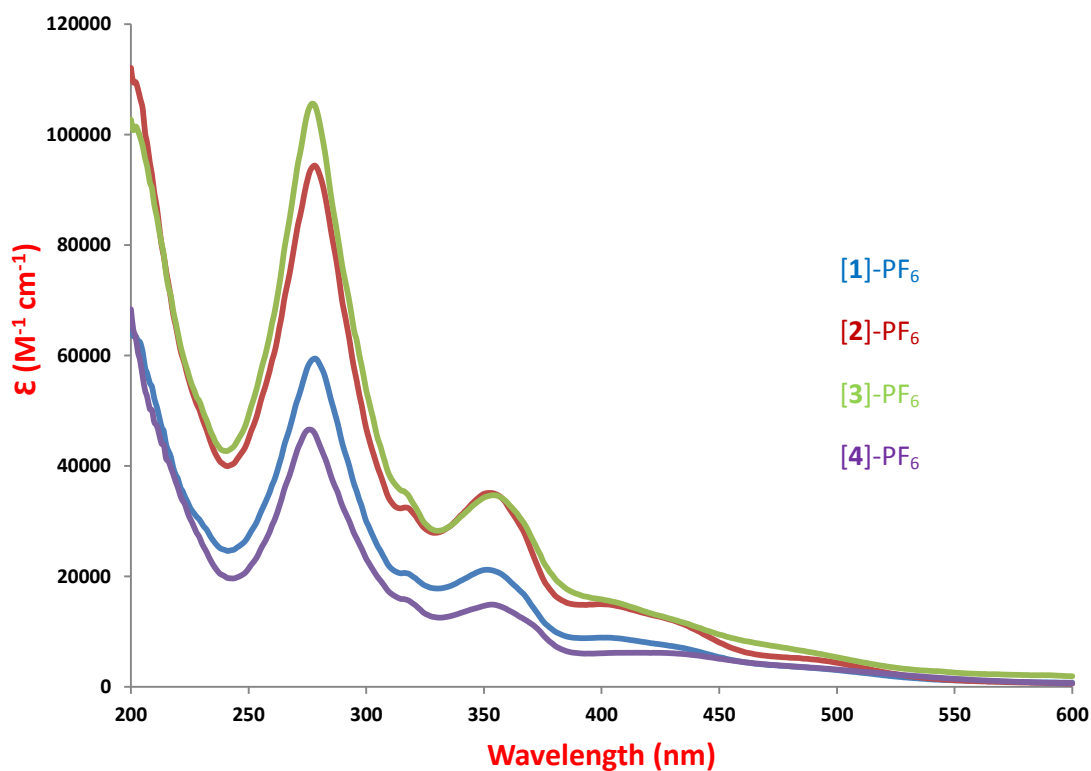


**Figure 2.6:** UV-Visible absorption spectra for the complexes **[1]**, **[2]**, **[3]** and **[4]** as PF<sub>6</sub> salts in acetonitrile at room temperature

These UV–Visible spectra are dominated by high-energy bands between 270–300 nm which correspond to  $\pi \rightarrow \pi^*$  transitions of the aromatic nitrogen donor ligands. The corresponding spectrum of free dppz in acetonitrile exhibits a moderately intense band in the near-UV with two principle maxima at  $\lambda = 358$  and  $376$  nm, which are characteristic of  $\pi \rightarrow \pi^*$ (dppz) transitions.<sup>8</sup> Consequently, the moderately intense bands in the near-UV regions for complexes **1** (351nm), **2** (350 nm), **3** (355 and 368 nm) and **4** (352 and 395 nm) are assigned to analogous transitions.

Compound	Absorption		Assignment
	$\lambda_{\max}$ (nm)	$10^{-3} \epsilon$ ( $M^{-1}cm^{-1}$ )	
(1) [Ru(tpm)(dppz)( $\mu$ -L1)][PF <sub>6</sub> ] <sub>2</sub>	278	59.4	$\pi \rightarrow \pi^*$
	317	20.5	$\pi \rightarrow \pi^*$
	351	21.2	$\pi \rightarrow \pi^*$
	401	8.9	$\pi \rightarrow \pi^*$
	431	6.0	MLCT
	494	3.3	MLCT
(2) [Ru(tpm)(dppz)( $\mu$ -L2)][PF <sub>6</sub> ] <sub>2</sub>	278	94.4	$\pi \rightarrow \pi^*$
	317	33.9	$\pi \rightarrow \pi^*$
	350	34.4	$\pi \rightarrow \pi^*$
	401	15.6	$\pi \rightarrow \pi^*$
	431	12.0	MLCT
	491	3.4	MLCT
(3) [{(tpm)Ru(dppz)} <sub>2</sub> ( $\mu$ -L1)][(PF <sub>6</sub> ) <sub>4</sub> ]	276	105.6	$\pi \rightarrow \pi^*$
	318	33.9	$\pi \rightarrow \pi^*$
	355	34.6	$\pi \rightarrow \pi^*$
	402	15.6	$\pi \rightarrow \pi^*$
	486	6.5	MLCT
(4) [{(tpm)Ru(dppz)} <sub>2</sub> ( $\mu$ -L2)][(PF <sub>6</sub> ) <sub>4</sub> ]	276	46.4	$\pi \rightarrow \pi^*$
	318	15.6	$\pi \rightarrow \pi^*$
	352	14.9	$\pi \rightarrow \pi^*$
	405	6.1	$\pi \rightarrow \pi^*$
	483	3.57	MLCT

**Table 2.2:** UV-Visible data for the complexes [1], [2], [3] and [4] as PF<sub>6</sub> salts recorded in acetonitrile.

The MLCT Ru( $d\pi$ ) $\rightarrow$ dppz( $\pi^*$ ) <sup>1</sup>MLCT bands for **1–4** all appear in the region of the spectrum typical for ruthenium(II) complexes with coordinated polyimine ligands. Excitation into the MLCT band of complexes **1–4** in acetonitrile solutions results in characteristic broad and unstructured emission originating from the Ru( $d\pi$ ) $\rightarrow$ dppz( $\pi^*$ ) <sup>3</sup>MLCT manifold, see **Table 2.3**.

Complex	Counterion	solvent	$\lambda_{\text{ex}}/ \text{nm}$	$\lambda_{\text{em}}/ \text{nm}$
(1) [Ru(tpm)(dppz)( $\mu$ -L1)][PF <sub>6</sub> ] <sub>2</sub>	[PF <sub>6</sub> ]	Acetonitrile	429	661
(2) [Ru(tpm)(dppz)( $\mu$ -L2)][PF <sub>6</sub> ] <sub>2</sub>	[PF <sub>6</sub> ]	Acetonitrile	430	659
(3) [Ru(tpm)Ru(dppz) <sub>2</sub> ( $\mu$ -L1)][PF <sub>6</sub> ] <sub>4</sub>	[PF <sub>6</sub> ]	Acetonitrile	431	641
(4) [Ru(tpm)Ru(dppz) <sub>2</sub> ( $\mu$ -L2)][PF <sub>6</sub> ] <sub>4</sub>	[PF <sub>6</sub> ]	Acetonitrile	439	661

**Table 2.3:** Emission data for the complexes [1], [2], [3] and [4], where  $\lambda_{\text{ex}}$  = excitation wavelength,  $\lambda_{\text{em}}$  = emission wavelength.

The corresponding absorbances for these complexes as chloride salts in water are also summarised below in **table 2.4**. The spectra for these complexes chloride look very similar to one another.

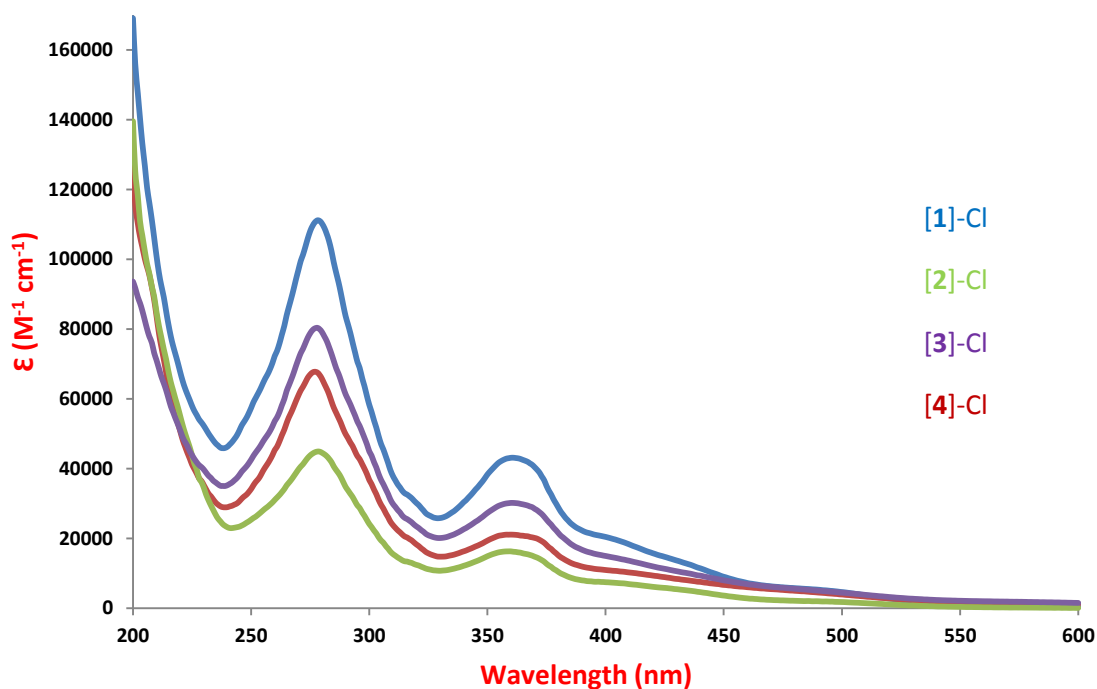


**Figure 2.7:** UV-Visible absorption spectra for the complexes [1], [2], [3] and [4] as Chloride salts in in 5 mM tris buffer, 25 mM NaCl, pH 7.4 at room temperature.

Compound	Absorption		Assignment
	$\lambda_{\max}$ (nm)	$10^{-3}\epsilon$ ( $M^{-1}cm^{-1}$ )	
(1) [Ru(tpm)(dppz)( $\mu$ -L1)]Cl <sub>2</sub>	279	110.3	$\pi \rightarrow \pi^*$
	318	30.8	$\pi \rightarrow \pi^*$
	359	43.1	$\pi \rightarrow \pi^*$
	402	20.1	$\pi \rightarrow \pi^*$
	431	13.5	MLCT
	495	4.7	MLCT
(2) [Ru(tpm)(dppz)( $\mu$ -L2)]Cl <sub>2</sub>	278	44.9	$\pi \rightarrow \pi^*$
	317	13.1	$\pi \rightarrow \pi^*$
	356	16.1	$\pi \rightarrow \pi^*$
	402	7.4	$\pi \rightarrow \pi^*$
	431	5.3	MLCT
	491	1.9	MLCT
(3) [{(tpm)Ru(dppz)} <sub>2</sub> ( $\mu$ -L1)]Cl <sub>4</sub>	278	80.3	$\pi \rightarrow \pi^*$
	318	24.6	$\pi \rightarrow \pi^*$
	358	30.1	$\pi \rightarrow \pi^*$
	402	14.7	$\pi \rightarrow \pi^*$
	488	5.1	MLCT
(4) [{(tpm)Ru(dppz)} <sub>2</sub> ( $\mu$ -L2)]Cl <sub>4</sub>	276	67.8	$\pi \rightarrow \pi^*$
	318	19.4	$\pi \rightarrow \pi^*$
	358	21.1	$\pi \rightarrow \pi^*$
	409	10.3	$\pi \rightarrow \pi^*$
	488	5.1	MLCT

**Table 2.4:** UV-Visible data for the complexes [1], [2], [3] and [4] as chloride salts recorded in 5mM tris buffer, 25 mM NaCl, pH 7.4 at 25 °C.

### 2.3.4 DNA Binding Studies

The well-defined spectroscopic characteristics of a metal complex often change when they interact with DNA. This is because the complex is subjected to a change in local microenvironment from being completely solvated in aqueous solution to being in the hydrophobic environment of a DNA helix; either within the grooves or between base stacks. This change in local microenvironment can be observed in the UV-Visible spectrum of the complex. During the binding process, the central metal ion and the aromatic ligands come into close proximity to the poly-anionic backbone of the DNA and the hydrophobic interior of the DNA grooves. This causes alterations in the metal centred MLCT band and the ligand centred  $\pi \rightarrow \pi^*$  bands of the UV-Visible spectrum of the complexes<sup>9,10,11</sup>. These shifts are often to a longer wavelength (bathochromic shift) and are frequently accompanied by absorption decreases (hypochromic shift) indicating that, upon binding to DNA, the energy of the transition has been altered by stabilisation or destabilisation of the HOMO/LUMO orbitals involved in the transitions.<sup>11</sup>

Excited state luminescence emission spectra of the complex are also often sensitive to local environment. Water molecules can act as excited states quenchers, specifically where they can form hydrogen bonds to nitrogen donor sites on the complexes. Upon binding to DNA the ligand based nitrogen donor sites are protected from the aqueous solvent by the hydrophobic interior of the grooves and the base stack. As a result the excited state of the complex can change significantly, resulting in large changes in emission.<sup>3</sup>

In this study all of the metal complexes exhibit well-defined UV-visible spectra in both lipophilic and aqueous environments. Therefore, the change in the absorption and emission properties of the metal complexes can be used as a spectroscopic tool to study the binding interactions of the metal complexes with DNA.

The degree of shift in any given band from the titration of known concentration of drug with DNA in UV-Visible spectrum or the luminescence spectrum is proportional to the fraction of drug bound to the DNA. For hypochromic shifts in the UV-Visible spectrum, the fraction bound of complex ( $\chi$ ) to DNA is estimated from the equation:

$$\chi = \frac{A_f - A_{obs}}{A_f - A_b}$$

**Equation 2.1**

Where  $A_f$  is the absorption of the free unbound drug,  $A_b$  is the absorption of the fully bound drug  $x$  and  $A_{obs}$  is the absorption at a given point. Similarly for luminescence titrations where the emission intensity of the drugs increases upon binding to DNA the fraction bound is given by:

$$\chi = \frac{I_{obs} - I_f}{I_b - I_f} \quad \text{Equation 2.2}$$

Where  $I_{obs}$ ,  $I_f$  and  $I_b$  are the emission intensities of the observed, free unbound and fully bound complex respectively.

If  $\chi$  is plotted against the ratio of the DNA concentration to drug concentration ( $[DNA]/[Drug]$ ), also called the mixing ratio (R) then a saturation curve can be constructed.

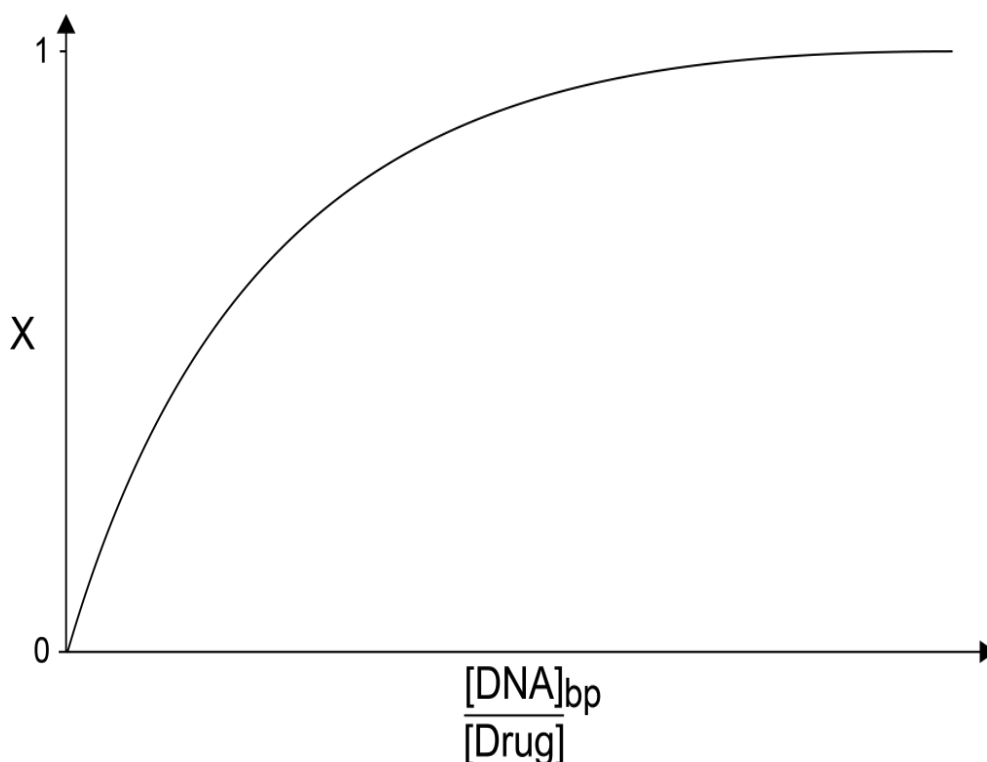


**Figure 2.8:** Schematic of a binding showing saturation binding

The concentration of bound drug ( $C_b$ ) can be easily calculated at any given time from knowing the initial concentration of complex ( $C_i$ ) and the fraction bound ( $\chi$ ).

$$C_b = \chi \cdot C_i$$

**Equation 2.3**

$C_f$  is the concentration of free drug, then

$$C_i = C_f + C_b$$

**Equation 2.4**

Rearranging equation 2.4 to make  $C_f$  the subject gives the following equation.

$$C_f = C_i - C_b$$

**Equation 2.5**

Finding the concentrations of free unbound and bound drug at any given time allows the binding ratio ( $r$ ), which is described as the ratio of bound complex to total concentration of DNA to be determined.

$$r = \frac{C_b}{[DNA]}$$

**Equation 2.6**

By plotting  $r/C_f$  vs.  $r$  from the Scatchard equation shown below, the intrinsic equilibrium binding constant ( $K_i$ ) and the number of DNA binding sites occupied by the bound complex ( $n$ ) can be found.

$$\frac{r}{C_f} = K_i(n - r)$$

**Equation 2.7**

The Scatchard model was developed for the binding of small ligands to non-interacting isolated binding sites on proteins;<sup>12</sup> although it works well for simple systems with 1:1 binding solutions, in more complicated systems, where data is no longer linear, the plot  $r/C_f$  vs.  $r$  quickly begins to show weaknesses. To fit the data more accurately a more complicated plot can be used (**Equation 2.8**). This is done so using the McGhee Von Hippel model<sup>13</sup> which makes a number of assumptions; essentially it takes into account overlapping binding sites which the Scatchard Model did not.

$$\frac{r}{C_f} = K \cdot (1 - nr) \cdot \left[ \frac{(1 - nr)}{1 - (n - 1)r} \right]^{n-1}$$

**Equation 2.8**

As the binding reaches saturation, the numbers of free binding sites remaining require a significant increase in effective concentration of complex to bind.<sup>14</sup> This has a significant effect on the data and artificially increases the observed binding constant. The model is fitted to experimental data between 30% and 90% bound drugs to minimise these artificial effects.

### 2.3.5 UV-Visible titrations

The interaction of [1]Cl<sub>2</sub>, [2]Cl<sub>2</sub>, [3]Cl<sub>4</sub> and [4]Cl<sub>4</sub> with CT-DNA in aqueous buffer (25 mM NaCl, 5 mM tris, pH 7.0) was investigated using UV–visible and emission spectroscopic titrations. Addition of CT-DNA to a solution of any of the complexes results in characteristically large hypochromicity in both MLCT and  $\pi \rightarrow \pi^*$  absorption bands due to the changes in the local microenvironments of the metal complexes.

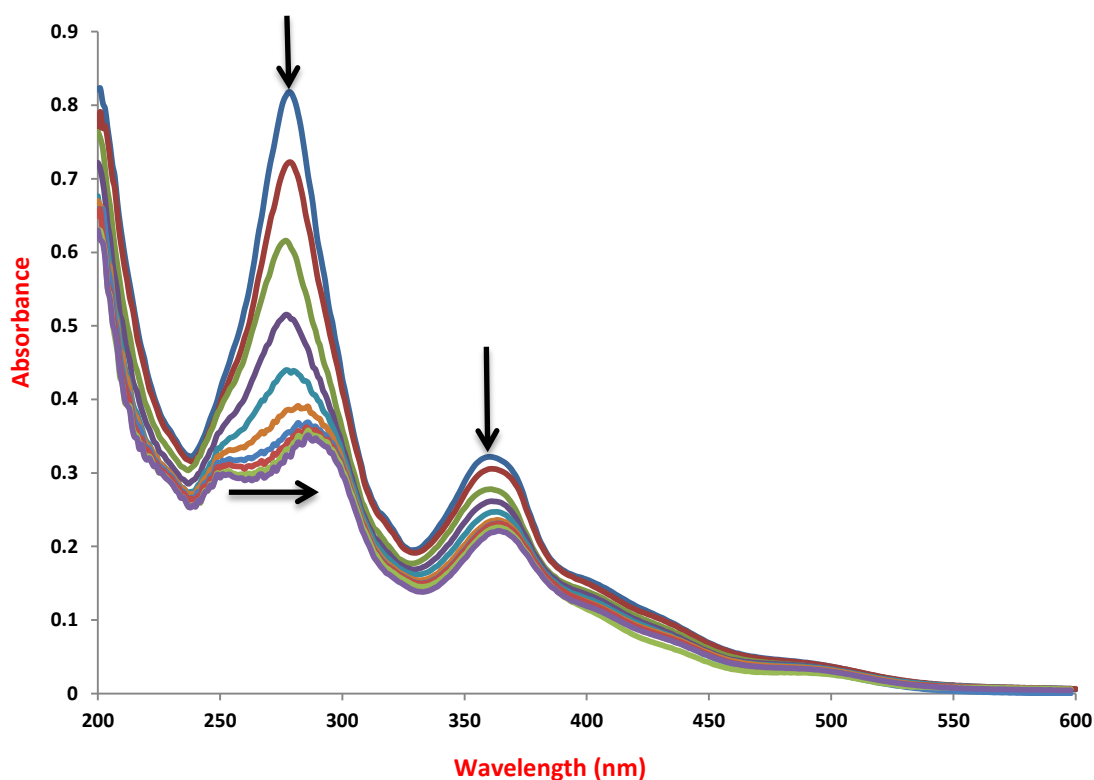


**Figure 2.9:** UV-Visible titration of 1.00 mM bp<sup>-1</sup> CT-DNA into a solution of 15  $\mu$ M [Ru(tpm)(dppz)( $\mu$ -L1)]Cl<sub>2</sub> ([1]Cl<sub>2</sub>) in 5 mM tris buffer, 25 mM NaCl, pH 7.4 at 25 °C.

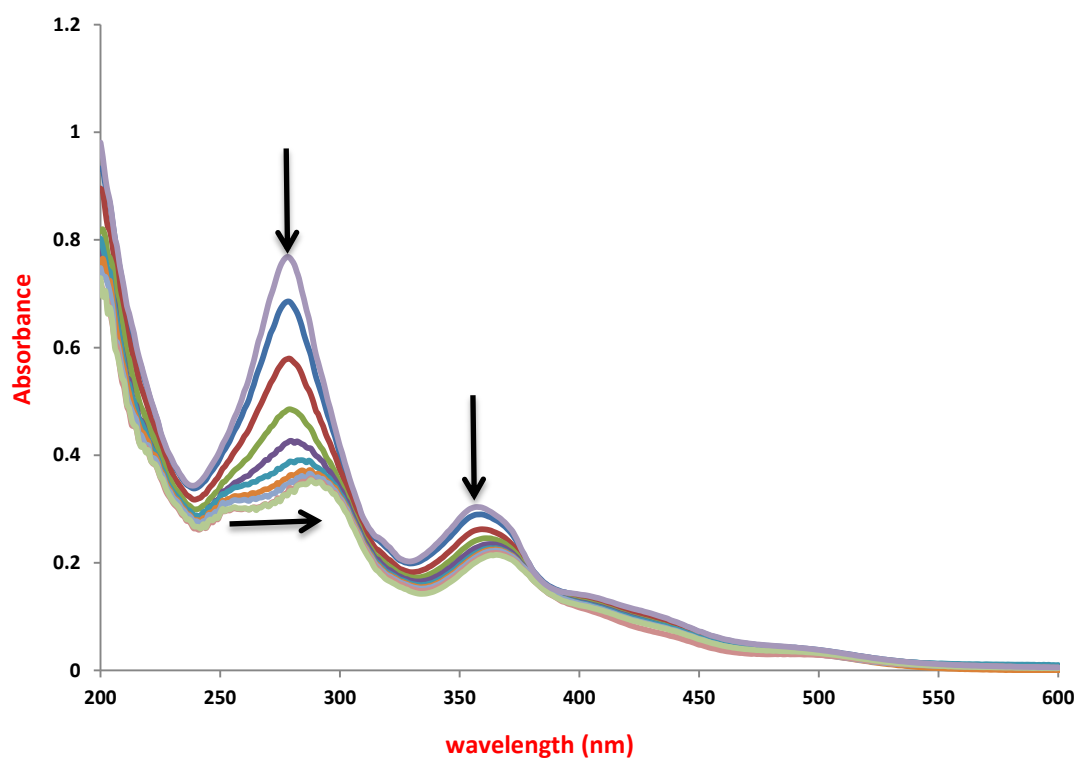


**Figure 2.10:** UV-Visible titration of 1.00 mM bp<sup>-1</sup> CT-DNA into a solution of 15 μM [Ru(tpm)(dppz)(μ-L2)]Cl<sub>2</sub> (**[2]**Cl<sub>2</sub>) in 5 mM tris buffer, 25 mM NaCl, pH 7.4 at 25 °C.

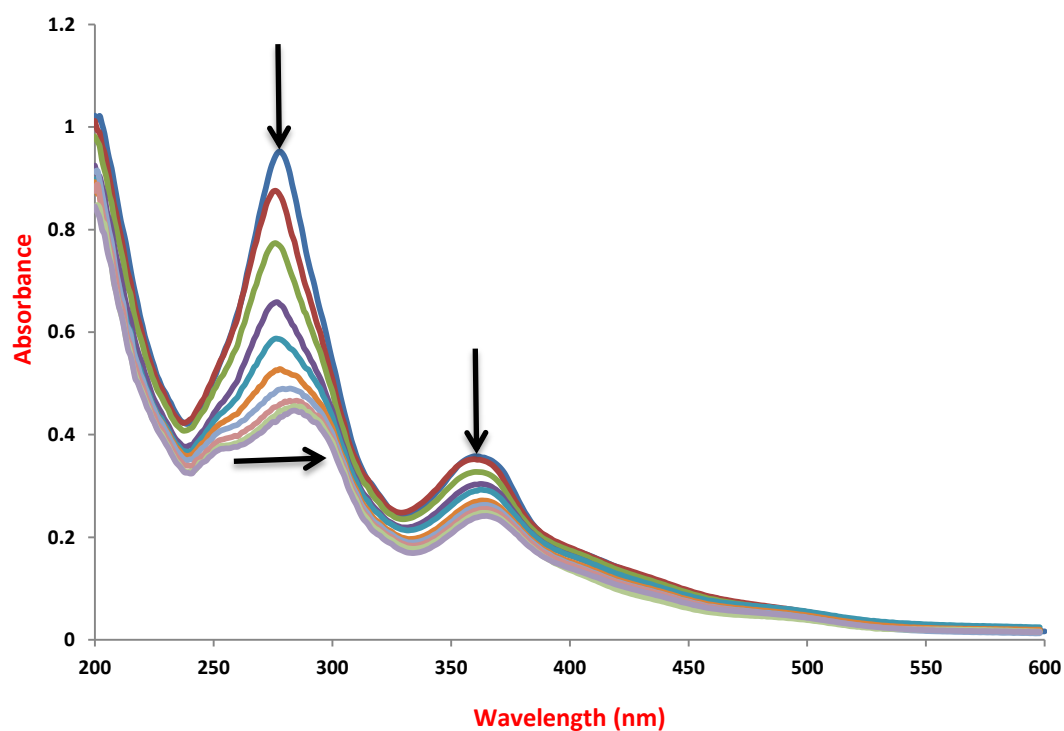


**Figure 2.11:** UV-Visible titration of 1.00 mM bp<sup>-1</sup> CT-DNA into a solution of 15 μM [{(tpm)Ru(dppz)}<sub>2</sub>(μ-L1)]Cl<sub>4</sub> (**[3]**Cl<sub>4</sub>) in 5 mM tris buffer, 25 mM NaCl, pH 7.4 at 25 °C.

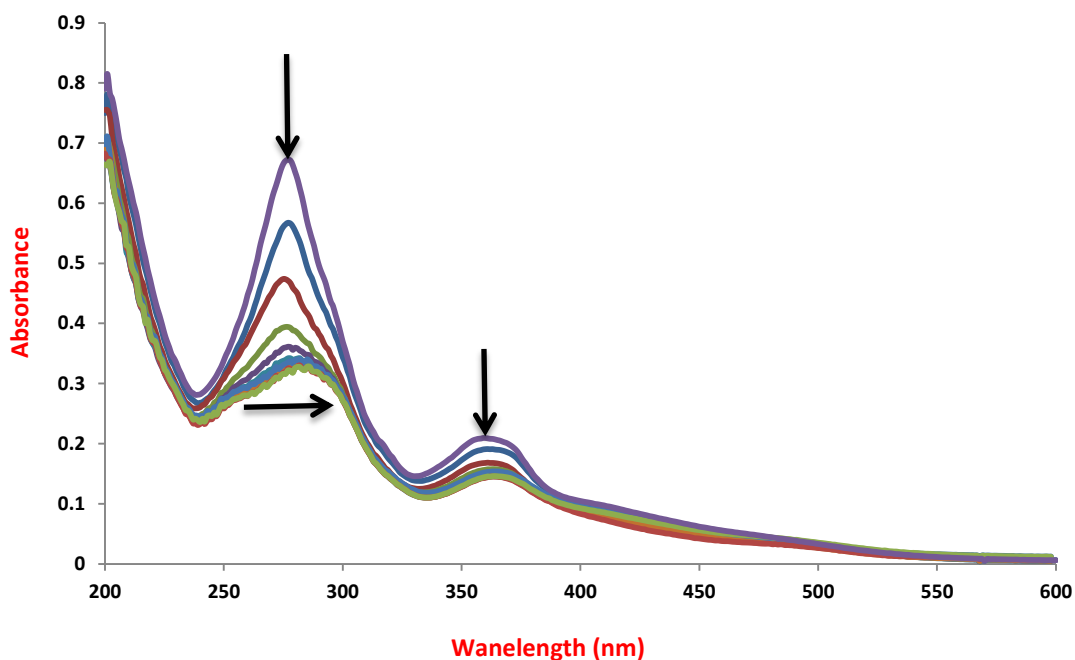


**Figure 2.12:** UV-Visible titration of 1.00 mM bp<sup>-1</sup> CT-DNA into a solution of 15 μM [(tpm)Ru(dppz)<sub>2</sub>(μ-L2)]Cl<sub>4</sub> ([4]Cl<sub>4</sub>) in 5 mM tris buffer, 25 mM NaCl, pH 7.4 at 25 °C.

The bands at ~277 nm and ~359 nm in all complexes show hypochromicity as CT-DNA is titrated into the complex solution. The hypochromicity has usually been ascribed to the interaction between the electronic states of the compound and those of the DNA bases.<sup>15</sup> A bathochromic shift, characteristic of intercalation<sup>16</sup> is seen at ~277 nm as the band moves towards ~292 nm. The red shift has been linked with the decrease in the energy gap between the HOMO and LUMO molecular orbitals after binding of the complex to DNA.<sup>17</sup>

The saturation binding curves obtained from the titrations are shown in **(Figure 2.13)**.

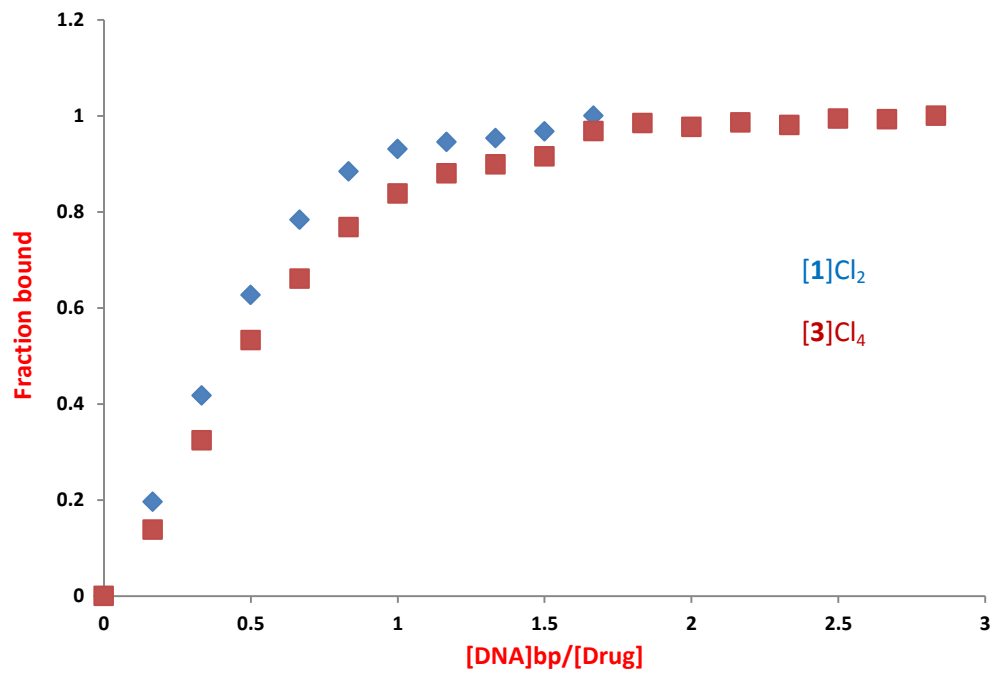


**Figure 2.13:** Binding curves obtained from the UV-Vis titrations of [1]Cl<sub>2</sub> and [3]Cl<sub>4</sub> binding to CT-DNA

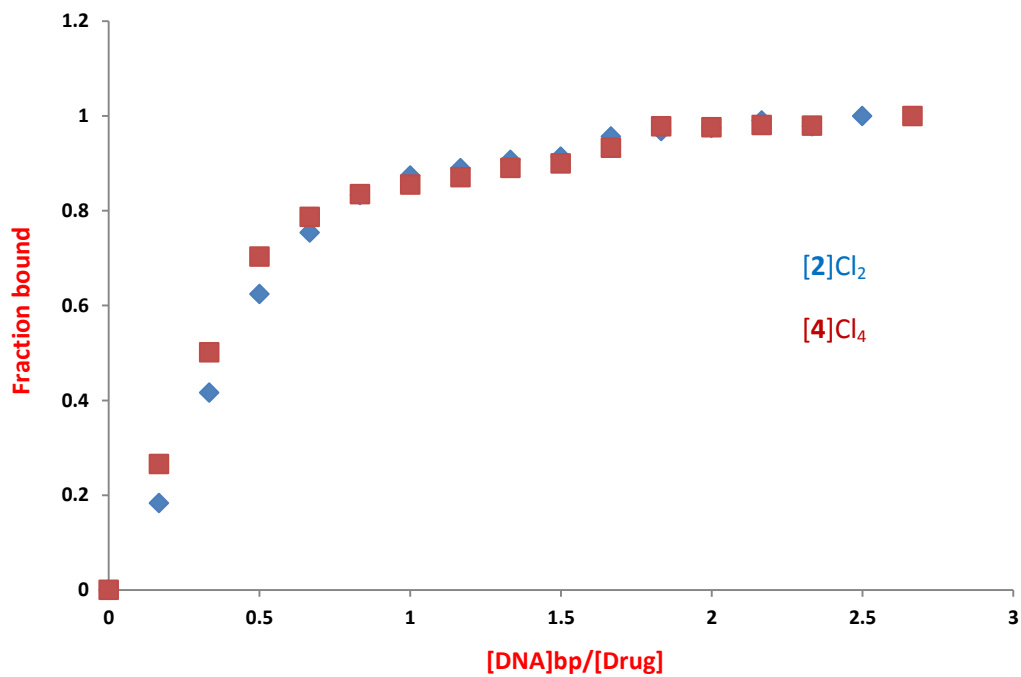


**Figure 2.13:** Binding curves obtained from the UV-Vis titrations of [2]Cl<sub>2</sub> and [4]Cl<sub>4</sub> binding to CT-DNA

To study further the interaction of complexes **1-4** with DNA and to explain the different photophysical responses of the molecules, emission titrations have also been carried out with the CT-DNA.

### 2.3.6 Luminescence emission titrations

Luminescence titrations for all the complexes were carried out using similar procedure to the UV-Vis titrations. All of the complexes display virtually no emission in tris buffer. Addition of CT-DNA into the complexes resulted in significant enhancements of the  $^3\text{MLCT}$  luminescence emission for each complex, indicating that all the complexes are behaving as DNA light switch systems.

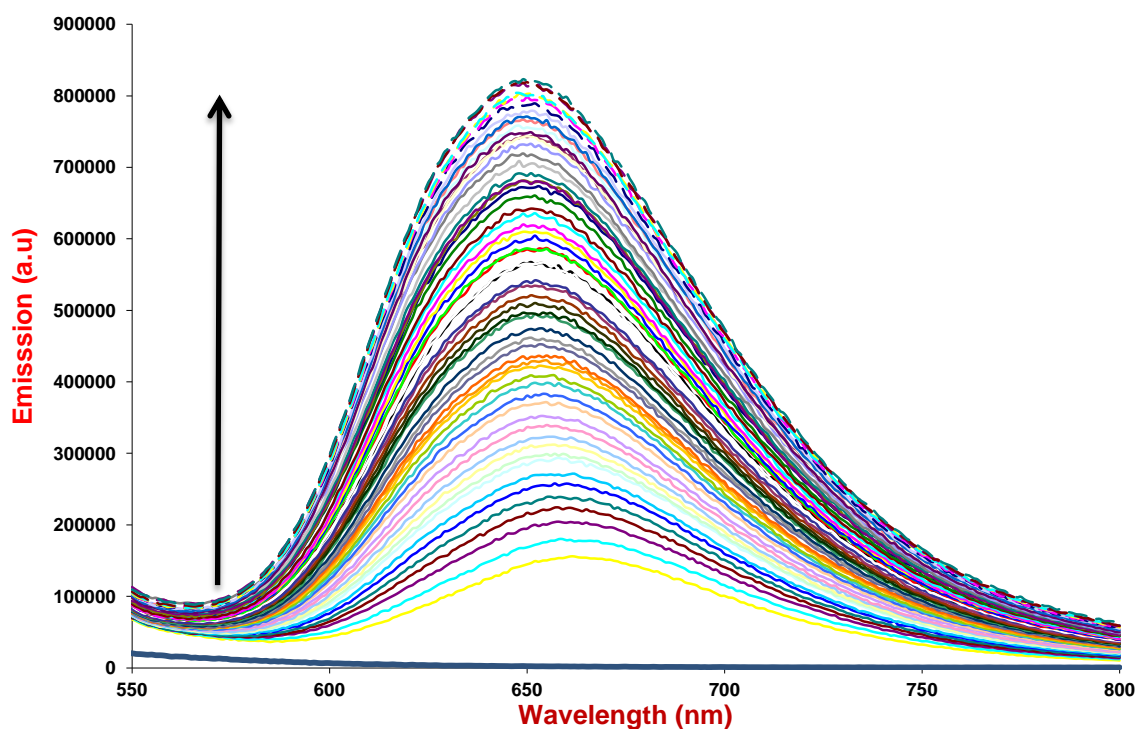


**Figure 2.14:** Luminescence titration of  $151 \mu\text{M bp}^{-1}$  CT-DNA into a solution of  $15 \mu\text{M [1]Cl}_2$  in 5 mM tris buffer, 25 mM NaCl, pH 7.4 at 25 °C.  $\lambda_{\text{ex}} = 420 \text{ nm}$ .

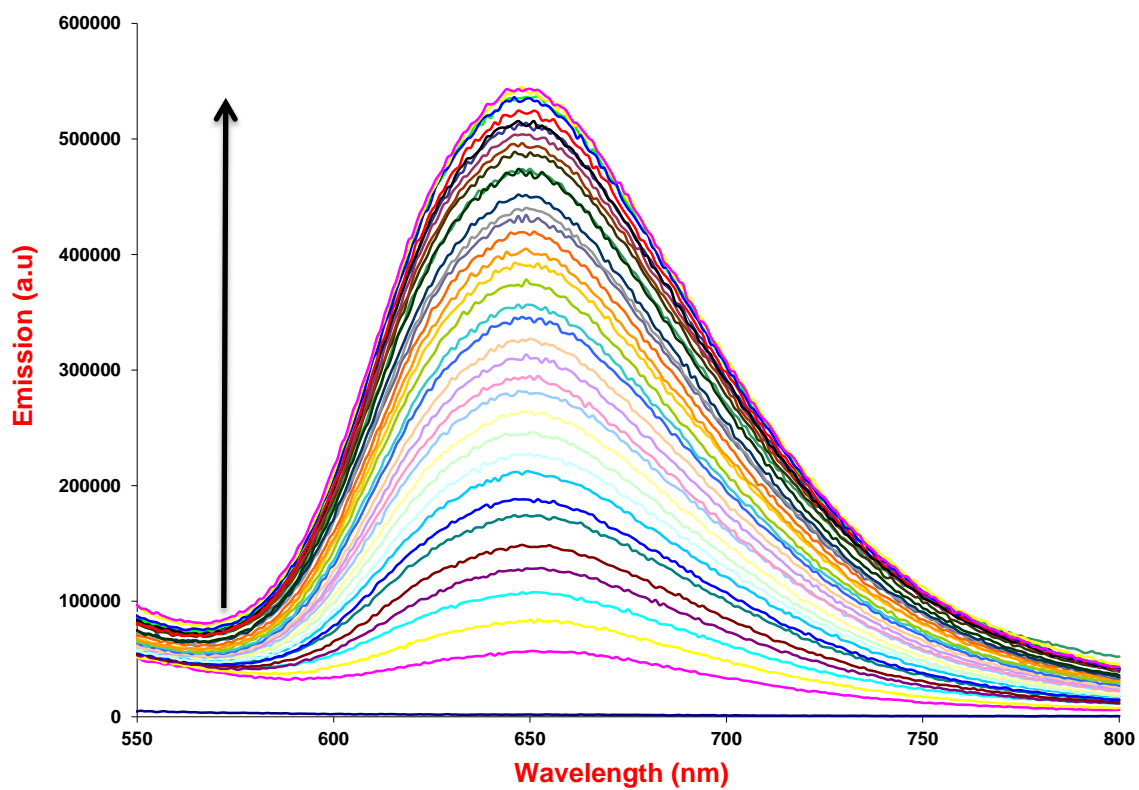


**Figure 2.15:** Luminescence titration of  $151 \mu\text{M bp}^{-1}$  CT-DNA into a solution of  $15 \mu\text{M [2]Cl}_2$  in 5 mM tris buffer, 25 mM NaCl, pH 7.4 at 25 °C.  $\lambda_{\text{ex}} = 430 \text{ nm}$ .

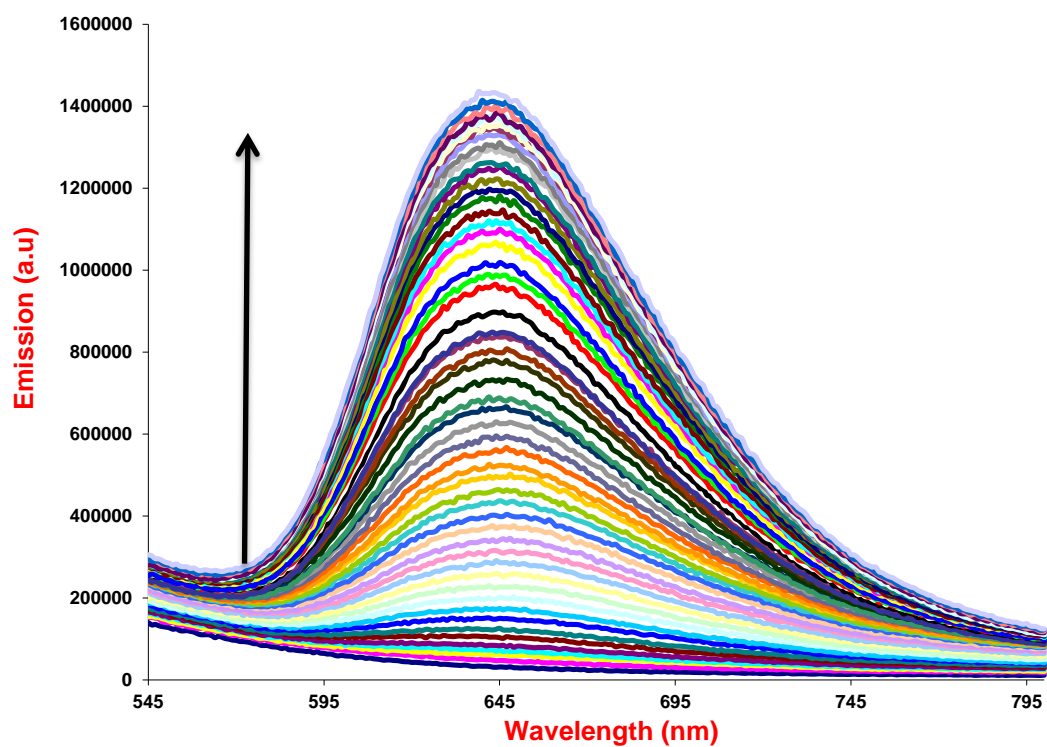


**Figure 2.16:** Luminescence titration of  $1.0 \text{ mM bp}^{-1}$  CT-DNA into a solution of  $15 \mu\text{M [3]Cl}_4$  in 5 mM tris buffer, 25 mM NaCl, pH 7.4 at 25 °C.  $\lambda_{\text{ex}} = 440 \text{ nm}$ .

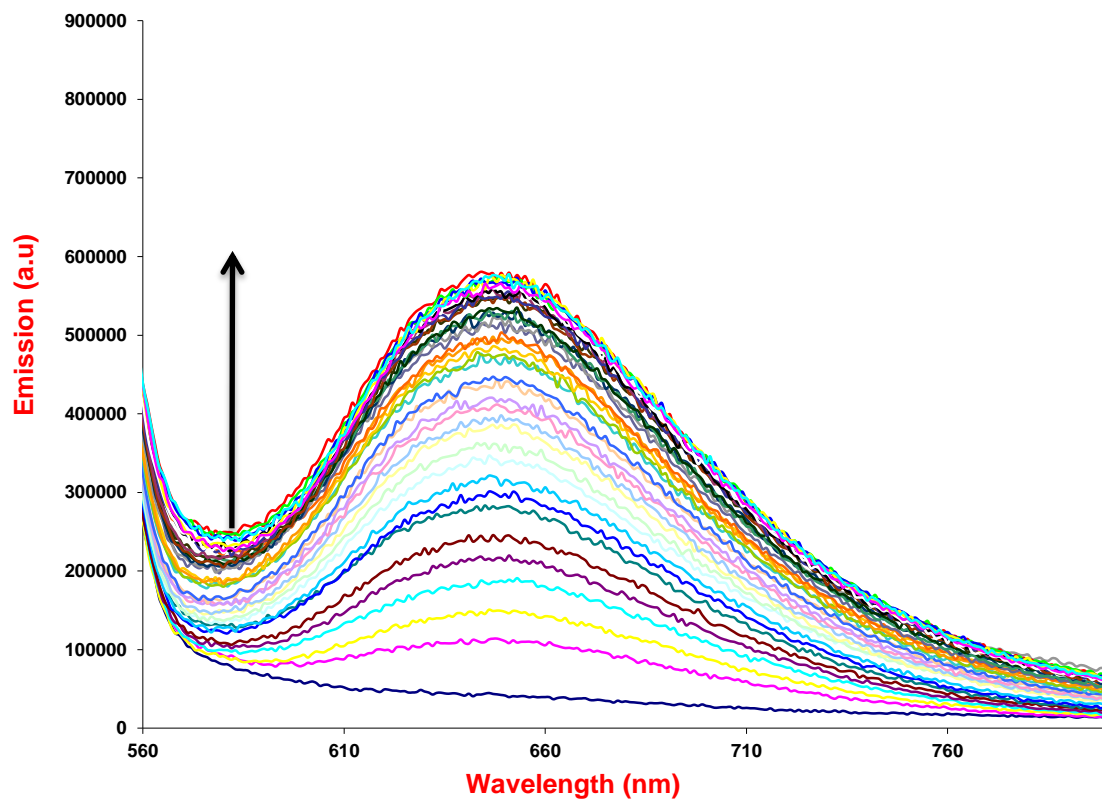


**Figure 2.17:** Luminescence titration of  $151 \mu\text{M bp}^{-1}$  CT-DNA into a solution of  $15 \mu\text{M [4]Cl}_4$  in 5 mM tris buffer, 25 mM NaCl, pH 7.4 at  $25^\circ\text{C}$ .  $\lambda_{\text{ex}} = 460 \text{ nm}$ .

The binding curve for the interactions of these complexes with CT-DNA shows that saturation binding has taken place.

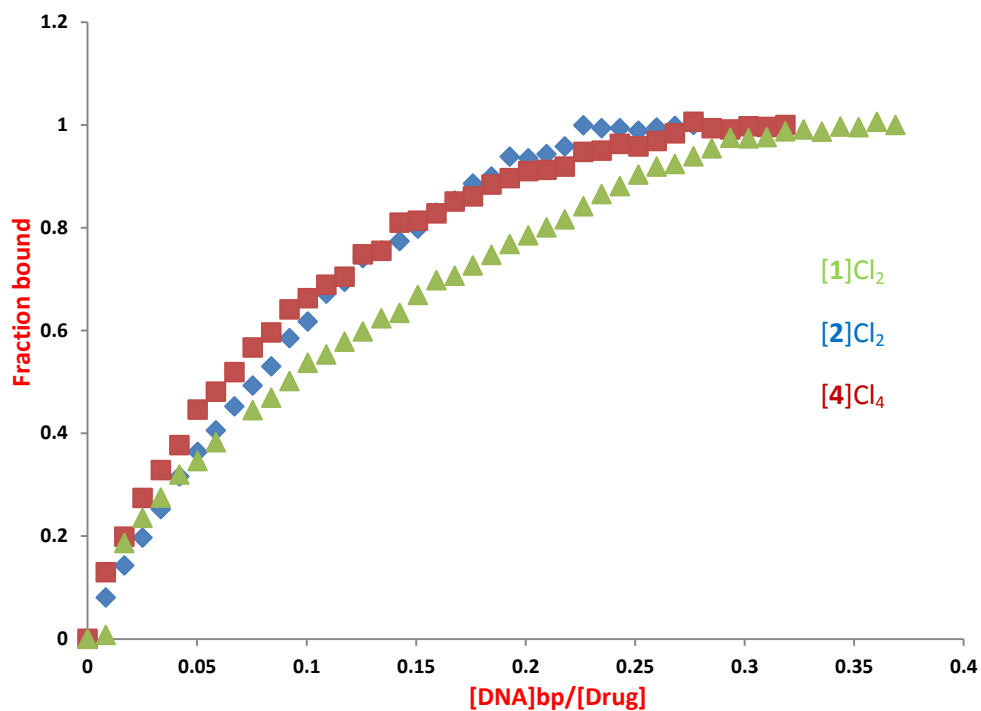


**Figure 2.18:** Binding curves obtained from the luminescence titrations of [1]Cl<sub>2</sub>, [2]Cl<sub>2</sub> and [4]Cl<sub>4</sub> binding to 151 μM CT-DNA, 25mM NaCl, 5mM Tris-HCl, pH 7.4, 25°C.

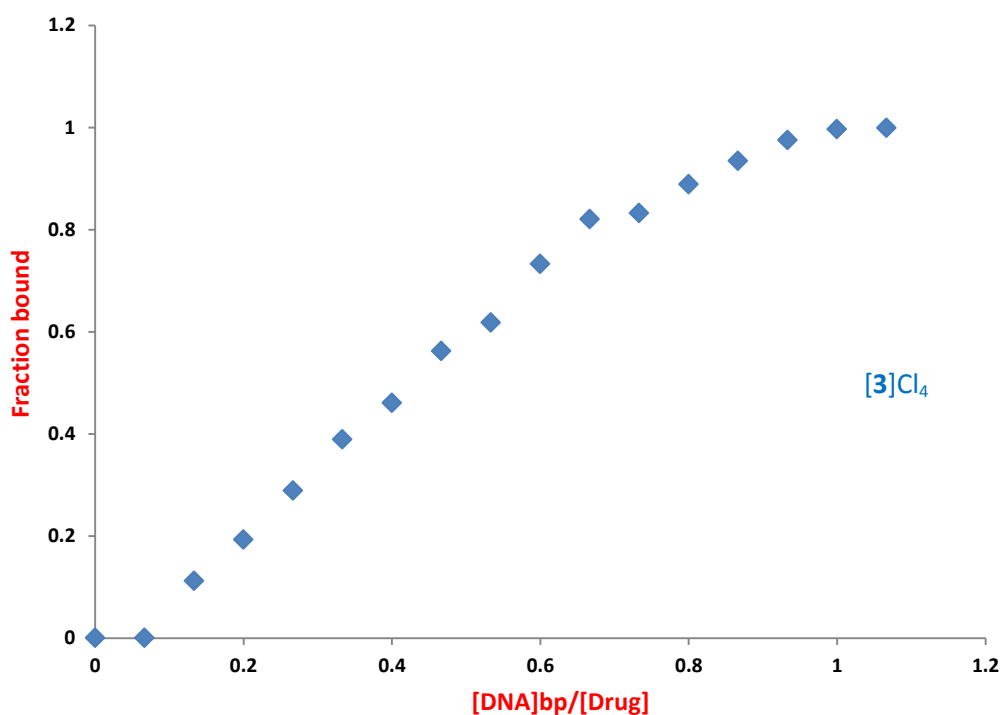


**Figure 2.19:** Binding curves obtained from the luminescence titrations of [3]Cl<sub>4</sub> binding to 1.00 mM CT-DNA, 25mM NaCl, 5mM Tris-HCl, pH 7.4, 25°C.

Attempts to fit the binding data for the luminescence and absorption titrations to the McGhee Von Hippel model were unsuccessful. It may be that these complexes bind to DNA very strongly preventing fits to the model or that in these conditions there is more than one binding mode. For whatever reason, attempts to fit these titrations to the model produced unfeasibly large complex:DNA binding ratios. To explore this issue, luminescence titrations at high salt concentration (200 mM NaCl) were carried out and as a result of this increase in ion strength; fits to the Scatchard plots for the complexes became possible. In these conditions, the monometallic complex [1]Cl<sub>2</sub> was found to have a very similar binding affinity compared to dinuclear complex [3]Cl<sub>4</sub>, indeed, within experimental error it is identical.

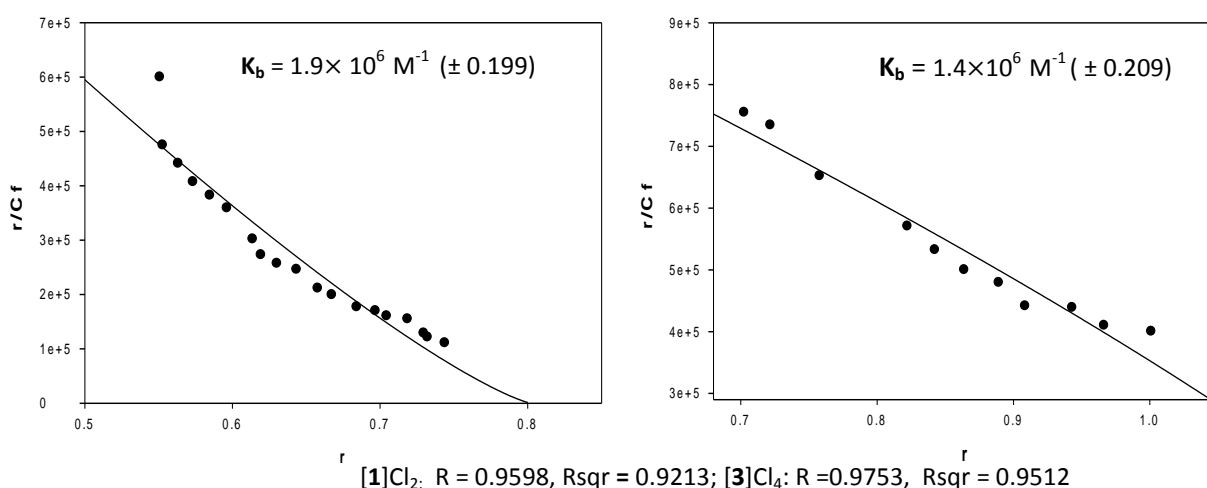


**Figure 2.20:** Scatchard plots for the complexes [1]Cl<sub>2</sub> (right) and [3]Cl<sub>4</sub> (left) obtained from the luminescence titration of CT-DNA in 5 mM tris buffer, 200 mM NaCl, pH 7.4. Data fitted using McGhee Von Hippel binding model.

In addition, as an alternative to McGhee Von Hippel binding model, using the absorption data at low NaCl concentration, the model first developed by Wolfe, *et al.* was used as well to estimate the binding constants  $K_b$  for the interaction of these complexes with CT-DNA. This model uses the changes of absorption with increasing concentration of DNA and the following equation<sup>18</sup> represents the relationship:

$$\frac{[DNA]}{(\epsilon_a - \epsilon_f)} = \frac{[DNA]}{(\epsilon_b - \epsilon_f)} + \frac{1}{K_b(\epsilon_b - \epsilon_f)}$$

Where  $[DNA]$  is the concentration of DNA,  $\varepsilon_a$ ,  $\varepsilon_f$  and  $\varepsilon_b$  corresponds to the apparent absorption coefficient  $A_{obs}/[complex]$ , the extinction coefficient for the free complex and the extinction coefficient for the complex in the fully bound form, respectively.

In plots of  $[DNA]/(\varepsilon_a - \varepsilon_f)$  versus  $[DNA]$  (**Figure 2.21 and 2.22**),  $K_b$  is given by the ratio of slope to the intercept and the data are shown in **Table 2.4**.

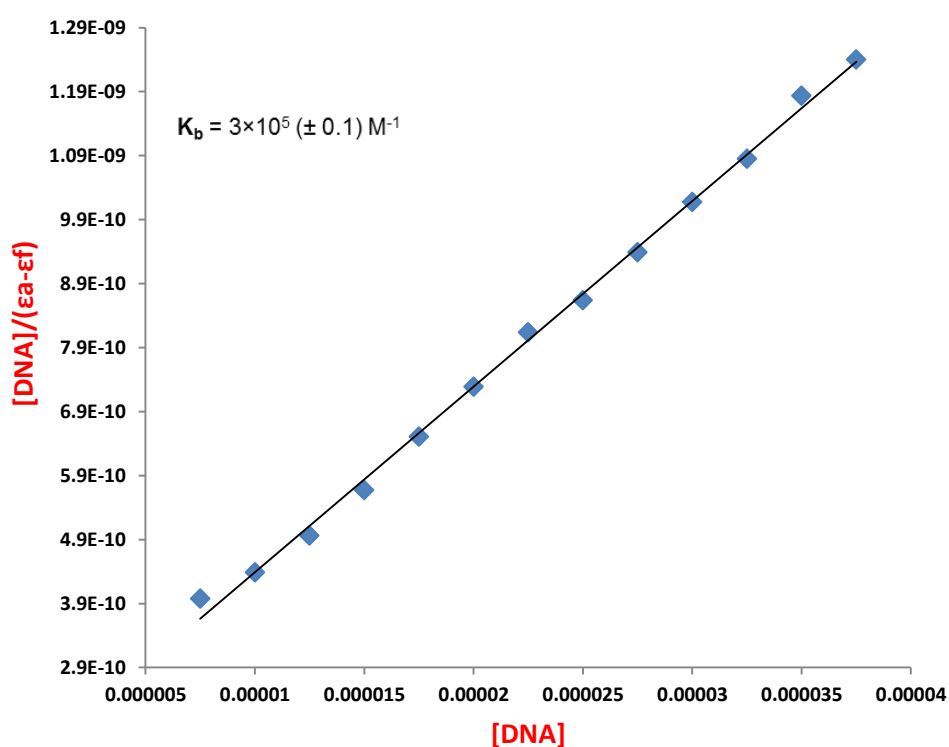


**Figure 2.21:** Scatchard plots for the complex  $[2]Cl_2$  obtained from the absorption spectroscopy of CT-DNA. Inserted plot,  $[DNA]/(\varepsilon_a - \varepsilon_f)$  versus  $[DNA]$  for the absorption titrations.

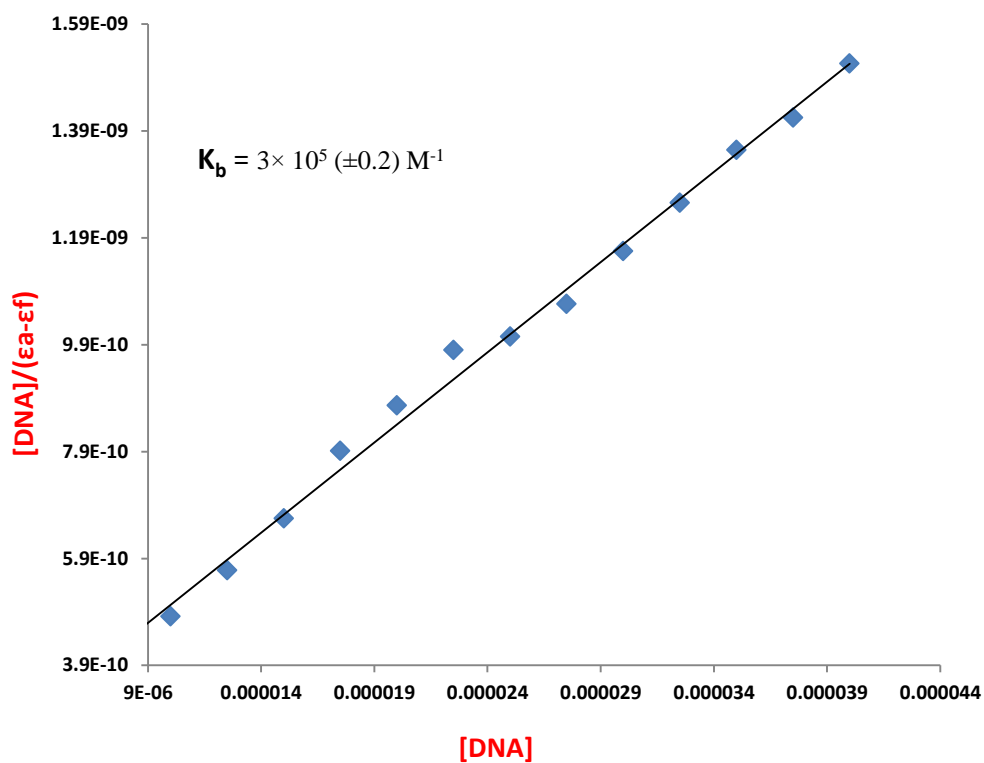


**Figure 2.22:** Scatchard plots for the complex [4]Cl<sub>4</sub> obtained from the absorption spectroscopy of CT-DNA. Inserted plot, [DNA]/(εa-εf) versus [DNA] for the absorption titrations.

Complex	$K_b$ ( $\text{M}^{-1}$ )
[1]Cl <sub>2</sub>	$2 \times 10^5 (\pm 0.2)$
[2]Cl <sub>2</sub>	$3 \times 10^5 (\pm 0.1)$
[3]Cl <sub>4</sub>	$2 \times 10^5 (\pm 0.1)$
[4]Cl <sub>4</sub>	$3 \times 10^5 (\pm 0.2)$

**Table 2.4:** Binding constants obtained by UV-Visible titrations of CT-DNA with complexes [1-4],  $K_b$  is Intrinsic binding constants.

Surprisingly the  $K_b$  value obtained using the simpler model and the UV-Visible titration data at 25 mM [NaCl] are an order of magnitude lower than those obtained from McGhee Von Hippel binding model for the luminescent studies on CT-DNA at 200 mM [NaCl]. This may be due to the different assumptions in the models or it may be that there are different binding modes when the dielectric of the solutions is changed. This is an issue that can be explored in more detail in the future.

In either case however, the trend in the data is similar, indicating that there is very little (if any) enhancement of binding affinity of bimetallic complexes [3] and [4] with respect to analogous monometallic complexes [1] and [2]. This result is interpreted by a consideration of the rigidity of the linker employed in the complex.

The observations of large hypochromicity in both MLCT and  $\pi \rightarrow \pi^*$  absorption bands and also the enhanced emission intensity upon addition of CT-DNA are all consistent with the interaction of a metallo-intercalator and DNA.<sup>19-23</sup> However these observations do not provide definitive proof of an intercalative DNA binding modes for [1]Cl<sub>2</sub>, [2]Cl<sub>2</sub>, [3]Cl<sub>4</sub> and [4]Cl<sub>4</sub>. One simple method for authoritatively distinguishing binding modes is the hydrodynamic method of viscometry.

### 2.3.7 Viscosity

Viscosity measurements afford a direct and sensitive method to confirm if a compound is a true intercalator, as an increase in the length of a DNA sequence will occur when base pairs separate to accommodate an intercalating molecule. To check out the validity of viscosity measurements Hoechst 33258 (H33258) and ethidium bromide (EtBr) were used as a control compounds. Due to its groove binding mode, Hoechst 33258 does not induce any changes in viscosity upon interaction with DNA, while the known intercalator ethidium bromide does increase the relative viscosity of DNA.

It was found that the relative specific viscosity of CT-DNA increased upon addition of [1]Cl<sub>2</sub>, [2]Cl<sub>2</sub>, [3]Cl<sub>4</sub> or [4]Cl<sub>4</sub>. These measurements also reveal that the nature of the functional group has an effect on the viscosity changes caused by the complexes. It is also notable that, in both case, these monometallic complexes [1] and [2] appear to lengthen DNA more than dinuclear complexes [3] and [4]. It seems that in the dinuclear complexes the linker restricts

full insertion of the complex between DNA base pairs, whilst in the case of the mononuclear complexes it is easier for the linker to sit within the minor groove, resulting in enhanced binding compared to their dinuclear analogues. The changes in DNA viscosity for complexes **1** and **3** does confirm that they bind to DNA through intercalation, but suggest that for the dinuclear complex perhaps only one site is fully intercalating. However, as **Figure 2.24** shows the viscosity changes induced by **2** and **4** are considerably smaller than those induced by **1** and **3**. This suggests that either these complexes are not intercalating or are more selective so that they only bind at a smaller number of sites to produce an overall lower bulk change in viscosity.

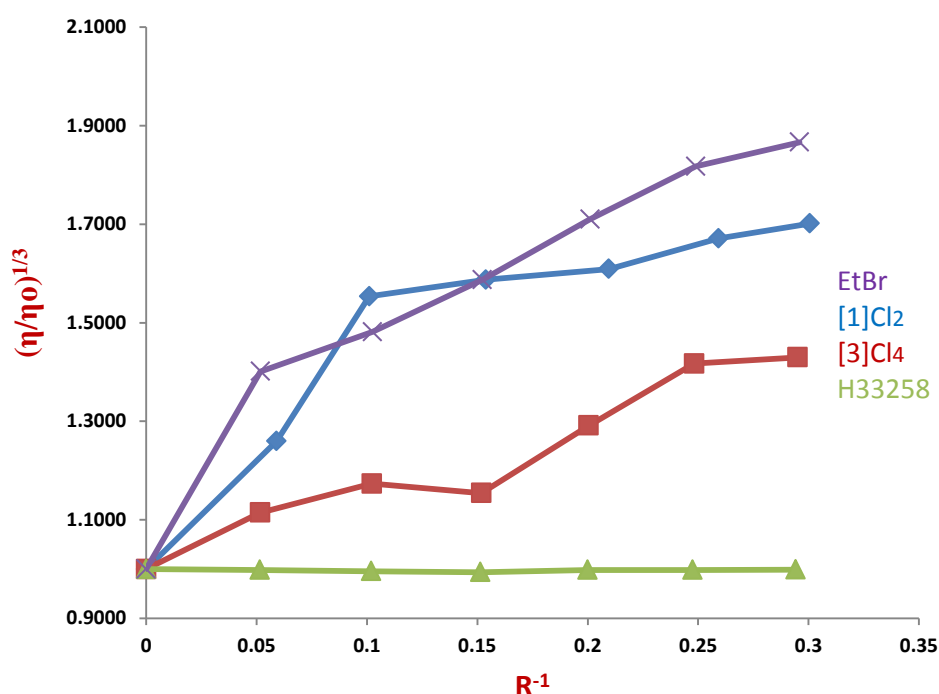


**Figure 2.23:** plot of relative viscosity  $(\eta/\eta_0)^{1/3}$  of CT-DNA versus  $R^{-1}$  ( $R = [\text{DNA}]/[\text{Compound}]$ ) upon addition of EtBr, H33258, [1]Cl<sub>2</sub> and [3]Cl<sub>4</sub>. Experimental conditions: 5 mM Tris, 25 mM NaCl, pH 7.4 at 26°C.

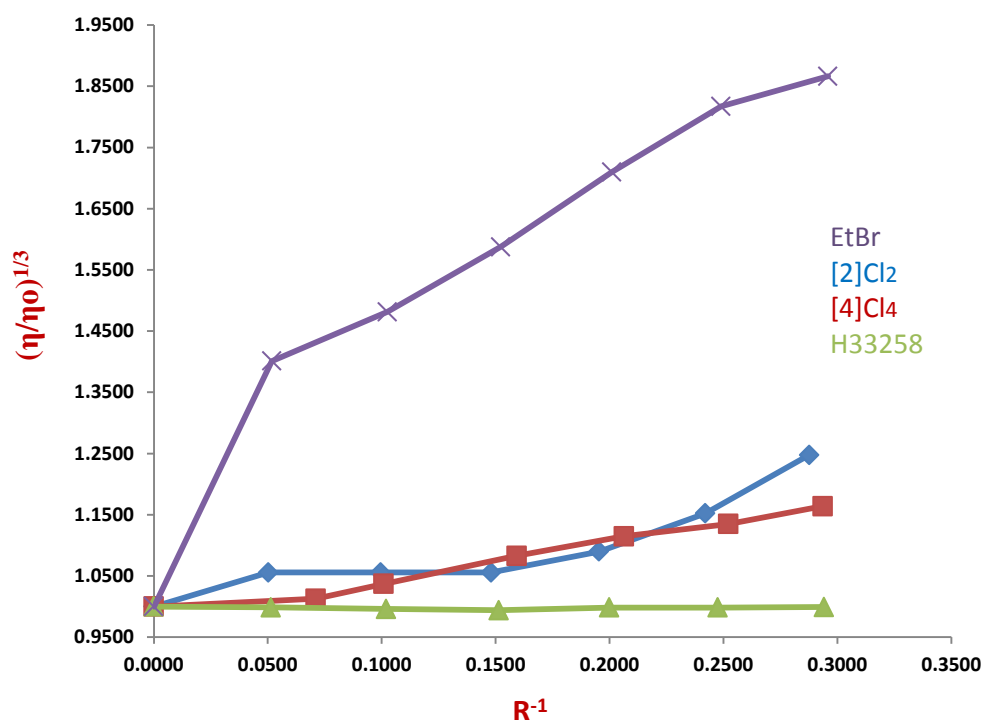


**Figure 2.24:** plot of relative viscosity  $(\eta/\eta_0)^{1/3}$  of CT-DNA versus  $R^{-1}$  ( $R = [\text{DNA}]/[\text{Compound}]$ ) upon addition of EtBr, H33258, [2]Cl<sub>2</sub> and [4]Cl<sub>4</sub>. Experimental conditions: 5 mM Tris, 25 mM NaCl, pH 7.4 at 26°C.

Four new polypyridyl ruthenium (II) complexes containing a linker group and their DNA binding properties have been established. The combination of viscometry, fluorescence and absorption spectroscopy data show that these complexes bind to DNA, most likely through intercalation. Complexes [1] and [3] seem to intercalate more strongly than complexes [2] and [4]. It seems the more rigid linker group may restrict full insertion of intercalative sites between the DNA base pairs. For the more flexible linker, the complex can sit more comfortably within the minor groove resulting in enhanced the binding compared. Whatever the reason, it is clear that the binding affinity of these complexes towards DNA is affected by the nature of the functional group in a linker.

To further investigate the properties of these complexes with DNA, isothermal titration calorimetry (ITC) was used as this can provide a complete thermodynamic profile on the interaction of metal complexes with biomolecules – *vide infra*.

## References

- (1) Erkkila, K. E.; Odom, D. T.; Barton, J. K.: *Chemical Reviews* **1999**, *99*, 2777-2796.
- (2) Mesmaeker, A. D.: *Chemical Communications* **1996**, 1013-1014.
- (3) Friedman, A. E.; Chambron, J. C.; Sauvage, J. P.; Turro, N. J.; Barton, J. K.: *Journal of the American Chemical Society* **1990**, *112*, 4960-4962.
- (4) Jenkins, Y.; Friedman, A. E.; Turro, N. J.; Barton, J. K.: *Biochemistry* **1992**, *31*, 10809-10816.
- (5) Hartshorn, R. M.; Barton, J. K.: *Journal of the American Chemical Society* **1992**, *114*, 5919-5925.
- (6) Metcalfe, C.; Adams, H.; Haq, I.; Thomas, J. A.: *Chemical Communications* **2003**, 1152.
- (7) Metcalfe, C.; Thomas, J. A.: *Chemical Society Reviews* **2003**, 215.
- (8) Waterland, M. R.; Gordon, K. C.; McGarvey, J. J.; Jayaweera, P. M.: *Journal of the Chemical Society, Dalton Transactions* **1998**, 609.
- (9) Fees, J.; Kaim, W.; Moscherosch, M.; Matheis, W.; Klima, J.; Krejcik, M.; Zalis, S.: *Inorganic Chemistry* **1993**, *32*, 166-174.
- (10) Amouyal, E.; Homsy, A.; Chambron, J. C.; Sauvage, J. P.: *Journal of the Chemical Society, Dalton Transactions* **1990**, 1841-1845.
- (11) Duveneck, G. L.; Kumar, C. V.; Turro, N. J.; Barton, J. K.: *The Journal of Physical Chemistry* **1988**, *92*, 2028-2032.
- (12) Scatchard, G.: *Annals of the New York Academy of Sciences* **1949**, *51*, 660-672.
- (13) McGhee, J. D. and Von Hippel, P. H.: *Journal of Molecular Biology* **1974**, *86*, 469-89.
- (14) Crothers, D. M.: *Biopolymer* **1968**, *6*, 575-84.

- (15) Wang, B. D.; Yang, Z. Y.; Crewdson, P.; Wang, D. Q.: *Journal of Inorganic Biochemistry* **2007**, *101*, 1492-1504.
- (16) Dougherty, G., Pilbrow, J. R. : *International Journal of Biochemistry* **1984**, *16*, 1179–1192.
- (17) Arjmand, F.; Aziz, M.: *European Journal of Medicinal Chemistry* **2009**, *44*, 834-844.
- (18) Wolfe, A.; Shimer Jr, G. H.; Meehan, T.: *Biochemistry* **1987**, *26*, 6392-6396.
- (19) Erkkila, K. E.; Odom, D. T.; Barton, J. K.: *Chemical Review* **1999**, *99*, 2777.
- (20) Friedman, A. E.; Chambron, J. C.; Sauvage, J. P.; Turro, N. J.; Barton, J. K.: *Journal of the American Chemical Society* **1990**, *112*, 4960.
- (21) Friedman, A. E.; Kumar, C. V.; Turro, N. J.; Barton, J. K.: *Nucleic Acid Research* **1991**, *19*, 2595.
- (22) Hartshorn, R. M.; Barton, J. K.: *Journal of the American Chemical Society* **1992**, *114*, 5919.
- (23) Nordén, B.; Lincoln, P.; Akerman, B.; Tuite, E.: *Metal Ions in Biological Systems*; Sigel, H., Sigel, A., Eds.; Marcel Dekker: New York, 1996; Vol. 33; pp 177.

## Chapter 3

### *The effect of the nature and positioning of the functional group on the binding mode and affinity of Ruthenium polypyridyl complexes*

---

3.1 Introduction.....	77
3.2 Syntheses.....	78
3.3.1 Linker syntheses.....	78
3.3.2 Synthesis of complexes.....	79
3.3.2.1 Monometallic complexes.....	79
3.3.2.2 Bimetallic complexes.....	80
3.3 Characterization.....	81
3.3.1 <sup>1</sup> H NMR spectroscopy studies.....	81
3.3.1.1 [Ru(tpm)(dppz)(μ-L'2)][(PF <sub>6</sub> ) <sub>2</sub> ].....	81
3.3.2 Photophysical studies.....	84
3.4 DNA Binding Studies.....	88
3.4.1 Absorption titration.....	88
3.4.2 Luminescence titration.....	90
3.4.3. Luminescence lifetimes.....	96
3.4.4. Viscosity Measurements.....	96
References.....	100

### 3.1 Introduction

In the previous chapter, four new ruthenium dppz complexes were reported. Binding studies show that the mononuclear complexes intercalate into CT-DNA with almost the same affinities as the related dinuclear complexes, probably due to the linkers of the dinuclear complexes restricting tight intercalation of the complex between DNA base pairs. Given this observation, it is of interest to investigate how the nature and difference in positioning of the tether group affects the biological activity and DNA binding affinities of analogous systems. Previously in the Thomas group, work on achiral  $[\text{Ru}(\text{tpm})(\text{dppz})\text{L}]^{2+}$  cation systems containing monodentate ancillary pyridyl ligands (**Figure 3.1**) have shown that the nature and position of a single functional group can greatly modulate the DNA binding properties of the resultant complex<sup>1</sup> and, in the case of the 4-aminopyridine complex, can even entirely “switch off” intercalative binding, due to the close contacts made by coordinated ancillary ligands held in the minor groove – see later for further details.

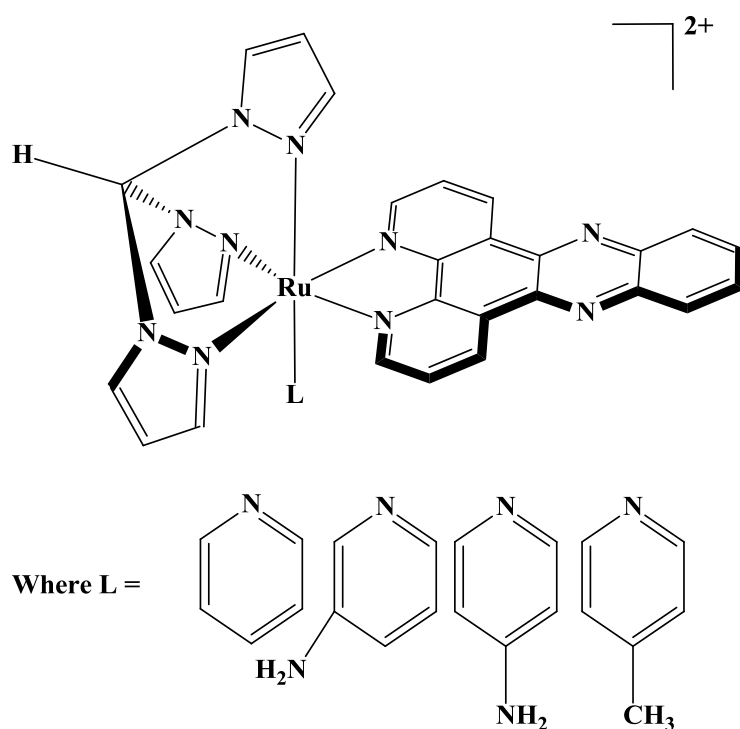


**Figure 3.1:** The structure of  $[\text{Ru}(\text{tpm})(\text{dppz})\text{L}]^{2+}$  complexes

This chapter describes work aimed at synthesizing four ruthenium complexes bearing new linkers designed to interact with DNA and comparing their photophysical and electrochemical properties with the ruthenium complexes reported in the previous chapter.

## 3.2 Syntheses

### 3.3.1 Linker syntheses

**N,N'-bis(3-pyridylmethyl)-1,6-hexanediamine (L'1)** was synthesized by refluxing a solution of 3-pyridinecarboxaldehyde and 1,6-hexanediamine in ethanol. Addition of  $\text{NaBH}_4$  and extracting the aqueous solution with  $\text{CH}_2\text{Cl}_2$  yielded a cream coloured viscous oil product.

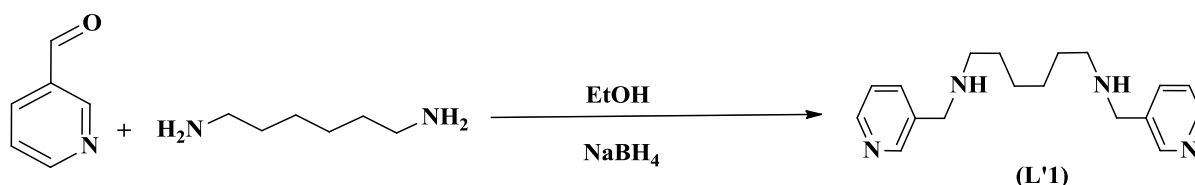


**Figure 3.2:** Synthesis of N,N'-bis(3-pyridylmethyl)-1,6-hexanediamine (L'1)

**N,N'-bis(3-pyridylmethyl)-1,4-benzenedimethyleneamine (L'2)** was prepared by stirring a mixture of benzene-1,4-dicarboxaldehyde and 3-(aminomethyl)pyridine in  $\text{CH}_2\text{Cl}_2$  (100 ml) with anhydrous  $\text{MgSO}_4$  (at room temperature for 24 h). Addition of  $\text{NaBH}_4$  and extracting the aqueous solution with  $\text{CH}_2\text{Cl}_2$  yielded a golden coloured viscous oil product.

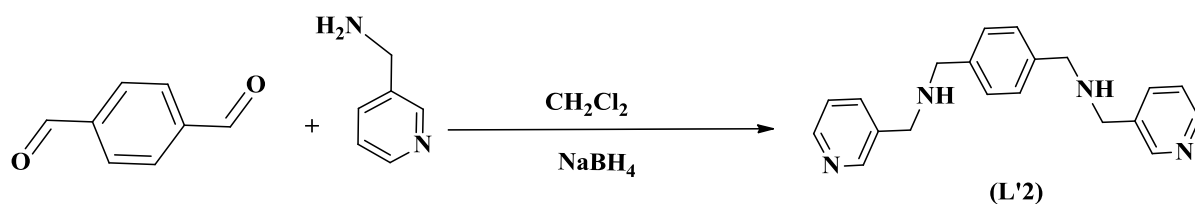


**Figure 3.3:** Synthesis of N,N'-bis(3-pyridylmethyl)-1,4-benzenedimethyleneamine (L'2)

### 3.3.2 Synthesis of complexes

#### 3.3.2.1 Monometallic complexes

$[\text{Ru}(\text{tpm})(\text{dppz})(\mu\text{-L}'1)](\text{PF}_6)_2$  [5] and  $[\text{Ru}(\text{tpm})(\text{dppz})(\mu\text{-L}'2)](\text{PF}_6)_2$  [6]. Complexes [5] and [6] were prepared by refluxing  $[\text{Ru}(\text{tpm})(\text{dppz})\text{Cl}]^+$  and  $\text{AgNO}_3$  in ethanol:water followed by the addition of the L'1 or L'2 ligand.  $\text{AgNO}_3$  was added to remove the axial chloride ligand and precipitated as  $\text{AgCl}$  which was removed by filtration through celite. The resultant complexes were precipitated as  $\text{PF}_6^-$  salts by reducing the solvent volume and adding an excess of the appropriate counter ion (**Figure 3.4**). Both ruthenium complexes were further purified by column chromatography on alumina eluted with acetonitrile:toluene.

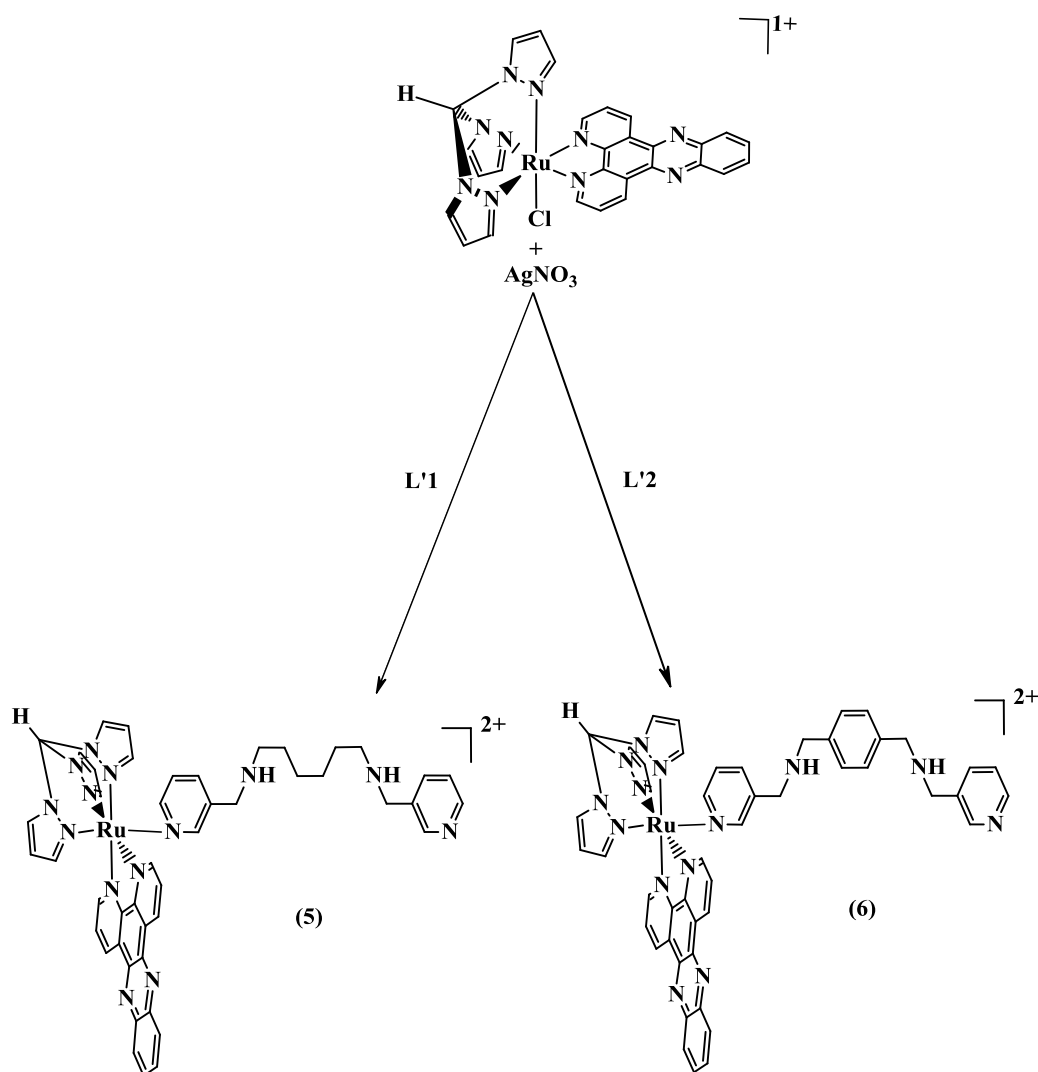


**Figure 3.4:** Synthesis of complexes [5] and [6]

### 3.3.2.2 Bimetallic complexes

$[\{\text{Ru}(\text{tpm})(\text{dppz})\}_2(\mu\text{-L}'1)](\text{PF}_6)_4$  [7],  $[\{\text{Ru}(\text{tpm})(\text{dppz})\}_2(\mu\text{-L}'2)](\text{PF}_6)_4$  [8].

Both complexes [7] and [8] were synthesized in an identical procedure starting by refluxing  $[\text{Ru}(\text{tpm})(\text{dppz})\text{Cl}]^+$  and  $\text{AgNO}_3$  in ethanol:water. After filtration  $[(\text{tpm})\text{Ru}(\text{dppz})(\text{L}'1)](\text{PF}_6)_2$  or  $[(\text{tpm})\text{Ru}(\text{dppz})(\text{L}'2)](\text{PF}_6)_2$  in acetone was added to the resultant solution, which was then refluxed for 3 days. The solution was concentrated and purification was achieved via ion-exchange chromatography on Sephadex CM-25 resin eluted with water acetone mixtures (5:3) containing increasing concentrations of NaCl. The fractions containing the product were concentrated and the product was precipitated by addition of  $\text{NH}_4\text{PF}_6$ .

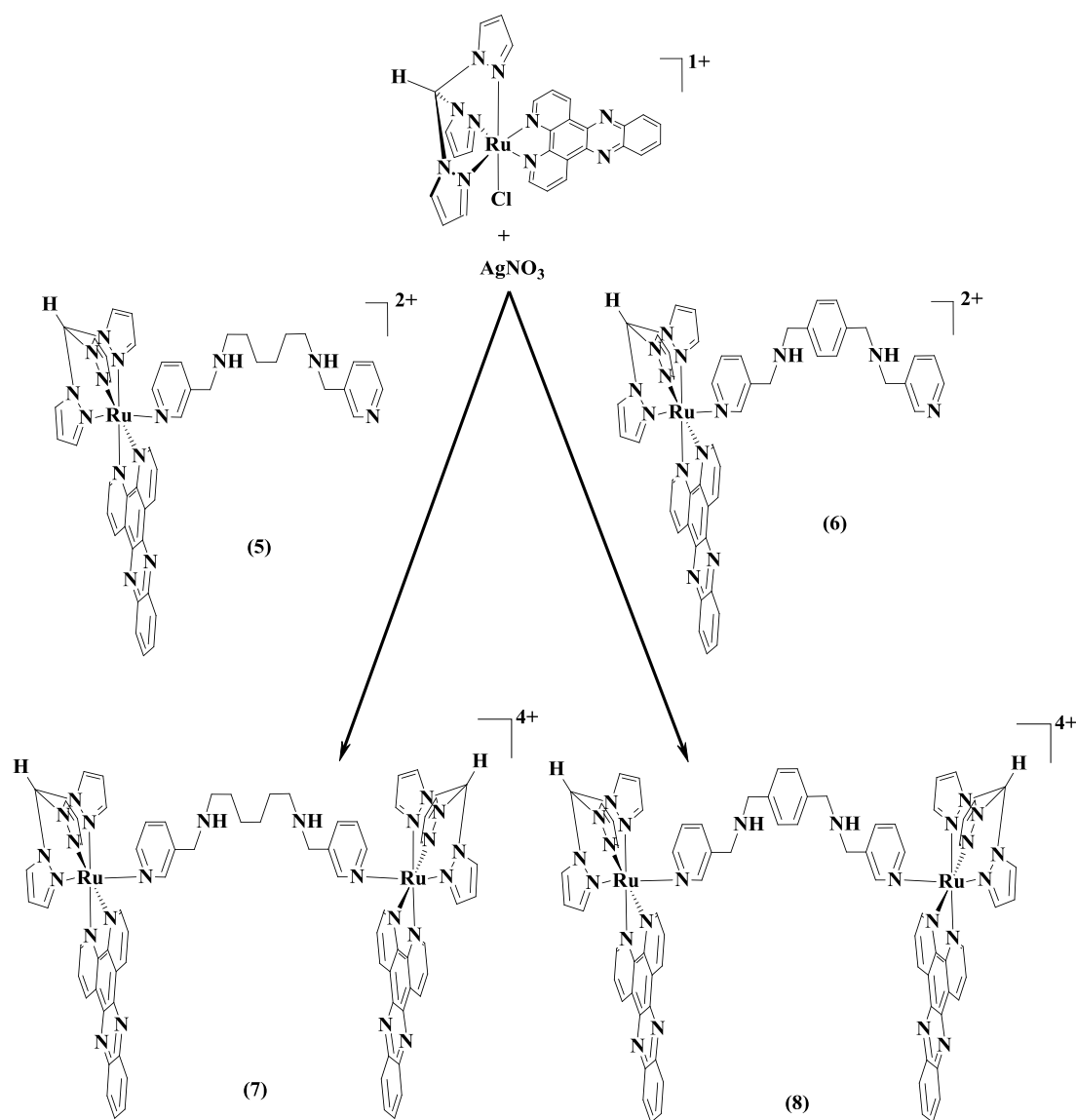


**Figure 3.5:** Synthesis of complexes [7] and [8]

### 3.3 Characterization

#### 3.3.1 $^1\text{H}$ NMR spectroscopy studies

##### 3.3.1.1 $[\text{Ru}(\text{tpm})(\text{dppz})(\mu\text{-L}'2)][(\text{PF}_6)_2]$

The downfield  $^1\text{H}$  NMR region of the spectrum for  $[\text{Ru}(\text{tpm})(\text{dppz})(\mu\text{-L}'2)](\text{PF}_6)_2$  is shown below in **Figure 3.6** along with the molecular structure and proton labelling scheme.

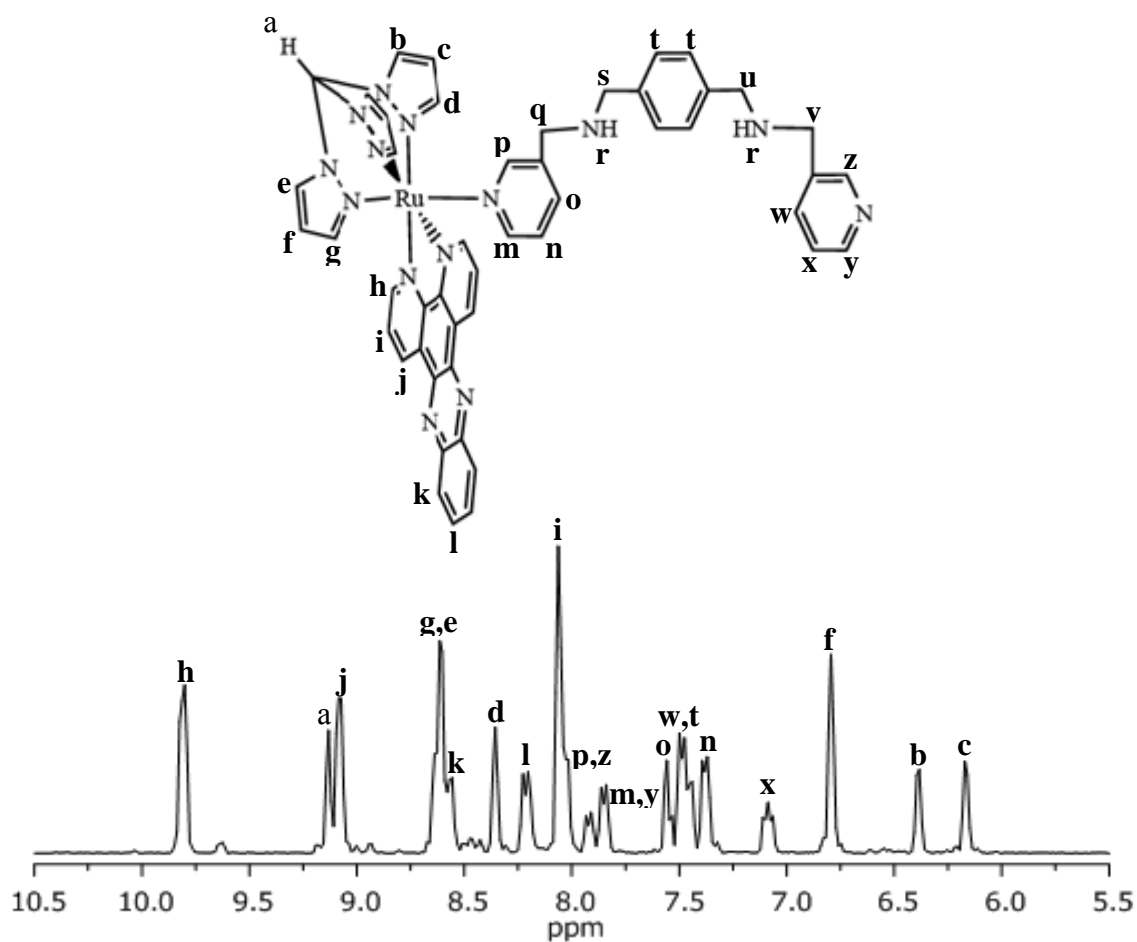


**Figure 3.6:** Downfield region of 400 MHz  $^1\text{H}$  NMR spectrum of **[6]** in acetonitril- $\text{d}^3$  along with chemical structure and proton labelling scheme.

The 500 MHz  $^1\text{H}$  NMR-COSY spectrum (**Figure 3.7**) shows the cross coupling between the different ligand sets, Tpm (blue), dppz (red) and L'2 (green).

The typical de-shielded methane proton of the tpm moiety is found as a singlet at 9.13ppm (a). Cross coupling analysis shows that the pyrazole protons appearing at 8.60ppm (b), 6.38ppm (c) and 6.80ppm, which integrate for two hydrogen atoms each are the axial pyrazole and the signals as 8.63ppm (e), 7.05ppm (f) and 6.17ppm (g) (which all integrate for two hydrogens) are the two equatorial protons. The phenanthroline protons of dppz appear at 9.81ppm (h), 8.21ppm (i) and 9.08ppm (j), with all three signals integrating to two protons each. Due to its proximity to nitrogen, proton h has the highest chemical shift. The two phenazine protons appear at 8.57ppm and 8.41ppm respectively. All seven sets of pyridine protons within the linker are rendered inequivalent due to coordination of one of the pyridine moieties of the ( $\mu$ -L'2) ligand to the ruthenium centre. The two aromatic sets appear at 8.06ppm (p) and 7.56ppm (z). The large coupling constant indicates that these protons are adjacent to ring nitrogens, and the one coordinated to the ruthenium was assumed to be with the furthest downfield shift. The other aromatic protons appear at 7.85ppm (n) and 7.36ppm (x). The two triplets at 2.55ppm and 2.60ppm which are closely positioned are protons (q) and (s) on the alkyl linker. While the amino group protons appear as a singlet at 2.01ppm (r), multiplets appear at 1.59ppm and 1.52ppm are protons (v) and (u) respectively.

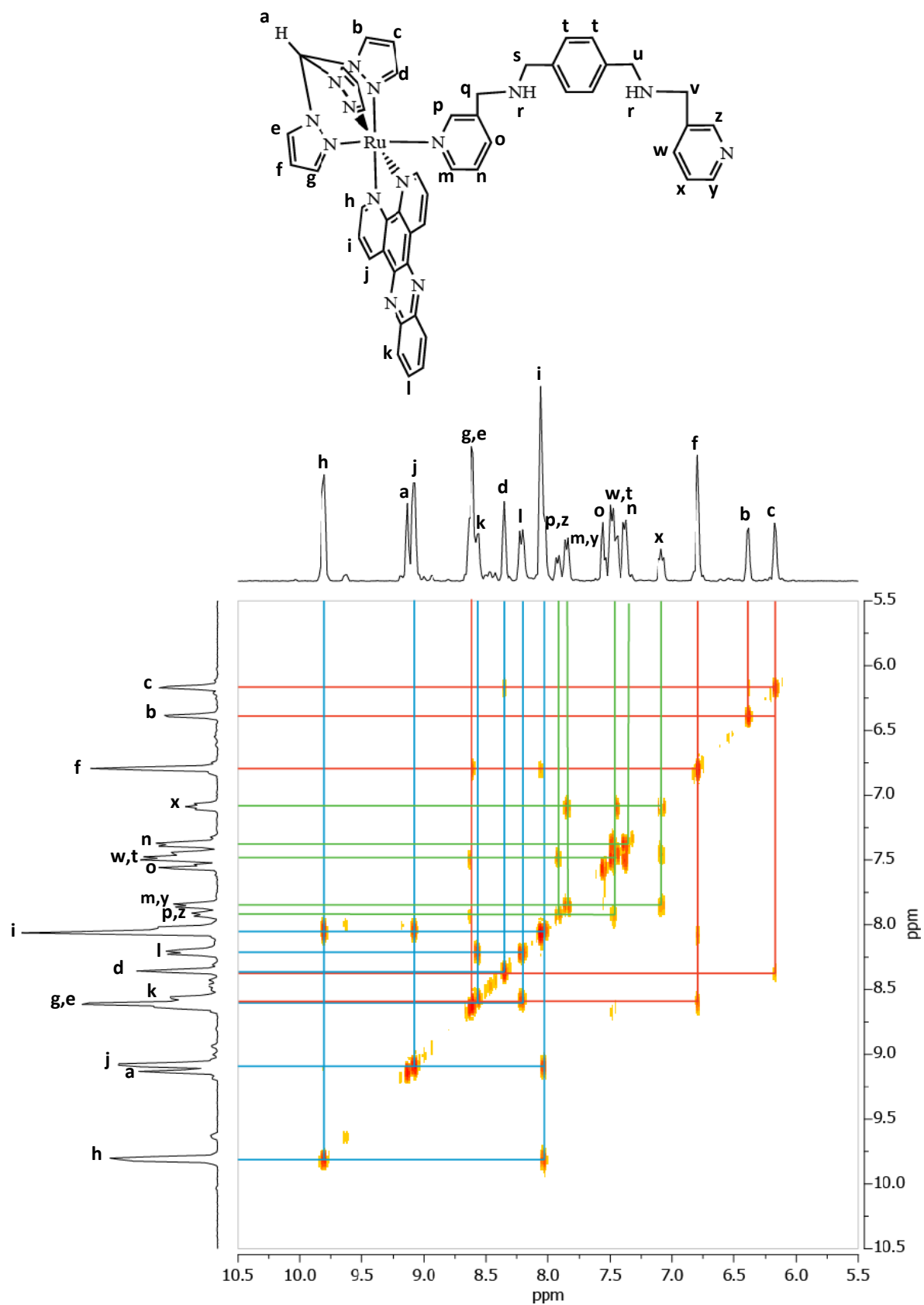


**Figure 3.7:** 500 MHz  $^1\text{H}$  NMR-COSY of [6] in acetonitrile- $\text{d}_3$

The  $^1\text{H}$  NMR spectrum of the bimetallic ruthenium complex  $[\{\text{Ru}(\text{tpm})(\text{dppz})\}_2(\mu\text{-L}'2)](\text{PF}_6)_4$  is well resolved and is quite simple due to the symmetry of the molecule. Therefore, 2D-COSY NMR was not needed to fully assign the spectrum of this complex.

### 3.3.2 Photophysical studies

The photophysical properties of complexes [5-8] were recorded in acetonitrile solutions at room temperature (**Figure 3.8**). All the complexes show a band between 220-320 nm that can be assigned to high energy  $\pi\rightarrow\pi^*$  transition in aromatic nitrogen donor ligands. The UV-Vis spectrum of the dppz ligand in DMF shows structured transitions between 340-380 nm, which can be assigned to ( $\pi\rightarrow\pi^*$ ) transitions.<sup>2</sup> All complexes show A band around 360 nm; in [5] and [8] this band is found at 357 nm, for [6] it occurs at 355 nm and for [7] it is seen at 359 nm. Metal ligand charge transfer transitions (MLCT) are observed for all the complexes at around 400-500 nm; this is typical for ruthenium (II) complexes with coordinated polyimine ligands. Data are summarised in **table 3.1**.

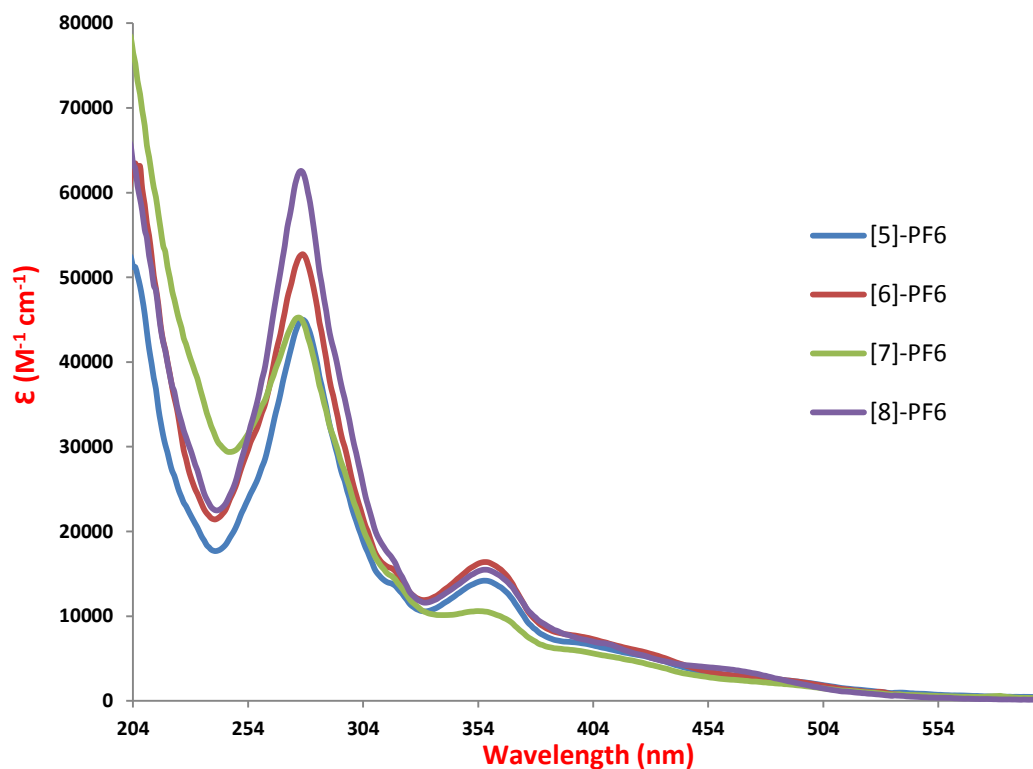


**Figure 3.8:** UV-Visible absorption spectra for the complexes [5], [6], [7] and [8] as  $\text{PF}_6$  salts in acetonitrile at room temperature

Compound	$\lambda_{\text{max}}$ (nm)	$10^{-3}\epsilon$ ( $\text{M}^{-1}\text{cm}^{-1}$ )	Assignment
<b>(5)</b> $[\text{Ru}(\text{tpm})(\text{dppz})(\mu\text{-L}'1)][\text{PF}_6]_2$	231	20.45	$\pi \rightarrow \pi^*$
	277	45.10	$\pi \rightarrow \pi^*$
	318	13.27	$\pi \rightarrow \pi^*$
	358	14.10	$\pi \rightarrow \pi^*$
	402	6.67	MLCT
	432	4.82	MLCT
	492	2.30	MLCT
<b>(6)</b> $[\text{Ru}(\text{tpm})(\text{dppz})(\mu\text{-L}'2)][\text{PF}_6]_2$	223	34.50	$\pi \rightarrow \pi^*$
	279	52.29	$\pi \rightarrow \pi^*$
	318	14.92	$\pi \rightarrow \pi^*$
	361	16.01	$\pi \rightarrow \pi^*$
	402	7.35	MLCT
	432	5.24	MLCT
	490	2.36	MLCT
<b>(7)</b> $[\{(\text{tpm})\text{Ru}(\text{dppz})\}_2(\mu\text{-L}'1)][\text{PF}_6]_4$	231	38.04	$\pi \rightarrow \pi^*$
	277	44.66	$\pi \rightarrow \pi^*$
	318	13.93	$\pi \rightarrow \pi^*$
	361	10.25	$\pi \rightarrow \pi^*$
	396	5.93	MLCT
	424	4.52	MLCT
	492	1.83	MLCT
<b>(8)</b> $[\{(\text{tpm})\text{Ru}(\text{dppz})\}_2(\mu\text{-L}'2)][\text{PF}_6]_4$	231	27.21	$\pi \rightarrow \pi^*$
	277	62.56	$\pi \rightarrow \pi^*$
	316	16.71	$\pi \rightarrow \pi^*$
	356	15.48	$\pi \rightarrow \pi^*$
	410	6.66	MLCT
	471	3.39	MLCT

**Table 3.1:** UV-Visible data for the complexes [5], [6], [7] and [8] as  $\text{PF}_6$  salts recorded in acetonitrile.

The UV-Visible data for these complexes [5],[6],[7] and [8] recorded in tris buffer as their respective chloride salts is also summarised below in **Table 3.2**. The spectra for these chloride salts look very similar to one another.

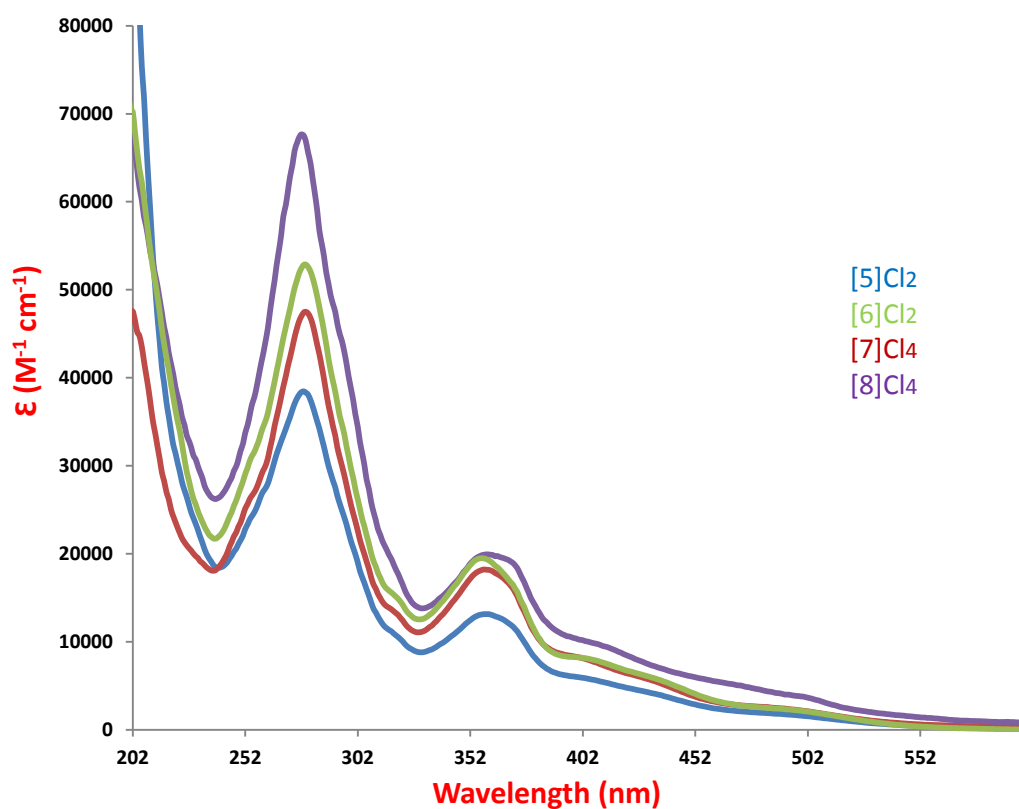


**Figure 3.9:** UV-Visible absorption spectra for the complexes [5], [6], [7] and [8] as chloride salts in 5 mM tris buffer, 25 mM NaCl, pH 7.4 at room temperature

Compound	$\lambda_{\text{max}}$ (nm)	$10^{-3} \epsilon$ ( $\text{M}^{-1}\text{cm}^{-1}$ )	Assignment
<b>(5) [Ru(tpm)(dppz)(<math>\mu</math>-L'1)]Cl<sub>2</sub></b>	232	23.63	$\pi \rightarrow \pi^*$
	279	38.08	$\pi \rightarrow \pi^*$
	320	10.30	$\pi \rightarrow \pi^*$
	360	13.10	$\pi \rightarrow \pi^*$
	405	5.76	MLCT
	439	4.09	MLCT
	498	2.17	MLCT
<b>(6) [Ru(tpm)(dppz)(<math>\mu</math>-L'2)]Cl<sub>2</sub></b>	224	32.30	$\pi \rightarrow \pi^*$
	280	52.55	$\pi \rightarrow \pi^*$
	319	14.88	$\pi \rightarrow \pi^*$
	359	19.29	$\pi \rightarrow \pi^*$
	403	8.10	MLCT
	435	5.75	MLCT
	498	2.19	MLCT
<b>(7) [{(tpm)Ru(dppz)}<sub>2</sub>(<math>\mu</math>-L'1)]Cl<sub>4</sub></b>	228	20.36	$\pi \rightarrow \pi^*$
	281	46.79	$\pi \rightarrow \pi^*$
	321	14.21	$\pi \rightarrow \pi^*$
	362	18.91	$\pi \rightarrow \pi^*$
	405	8.04	MLCT
	433	5.91	MLCT
	493	2.30	MLCT
<b>(8) [{(tpm)Ru(dppz)}<sub>2</sub>(<math>\mu</math>-L'2)]Cl<sub>4</sub></b>	231	29.29	$\pi \rightarrow \pi^*$
	278	67.49	$\pi \rightarrow \pi^*$
	317	18.80	$\pi \rightarrow \pi^*$
	359	19.40	$\pi \rightarrow \pi^*$
	417	8.85	MLCT
	499	3.77	MLCT

**Table 3.2:** UV-Visible data for the complexes [5], [6], [7] and [8] as chloride salts recorded in 5mM tris buffer, 25 mM NaCl, pH 7.4 at 25 °C.

## 3.4 DNA Binding Studies

### 3.4.1 Absorption titration

Initial evidence of these complexes binding to DNA comes from the absorption titration experiments. Upon addition of CT-DNA to buffered solutions of the complexes, their UV-Vis spectra show hypochromic and red shifts of the peak maxima in both MLCT and  $\pi \rightarrow \pi^*$  absorption bands. **Figures 3.10** and **3.11** show typical UV-Vis titrations.

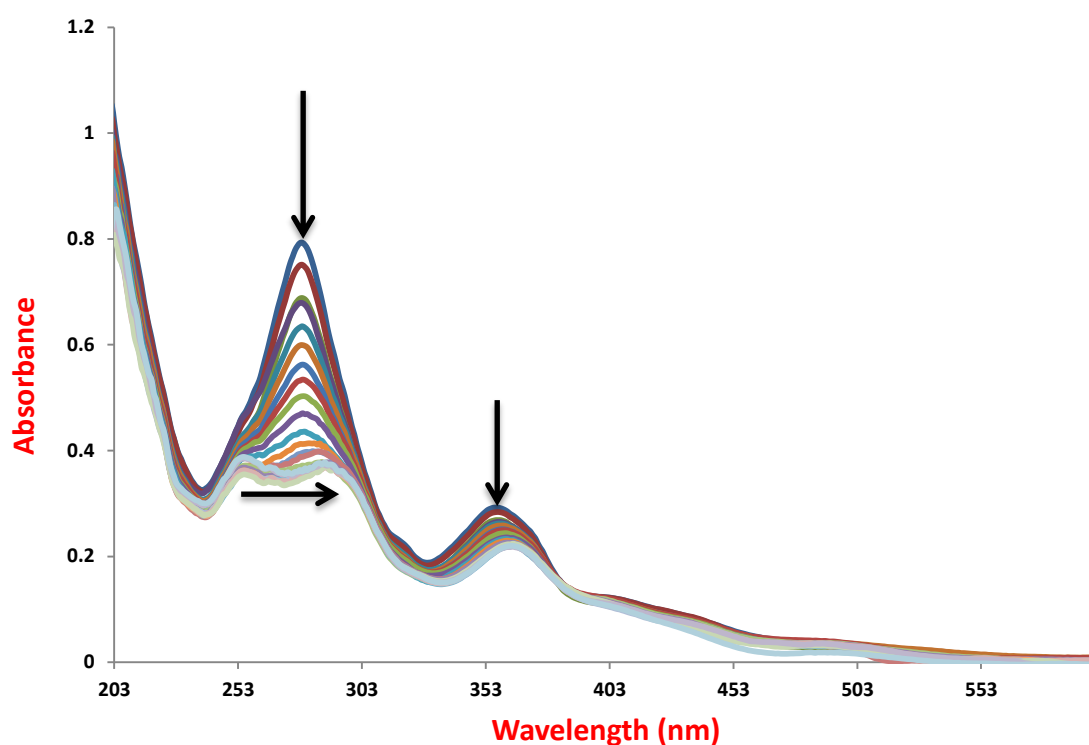


**Figure 3.10:** UV-Visible titration of 1.01 mM bp<sup>-1</sup> CT-DNA into a solution of 15  $\mu$ M [6]Cl<sub>2</sub> in 5 mM tris buffer, 25 mM NaCl, pH 7.4 at 25 °C.

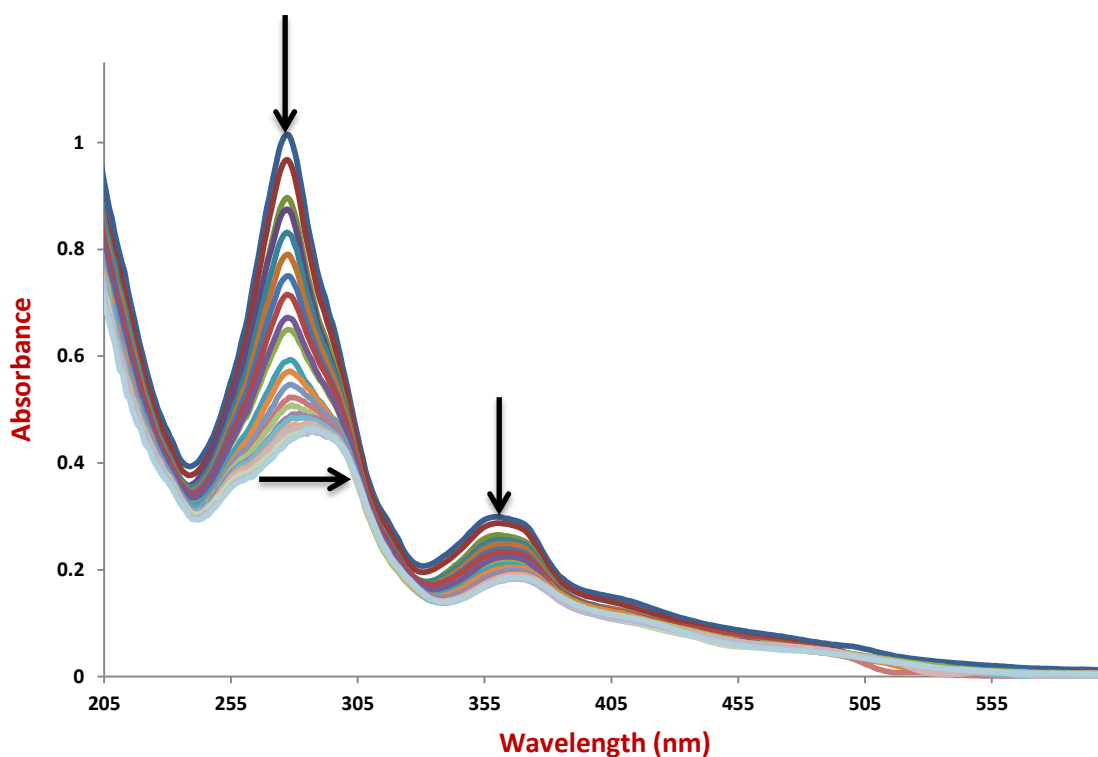


**Figure 3.11:** UV-Visible titration of 1.01 mM bp<sup>-1</sup> CT-DNA into a solution of 15 μM [8]Cl<sub>4</sub> in 5 mM tris buffer, 25 mM NaCl, pH 7.4 at 25 °C.

For all complexes, the bands at ~278 nm and ~357 nm show a high degree of hypochromicity. There is also a significant bathochromic shift of about ~10 nm as the band at ~278 nm reaches saturation. Hypochromicity and bathochromic shifts generally indicate intercalative binding<sup>3</sup> as these effects are the result of the interaction between the electronic states of the ligand and the DNA base pairs.<sup>4,5</sup>

The saturation binding curves of [5-8] obtained from the titrations are shown in (**Figure 3.12**); in each case saturation binding has taken place.

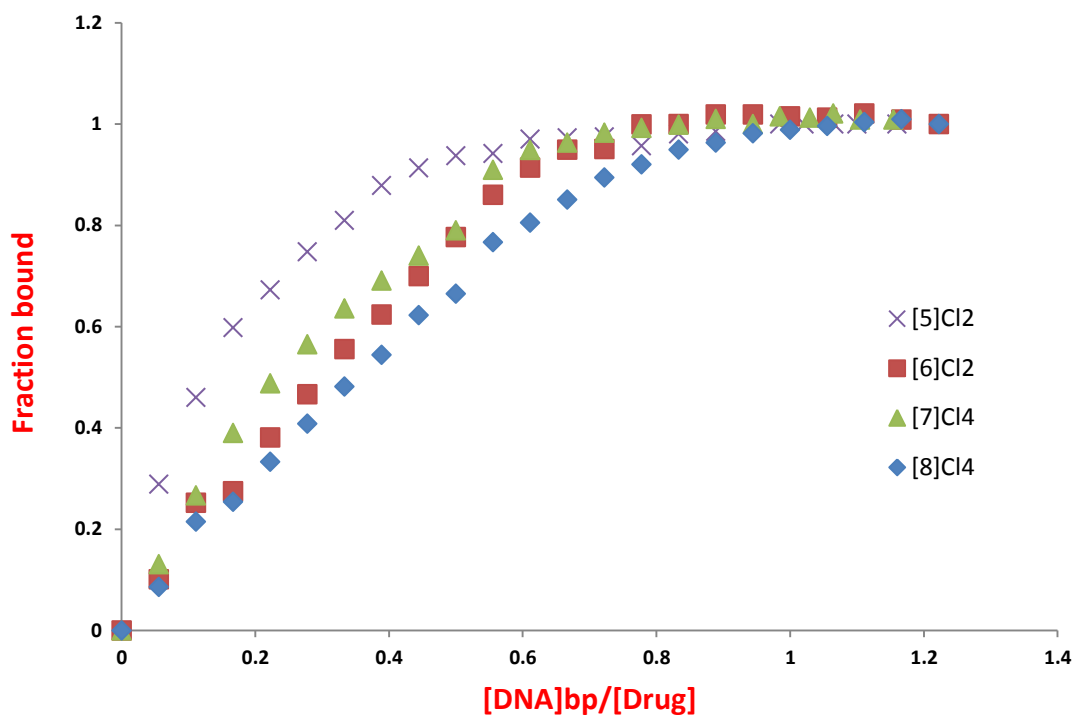


**Figure 3.12:** Binding curves obtained from the UV-Vis titrations of [5]Cl<sub>2</sub>, [6]Cl<sub>2</sub>, [7]Cl<sub>4</sub> and [8]Cl<sub>4</sub> binding to CT-DNA

The previously described complexes [1], [2], [3] and [4] all bind to DNA with the dppz ligand in a solvent protected site. On the basis of the similarities in structures and absorption characteristics between these Ru(II)dppz complexes and complexes [5], [6], [7] and [8], it seems that the latter complexes bind to CT-DNA in a similar manner.

### 3.4.2 Luminescence titration

To further investigate the binding mode between complex and CT-DNA, luminescence titration experiment was carried out. The complexes luminescence in tris buffer with wavelength maxima around ~640 nm, **Figure 3.13** and **3.14** show the emission spectra of the complexes [6]Cl<sub>2</sub> and [8]Cl<sub>4</sub> in the presence and absence of CT-DNA. All the complexes have a light switch effect with emission from all four complexes being quenched by water molecules, while binding to DNA enhances luminescence by several orders of magnitude. All the complexes were excited at the wavelength characteristic of the transition MLCT. In the

case of [5]Cl<sub>2</sub> the excitation wavelength is at 425 nm, for [6]Cl<sub>2</sub>,  $\lambda_{ex}$  = 435 nm, and  $\lambda_{ex}$  = 445 and 460 nm for [7]Cl<sub>4</sub> and [8]Cl<sub>4</sub> respectively. The emission of [6]Cl<sub>2</sub> and [8]Cl<sub>4</sub> are around 640 nm, while the emission of [5]Cl<sub>2</sub> and [7]Cl<sub>4</sub> are around 645 nm. Data are summarised in **Table 3.3**.

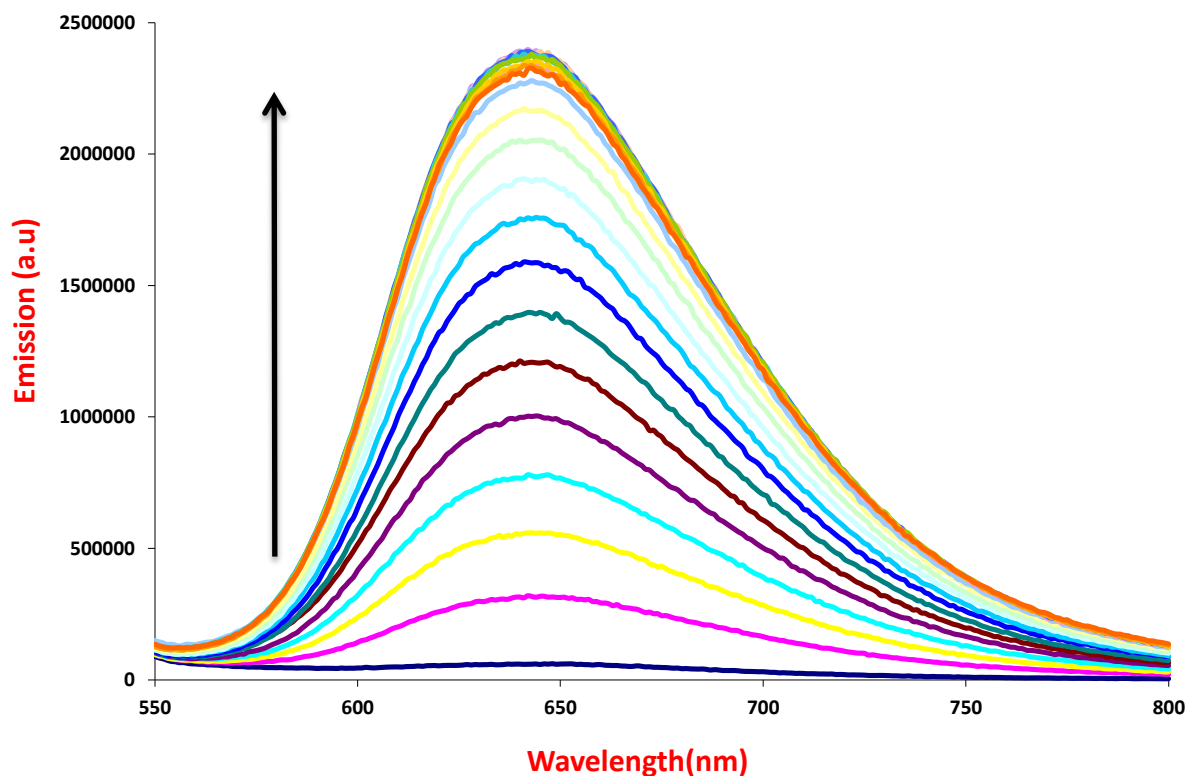


**Figure 3.13:** Luminescence titration of 1.01 mM M bp<sup>-1</sup> CT-DNA into a solution of 15  $\mu$ M [6]Cl<sub>2</sub> in 5 mM tris buffer, 25 mM NaCl, pH 7.4 at 25 °C.  $\lambda_{ex}$  = 431 nm.

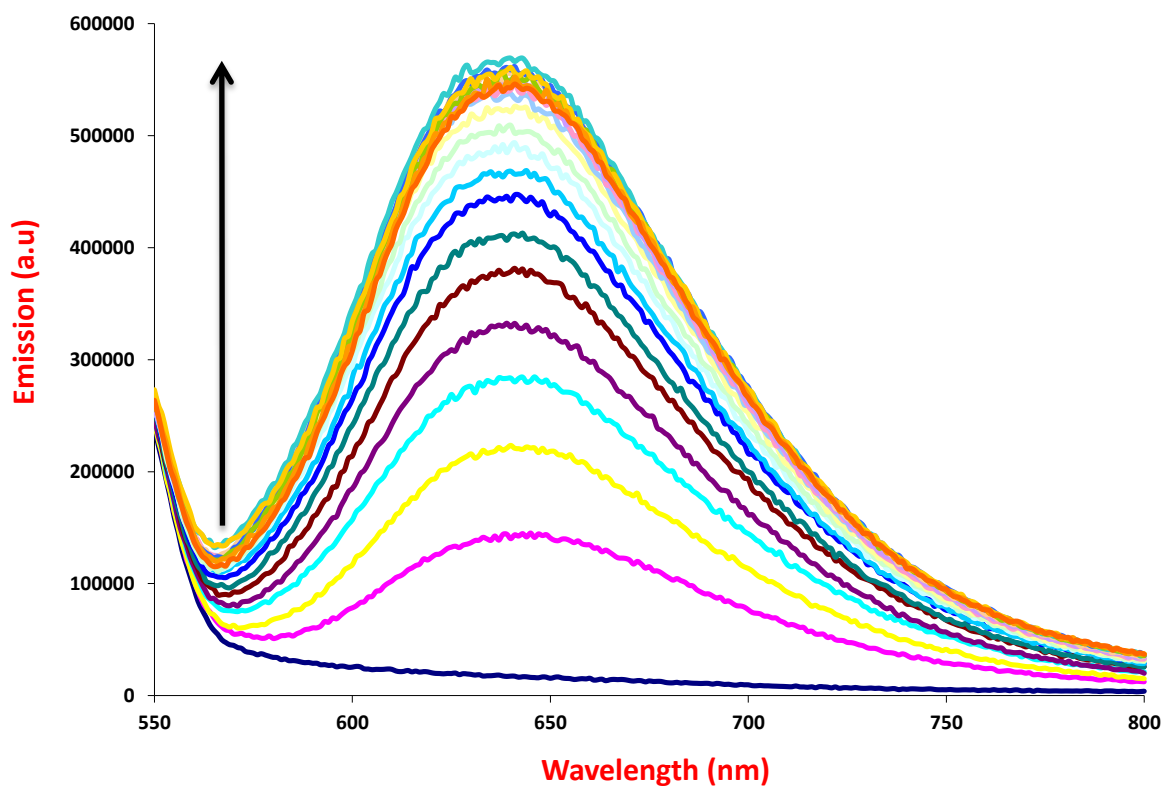


**Figure 3.14:** Luminescence titration of 1.01 mM bp<sup>-1</sup> CT-DNA into a solution of 15 μM [8]Cl<sub>4</sub> in 5 mM tris buffer, 25 mM NaCl, pH 7.4 at 25 °C. λ<sub>ex</sub> = 437 nm.

Complex	Emission	
	λ <sub>ex</sub> (nm)	λ <sub>em</sub> (nm)
[5]Cl <sub>2</sub>	425	645
[6]Cl <sub>2</sub>	435	639
[7]Cl <sub>4</sub>	445	642
[8]Cl <sub>4</sub>	460	640

**Table 3.3:** Emission data for the complexes [5-8] in 5 mM tris buffer, 25 mM NaCl, pH 7.4 at 25 °C.

The binding curve for the interaction of these complexes with CT-DNA shows that saturation binding has taken place (**Figure 3.15**).

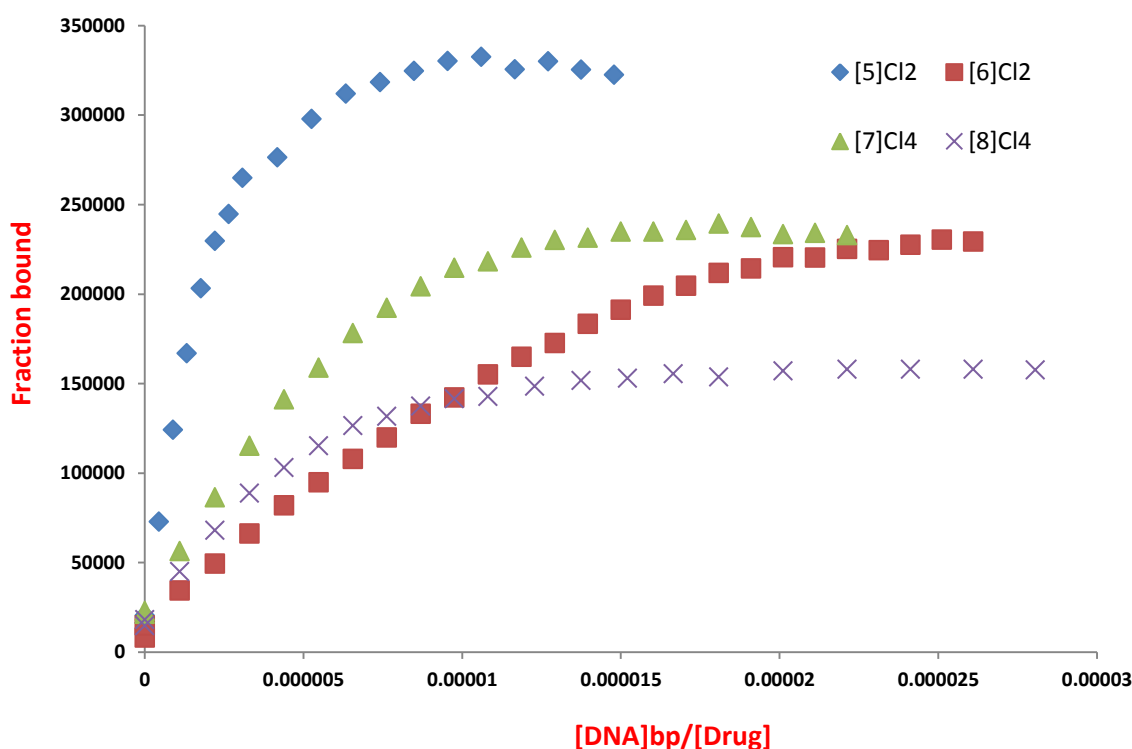


**Figure 3.15:** Binding curves obtained from the Luminescence titrations of [5]Cl<sub>2</sub>, [6]Cl<sub>2</sub>, [7]Cl<sub>4</sub> and [8]Cl<sub>4</sub> binding to 1.01 mM CT-DNA, 25mM NaCl, 5mM Tris-HCl, pH 7.4, 25°C

The binding data for the luminescence and absorption titrations of these complexes again did not fit to the McGhee Von Hippel model properly for the same reasons as explained in chapter two. To address this problem, the binding constants  $K_b$  for the interaction of these complexes with CT-DNA were calculated by using a simpler model.<sup>6</sup>

In plots of  $[DNA]/(\epsilon_a - \epsilon_f)$  versus  $[DNA]$ ,  $K_b$  is given by the ratio of slope to the intercept and the data are shown in **Table 3.4**.

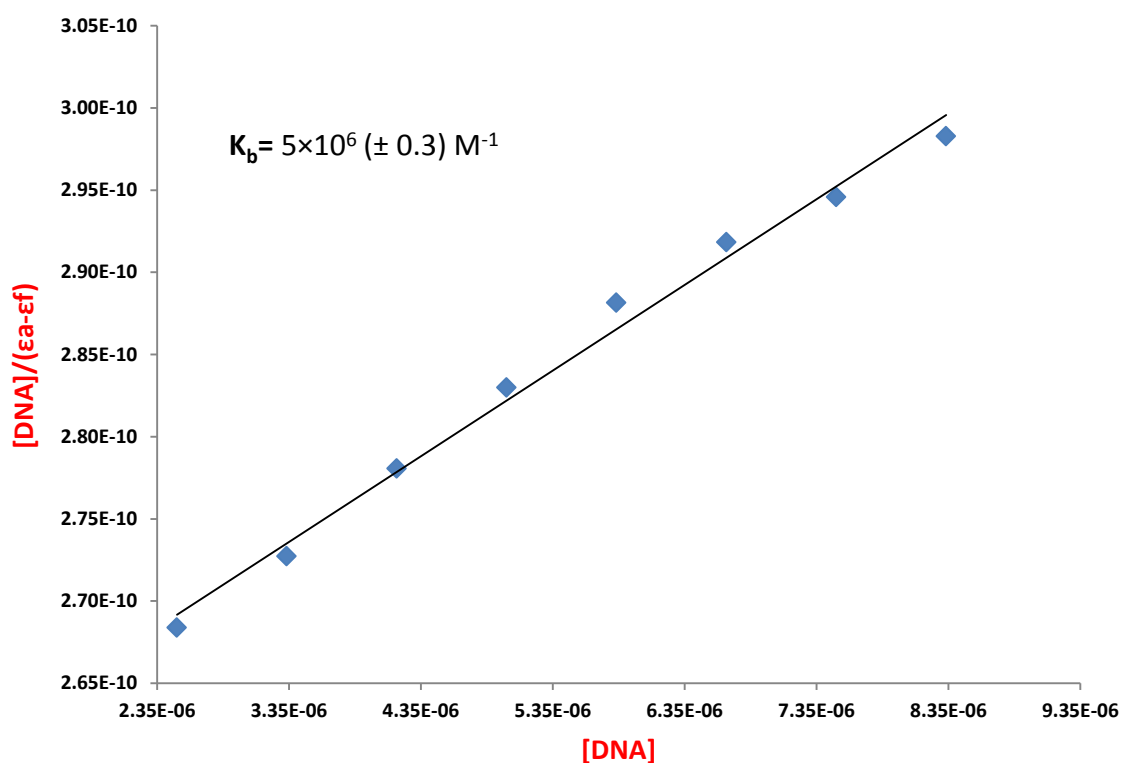
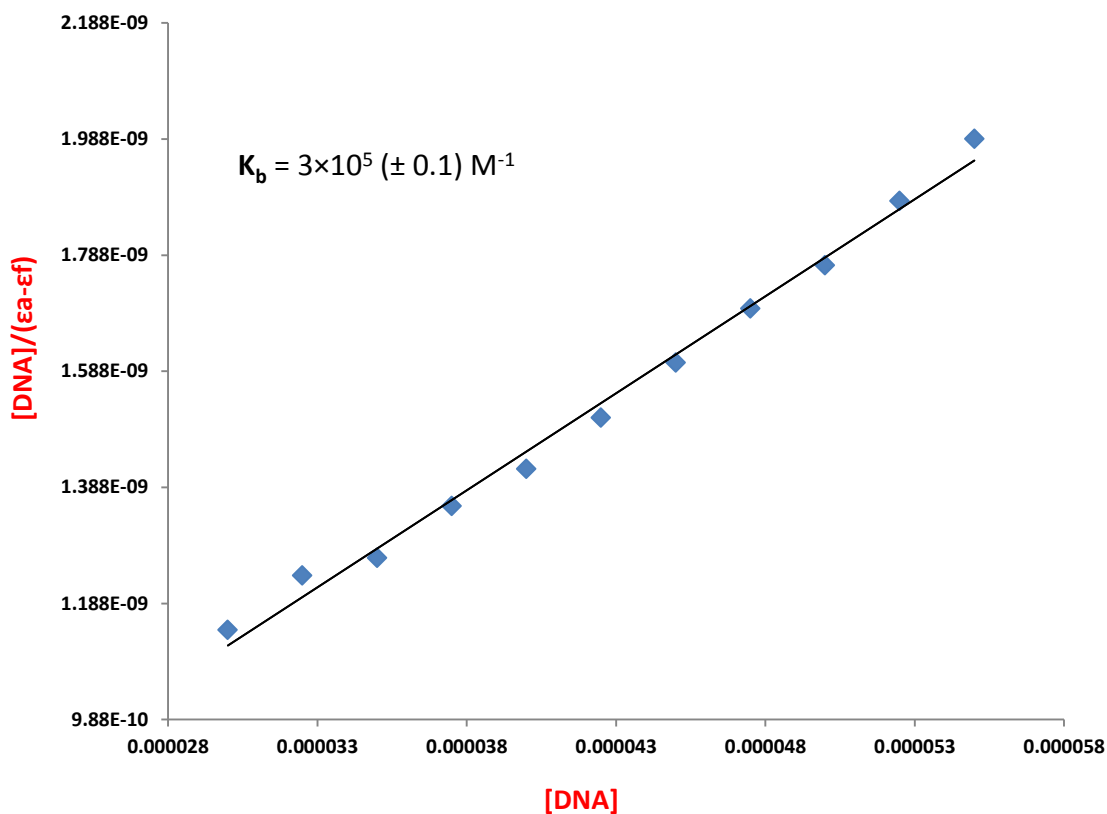


**Figure 3.16:** Scatchard plots for the complex [6]Cl<sub>2</sub> (top) and complex [8]Cl<sub>4</sub> (bottom) obtained from the absorption spectroscopy of CT-DNA. Inserted plot, [DNA]/(εa-εf) versus [DNA] for the absorption titrations.

For the two monometallic complexes [5]Cl<sub>2</sub> and [6]Cl<sub>2</sub> the intrinsic binding constant constants were determined as  $4.0 \times 10^5 \text{ M}^{-1}$  and  $3.0 \times 10^5 \text{ M}^{-1}$  respectively. However, the intrinsic binding constant constants for both dinuclear complexes [7]Cl<sub>4</sub> and [8]Cl<sub>4</sub> were obtained as  $9.0 \times 10^6 \text{ M}^{-1}$  and  $5.0 \times 10^6 \text{ M}^{-1}$  respectively. This shows an over one order of magnitude increase in binding affinity for the dinuclear over the mononuclear complexes.

Complex	$K_b \text{ (M}^{-1}\text{)}$
[5]Cl <sub>2</sub>	$4 \times 10^5 (\pm 0.08)$
[6]Cl <sub>2</sub>	$3 \times 10^5 (\pm 0.1)$
[7]Cl <sub>4</sub>	$9 \times 10^6 (\pm 0.2)$
[8]Cl <sub>4</sub>	$5 \times 10^6 (\pm 0.3)$

**Table 3.4:** Binding constants obtained by UV-Visible titrations of CT-DNA with complexes [5-8],  $K_b$  is intrinsic binding constants.

Since the size and shape of complexes [1-4] and [5-8] are almost identical, the increased binding affinity of [5-8] over [1-4] for CT-DNA must be due to the connectivity within the tether ligand.

In optical titrations with mononuclear  $[\text{Ru}(\text{tpm})(\text{pyNH}_2)(\text{dppz})]^{n+}$  complexes (where pyNH<sub>2</sub> = 3- or 4-amino pyridine) it was found that although the 3-pyNH<sub>2</sub>-based complex binds by intercalation, the coordinated 4-pyNH<sub>2</sub> complex is a low affinity groove binder that does not display the light switch effect. NMR studies revealed that this is due to unfavourable interactions made by the 4-NH<sub>2</sub> of the coordinated pyridine which projects into the minor groove of the duplex. It seems that effects like this are responsible for the different affinities of the systems reported in this chapter and chapter two.

It seems clear that attachment of the chain of the tether in the 3-position of the coordinated pyridine allows for a closer association between the dinuclear system and their DNA target.

In summary the spectroscopic binding studies on the ruthenium monometallic complexes reveal a good affinity for DNA with the dinuclear complexes showing a 10 fold enhanced affinity over the mononuclear complexes.

### 3.4.3. Luminescence lifetimes

Luminescence lifetimes for all the complexes [1-8] were recorded in acetonitrile. Data and the quality of fits to a single exponential function ( $X^2$ ) are summarised in **Table 3.5**. The longest lived lifetime among this series of complexes is around~ 75 ns for complex [6], whereas the shortest luminescence lifetime is about~ 53 for the complex [2] in acetonitrile. Foxon et al. prepared a family of substituted dppz ligands, one of which was  $[\text{Ru}(\text{tpm})(\text{pyridine})\text{dppz}]^{2+}$  with a luminescence lifetime 77 ns.<sup>7</sup> This luminescence lifetime value correlates well with the data observed for the complexes [1-8] in acetonitrile.

Complex	[1][PF <sub>6</sub> ] <sub>2</sub>	[2][PF <sub>6</sub> ] <sub>2</sub>	[3][PF <sub>6</sub> ] <sub>4</sub>	[4][PF <sub>6</sub> ] <sub>4</sub>	[5][PF <sub>6</sub> ] <sub>2</sub>	[6][PF <sub>6</sub> ] <sub>2</sub>	[7][PF <sub>6</sub> ] <sub>4</sub>	[8][PF <sub>6</sub> ] <sub>4</sub>
$t_{(\text{ns})}$	68.90	53.23	57.54	67.91	73.70	75.36	55.89	73.60
$X^2$	1.06	1.16	1.00	1.10	1.15	1.19	1.01	1.04

**Table 3.5:** Luminescence lifetime data for complexes [1-8] in dry acetonitrile at room temperature

### 3.4.4. Viscosity Measurements

In the absence of crystallographic structural data, viscosity measurements of CT-DNA are considered as the least ambiguous and the most critical tests of a binding model in solution.<sup>8,9</sup> Therefore, the effect of new complexes [5-8] on the viscosity of CT-DNA has been explored as shown in **Figures 3.17** and **3.18**.

Clearly, these new complexes produce very large positive viscosity changes, definitively confirming that these complexes intercalate into DNA duplex. Furthermore, these studies show that the 3-py based complexes [5-8] lengthen the DNA sequences appreciably more than 4-py based complexes [1-4] suggesting that these complexes intercalate more deeply than the 4-py based complexes. It is also interesting to note that the viscosity changes induced by [8]Cl<sub>4</sub> is significantly larger than that of [6]Cl<sub>2</sub>. This the first time that this kind of dinuclear complex shows such an increase over its mononuclear analogue and suggests that in this case the dinuclear complexes is a true bis-intercalator.

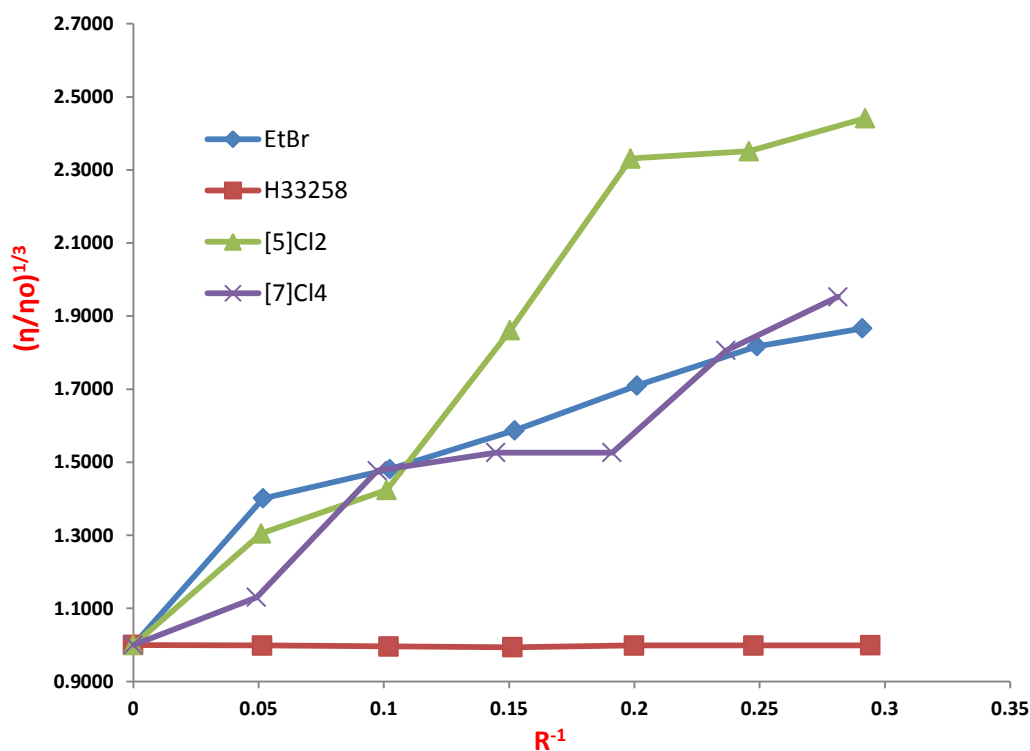


**Figure 3.17:** plot of relative viscosity  $(\eta/\eta_0)^{1/3}$  of CT-DNA versus  $R^{-1}$  ( $R = [\text{DNA}]/[\text{Compound}]$ ) upon addition of EtBr, H33258, [5]Cl<sub>2</sub> and [7]Cl<sub>4</sub>. Experimental conditions: 5 mM Tris, 25 mM NaCl, pH 7.4 at 26°C.

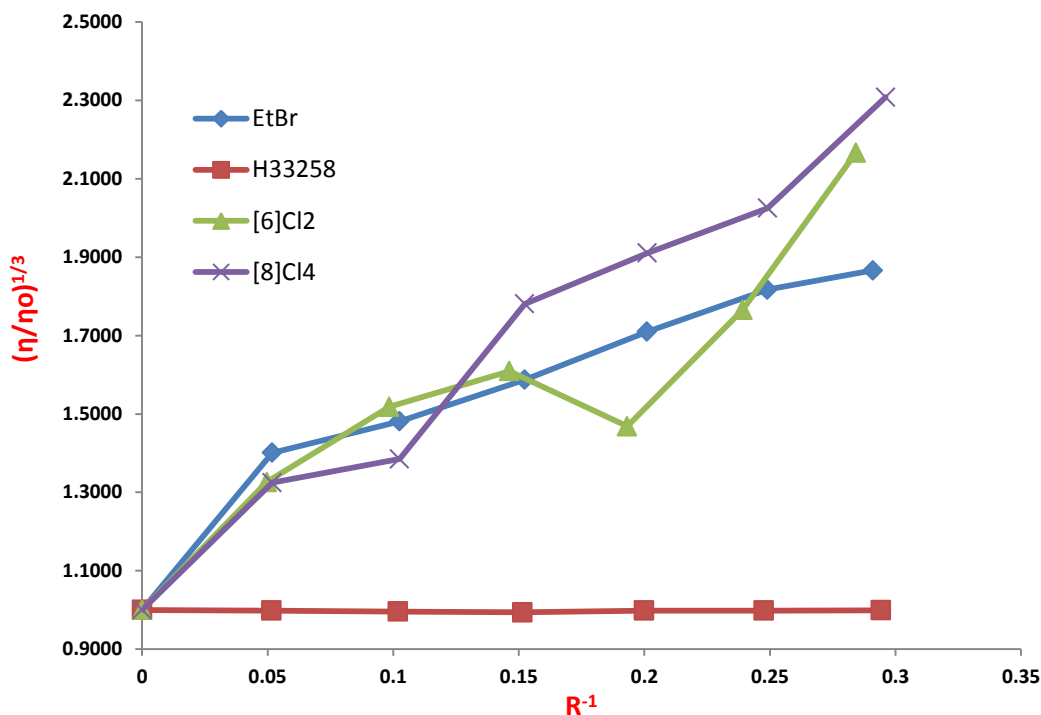


**Figure 3.18:** Plot of relative viscosity  $(\eta/\eta^0)^{1/3}$  of CT-DNA versus  $R^{-1}$  ( $R = [\text{DNA}]/[\text{Compound}]$ ) upon addition of EtBr, H33258, [6]Cl<sub>2</sub> and [8]Cl<sub>4</sub>. Experimental conditions: 5 mM Tris, 25 mM NaCl, pH 7.4 at 26°C.

In this chapter, the synthesis and characterization by UV-visible spectroscopy, luminescence titrations, <sup>1</sup>H NMR and mass spectrometry of four new ruthenium complexes, [Ru(tpm)(dppz)(μ-L'1)](PF<sub>6</sub>)<sub>2</sub> [5], [Ru(tpm)(dppz)(μ-L'2)](PF<sub>6</sub>)<sub>2</sub> [6], [{Ru(tpm)(dppz)}<sub>2</sub>(μ-L'1)](PF<sub>6</sub>)<sub>4</sub> [7] and [{Ru(tpm)(dppz)}<sub>2</sub>(μ-L'2)](PF<sub>6</sub>)<sub>4</sub> [8], have been investigated and their binding with CT-DNA has been studied. Absorption titrations showed ~10nm bathochromic shift of the absorption band at ~ 278 nm along with significant hypochromicity. Viscosity measurements confirmed that the complex-DNA interaction is through intercalation. These results confirm that both mono and di complexes are avid binders of CT DNA and that the dipyrrophenazine ligand on them is engaged in the intercalative interaction with DNA. Furthermore, in comparison with complexes [1-4] the interactions of complexes [5-8] with DNA are stronger. Of particular note is the fact that the dinuclear complexes show enhanced binding compared to their mononuclear analogues. Indeed, the viscosity measurement presents clear evidence that [8]Cl<sub>4</sub> is in fact a bis-intercalator.

The results described in this study highlight how the nature and positioning of functional groups within the complexes affect binding affinities. Results from the isothermal titration calorimetry for complexes [1-4] and [5-8] are discussed in chapter 4.

## References

- (1) Waywell, P.; Gonzalez, V.; Gill, M. R.; Adams, H.; Meijer, A. J.; Williamson, M. P.; Thomas, J. A.: *Chemistry-A European Journal* **2010**, 16, 2407-2417.
- (2) Fees, J.; Kaim, W.; Moscherosch, M.; Matheis, W.; Klima, J.; Krejcik, M.; Zalis, S.: *Inorganic Chemistry* **1993**, 32, 166-174.
- (3) Shahabadi, N.; Mohammadi, S.; Alizadeh, R.: *Bioinorganic Chemistry and Applications* **2011**, 2011.
- (4) Dougherty, G.; Pilbrow, J. R.: *International Journal of Biochemistry* **1984**, 16, 1179-1192.
- (5) Metcalfe, C.; Adams, H.; Haq, I.; Thomas, J. A.: *Chemical Communications* **2003**, 1152-1153.
- (6) Wolfe, A.; Shimer Jr, G. H.; Meehan, T.: *Biochemistry* **1987**, 26, 6392-6396.
- (7) Foxon, S. P.; Metcalfe, C.; Adams, H.; Webb, M.; Thomas, J. A.: *Inorganic Chemistry* **2007**, 46, 409-416.
- (8) Cohen, G.; Eisenberg, H.: *Biopolymers* **1969**, 8, 45-55.
- (9) Satyanarayana, S.; Dabrowiak, J. C.; Chaires, J. B.: *Biochemistry* **1992**, 31, 9319-9324.

## Chapter 4

### *Isothermal Titration Calorimetry*

---

4.1 Introduction.....	101
4.2 General principles of the ITC experimental setup .....	101
4.3 Titration curve and binding constant .....	105
4.4 ITC calibration .....	107
4.5 Heat of dilution .....	108
4.6 Data analysis .....	108
4.7 ITC studies .....	109
4.7.1 Set one: Complexes [1]Cl <sub>2</sub> , [2]Cl <sub>2</sub> , [3]Cl <sub>4</sub> and [4]Cl <sub>4</sub> titrated into CT-DNA solution. .....	109
4.7.2 Set two: Complexes [5]Cl <sub>2</sub> , [6]Cl <sub>2</sub> , [7]Cl <sub>4</sub> and [8]Cl <sub>4</sub> titrated into CT-DNA solution. .....	117
References.....	122

## 4.1 Introduction

In recent years isothermal titration calorimetry (ITC) has become an increasingly popular technique and has found wide-ranging application in the study of chemical binding phenomena, especially biochemical processes. ITC is the only technique currently available that directly measures enthalpy changes associated with interactions. ITC can be used to measure the binding affinity ( $K_a$ ), enthalpy changes ( $\Delta H$ ), entropy changes ( $\Delta S$ ) and binding stoichiometry ( $n$ ) of the interaction between two or more molecules in solution.

## 4.2 General principles of the ITC experimental setup

A typical ITC instrument consists of two identical cells, one is a reference containing the same solvent used in the sample cell (for aqueous solution the reference cell is filled with distilled water) and the other, a sample cell (working cell) containing the host (macromolecule) for the interaction and the syringe is filled with the guest, also dissolved in the same solvent. Both cells are maintained at constant temperature within an insulated, adiabatic system.

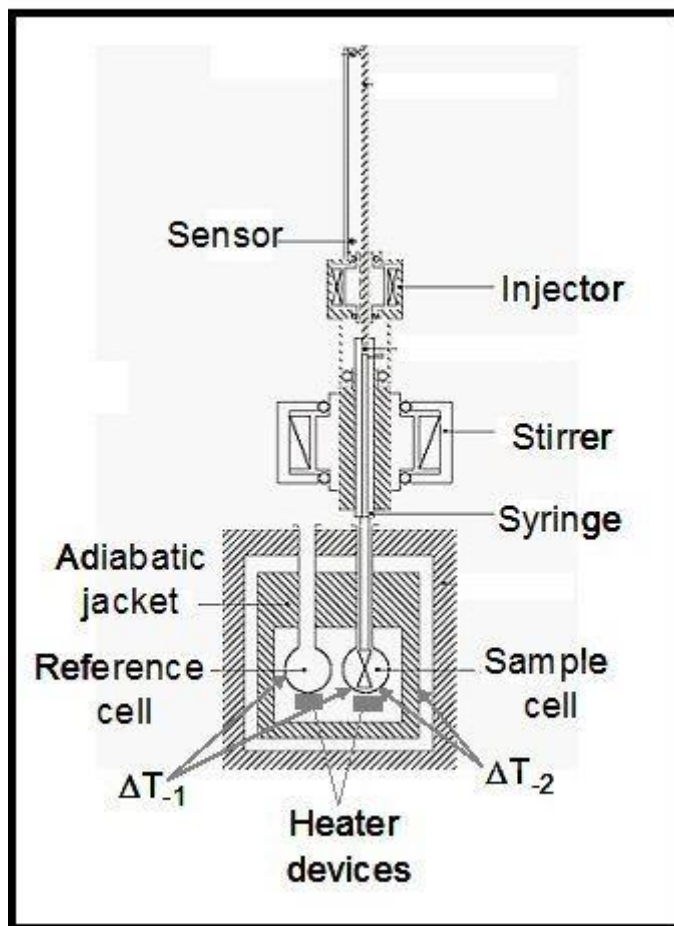


**Figure 4.1:** ITC experimental schematic

After equilibration the syringe injects a certain volume of guest solution into the host solution at prefixed time intervals. Upon making an injection of the guest, heat is either absorbed or released. These tiny heat effects produce a difference in temperature between the cells that is detected by semi-conductor thermopiles, and the calorimeter applies thermal power to return the system to thermal equilibrium. The energy difference between the two cells for each injection is measured and integrated and the process repeated until eventually the saturation point of the titration is reached.

For a reaction of 1:1 stoichiometry, the following equation describes the binding equilibrium (where M is a macromolecule and L represents a ligand):



Equation 4.1

$$K_a = \frac{[ML]}{[M][L]}$$

Equation 4.2

At any given time, the total concentration of either the macromolecule or the ligand can be written

$$[M]_{tot} = [M] + [ML]$$

Equation 4.3

$$[L]_{tot} = [L] + [ML]$$

Equation 4.4

Using equations 4.3 and 4.4 into equation 4.2, this expands to give the following equation.

$$K_a = \frac{[ML]}{[M]_{tot}[L]_{tot} - [ML]([M]_{tot} + [L]_{tot}) + [ML]^2}$$

Equation 4.5

$$[ML] = \frac{[M]_{tot} + [L]_{tot} + \frac{1}{K_a} - \sqrt{([L]_{tot} + [M]_{tot} + \frac{1}{K_a})^2 - 4[M]_{tot}[L]_{tot}}}{2}$$

Equation 4.6

Differentiation and rearrangement of 4.6 gives the following quadratic equation.

$$\frac{d[ML]}{d[L]_{tot}} = \frac{1}{2} + \frac{[M]_{tot} - \left( \frac{[L]_{tot} + [M]_{tot} + \frac{1}{Ka}}{2} \right)}{\sqrt{\left( [L]_{tot} + [M]_{tot} + \frac{1}{Ka} \right)^2 - 4[L]_{tot}[M]_{tot}}}$$

**Equation 4.7**

Since, for each injection, the heat absorbed or released is proportional to the change in [ML]:

$$dq = V \cdot \Delta H^\circ \cdot d[ML]$$

**Equation 4.8**

Where  $V$  is the sample cell volume and  $\Delta H^\circ$  is the molar enthalpy of the binding.

Therefore substitution of **4.8** into **4.7**:

$$\frac{1}{V_0} \left( \frac{dq}{d[L]_{tot}} \right) = \Delta H^\circ \left\{ \frac{1}{2} + \frac{[M]_{tot} - \left( \frac{[L]_{tot} + [M]_{tot} + \left( \frac{1}{Ka} \right)}{2} \right)}{\sqrt{\left( [L]_{tot} + [M]_{tot} + \frac{1}{Ka} \right)^2 - 4[L]_{tot}[M]_{tot}}} \right\}$$

**Equation 4.9**

Binding curves can be generated using equation **4.9**, and therefore the binding constant and enthalpies for the interaction can be calculated. The free energy change for a reaction can be calculated from the equilibrium constant:

$$\Delta G^\circ = -RT \ln Ka$$

**Equation 4.10**

Where  $\Delta G^\circ$  is the Gibb's free energy, R is the gas constant ( $R = 1.98 \times 10^{-3}$  kcal/mol.deg) and T the temperature in Kelvin ( $T(K) = 273 + T(^\circ C)$ ). Finally, knowing  $\Delta G^\circ$  and  $\Delta H^\circ$ ,  $\Delta S^\circ$  can be calculated by:

$$\Delta G^\circ = \Delta H^\circ - T\Delta S^\circ$$

**Equation 4.11**

### 4.3 Titration curve and binding constant

The shape of binding isotherm produced in the ITC experiment depends on the Wiseman  $c$ -parameter:<sup>1-3</sup> Provided that concentration is expressed as the total concentration of binding sites, the shape of a binding curve for macromolecules with  $n$  identical sites will be exactly the same as for a molecule with a single binding site having the same  $Ka$  value. To account for this, the  $c$  parameter is defined as

$$c = Ka[M]_{tot}n$$

**Equation 4.12**

The importance of this is that the precision with which a titration curve can be simulated depends on the value of  $c$  without using actual numerical values for  $n$ ,  $Ka$ ,  $\Delta H^\circ$ ,  $[M]_{tot}$  or  $[L]_{tot}$ .

A high value of  $c$  can result from a high concentration of macromolecule/ligand and/or a high value of  $Ka$ . Typical curves showing the influence of values of  $Ka$  are shown in **Figure 4**.

Very large  $c$  values ( $c = \infty$ ) lead to tight binding and the isotherm curve is rectangular in shape with the height corresponding directly to  $\Delta H^\circ$  and the sharp drop occurring exactly at the stoichiometric equivalence point  $n$  in the molar ratio. As  $c$  is decreased by reducing  $[M]_{\text{tot}}$  and keeping the other parameters constant, the drop near the equivalence point becomes very broad transitions and the intercept at the Y-axis becomes lower than the true  $\Delta H^\circ$ .

By deconvolution from the total area under the curve and its shape, this parameter is easily obtained. Very weak binding (cf.  $c = 0.1$ ) yields a nearly horizontal trace, which again like very tight binding yields little information on the precise value of  $Ka$ . The shape of the isotherm is only sensitive to  $c$  values in the range  $1 \leq c \leq 1000$ , corresponding to binding of intermediate strength. This range has been referred to as the “experimental K window”. When available, the middle of the window from  $c = 5$  to 500 is ideal for measuring  $Ka$ . Therefore, in general, the concentration of the metal complex in the syringe was kept around five times higher than that of the concentration of the DNA solution in the working cell.<sup>4</sup>

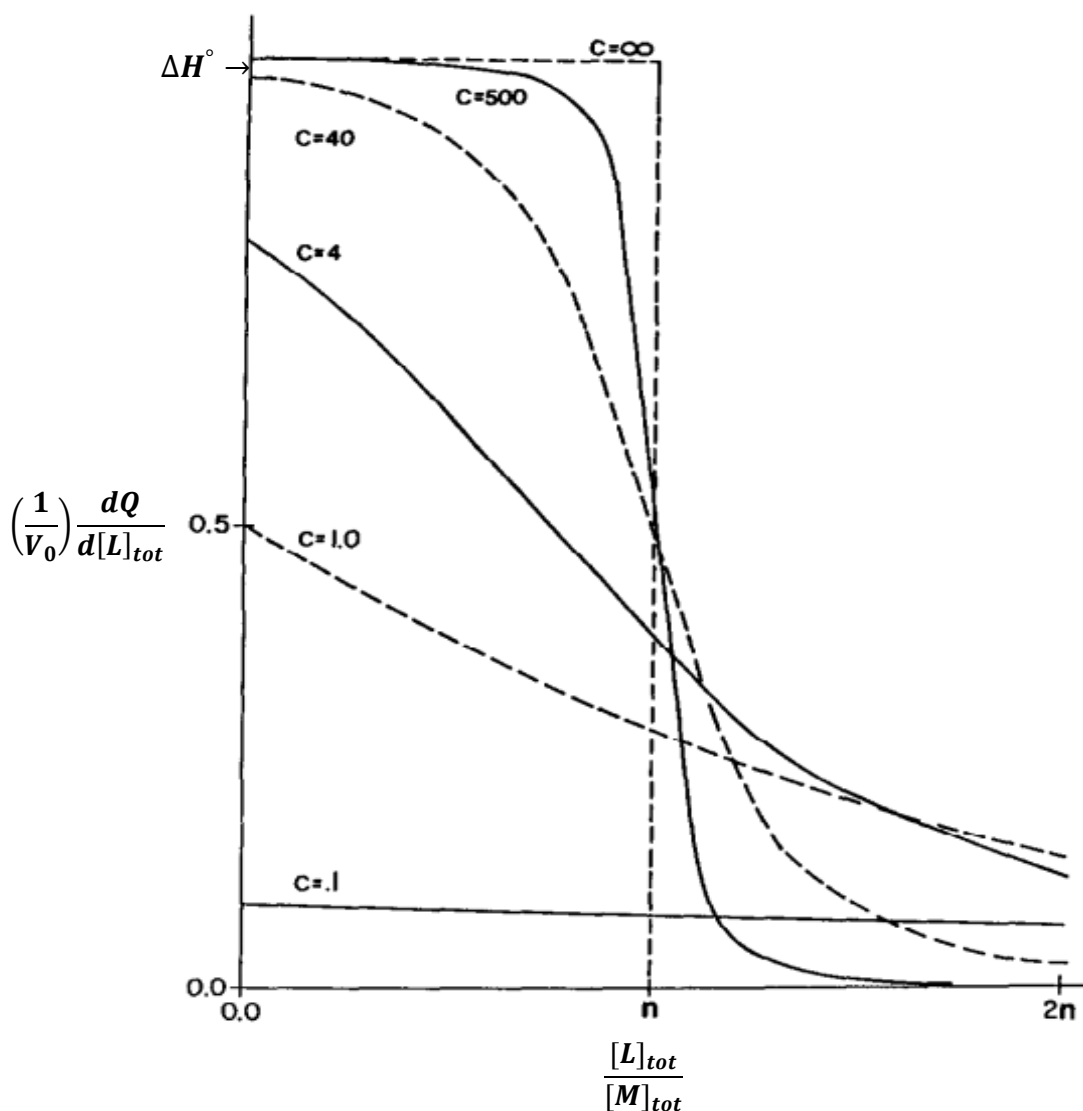


**Figure 4.2:** Simulated binding isotherms for various values of the parameter  $c$

## 4.4 ITC calibration

Calorimetric techniques are uniquely exposed to systematic experimental errors. These errors are frequently affected by contributions from process accompanying the interaction being investigated. Furthermore, errors such as evaporation, condensation and incomplete mixing are difficult to control and include. Calibration errors are another possible contribution to systematic errors. Unfortunately, although there are several methods available, there is not commonly accepted method of calibration for ITC. Electrical calibration is the most commonly used one, here the calorimetric signal is standardised by using an internal heater

provided with most ITC instruments and it releases a pulse of an accurately known quantity of heat by converting the electrical signal to power output. Other calibration methods used involve acid-base interactions such as addition of standardised aqueous HCl to NaOH solutions.<sup>5</sup>

## 4.5 Heat of dilution

The ITC data from a titration can require some correction before analysis. These background heats are measured in separate experiments. For example, buffer is injected into buffer to determine if any interaction occurs which may effect in the reaction. Ligand is also injected into buffer to measure the heat of dilution of the ligand and to confirm that heat changes are uniform throughout the titration process. Finally, buffer is injected into the macromolecular hosts. After these corrections, the isotherm can be fit to an appropriate model to obtain the binding constant and the stoichiometry.

## 4.6 Data analysis

The model required to fit the data depends on the system of interest. The widely used Origin software typically includes functions describing equilibria for which analysis of calorimetric data to multiple independent binding sites is well established. More complex models, such as multiple co-operative binding events, require more independent variables and although apparent improvement of the fits can be accomplished, this does not mean that the most suitable model has been chosen. It should be noted that enthalpy is the only parameter that is model independent. Often in cases involving biological molecules more than one independent interaction, such as several coupled equilibria, can occur. These types of binding can be accommodated by software supplied with most current instrumentation and thus provide the enthalpies and stoichiometries as for the single site model. Usually performing the titrations at different temperatures will confirm the presence of two or more independent binding events.<sup>6</sup>

## 4.7 ITC studies

### 4.7.1 Set one: Complexes [1]Cl<sub>2</sub>, [2]Cl<sub>2</sub>, [3]Cl<sub>4</sub> and [4]Cl<sub>4</sub> titrated into CT-DNA solution.

To further characterise the interaction of the complexes with nucleic acids, the binding thermodynamics of the first set of ruthenium complexes [1-4] with CT-DNA at 25 °C were determined by ITC. This work was carried out at the School of Chemistry in Cardiff University under the supervision of Dr Neik Buurma.

Blank titrations were performed before titrations of ruthenium complexes solutions into CT-DNA solution were carried out. In these blanks, each of the four ruthenium complexes were titrated separately into tris buffer solution, to establish whether the metal complexes exhibited any interactions with the buffer. No measureable heat was detected in any of the cases, other than that due to dilution of the ruthenium complexes. Furthermore, in similar blank titrations in which buffer solution was titrated into DNA solution, no heat was detected due to interactions between the CT-DNA and the buffer.

In these titrations the values for the reaction stoichiometric ratios,  $K_b$  and  $\Delta H^\circ$  determined from simulation and  $\Delta S^\circ$  obtained by calculation from  $K_b$ , and  $\Delta H^\circ$  are summarised in **Table 4.1, 4.2 and 4.3** and discussed in a full details later.

A typical ITC trace that results from the interaction between complex [1]Cl<sub>2</sub>, and CT-DNA can be seen below.

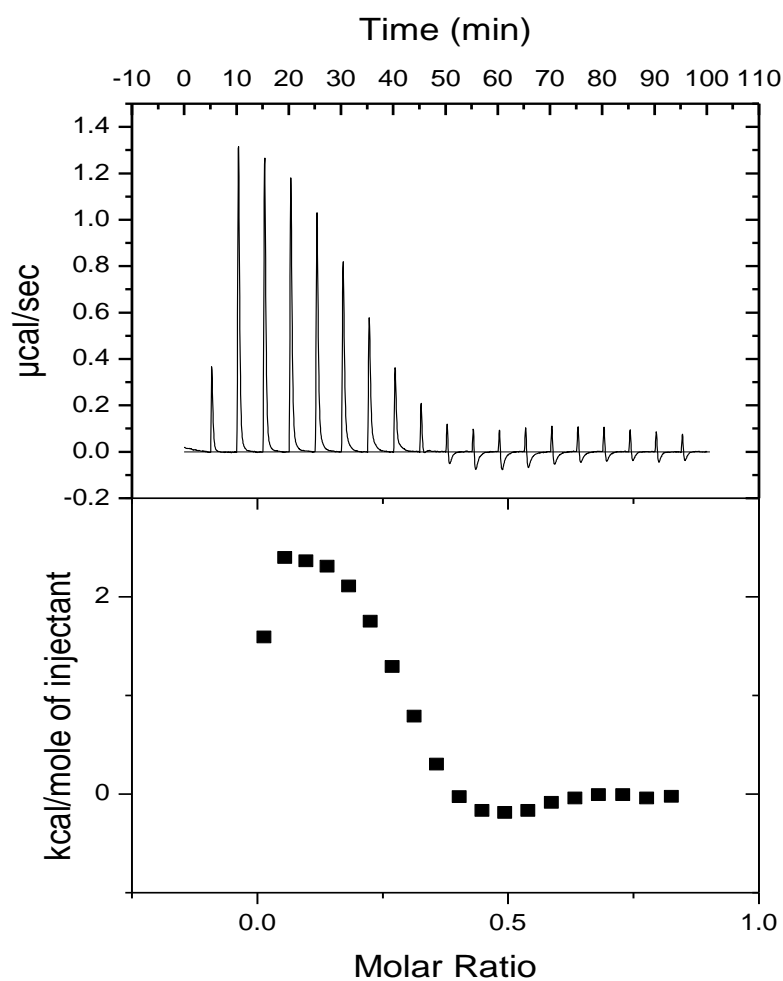


**Figure 4.3:** ITC raw data for the interaction of [1]Cl<sub>2</sub> (1.00 mM) with CT-DNA (0.25 mM) in 5mM Tris, 25mM NaCl, pH 7.4 at 25 °C.

This output is consistent with an endothermic reaction and is simulated as a single binding event. In this case, the interaction of this complex with CT-DNA showed a positive change in enthalpy ( $2.5 \text{ kcal mol}^{-1}$ ) and positive entropy indicating that the interaction is entropically driven. The binding constant obtained by ITC was  $6.40 \times 10^5 \text{ M}^{-1}$ ,  $\Delta H^\circ = 2.59 \text{ kcal mol}^{-1}$ ,  $T\Delta S^\circ = 10.50 \text{ kcal mol}^{-1}$  and the site size was 3.77 bp per binding event. Hydrophobic interactions are usually characterised by small enthalpy changes and large entropy changes.<sup>7</sup> Electrostatic interactions are more difficult to determine, but the interaction of cations with DNA is usually entropically driven with small unfavourable changes in enthalpy.<sup>8</sup>

The thermodynamic data for the interaction of [1]Cl<sub>2</sub> with CT-DNA is shown in the table below.

<i>Complex</i>	$K_b/M(bp)^{-1}$	<i>S/bp</i>	$\Delta H/kcal\ mol^{-1}$	$\Delta G/kcal\ mol^{-1}$	$-T\Delta S/kcal\ mol^{-1}$
[1]Cl <sub>2</sub>	$6.40 \times 10^5$	3.77	2.59	-7.91	-10.50

**Table 4.1:** ITC thermodynamic data for the interaction of [1]Cl<sub>2</sub> with CT-DNA at 25°C

When the differential heat flow is plotted against molar ratio for titration of a 1.00 mM solution of [1]Cl<sub>2</sub> into a 0.25 mM CT-DNA solution, then a comparison curve between experimental and calculated heat of the binding interaction can be constructed. The graph shows almost an identical agreement between the experimental and calculated values of the integrated heat effects against molar ratio.

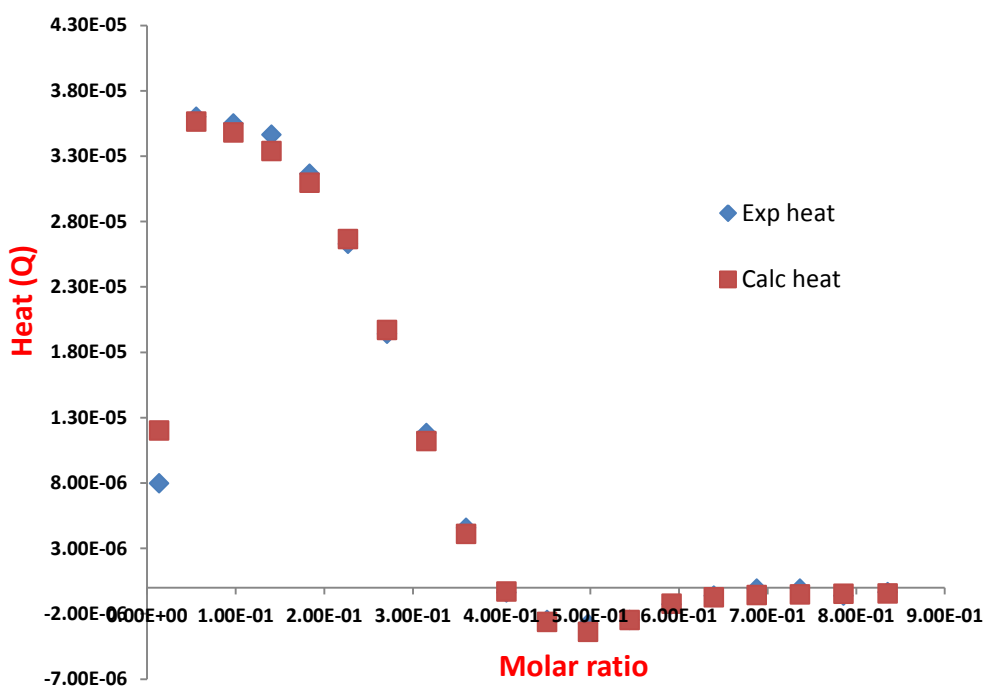


**Figure 4.4:** Integrated heat effects for titration of a 1.00 mM solution of [1]Cl<sub>2</sub> into a 0.25 mM CT-DNA

In the interaction of [2]Cl<sub>2</sub> and [3]Cl<sub>4</sub> with CT-DNA, two modes of binding ( $K_{b1}$  and  $K_{b2}$ ) were distinguished (**Figure 4.5**), both showed small positive enthalpies and positive changes in entropy for the first event binding, indicating that the reaction is also entropic favoured.

The observation of two binding modes is in agreement with the data obtained from integrated heat effects which showed two different bindings stoichiometries for the interaction of [2]Cl<sub>2</sub> and [3]Cl<sub>4</sub> with CT-DNA (**Figure 4.6**). The affinities of these complexes with DNA for the first events are in the order of  $8.95 \times 10^5 \text{ M}^{-1}$  and  $4.49 \times 10^5 \text{ M}^{-1}$  and the second events show binding affinities in  $1.23 \times 10^5 \text{ M}^{-1}$  and  $3.22 \times 10^5 \text{ M}^{-1}$  ranges for the complexes [2]Cl<sub>2</sub> and [3]Cl<sub>4</sub> respectively.

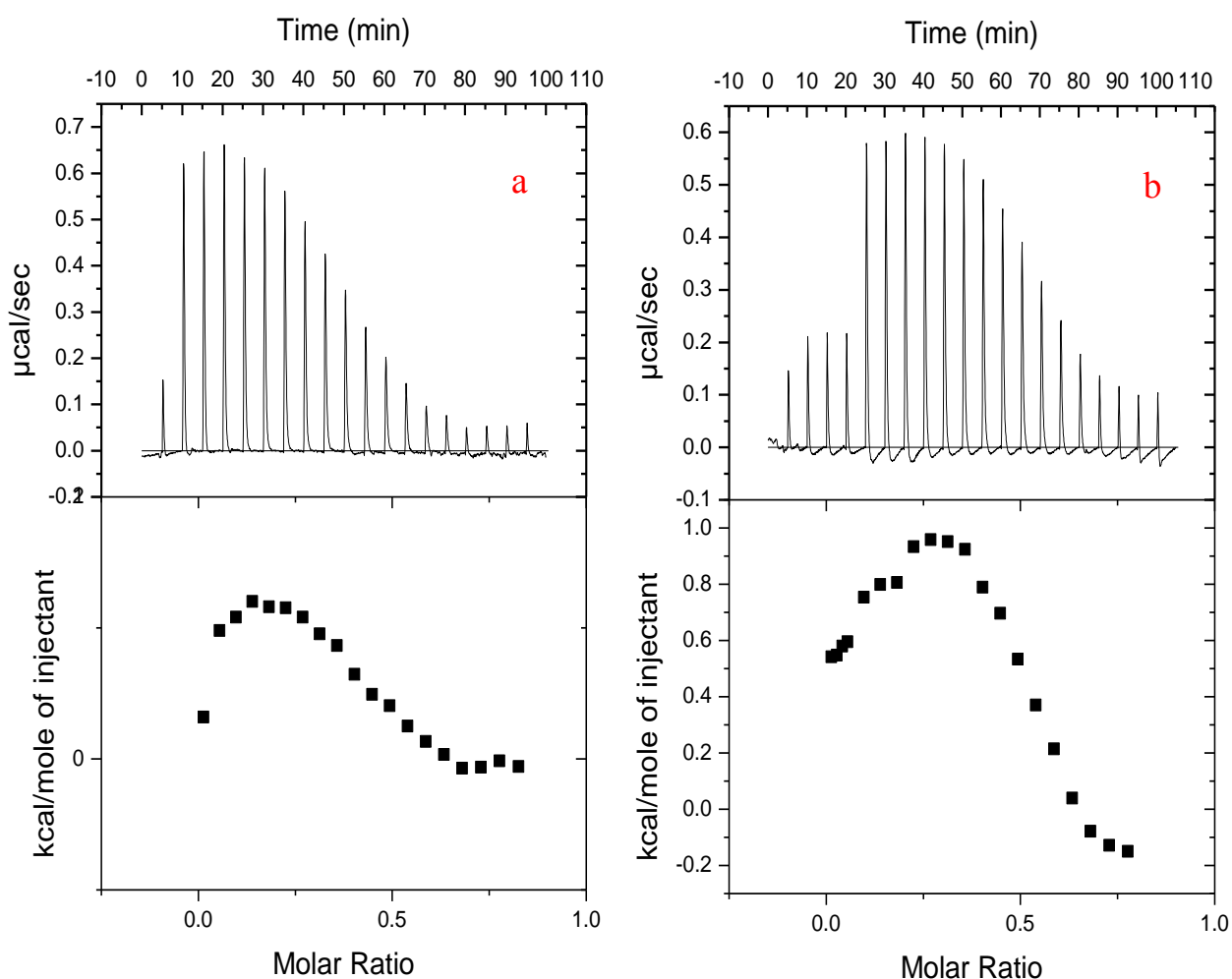


**Figure 4.5:** ITC raw data for the interaction of [2]Cl<sub>2</sub> (1.00 mM) (a) and [3]Cl<sub>4</sub> (1.00 mM) (b) with CT-DNA and (0.25 mM) in 5mM Tris, 25mM NaCl, pH 7.4 at 25 °C.

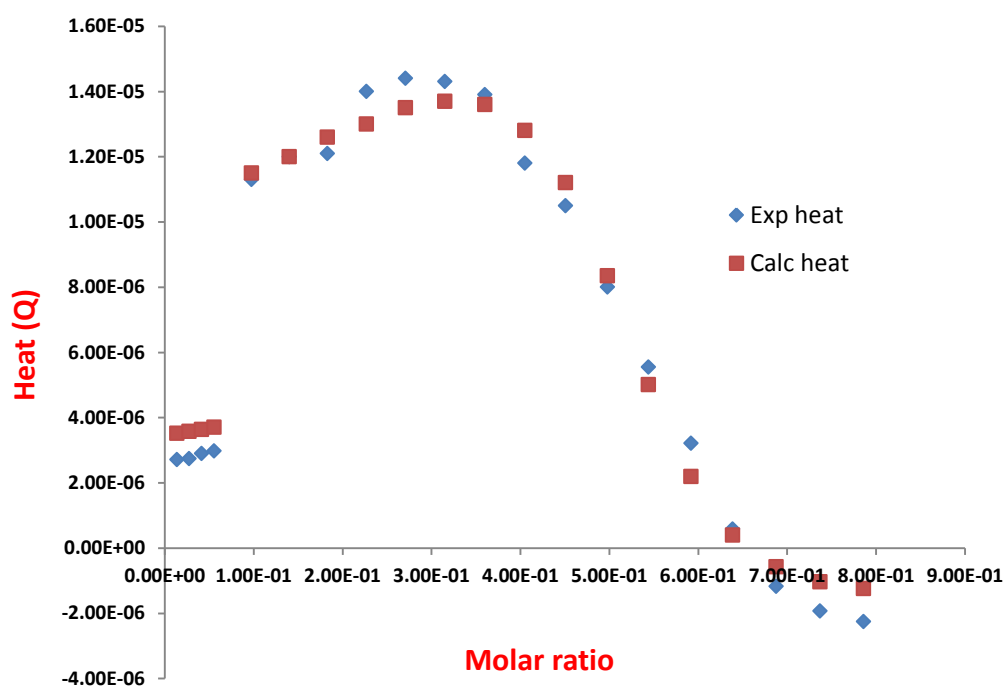
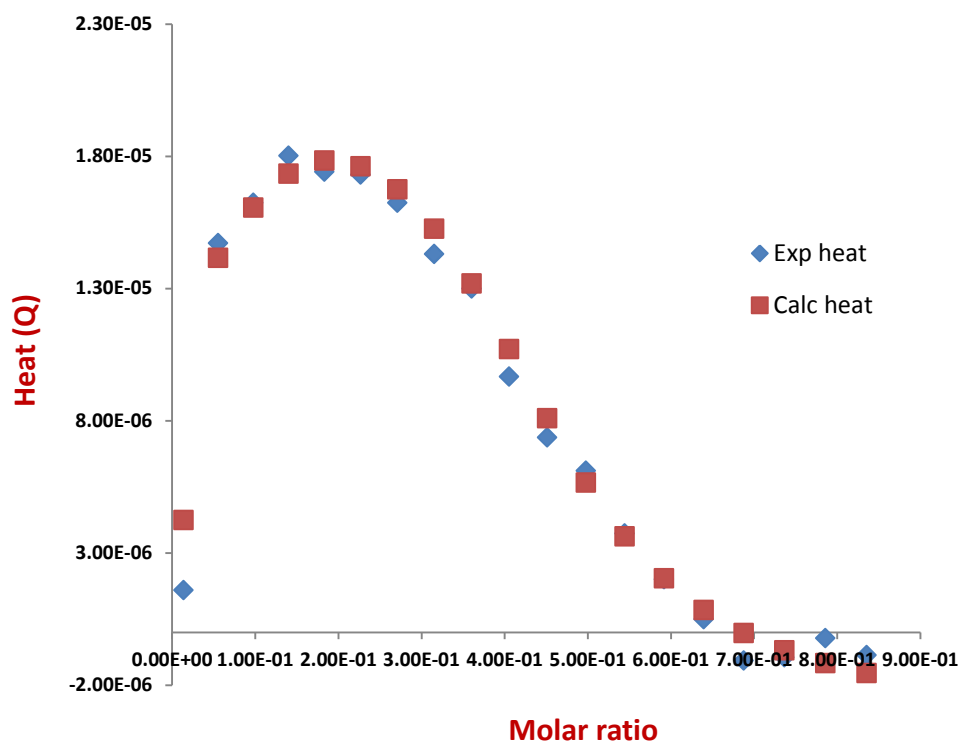


**Figure 4.6:** Integrated heat effects for titration of a 1.00 mM solution of [2]Cl<sub>2</sub> (top) and [3]Cl<sub>4</sub> (bottom) into a 0.25 mM CT- DNA

The second binding events of [2]Cl<sub>2</sub> and [3]Cl<sub>4</sub> are endothermic in nature with a positive enthalpies and positive entropies term. However, [3]Cl<sub>4</sub> showed larger positive enthalpy and entropy, thermodynamic parameters for both complexes [2]Cl<sub>2</sub> and [3]Cl<sub>4</sub> are shown below (Table 4.2). Both binding events for complexes [2]Cl<sub>2</sub> and [3]Cl<sub>4</sub> are entropically favoured.

Complex	[2]Cl <sub>2</sub>	[3]Cl <sub>4</sub>
K <sub>b1</sub> /M(bp) <sup>-1</sup>	8.95 × 10 <sup>5</sup>	4.49 × 10 <sup>5</sup>
S1/bp	12.77	1.99
ΔH1/kcal mol <sup>-1</sup>	0.59	0.47
ΔG1/kcal mol <sup>-1</sup>	-8.08	-7.67
(-TΔS1)/kcal mol <sup>-1</sup>	-8.68	-8.68
K <sub>b2</sub> /M(bp) <sup>-1</sup>	1.23 × 10 <sup>5</sup>	3.22 × 10 <sup>5</sup>
S2/bp	2.83	20.7
ΔH2/kcal mol <sup>-1</sup>	1.84	15.8
ΔG2/kcal mol <sup>-1</sup>	-6.91	-7.48
(-TΔS2)/kcal mol <sup>-1</sup>	-8.77	-23.28

**Table 4.2:** ITC thermodynamic data for the interaction of [2]Cl<sub>2</sub> and [3]Cl<sub>4</sub> with CT-DNA at 25°C

Again, the thermodynamic parameters obtained for [1],[2] and [3] are in good agreement with the data obtained by Chaires *et al.*<sup>9</sup> for the interaction of Δ- and Λ- [Ru(phen)<sub>2</sub>(dppz)]<sup>2+</sup> with CT-DNA at 25 °C, where interactions are entropically driven with small positive changes in enthalpy, which is typical for hydrophobic interactions (as a consequence of transferring the dppz ligand from the aqueous solution to inside the DNA), release of counter ions and changes in hydration.

Calorimetric data for the binding of [4]Cl<sub>4</sub> to CT-DNA revealed one distinct binding event (Figure 4.7). Surprisingly, the titration curve for binding of [4]Cl<sub>4</sub> to CT-DNA was exothermic, resulting in negative peaks in the plots of power versus time and a ΔH° of -9.45

$kcal\ mol^{-1}$ , as well as a much reduced entropic term of  $T\Delta S^\circ = -2.66\ kcal\ mol^{-1}$  resulting in a binding affinity of  $9.63 \times 10^4\ M^{-1}$ . This profile suggests that the complex is stabilized by hydrogen bonding as well as van der Waals interactions.

The thermodynamic profile for the interaction of [4]Cl<sub>4</sub> with CT-DNA is shown in the table below.

<i>Complex</i>	$K_b/M(bp)^{-1}$	<i>S/bp</i>	$\Delta H/kcal\ mol^{-1}$	$\Delta G/kcal\ mol^{-1}$	$T\Delta S/kcal\ mol^{-1}$
[4]Cl <sub>4</sub>	$9.63 \times 10^4$	2.4	-9.45	-6.79	-2.66

**Table 4.3:** ITC thermodynamic data for the interaction of [4]Cl<sub>4</sub> with CT-DNA at 25°C

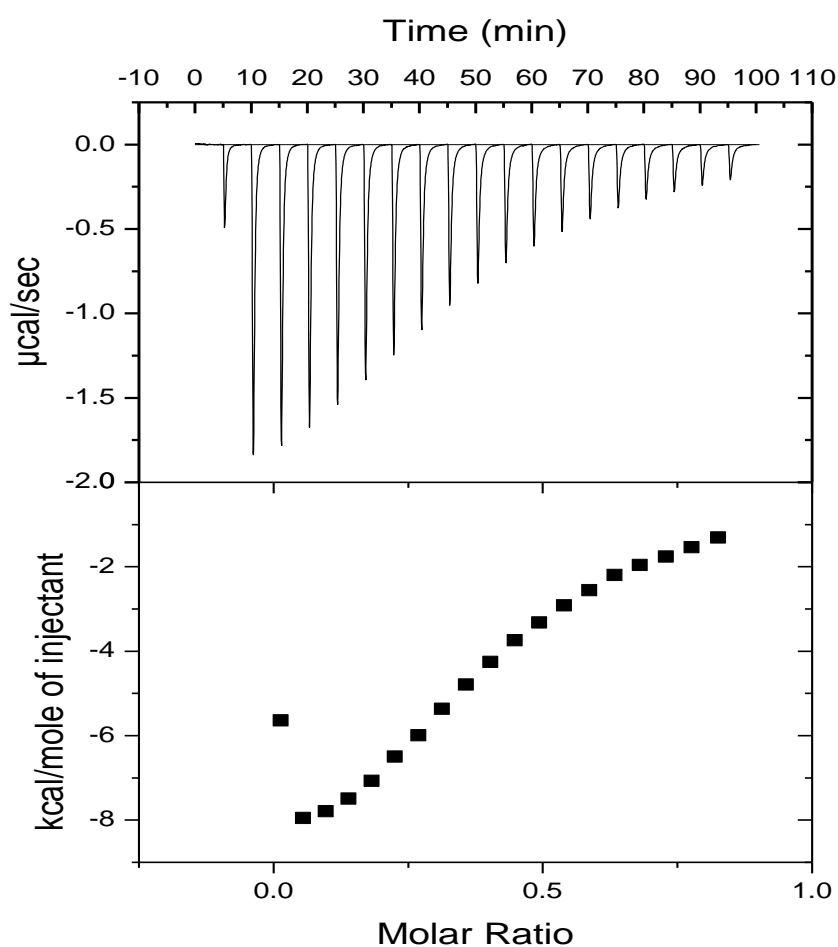


**Figure 4.7:** ITC raw data for the interaction of [4]Cl<sub>4</sub> (1.00 mM) with CT-DNA (0.25 mM) in 5mM Tris, 25mM NaCl, pH 7.4 at 25 °C.

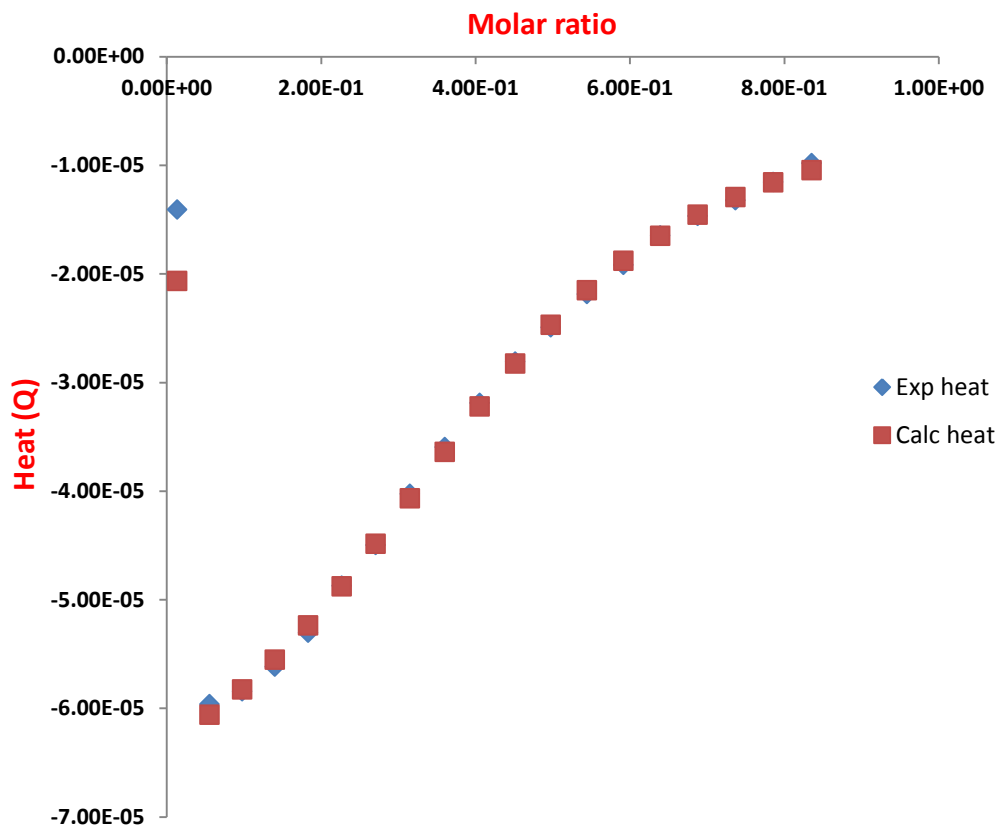


**Figure 4.8:** Integrated heat effects for titration of a 1.00 mM solution of [4]Cl<sub>4</sub> into a 0.25 mM CT-DNA

Comparing the binding affinities of the complexes [1-4] produced by ITC show that the monometallic complexes [1]Cl<sub>2</sub> and [2]Cl<sub>2</sub> bind to CT-DNA more strongly than their analogous dinuclear complexes [3]Cl<sub>3</sub> and [4]Cl<sub>4</sub>. Binding parameters obtained from ITC are in good agreements with the data obtained from titration spectroscopies and viscosity measurements.

#### 4.7.2 Set two: Complexes [5]Cl<sub>2</sub>, [6]Cl<sub>2</sub>, [7]Cl<sub>4</sub> and [8]Cl<sub>4</sub> titrated into CT-DNA solution.

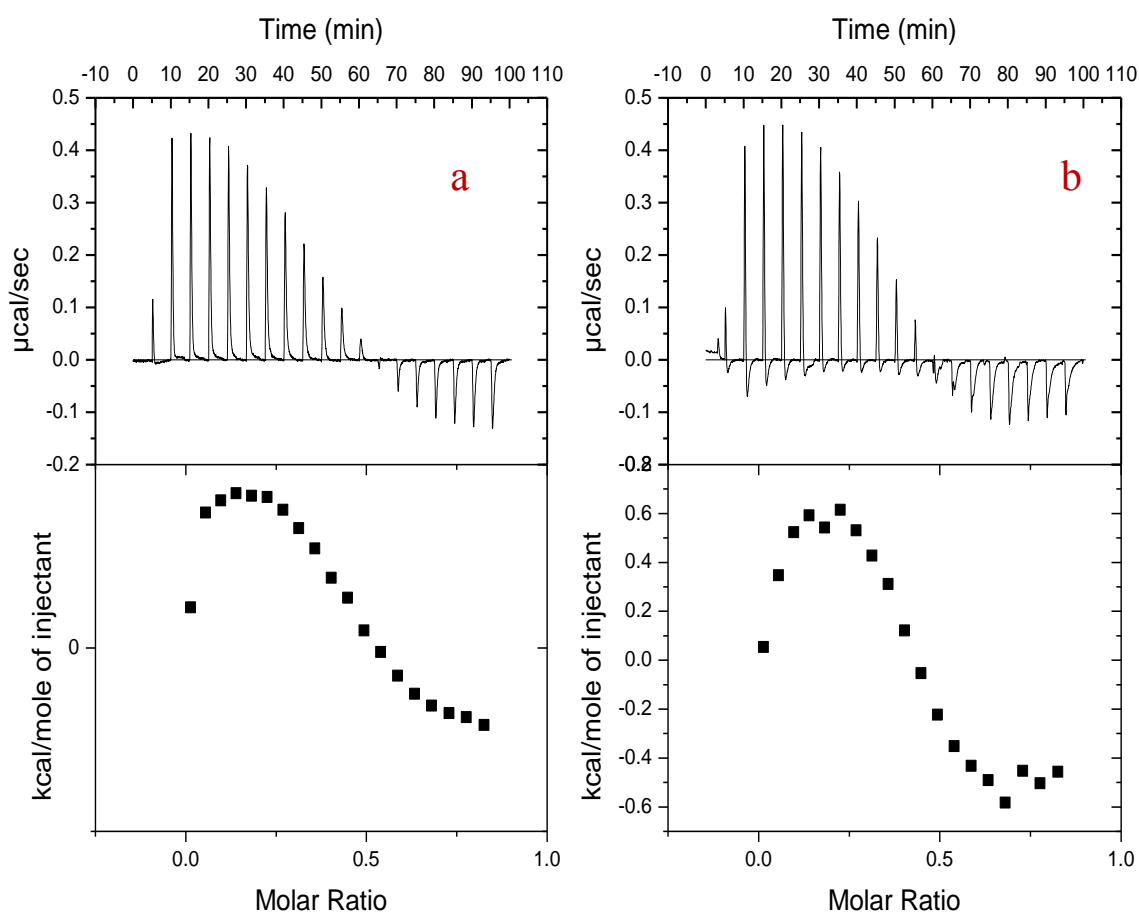
The thermodynamics of the binding of [5]Cl<sub>2</sub>, [6]Cl<sub>2</sub>, [7]Cl<sub>4</sub> and [8]Cl<sub>4</sub> with CT-DNA at 25 °C were also studied. A comparison of the enthalpic and entropic contributions to binding is shown in **table 4.4**.

Complex	[5]Cl <sub>2</sub>	[6]Cl <sub>2</sub>	[7]Cl <sub>4</sub>	[8]Cl <sub>4</sub>
K <sub>b1</sub> /M(bp) <sup>-1</sup>	1.74 × 10 <sup>5</sup>	7.30 × 10 <sup>6</sup>	2.15 × 10 <sup>5</sup>	4.07 × 10 <sup>7</sup>
S1/bp	7.81	30.03	2.10	3.34
ΔH1/kcal mol <sup>-1</sup>	0.22	0.27	0.917	-0.14
ΔG1/kcal mol <sup>-1</sup>	-7.14	-9.35	-7.24	-10.37
(-TΔS1)/kcal mol <sup>-1</sup>	-7.37	-9.63	-8.16	-10.23
K <sub>b2</sub> /M(bp) <sup>-1</sup>	9.35 × 10 <sup>4</sup>	3.87 × 10 <sup>5</sup>	.....	3.39 × 10 <sup>5</sup>
S2/bp	2.94	2.65	.....	3.50
ΔH2/kcal mol <sup>-1</sup>	2.39	1.24	.....	-0.64
ΔG2/kcal mol <sup>-1</sup>	-6.77	-7.61	.....	-7.53
(-TΔS2)/kcal mol <sup>-1</sup>	-9.16	-8.85	.....	-6.89

**Table 4.4:** ITC thermodynamic data for the interactions of [5]Cl<sub>2</sub>, [6]Cl<sub>2</sub>, [7]Cl<sub>4</sub> and [8]Cl<sub>4</sub> with CT-DNA at 25°C

In the interactions of the complexes [5-8] with CT-DNA, two modes of binding were seen (Figure 4.9).

The interaction of most of these complexes with CT-DNA for the first event show small positive changes in enthalpy (from 0.22 kcal mol<sup>-1</sup> to 0.765 kcal mol<sup>-1</sup>) and positive entropies indicating that the interactions are entropically driven. The exception being complex [8]Cl<sub>4</sub> which shows a small negative enthalpy and positive entropy indicating that the interaction is both enthalpically and entropically favoured. The binding affinities of these complexes are reasonably large with values 1.74 × 10<sup>5</sup> M<sup>-1</sup>, 7.30 × 10<sup>6</sup> M<sup>-1</sup> and 4.07 × 10<sup>7</sup> M<sup>-1</sup> for [5],[6] and [8] respectively and corresponding binding sites of 7.81, 30.03 and 3.34. As mentioned before, hydrophobic interactions are usually characterised by small enthalpy changes and large entropy changes<sup>10</sup> and electrostatic interaction are usually entropically driven with small unfavourable changes in enthalpy.<sup>4</sup> In contrast, the titration of [7]Cl<sub>4</sub> was best fitted to a one set of site model, indicating one binding event. The thermodynamic profile of [7]Cl<sub>4</sub> binding to CT-DNA showed a small positive enthalpy (0.917 kcal mol<sup>-1</sup>) and positive change in entropy, indicating that the reaction is entropically favoured.



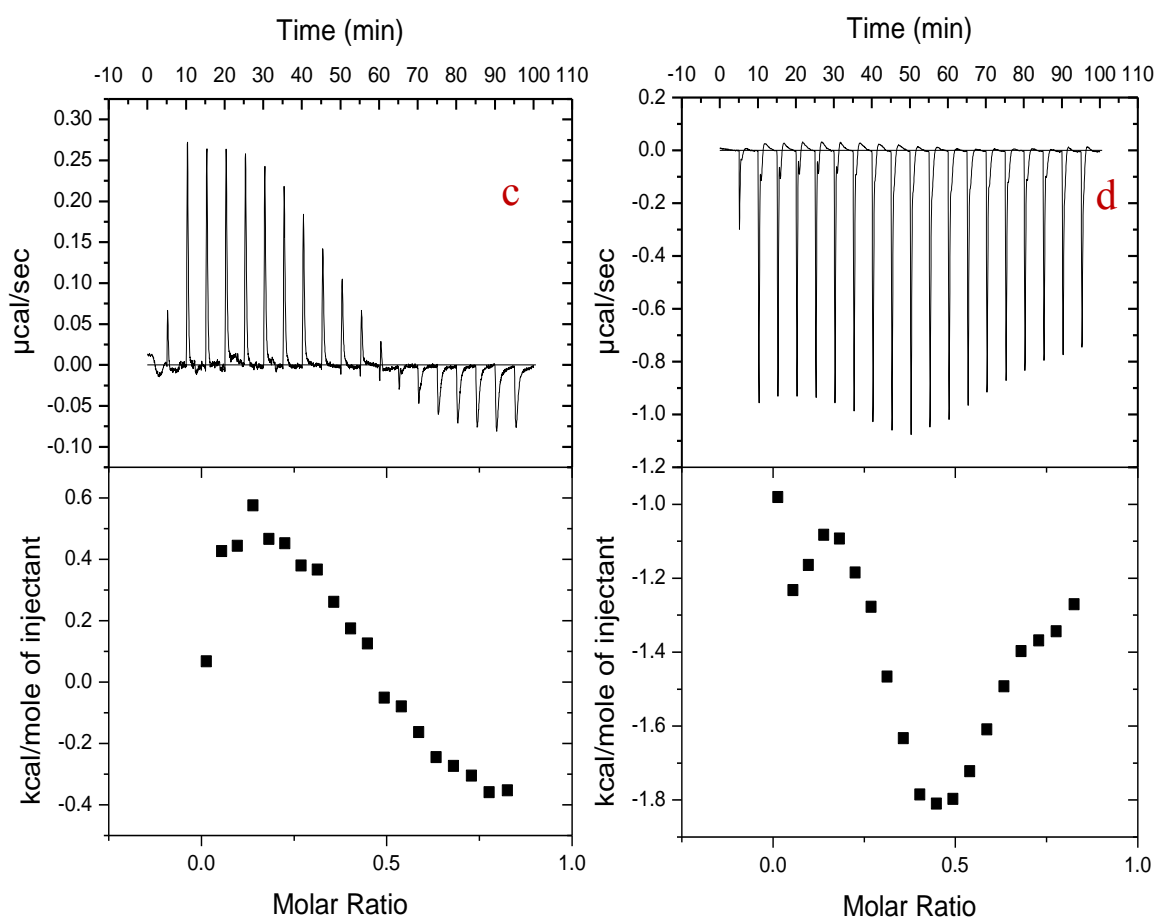


**Figure 4.9:** ITC raw data for the interactions of (a)  $[5]\text{Cl}_2$  (1.00 mM), (b)  $[6]\text{Cl}_2$  (1.00mM), (c)  $[7]\text{Cl}_4$  (1.00mM) and (d)  $[8]\text{Cl}_4$  (1.00mM) with CT-DNA (0.25 mM) in 5mM Tris, 25mM NaCl, pH 7.4 at 25 °C.

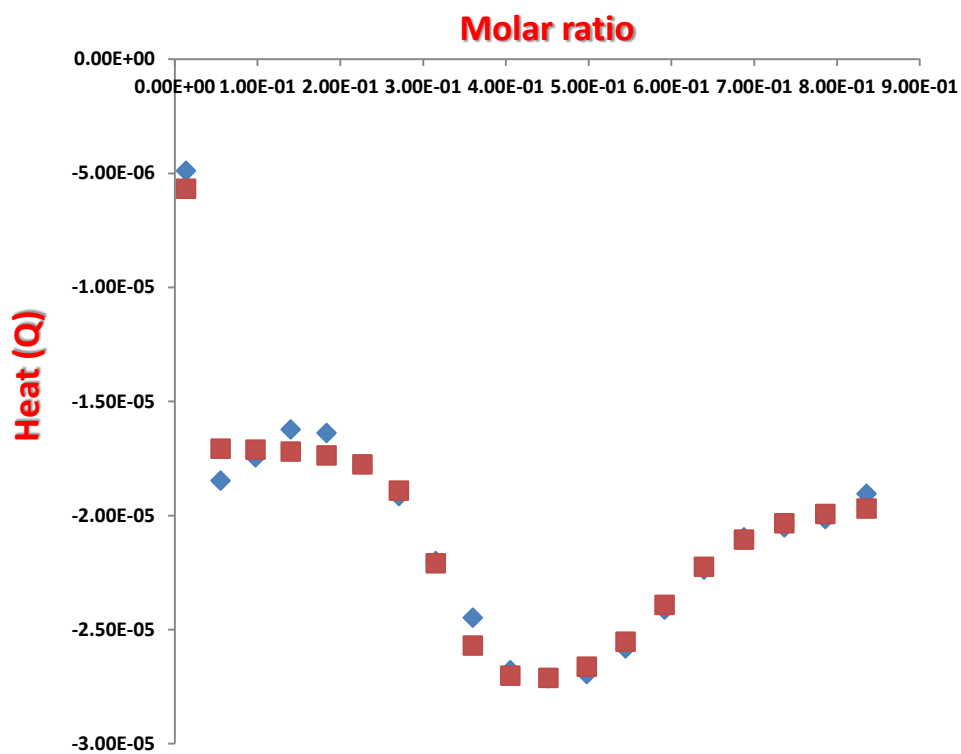
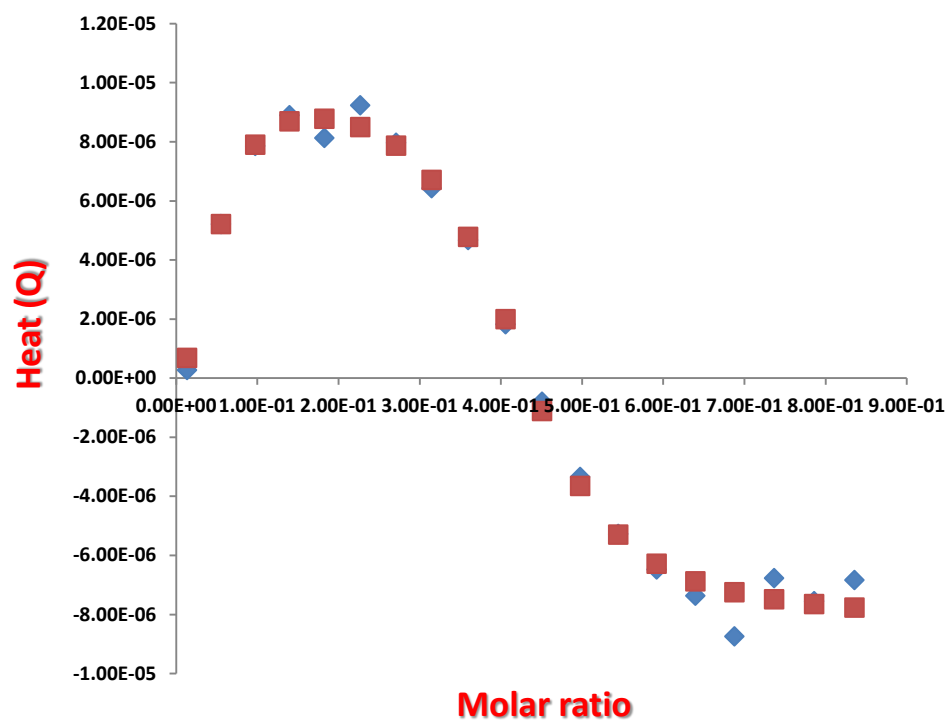


**Figure 4.10:** Integrated heat effects for titration of a 1.00 mM solution of [6]Cl<sub>2</sub> (top) and [8]Cl<sub>4</sub> (bottom) into a 0.25 mM CT- DNA

The second event is enthalpy and entropy favoured for the complex [8]Cl<sub>4</sub> with enthalpy between -0.64 kcal mol<sup>-1</sup>. This negative enthalpy can be interpreted as H-bonding and/or van der Waals specific recognitions. The binding affinity for this second interaction of [8] is in 10<sup>5</sup> M<sup>-1</sup> range with binding site size of 3.50 bp per ligand. However, the second event interactions of [5]Cl<sub>2</sub> and [6]Cl<sub>2</sub> with CT-DNA are entropically driven with small positive enthalpies around (2.39-1.24) kcal mol<sup>-1</sup> and positive entropy (TΔS<sub>2</sub> = 9.16 and 8.85 kcal mol<sup>-1</sup>) correspondingly. Binding site sizes for this binding event are about 2.94-2.65 bp per ligand. A comparison of binding affinities of [5-8] observed by ITC show that, with a binding affinity 4.07 × 10<sup>7</sup> M<sup>-1</sup>, dinuclear complex [8]Cl<sub>4</sub> binds to CT-DNA more strongly than its mononuclear analogue, complex [6]Cl<sub>2</sub>, (K<sub>b</sub> = 7.30 × 10<sup>6</sup> M<sup>-1</sup>). On the other hand, mononuclear complex [5]Cl<sub>2</sub> has a binding affinity 1.74 × 10<sup>5</sup> M<sup>-1</sup> and therefore interacts with CT-DNA with a comparable strength to its dinuclear analogue [7]Cl<sub>4</sub> which displays a binding affinity of 2.15 × 10<sup>5</sup> M<sup>-1</sup>. These results are in good agreements with the data obtained from spectroscopic titrations and viscosity measurements discussed in Chapter three.

In summary, the ITC evidence has been used to obtain complete thermodynamic profiles (ΔG°, ΔH°, ΔS°) for the interaction of both sets of complexes [1-4] and [5-8] with CT-DNA. The results show the binding of these complexes are generally entropically favoured. The binding affinities of these complexes suggest that complexes [5-8] interactively bind to CT-DNA more strongly than complexes [1-4]. Moreover, both ITC and spectroscopic studies show a significant increase in binding affinity for DNA for the monometallic and bimetallic complexes [5-8] containing 3-Py positioned tethers. These results have confirmed that the positioning of the functional group can have a profound effect on the binding affinities of these complexes.

## References

- (1) Harding, S. E.; Chowdhry, B. Z.: *Protein-Ligand Interactions, Structure and Spectroscopy: a practical approach*; Oxford University Press, 2001.
- (2) Pierce, M. M.; Raman, C.; Nall, B. T.: *Methods* **1999**, 19, 213-221.
- (3) Turnbull, W. B.; Daranas, A. H.: *Journal of the American Chemical Society* **2003**, 125, 14859-14866.
- (4) Wiseman, T.; Williston, S.; Brandts, J. F.; Lin, L. N.: *Analytical Biochemistry* **1989**, 179, 131-137.
- (5) Tame, J.; O'Brien, R.; Ladbury, J.: *Isothermal Titration Calorimetry of Biomolecules* 1998, John Wiley & Sons Ltd.: Chichester, Sussex.
- (6) Ladbury, J. E.; Chowdhry, B. Z.: *Chemistry and Biology* **1996**, 3, 791-801.
- (7) Srinivas, V.; Reddy, G. B.; Surolia, A.: *FEBS Letters* **1999**, 450, 181-185.
- (8) Matulis, D.; Rouzina, I.; Bloomfield, V. A.: *Journal of Molecular Biology* **2000**, 296, 1053-1063.
- (9) Haq, I.; Lincoln, P.; Suh, D.; Norden, B.; Chowdhry, B. Z.; Chaires, J. B.: *Journal of the American Chemical Society* **1995**, 117, 4788-4796.
- (10) Nordén, B.; Tjerneld, F.: *Biopolymers* **1982**, 21, 1713-1734.

## Chapter 5

### ***DNA Binding and Cleavage Properties of a heterobimetallic Ru<sup>II</sup>-Re<sup>I</sup> system and Ru<sup>II</sup>-Ru<sup>II</sup> Polypyridyl complex with mixed-bis-intercalating ligands (dppz-dppn)***

---

5.0 Introduction.....	123
5.1.1 DNA Binding and Cleavage Properties of a heterobimetallic Ru <sup>II</sup> -Re <sup>I</sup> system.....	123
5.1.2 Synthetic Studies.....	124
5.1.3 Characterization .....	126
5.1.3.1 Absorption spectrum of ruthenium-rhenium complex .....	126
5.1.4 DNA Binding Studies .....	128
5.1.4.1 Absorption titration .....	128
5.1.4.2 Luminescence titration .....	131
5.1.4.3 Isothermal Titration Calorimetry (ITC) .....	132
5.1.5 RuRe Phototoxicity.....	134
5.1.6 DNA Photocleavage.....	136
5.1.6.1 Phototoxicity of RuRe bis-intercalator towards A2780 and A2780cis cell lines... 138	
5.2 Ru <sup>II</sup> -Ru <sup>II</sup> Polypyridyl complex with mixed-bis-intercalating ligands (dppz-dppn).....	143
5.2.1 Introduction.....	143
5.2.2 Synthetic Studies.....	143
5.2.2.1 Ligand synthesis.....	143
5.2.2.2 Synthesis of complexes .....	144
5.2.3 Characterization .....	146
5.2.3.1 Absorption spectra.....	146
5.2.4 Transient Absorption Studies.....	151
5.2.5 DNA binding studies.....	153
5.2.5.1 UV-Vis titrations .....	153
5.2.5.2 Luminescence titrations.....	157
5.2.6 Singlet oxygen quantum yield .....	160
5.2.7 DNA photocleavage and Singlet Oxygen Production .....	162
5.2.8 Phototoxicity.....	163

5.2.8.1 Inductively coupled plasma mass spectrometry (ICP-MS).....	168
References.....	171

## 5.0 Introduction

In the previous chapters, the effect of the nature of linker molecule and positioning of the functional group within the linker on the binding affinity of a number of mono and bimetallic ruthenium complexes incorporating the well-characterised DNA intercalating ligand dppz have been discussed. A variety of techniques have been used to study the binding of this series of complexes with CT-DNA. In this chapter the synthesis, characterisation and DNA binding study of the new hetero-bimetallic Ru-Re complex bearing the same intercalating dppz ligand, and also homo-bimetallic Ru-Ru complexes having mixed intercalating dppz/dppn ligands are reported as well.

### 5.1.1 DNA Binding and Cleavage Properties of a heterobimetallic Ru<sup>II</sup>-Re<sup>I</sup> system

The design of multinuclear metal complexes containing electroactive and photoactive units has attracted the attention of many research groups.<sup>1</sup> The active units in these multicomponent systems are linked through covalent bonds and variety of organic or inorganic active components can be engaged.

Many multinuclear compounds incorporating photoactive and electroactive units based on  $d^6$  metal transition complexes have been constructed. In particular, ruthenium(II) and rhenium(I) polypyridyl complexes are popular in both fundamental studies and applications.<sup>2,3</sup> Based on the attractive electrochemical and excited-state properties, we have synthesized a new hetero-dinuclear dppz complex of ruthenium(II)-rhenium(I) system (**Figure 5.1.1**) and the electronic and photophysical properties of this complex have been studied.

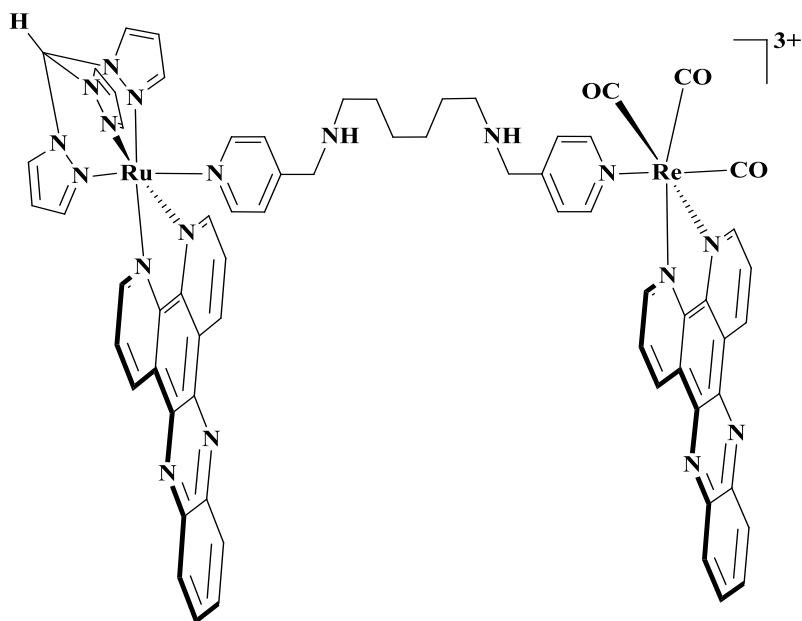


**Figure 5.1.1:** Chemical structure of Ru-Re complex

## 5.1.2 Synthetic Studies

The Ru<sup>II</sup>-Re<sup>I</sup> system  $[\{\text{Ru}(\text{tpm})(\text{dppz})\}(\mu\text{-L1})\{\text{fac}(\text{CO})_3\text{Re}(\text{dppz})\}]^{3+}$  was synthesized from the known mononuclear complexes  $[\text{Ru}(\text{tpm})(\text{dppz})(\mu\text{-L1})]^{2+}$ , described in chapter 2, and  $[\text{ReCl}(\text{CO})_3(\text{dppz})]$ .<sup>4</sup> The reaction was started by refluxing  $[\text{ReCl}(\text{CO})_3(\text{dppz})]$  and  $\text{AgCF}_3\text{SO}_3$  in ethanol overnight. The filtered solution was then returned to the reaction vessel followed by addition of excess  $[(\text{tpm})\text{Ru}(\text{dppz})(\text{L1})]\text{Cl}_2$  in an ethanol solution. The mixture was refluxed overnight again, and then evaporated to obtain a red-brown precipitate. Purification was achieved via anion metathesis, where the compound dissolved in the minimum amount of acetone and converted by counter-ion metathesis using acetone solutions of tetrabutylammonium chloride (10 molar equivalencies). This resulted in precipitation of the desired chloride product, which was filtered and washed with copious amounts of acetone.

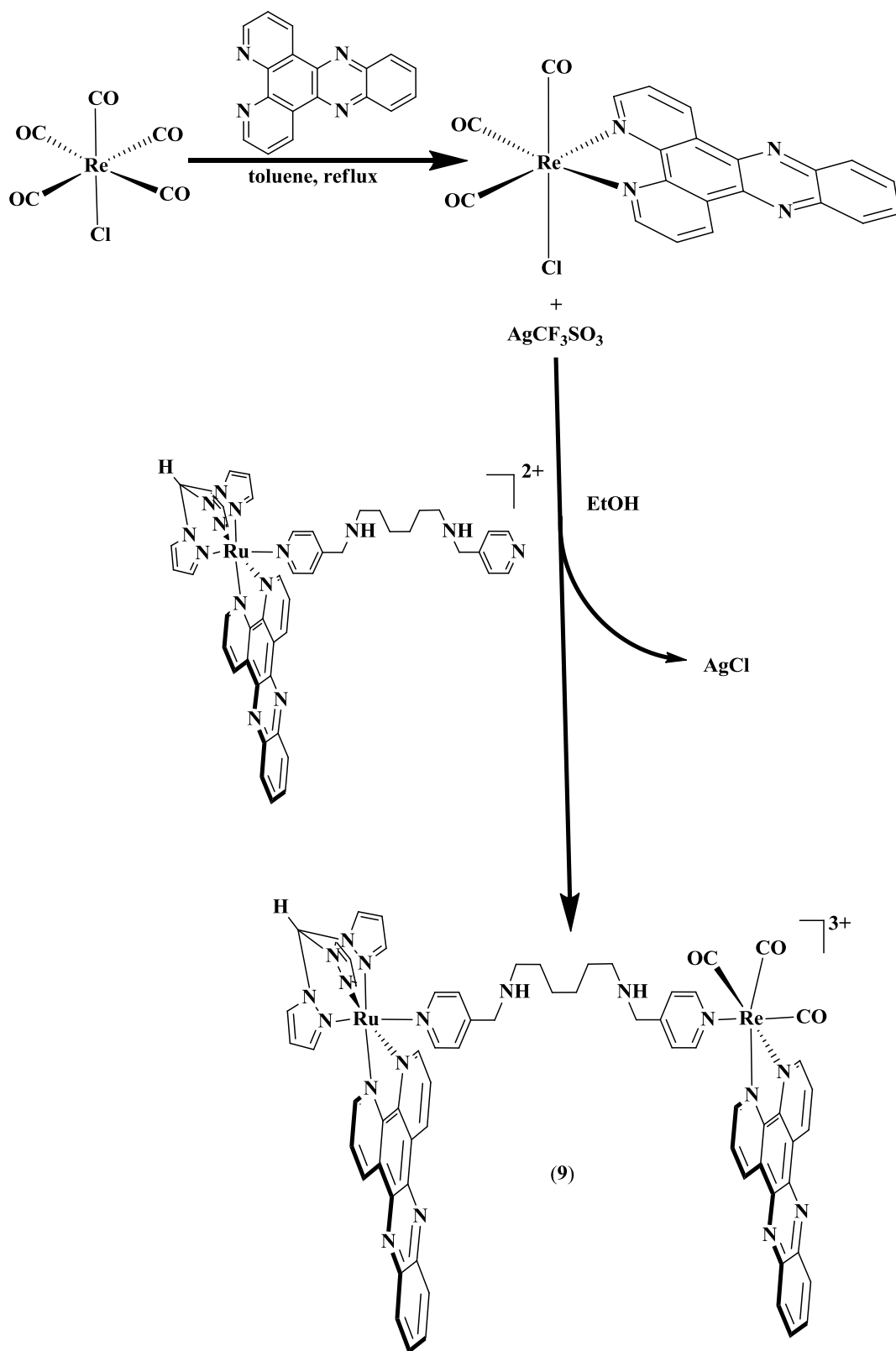


**Figure 5.1.2:** Synthesis of hetero-bimetallic complex  $[[\text{Ru}(\text{tpm})(\text{dppz})](\mu\text{-L1})\{\text{fac}(\text{CO})_3\text{Re}(\text{dppz})\}]^{3+}$

## 5.1.3 Characterization

### 5.1.3.1 Absorption spectrum of ruthenium-rhenium complex

The UV-visible absorption spectrum of the chloride salt of the complex was recorded in aqueous tris buffer at room temperature. Data are summarised in **Table 5.1.1**.

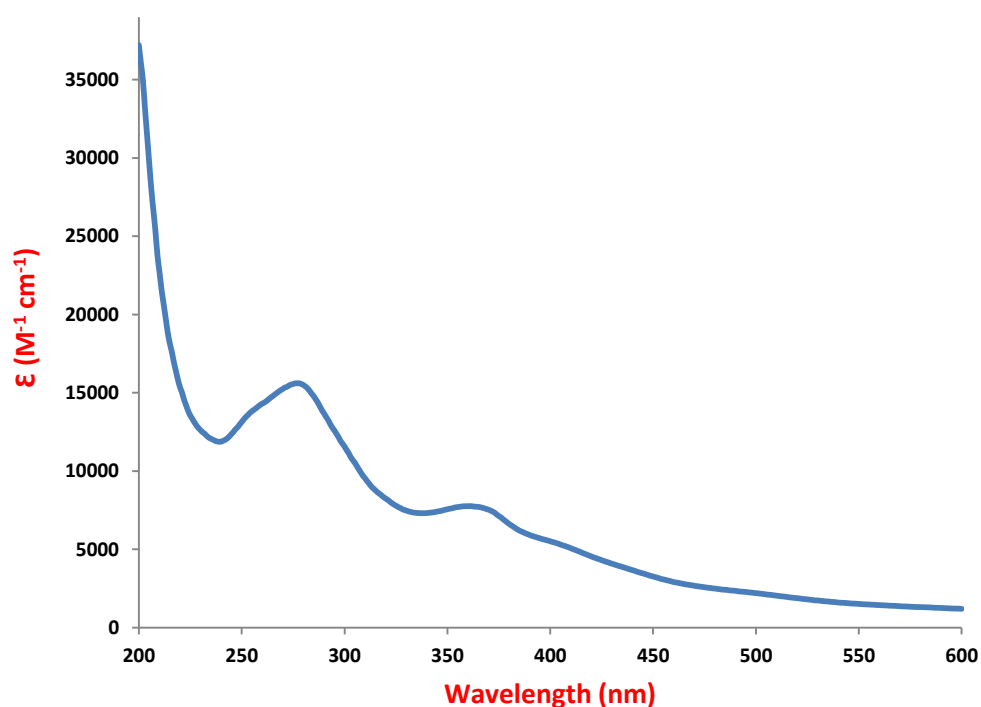


**Figure 5.1.3:** UV-Visible absorption spectrum for the complex [9] as a chloride salt in in 5 mM tris buffer, 25 mM NaCl, pH 7.4 at room temperature

The UV/Vis absorption spectrum of [9]Cl<sub>3</sub> in aqueous tris buffer shows high-energy  $\pi \rightarrow \pi^*$  transitions at 276 and 317 nm. Below 320 nm, a superposition of metal( $d\pi$ ) $\rightarrow$ dppz( $\pi^*$ ) MLCT and dppz( $\pi \rightarrow \pi^*$ ) intraligand (IL) transitions is observed.<sup>5-8</sup> Excitation at 431 nm results in unstructured luminescence characteristic of the Ru( $d\pi$ ) $\rightarrow$ dppz( $\pi^*$ ) <sup>3</sup>MLCT manifold at 642 nm.

	Absorption			Emission	
Complex	$\lambda_{\max}(\text{nm})$	$10^{-3} \epsilon (\text{M}^{-1}\text{cm}^{-1})$	Assignment	$\lambda_{\text{ex}}/\text{nm}$	$\lambda_{\text{em}}/\text{nm}$
[9]Cl <sub>3</sub>	254	13.82	$\pi \rightarrow \pi^*$	431	642
	276	15.57	$\pi \rightarrow \pi^*$		
	322	7.94	$\pi \rightarrow \pi^*$		
	364	7.70	MLCT		
	405	5.25	MLCT		
	489	2.43	MLCT		

**Table 5.1.1:** UV-Visible data for the complex [9] as a chloride salt recorded in 5mM tris buffer, 25 mM NaCl, pH 7.4 at 25 °C.

The data for complex [9] recorded in acetonitrile as a PF<sub>6</sub> salt is also summarised below in **Table 5.1.2**. The absorption spectrum for this compound is shown in **Figure 5.1.4**.

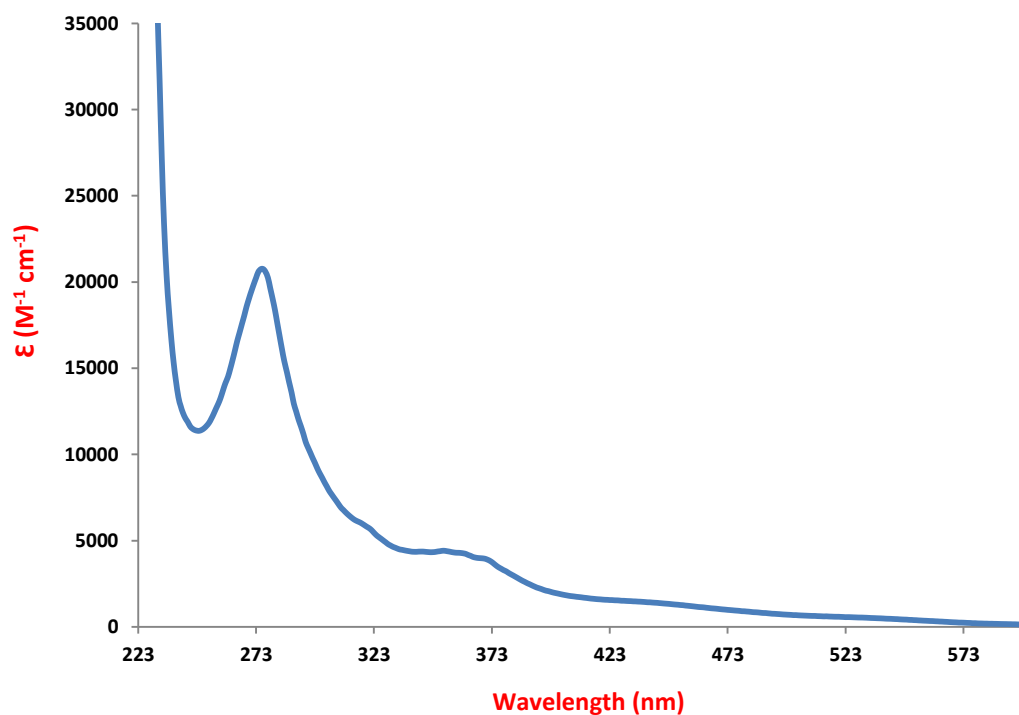


**Figure 5.1.4:** UV-Visible absorption spectrum for the complex [9] as PF<sub>6</sub> salt in acetonitrile at room temperature.

Complex	$\lambda_{\text{max}}$ (nm)	$10^{-3} \epsilon$ ( $\text{M}^{-1}\text{cm}^{-1}$ )	Assignment
[9][PF <sub>6</sub> ] <sub>3</sub>	276	20.60	$\pi \rightarrow \pi^*$
	321	5.71	$\pi \rightarrow \pi^*$
	361	4.25	MLCT
	440	1.40	MLCT
	470	1.01	MLCT

**Table 5.1.2:** UV-Visible data for the complex [9] as PF<sub>6</sub> salt recorded in acetonitrile at 25 °C.

## 5.1.4 DNA Binding Studies

### 5.1.4.1 Absorption titration

The interaction of [9] with calf-thymus DNA (CT-DNA) in aqueous buffer (25 mM NaCl, 5 mM tris buffer, pH 7.4) was investigated using electronic absorption spectroscopy. Addition of aliquots of CT-DNA results in distinctive changes in the UV/Vis spectrum of [9], with several bands between 279 and 490 nm showing large hypochromicity and significant bathochromic shifts. **Figure 5.1.5** shows a typical UV-Vis titration.

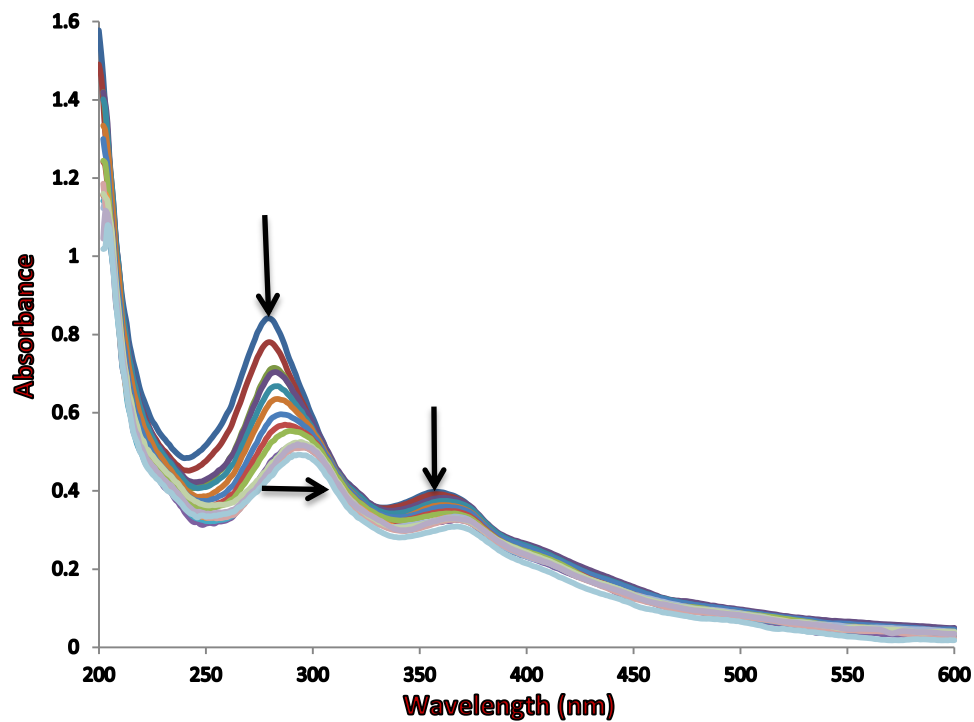


**Figure 5.1.5:** UV-Vis titration of 1.01 mM bp<sup>-1</sup> CT-DNA into a solution of 50 μM [9]Cl<sub>3</sub> in 5 mM tris buffer, 25 Mm NaCl, pH 7.4 at 25 °C.

To parameterise the interaction of complex [9] to DNA, changes in the 279 nm band were followed and the binding curve for [9] was constructed, **Figure 5.1.6**. It showed that saturation binding had taken place.

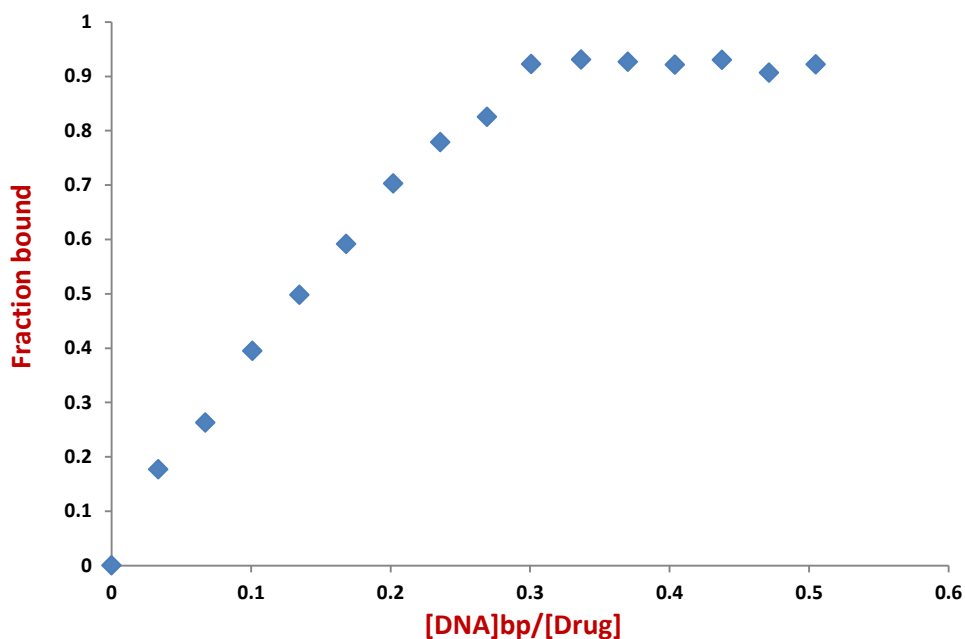


**Figure 5.1.6:** Binding curve obtained by UV-Vis titrations for [9]Cl<sub>3</sub> binding to CT-DNA

The binding constant for the interaction of the complex [9] with CT-DNA was calculated using previously derived, much used model<sup>9</sup> in which a plot of [DNA]/(ε<sub>a</sub>-ε<sub>f</sub>) versus [DNA] for the absorption titration of DNA with Ru<sup>II</sup>-Re<sup>I</sup> complex is used to give an estimate of the intrinsic binding constant (K<sub>b</sub>).

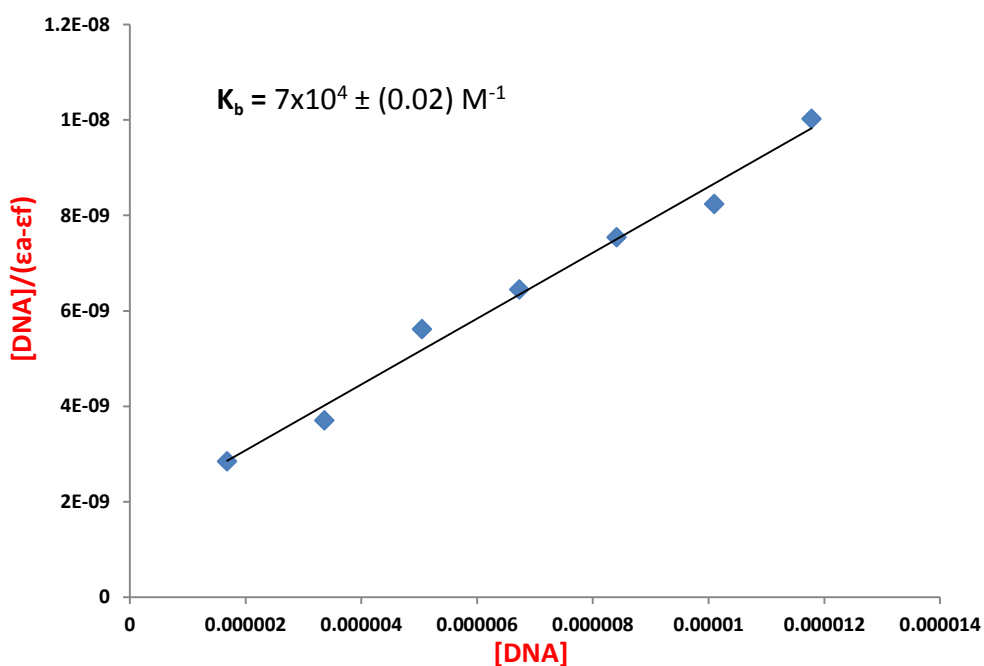


**Figure 5.1.7:** Scatchard plots for the complex [9]Cl<sub>3</sub> obtained from the UV-Visible titration of CT-DNA.

The binding affinity for the interaction of complex [9] with CT-DNA was estimated as  $7 \times 10^4 \text{ M}^{-1}$ . This value is lower than that of the corresponding dinuclear tetracation  $[\{\text{Ru}(\text{tpm})(\text{dppz})\}_2(\mu\text{-L1})]^{4+} [\text{3}]\text{Cl}_4$  ( $K_b = 2 \times 10^5 \text{ M}^{-1}$ ). The lower cationic charge of [9], indicating that electrostatic contributions are important in DNA metallo-intercalators interactions.

### 5.1.4.2 Luminescence titration

As expected, the emission intensity around 645 nm increases on the presence of DNA. The complex shows a true light switch effect, with no luminescence in aqueous solution, until addition of DNA to [9], causes the intense luminescence of [9] to be restored (Figure 5.1.8).

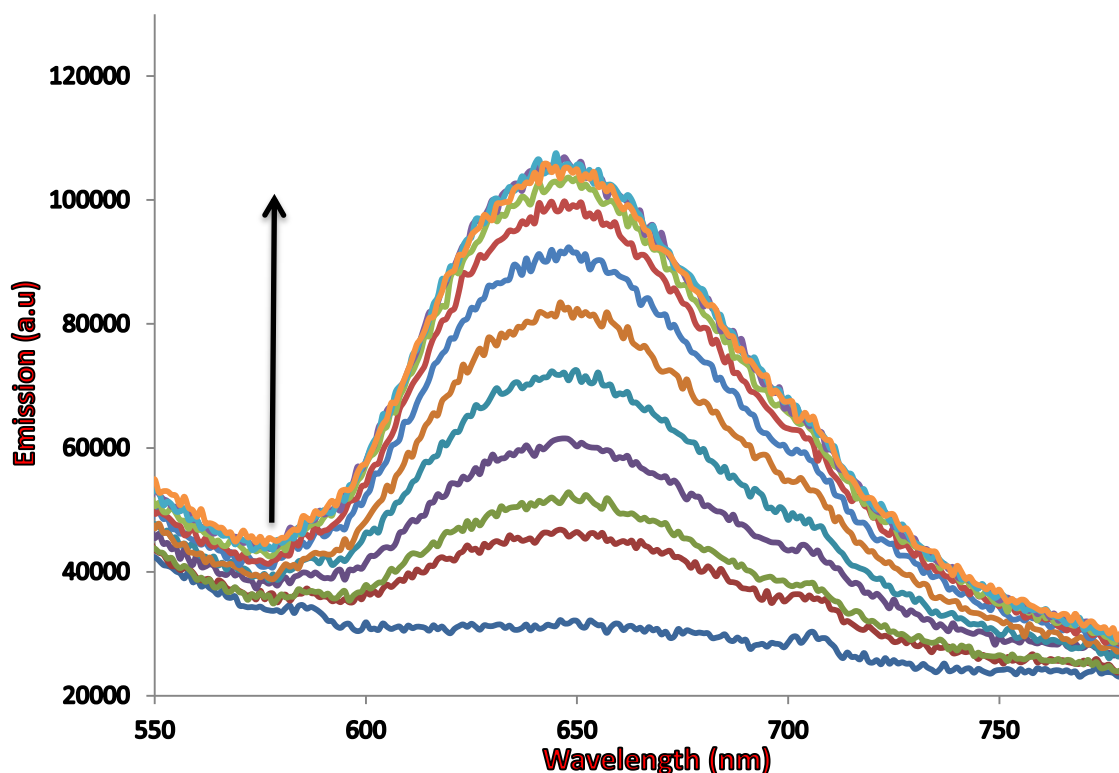
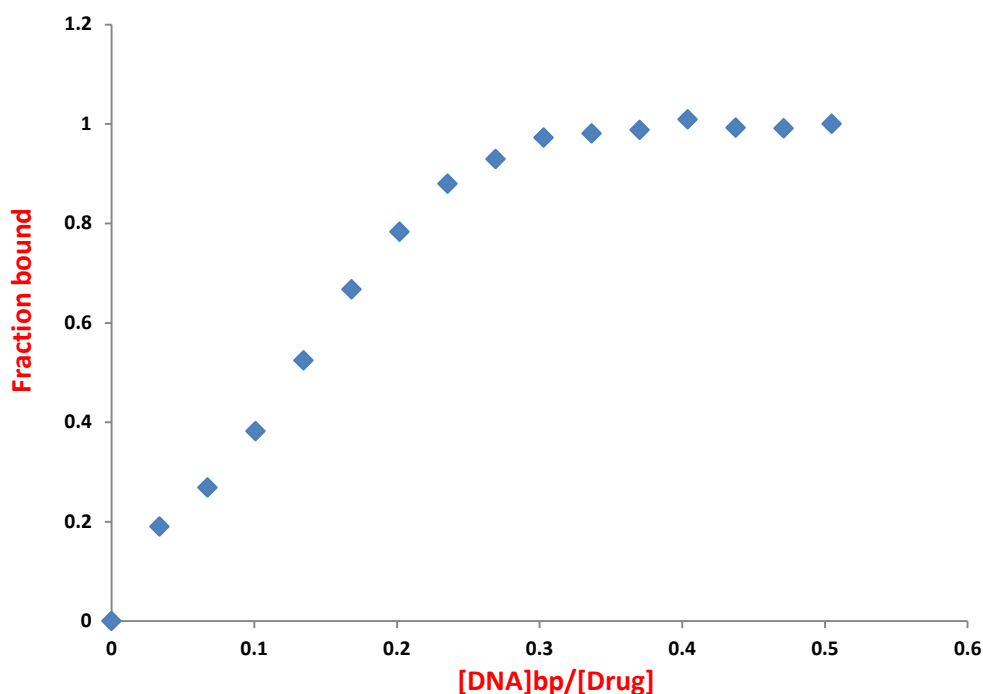


Figure 5.1.8: Luminescence titration of complex [9] with CT-DNA. (5 mM Tris buffer, 25 mM NaCl, pH 7.4, 25 °C).

The binding curve for the interaction of the complex with CT-DNA shows that saturation binding has taken place, however attempts to fit this data to the commonly employed McGhee-von Hippel model were unsuccessful.



**Figure 5.1.9:** Binding curve showing the luminescence titrations of [9]Cl<sub>3</sub> binding to CT-DNA

### 5.1.4.3 Isothermal Titration Calorimetry (ITC)

To further characterise the interaction of the complex with nucleic acid, the thermodynamic parameters of the binding of [9] with CT-DNA was determined using ITC.<sup>10</sup>

The differential heat flow and derived integrated heat effects of [9] are shown in **Figure 5.1.10** and the thermodynamic parameters are summarised in **Table 5.3**.

The data for [9] shows two experiments merged together to complete the binding isotherm, the syringe was refilled with ligand and the titration continued immediately. The small gap between experiments cannot be corrected due to the removal and replacement of the syringe from the cell. The titrations were not able to be completed in one experiment due to the fact that the syringe can only hold a fixed volume of liquid.

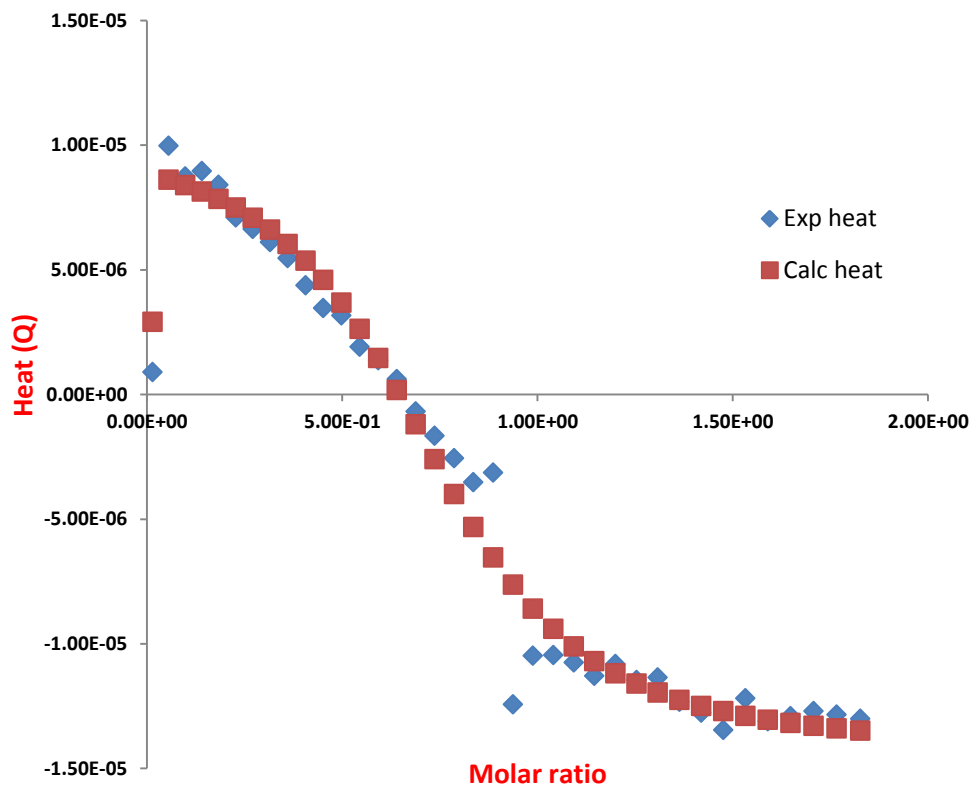


**Figure 5.1.10:** Integrated heat effects for titration of a 1.00 mM solution of [9]Cl<sub>3</sub> into a 0.25 mM CT- DNA

Complex	$K_b/M(\text{bp})^{-1}$	S/bp	$\Delta H/\text{kcal mol}^{-1}$	$\Delta G/\text{kcal mol}^{-1}$	$-T\Delta S/\text{kcal mol}^{-1}$
[9]Cl <sub>3</sub>	$7.58 \times 10^4$	1.30	1.65	-6.65	-8.29

**Table 5.1.3:** ITC thermodynamic data for the interaction of [9]Cl<sub>3</sub> with CT-DNA at 25°C

The overall thermodynamic picture that appears from calorimetry experiment for the interaction of [9] with CT-DNA is that the binding is enthalpically unfavourable (endothermic) and entropically favoured. Additionally, the binding constant obtained from

ITC for [9] is in good agreement with the binding value obtained from spectroscopic titrations, confirming that it is approximately 10-fold weaker than the interaction of the equivalent Ru<sup>II</sup>-Ru<sup>II</sup> complex [3] and further illustrating that electrostatic effects make an appreciable contribution to overall binding. However, the DNA binding affinity  $K_b$  value of [9] also represents less than an order of magnitude decrease in binding affinity relative to that of the corresponding Ru<sup>II</sup>-Re<sup>I</sup> complex with an estimated  $K_b$  value as  $6 \times 10^5 \text{ M}^{-1}$  reported by Simon P. Foxon and co-workers.<sup>11</sup> It seems that the more extended length or the presence of two amino groups within the linker has an effect on the binding affinity of this system.

Foxon and co-workers also reported that the first hetero-dinuclear Ru<sup>II</sup>-Re<sup>I</sup> dppz complex binds to duplex DNA with good affinity and displays both DNA light switch and cleavage properties.<sup>11</sup> On the basis of their report, the possibility that complex [9] could also display similar properties was investigated.

### 5.1.5 RuRe Phototoxicity

For many years the use of nucleic acid cleavage agents as structural probes and therapeutic agents has been studied. Some photocleavage compounds can react directly in an electronically excited state with a nucleic acid and cause an immediate scission of the nucleic acid chain. However, other compounds have excited states that indirectly lead to cleavage or damage of the nucleic acid.<sup>12</sup> In these latter cases, to fully reveal the sites and extent of damage, the nucleic acid must be subjected to a secondary treatment, such as incubation with hot piperidine.

The potential use of transition metal complexes as DNA structural probes and as anticancer agents have received significant attention.<sup>12</sup> Ruthenium (II) polypyridyl complexes are among these complexes and they have been extensively studied due to their rich photophysical, photochemical and redox properties.<sup>13</sup> It has been confirmed that many Ru<sup>II</sup> polypyridyl complexes possess DNA photocleavage activities via an <sup>1</sup>O<sub>2</sub> mechanism<sup>14</sup> (Figure 5.1.13).<sup>15</sup> The diversity of the chemical structures that are readily available through modifications of the coordinated ligands makes Ru(II) polypyridyl complexes that particularly useful for applications as biological probes and effectors.<sup>16</sup>

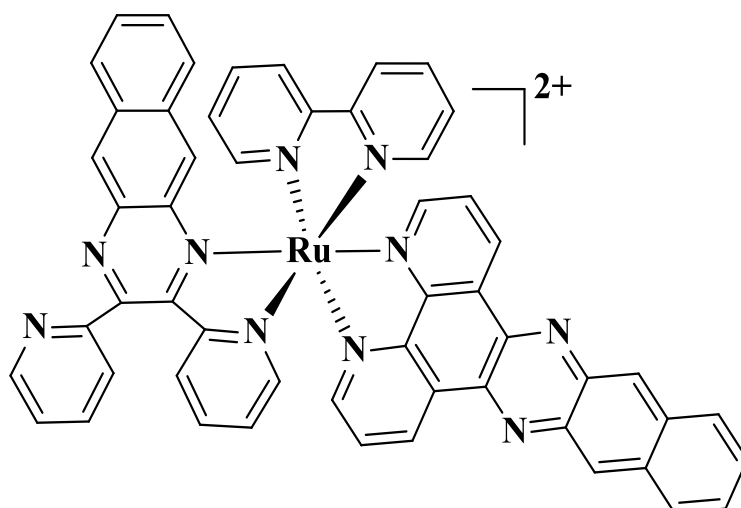


**Figure 5.1.13:** Structure of  $[\text{Ru}(\text{bpy})(\text{dpb})(\text{dppn})]^{2+}$  (**bpy** = 2,2'-bipyridine, **dpb** = 2,3-bis(2-pyridyl)benzoquinoline, **dppn** = 4,5,9,16-tetraazadibenzo[a,c]naphthacene)<sup>15</sup>

In addition to that, previous work on rhenium-based complexes has shown that they can produce photo-activated DNA damage as well. The intercalative binding interaction of  $[\text{Re}(\text{dppz})(\text{CO})_3(\text{py})][\text{SO}_3\text{CF}_3]$  and  $[\text{Re}(\text{dppn})(\text{CO})_3(\text{py})][\text{SO}_3\text{CF}_3]$  with calf thymus DNA has previously been studied (**Figure 5.1.14**).<sup>17</sup> The complexes have been established to stimulate cleavage of plasmid pBR322 DNA from the supercoiled form **I** to the open circular form **II** upon irradiation.

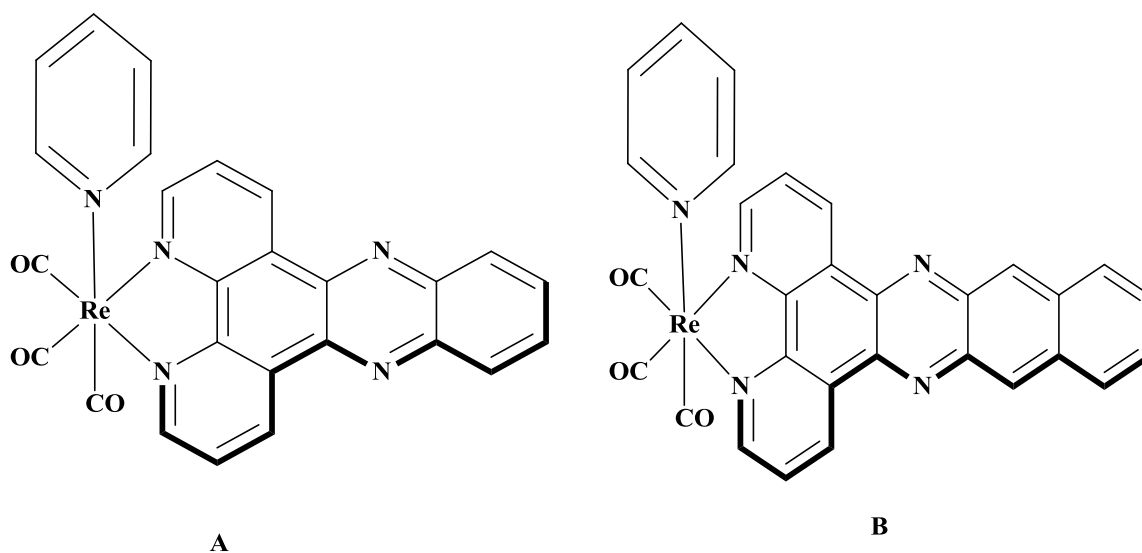


**Figure 5.1.14:** Structures of DNA cleavage molecules  $[\text{Re}(\text{dppz})(\text{CO})_3(\text{py})][\text{SO}_3\text{CF}_3]$  (**A**) and  $[\text{Re}(\text{dppn})(\text{CO})_3(\text{py})][\text{SO}_3\text{CF}_3]$  (**B**)

Irradiation of the plasmid pBR322 DNA in the presence of both complexes indicated that singlet oxygen was not involved in the cleavage process. For the dppz complex **A**, direct oxidation of DNA plasmid by the excited state of the molecule was involved.<sup>18</sup> For the dppn complex **B**, inhibition of cleavage in a degassed solution or through the presence of an appropriate quencher indicated that the superoxide radical ( $O_2^{\cdot-}$ ) was involved in this process; although the hydroxyl radical ( $\cdot OH$ ) was also implicated, as in the presence of hydroxyl scavengers decreased cleavage activity was also observed.<sup>17</sup>

Moreover, the photophysical studies of Re(dppz) (**A**) derivatives indicated that the lowest excited state is an intraligand triplet state of dppz  ${}^3IL_{dppz}$ . The difference in the photophysical properties of the rhenium types and the analogues Ru(II) and Os(II) with dppz arises as a result of the metal to ligand charge transfer states,  $d\pi(M) \rightarrow \pi^*(dppz)$   ${}^3MLCT$ . In the Re(I) system the  ${}^3MLCT$  state is at higher energy which allows the low-lying dppz-based intraligand triplet state  ${}^3IL_{dppz}$  to dominate the photophysics of the system.<sup>7</sup> In addition, previous studies showed that the RuRe system displays both DNA light switch and cleavage properties.<sup>10</sup> The  $\{Ru^{II}(dppz)\}$  unit supplies the light-switch function while the  $\{Re^I(dppz)\}$  unit cleaves DNA.

Although the DNA binding properties of bis-intercalator complex [**9**] have been studied above, its potential as a DNA photocleaving agent or as a phototoxic species is discussed in the next section.

### 5.1.6 DNA Photocleavage

Previous studies have shown that  $Re^I$  systems - and a  $Ru^{II}-Re^I$  complex reported by the Thomas group - can directly cleave DNA. So this issue was investigated using complex [**9**]. This possibility was first studied through DNA cleavage experiments

To detect DNA fragments produced by photocleavage two electrophoretic methods are generally used.<sup>19</sup> In one case, the target is supercoiled DNA. Single strand cleavage (“nicking”) converts the supercoiled DNA to a relaxed, circular form whereas double-strand cleavage produces linear DNA. The three forms are quickly separated on an agarose gel and detected by fluorescent staining.

In the second more informative method, the use of end-labeled targets is used to analyse nucleic acid photocleavage. In this case, the nucleic acid is enzymatically labelled at the

terminus of one strand with a radioactive, fluorescent, or chemiluminescent tag. A sequencing ladder of the labelled nucleic acid is then obtained by either chemical or enzymatic methods.

Photocleavage of the nucleic acid produces shorter strands that will migrate faster than the uncleaved target in polyacrylamide gel electrophoresis. The nucleotide at which the cleavage event took place can be identified by running the sequencing ladders in adjacent lanes on the gel. Due to its convenience, the former method described above is used, as only evidence of DNA cleavage was required at this early stage of study.

Nucleic acid fragments are mostly separated using electrophoresis through agarose or polyacrylamide gels. The cleavage reaction of plasmid DNA can be checked by agarose gel electrophoresis. Relatively fast migration will be observed for the intact supercoiled form (Form **I**) when circular plasmid DNA is subject to electrophoresis. The supercoil will relax to generate a slower moving open circular form (Form **II**) if scission occurs on one strand (nicking). If both strands are cleaved, a linear form (Form **III**) will be generated that migrates between Forms **I** and **II** (**Figure 5.1.11**).<sup>20</sup> Occasionally, if the cleaving agent is very active only small, very fast moving, fragments will be created and no plasmid will be observed. Single stranded cleavage of the sugar-phosphate backbone of double stranded DNA (“nicking”) is known to be induced by numerous organic and inorganic based systems. An excellent review by Armitage<sup>12</sup> discusses an enormous number of these.

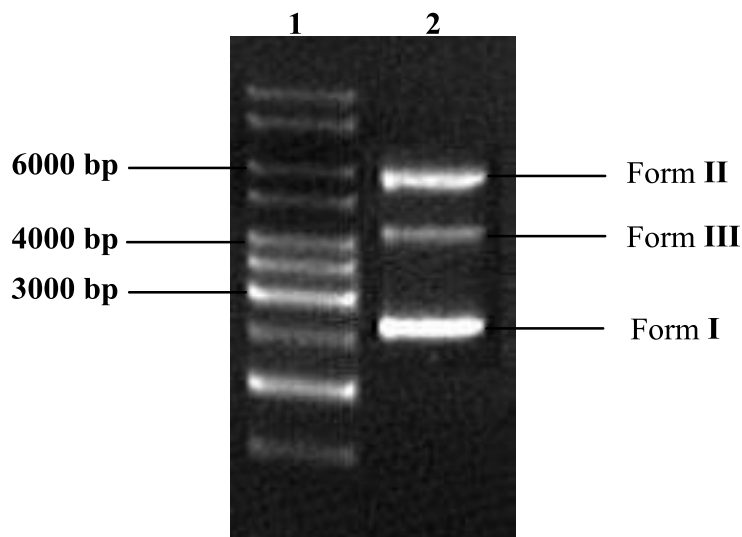


**Figure 5.1.11:** Agarose gel picture: (1) 1kb DNA Ladder; (2) Photoactivated cleavage of the plasmid DNA pBR 322 showing 3 different forms.

The DNA photocleavage property of [9] was investigated using supercoiled pBR 322 plasmid DNA and analysed by electrophoresis on an agarose gel. **Figure 5.1.12** shows a typical agarose gel photo of pBR 322 treated with [9] over a range of concentrations (10, 20 and 40  $\mu\text{M}$ ), irradiated for 60 mins at 470 nm. However, the gel photo showed no evidence of nicking at all. The experiment has repeated twice and the same result was obtained.

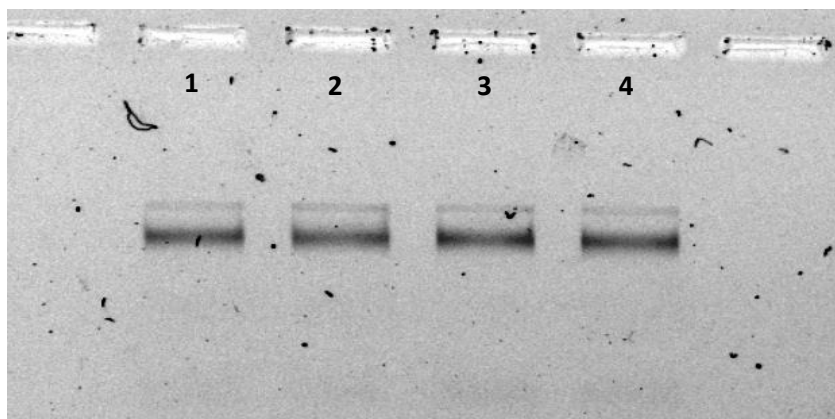


**Figure 5.1.12:** Photocleavage of supercoiled pBR322 DNA (0.1  $\mu\text{g}/\mu\text{L}$ ) by [9] under illuminated condition (470 nm, 100 mW, 60 minutes exposure) in 50 mM Tris-HCL buffer. Lane 1, DNA control; lane 2, DNA + 9 (10  $\mu\text{M}$ ); lane 3, DNA + 9 (20  $\mu\text{M}$ ); lane 4, DNA + 9 (40  $\mu\text{M}$ ) no nicking was observed.

These observations are surprising given the previous results described by Foxon, *et al* and suggests that the  $\text{Re}^{\text{I}}(\text{dppz})$ -based excited state is too short-lived to produce DNA damage. This is consistent with a faster rate of energy transfer to the Ru centre in 9 compared to the previously reported RuRe system, an effect that is perhaps mediated by the amino groups in the new linker ligand, an issue that can be explored through time resolved experiments.

### 5.1.6.1 Phototoxicity of RuRe bis-intercalator towards A2780 and A2780cis cell lines

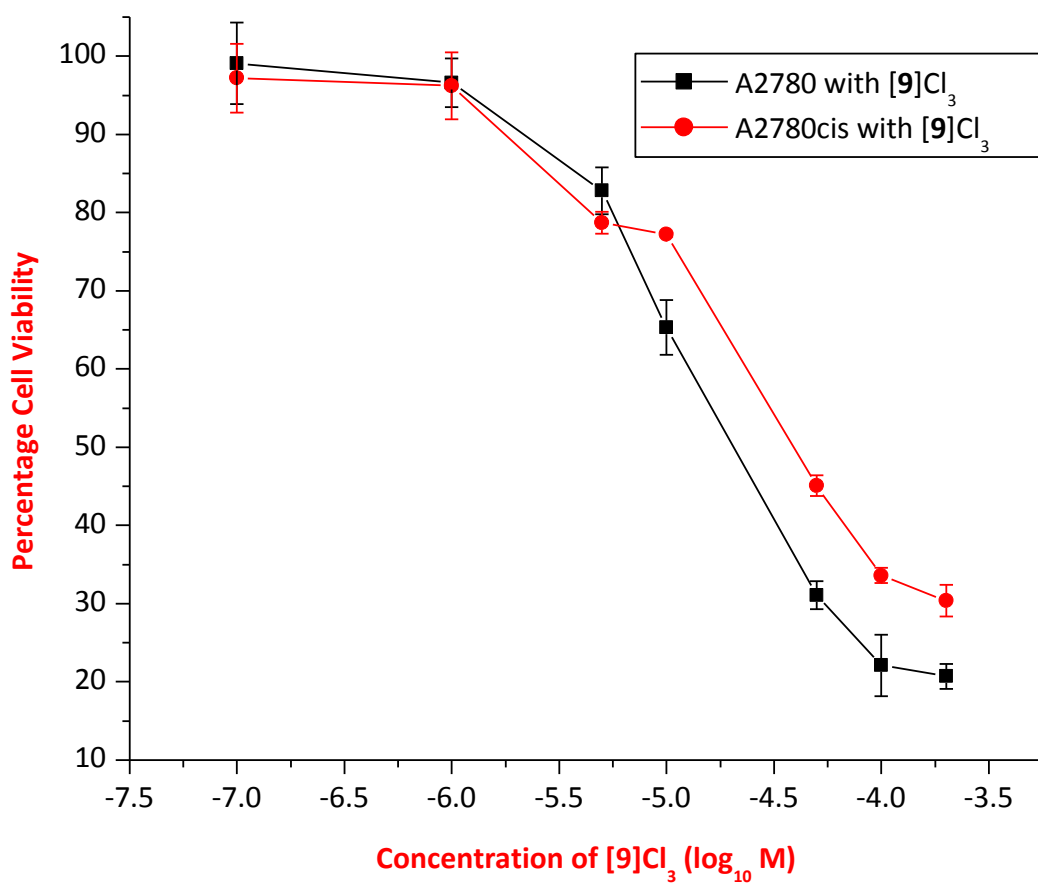
In addition to the differences in photophysical properties and the charge differences of ruthenium and rhenium systems, it was of interest to see if they possess any biological

activity. Thus, although it did not cleave DNA in cell-free conditions, the potential in cell phototoxic activity of complex [9] was also investigated.

The phototoxic index (**PI**) is a comparative measure of phototoxic activity for a molecule which can be calculated from the ratio between its toxicity in the dark and upon light irradiation.<sup>21</sup>

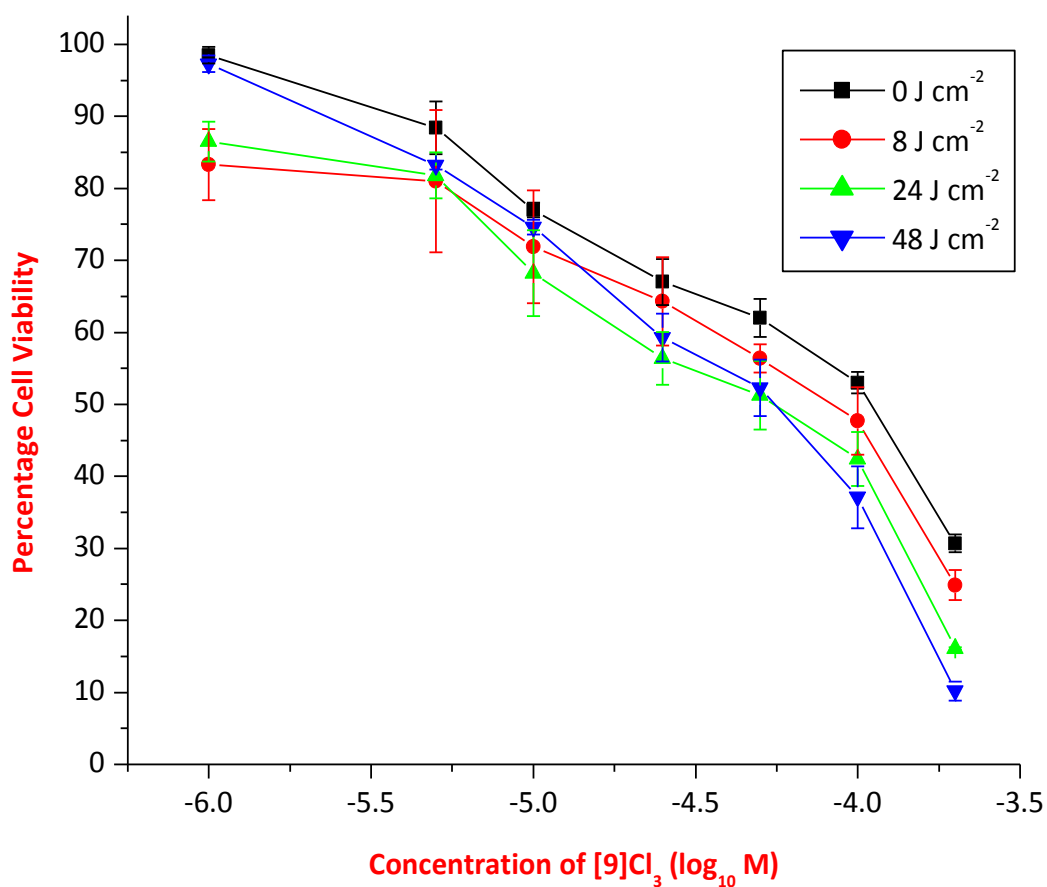
To further investigate, the possible phototoxicity of complex [9] and its effects on A2780 and A2780cis human ovarian cancer cell lines was investigated by Dr. Paul Jarman (A fellow member of the Thomas group). The 48 hour IC<sub>50</sub> determination protocol was originally used but four separate plates were employed and each was irradiated after 24 hours for a varying length of time. Three plates underwent timed exposures in the Light Irradiation Source Apparatus (LISA), which is used to irradiate the samples, while a dark control remained in the incubator throughout. To provide a comparison in assessing any phototoxicity upon irradiation, the dark control was essential. Untreated control wells served the usual purpose of delineating maximum cell viability. Besides, they could be used not only to make curves showing the effect of increasing compound concentration on cell viability, but - through inclusion in each plate individually - they also acted as a control for any damaging effects of the radiation alone. This confirmed the experiment was internally controlled for each variable and prevented any false positive results in which increased exposure to the irradiation increased toxicity despite of compound treatment.

Using a range of concentrations (0.1-200  $\mu\text{M}$ ), the IC<sub>50</sub> value of the complex [9] was determined after 48 hour to evaluate its influence against A2780 and A2780cis cell lines. The IC<sub>50</sub> value against the A2780 cell line was determined as 11  $\mu\text{M}$ , which is not as powerful as cisplatin (ca. 2  $\mu\text{M}$ ) but still comparatively active in therapeutic terms. However, against A2780cis, the IC<sub>50</sub> of 21  $\mu\text{M}$  is only a two-fold reduction in potency versus A2780 so that it now displays a similar level of cytotoxicity to cisplatin against this cell line (ca. 22  $\mu\text{M}$ ).



Cell Line	IC <sub>50</sub> (μM)
A2780	11
A2780cis	21

**Figure 5.1.15:** Cell viability data for RuRe complex [9]



Light Irradiation time (minutes)	IC <sub>50</sub> concentration (μM)	Percentage Viability at 100 μM [M] (% cells metabolising MTT +/- 1 SD)
0	112	53 +/- 2
5	89	48 +/- 5
15	58	42 +/- 4
30	58	37 +/- 4

**Figure 5.1.16:** A2780<sub>cis</sub> cell viability data for complex [9] upon irradiation

The phototoxicity of the RuRe complex against A2780cis cell line was carried out by using a concentration range of 1-200  $\mu\text{M}$ . The result shows no significant increase in toxicity against A2780cis after exposure to light. Thus, based on this characteristic, complex [9] is not a favourable lead for applications involving PDT; this is probably due to the low oxygen sensitisation observed in the previous section. Nevertheless, its dark toxicity – particularly against cisplatin resistant cells – indicates that it is a promising therapeutic lead. To further explore this issue, additional substantial biological investigations will be required.

In summary, the new hetero-dinuclear dppz complex is reported. The interaction of complex [9] with double-stranded calf thymus DNA has been studied by absorption and emission titrations. The complex binds to the duplex by intercalation with good affinity and displays a DNA light switch effect but not DNA cleavage properties. The thermodynamic parameters showed that the complex-DNA interaction is enthalpically unfavourable and entropically favoured. Moreover, although the molecule does not display significant phototoxicity, with a PI of 2, it displays significant dark cytotoxicity.

## 5.2 Ru<sup>II</sup>-Ru<sup>II</sup> Polypyridyl complex with mixed-bis-intercalating ligands (dppz-dppn)

### 5.2.1 Introduction

In an attempt to explore new systems with different properties, mono and dinuclear ruthenium complexes containing a longer intercalative motif dppn were targeted. The purpose of this research was to investigate the effect of an increase in intercalative surface area has on DNA binding and spectroscopic parameters of dinuclear systems. Moreover, the known differences between the excited states of the [Ru<sup>II</sup>(dppz)] and [Ru<sup>II</sup>(dppn)] units prompted us to further investigate the properties of dinuclear ruthenium systems containing both intercalating ligands.

### 5.2.2 Synthetic Studies

#### 5.2.2.1 Ligand synthesis

Benzo[*i*]dipyrido[3,2-*a*:2',3'-*c*]phenazine, (dppn) was prepared by condensation of 1,10-phenanthroline-5,6-dione (dpq) with 2,3-diaminonaphthalene in methanol<sup>22</sup> (Figure 5. 2.1).

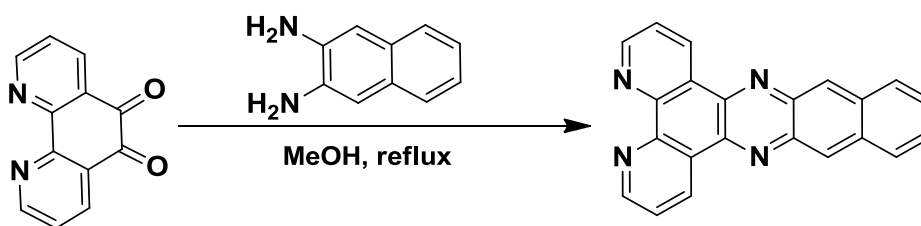


Figure 5.2.1: Synthesis of dppn.

### 5.2.2.2 Synthesis of complexes

#### **[Ru(tpm)(dppn)(L1)][PF<sub>6</sub>]<sub>2</sub> (10) and [{Ru(tpm)dppn}<sub>2</sub>L1][PF<sub>6</sub>]<sub>4</sub> (11)**

[Ru(tpm)(dppn)Cl]PF<sub>6</sub> was used as a starting material to prepare complexes [10], [11] and [12]. It was obtained by refluxing Ru(tpm)Cl<sub>3</sub> with dppn ligand in ethylene glycol at 120°C for 18 hours.<sup>23</sup> The solution was filtered through celite and the complex was precipitated by addition of saturated solution of NH<sub>4</sub>PF<sub>6</sub>.

The removal of the chloride ligand in [Ru(tpm)(dppn)Cl]<sup>+</sup> was accomplished by refluxing with silver nitrate for 2 hours in ethanol:water (3:1). The target complex [Ru(tpm)(dppn)(L1)]<sup>2+</sup> [10] was then synthesised by addition of the L1 ligand and refluxing for 72 hours. Precipitation of the complex occurred by addition of NH<sub>4</sub>PF<sub>6</sub>. It was then collected by centrifuging (**Figure 5.2.2**).

In addition, complex [{Ru(tpm)dppn}<sub>2</sub>L1]<sup>4+</sup> [11] was also synthesized. First [Ru(tpm)(dppn)Cl]<sup>+</sup> and AgNO<sub>3</sub> were heated to reflux in ethanol:water, then the filtrate solution was returned back to the reaction vessel and a solution of [10] in acetone was added to the reaction mixture and refluxed for 3 days. Precipitation of the product occurred by addition of NH<sub>4</sub>PF<sub>6</sub>, it was then collected by centrifuging and washed with water and diethyl ether before being dried under vacuum (**Figure 5.2.2**).

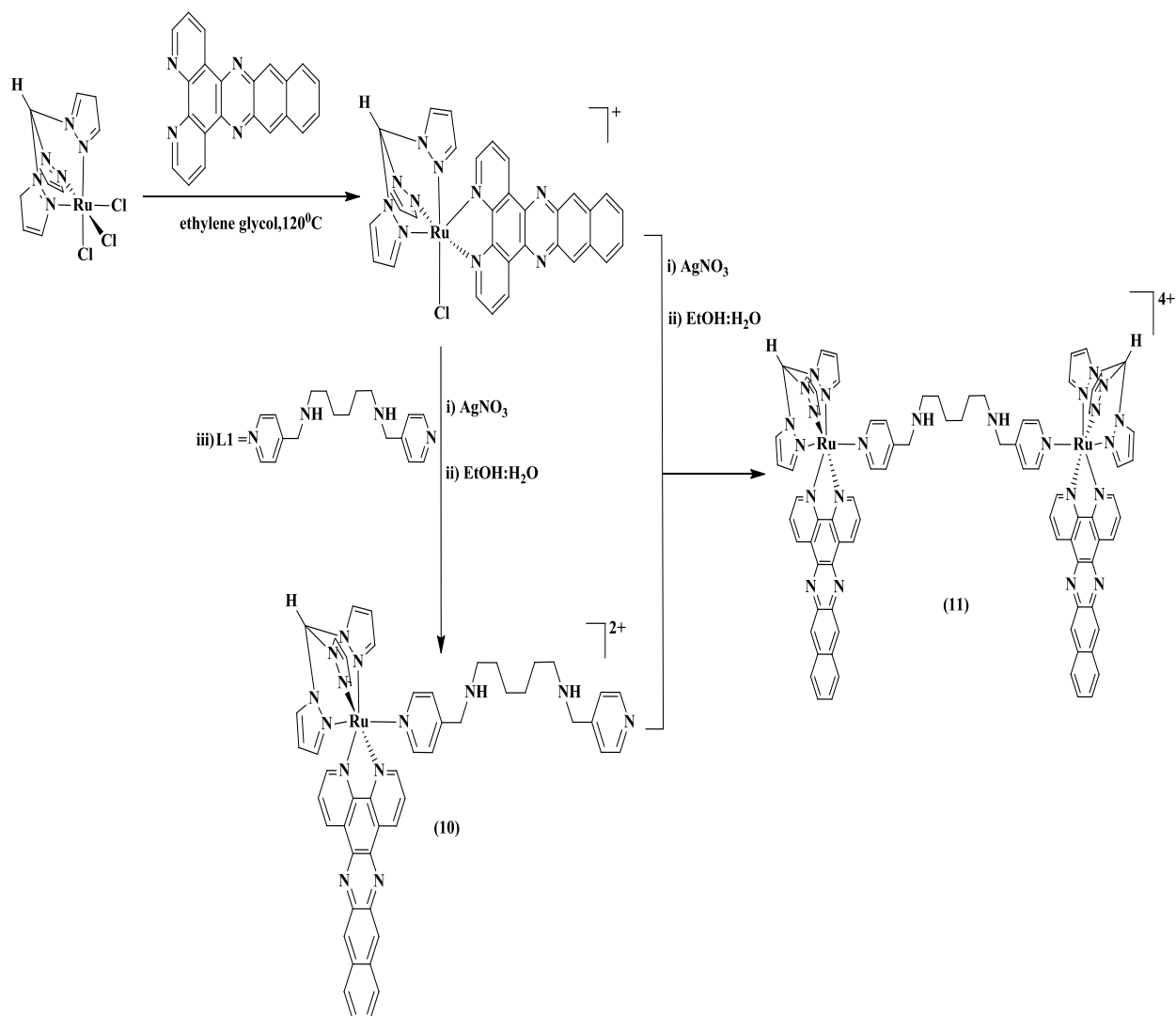


**Figure 5.2.2:** Synthesis of  $[Ru(tpm)(dppn)(L1)][PF_6]_2$  (**10**) and  $[Ru(tpm)(dppn)}_2L1][PF_6]_4$  (**11**)

Heteroleptic dincular complex  $[Ru(tpm)dppz-L1-Ru(tpm)dppn][PF_6]_4$  (**12**) was prepared in an identical manner to complex (**11**), except replacing the monomeric complex  $[10](PF_6)_2$  with  $[1]Cl_2$  (**Figure 5.2.3**).

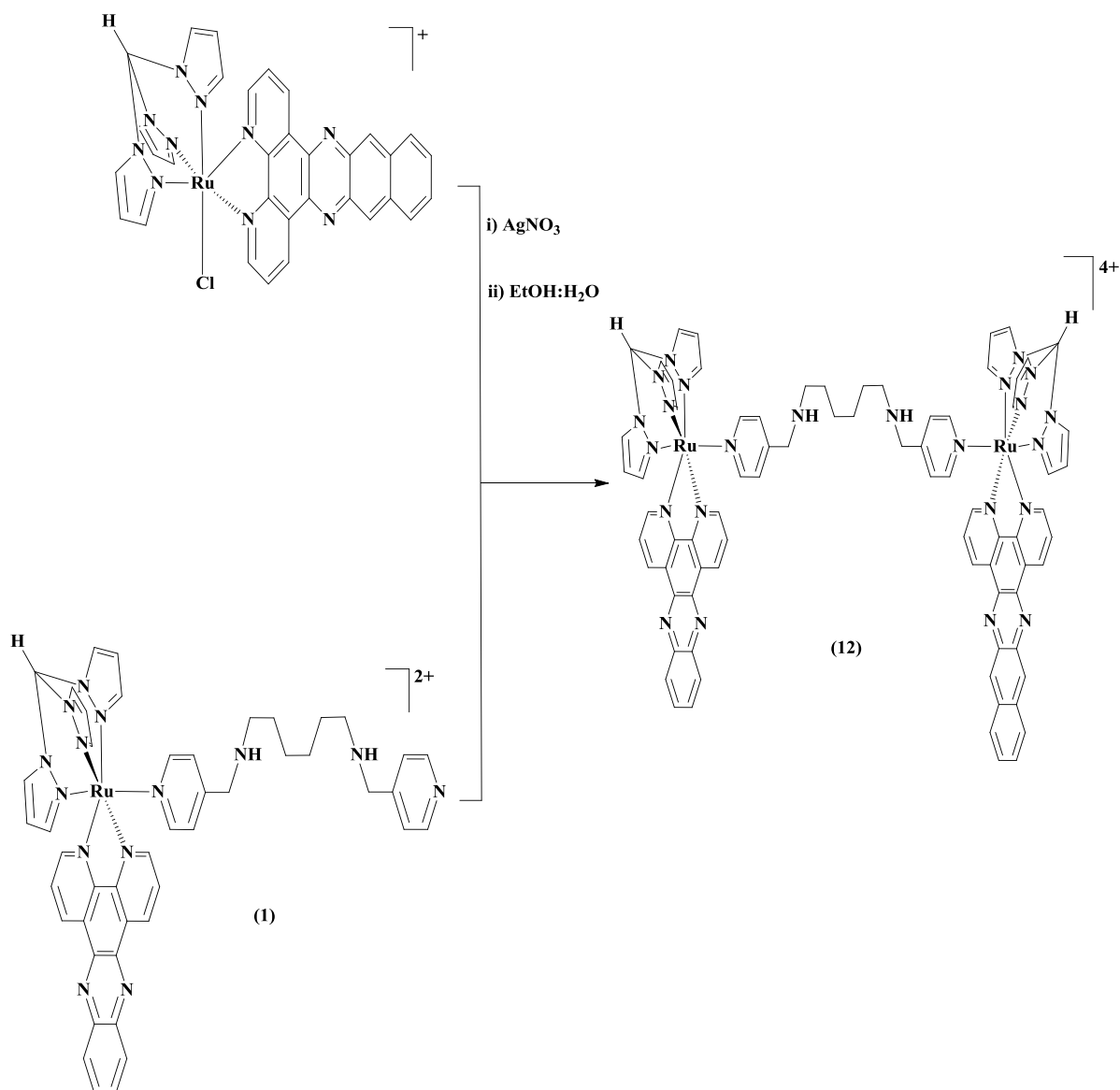


**Figure 5.2.3:** Synthesis of [Ru(tpm)dppz-L1-Ru(tpm)dppn][PF<sub>6</sub>]<sub>4</sub> (**12**)

## 5.2.3 Characterization

### 5.2.3.1 Absorption spectra

The UV-visible absorption spectra of complexes [10][PF<sub>6</sub>]<sub>2</sub>, [11][PF<sub>6</sub>]<sub>4</sub> and [12][PF<sub>6</sub>]<sub>4</sub> were recorded in acetonitrile at room temperature. The absorption spectra are shown in **Figure 5.2.4** and the spectroscopic data are summarised in **Table 5.2.1**.

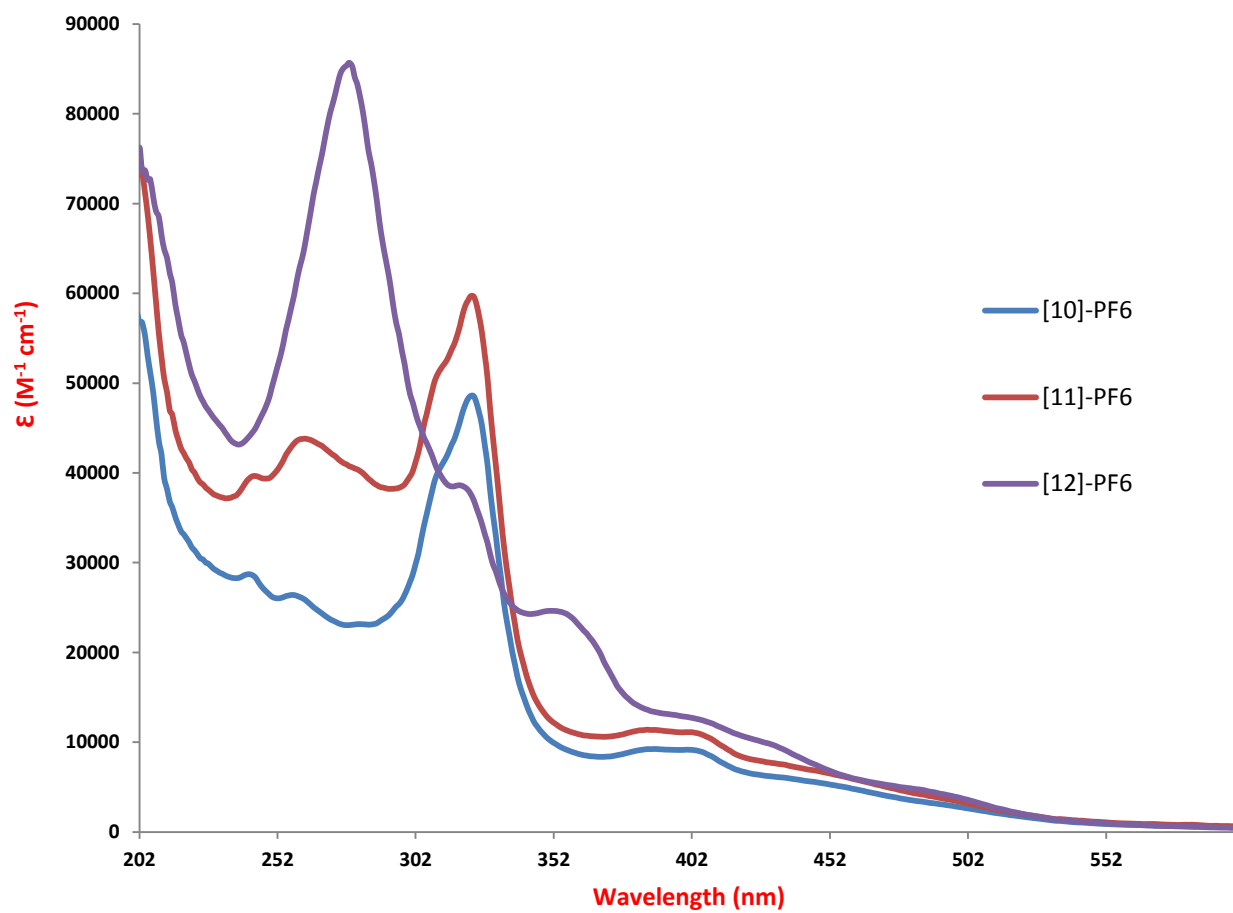


**Figure 5.2.4:** UV-Visible absorption spectra for the complexes [10], [11] and [12] as  $PF_6$  salts recorded in acetonitrile at room temperature.

Compound	$\lambda_{\text{max}}$ (nm)	$10^{-3}\epsilon(\text{M}^{-1}\text{cm}^{-1})$	Assignment
<b>(10) [Ru(tpm)(dppn)(L1)][PF<sub>6</sub>]<sub>2</sub></b>	241	28.69	$\pi \rightarrow \pi^*$
	257	26.39	$\pi \rightarrow \pi^*$
	280	23.15	$\pi \rightarrow \pi^*$
	310	40.61	$\pi \rightarrow \pi^*$
	323	48.55	$\pi \rightarrow \pi^*$
	387	9.22	$\pi \rightarrow \pi^*$
	404	8.98	$\pi \rightarrow \pi^*$
	453	5.23	MLCT
<b>(11) [{Ru(tpm)dppn}<sub>2</sub>L1][PF<sub>6</sub>]<sub>4</sub></b>	242	39.62	$\pi \rightarrow \pi^*$
	260	43.74	$\pi \rightarrow \pi^*$
	280	40.38	$\pi \rightarrow \pi^*$
	310	51.04	$\pi \rightarrow \pi^*$
	321	59.68	$\pi \rightarrow \pi^*$
	385	11.36	$\pi \rightarrow \pi^*$
	402	11.06	$\pi \rightarrow \pi^*$
	257	6.52	MLCT
<b>(12) [Ru(tpm)dppz-L1-Ru(tpm)dppn][PF<sub>6</sub>]<sub>4</sub></b>	231	45.34	$\pi \rightarrow \pi^*$
	277	85.36	$\pi \rightarrow \pi^*$
	318	38.54	$\pi \rightarrow \pi^*$
	354	24.49	$\pi \rightarrow \pi^*$
	404	12.58	$\pi \rightarrow \pi^*$
	434	9.35	MLCT
	490	9.35	MLCT

**Table 5.2.1:** UV-Visible data for the complexes **[10]**, **[11]** and **[12]** as PF<sub>6</sub> salts recorded in acetonitrile at room temperature.

The data for these complexes recorded in water as their respective chloride salts is also summarised below in **Table 5.2.2**. The absorption spectra for these compounds are shown in **Figure 5.2.5**.

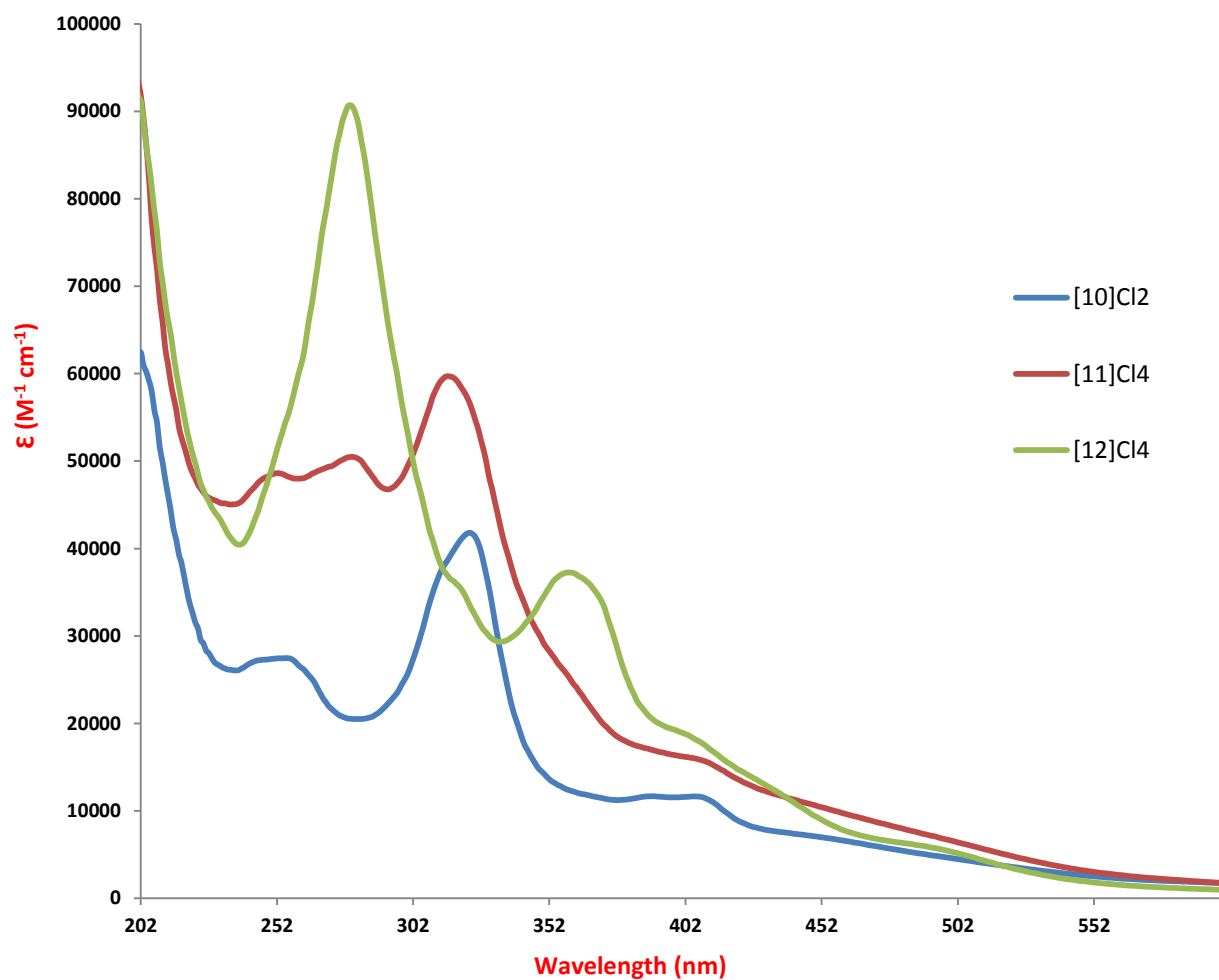


**Figure 5.2.5:** UV-Visible absorption spectra for the complexes [10], [11] and [12] as chloride salts recorded in 5mM tris buffer, 25 mM NaCl, pH 7.4 at 25 °C.

Compound	$\lambda_{\text{max}}$ (nm)	$10^{-3}\epsilon$ ( $\text{M}^{-1}\text{cm}^{-1}$ )	Assignment
<b>(10) [Ru(tpm)(dppn)(L1)]Cl<sub>2</sub></b>	248	27.38	$\pi \rightarrow \pi^*$
	261	26.35	$\pi \rightarrow \pi^*$
	313	37.59	$\pi \rightarrow \pi^*$
	322	41.74	$\pi \rightarrow \pi^*$
	387	11.62	$\pi \rightarrow \pi^*$
	406	11.63	$\pi \rightarrow \pi^*$
	457	7.89	MLCT
<b>(11) [{Ru(tpm)dppn}<sub>2</sub>L1]Cl<sub>4</sub></b>	250	49.04	$\pi \rightarrow \pi^*$
	267	48.86	$\pi \rightarrow \pi^*$
	280	50.47	$\pi \rightarrow \pi^*$
	314	59.74	$\pi \rightarrow \pi^*$
	359	24.59	$\pi \rightarrow \pi^*$
	408	17.54	$\pi \rightarrow \pi^*$
	453	8.63	MLCT
<b>(12) [Ru(tpm)dppz-L1-Ru(tpm)dppn]Cl<sub>4</sub></b>	252	51.34	$\pi \rightarrow \pi^*$
	280	89.66	$\pi \rightarrow \pi^*$
	320	35.16	$\pi \rightarrow \pi^*$
	361	37.03	$\pi \rightarrow \pi^*$
	404	18.47	$\pi \rightarrow \pi^*$
	438	11.71	MLCT
	490	5.94	MLCT

**Table 5.2.2:** UV-Visible data for the complexes **[10]**, **[11]** and **[12]** as chloride salts recorded in 5mM tris buffer, 25 mM NaCl, pH 7.4 at 25 °C.

The absorption bands centred at 250 and 260 nm are assigned to dppn based intraligand (IL)  $\pi \rightarrow \pi^*$  transitions. These bands appear unique to the dppn ligand as they have not been seen previously within spectra of the Ru(dppz) based systems. Previous work in the Thomas group

also shows the presence of these bands,<sup>24</sup> as well as that of the dominant band around 320 nm, and they are assigned to  $\pi \rightarrow \pi^*$  transitions. The UV–Visible spectrum of the dppz ligand in acetonitrile exhibits a moderately intense band in the near-UV with two principle maxima at  $\lambda = 358$  and 376 nm, which are characteristic of  $\pi \rightarrow \pi^*(\text{dppz})$  transitions. Therefore, the intense band at 361 nm for complex [12] is characteristic of  $\pi \rightarrow \pi^*(\text{dppz})$  transitions. The absorption spectrum of the free dppn ligand in acetonitrile is shown to have a similar ‘double humped’ absorption in the near-UV region with maxima at  $\lambda = 390$  and 411 nm.<sup>23</sup> Therefore, these peaks at 387 and 406 nm have been assigned as analogous dppn-based transitions. These transitions are more clearly seen when looking at the spectrum of the chloride salt which shows these peaks individually at 387 and 406 nm, as well as when observing the spectrum of the starting complex,  $[\text{Ru}(\text{tpm})(\text{dppn})\text{Cl}]^+$ . The bands around 450 and 490 nm have been assigned as belonging to MLCT transitions which typically occur at this energy.<sup>25</sup>

Complexes [10] and [11] do not display the characteristically intense  $^3\text{MLCT}$  based luminescence in both acetonitrile and water. However, complex [12] does display a change in emission spectrum around ~640 nm upon addition of CT-DNA.

## 5.2.4 Transient Absorption Studies

The study of the photoexcitation properties of ruthenium polypyridyl complexes have proven to be suitable in furthering the understanding of both energy and electron-transfer processes<sup>16,26,27</sup> and in the design of applied photoconversion systems.<sup>28-31</sup> The metal-to-ligand charge transfer (MLCT) transition is most often the process of interest in these complexes, in which a formal oxidation and reduction reactions of the metal and the ligand occurs upon photoexcitation. Studies suggest that the photoexcited electron of mixed ligand type complexes is localized on the lowest energy ligand, at least on long (> nanosecond) time scales.<sup>32-36</sup> However, the relaxation processes which lead to the formation of this state are not well understood. To this end, transient absorption studies on the new complexes were performed by Dr. Stuart Archer (a fellow member of the Thomas group). The transient difference spectra obtained in flash photolysis experiments for complexes  $[\mathbf{3}]^{4+}$ ,  $[\mathbf{11}]^{4+}$  and  $[\mathbf{12}]^{4+}$  in MeCN are shown in **Figure 5.2.6**.

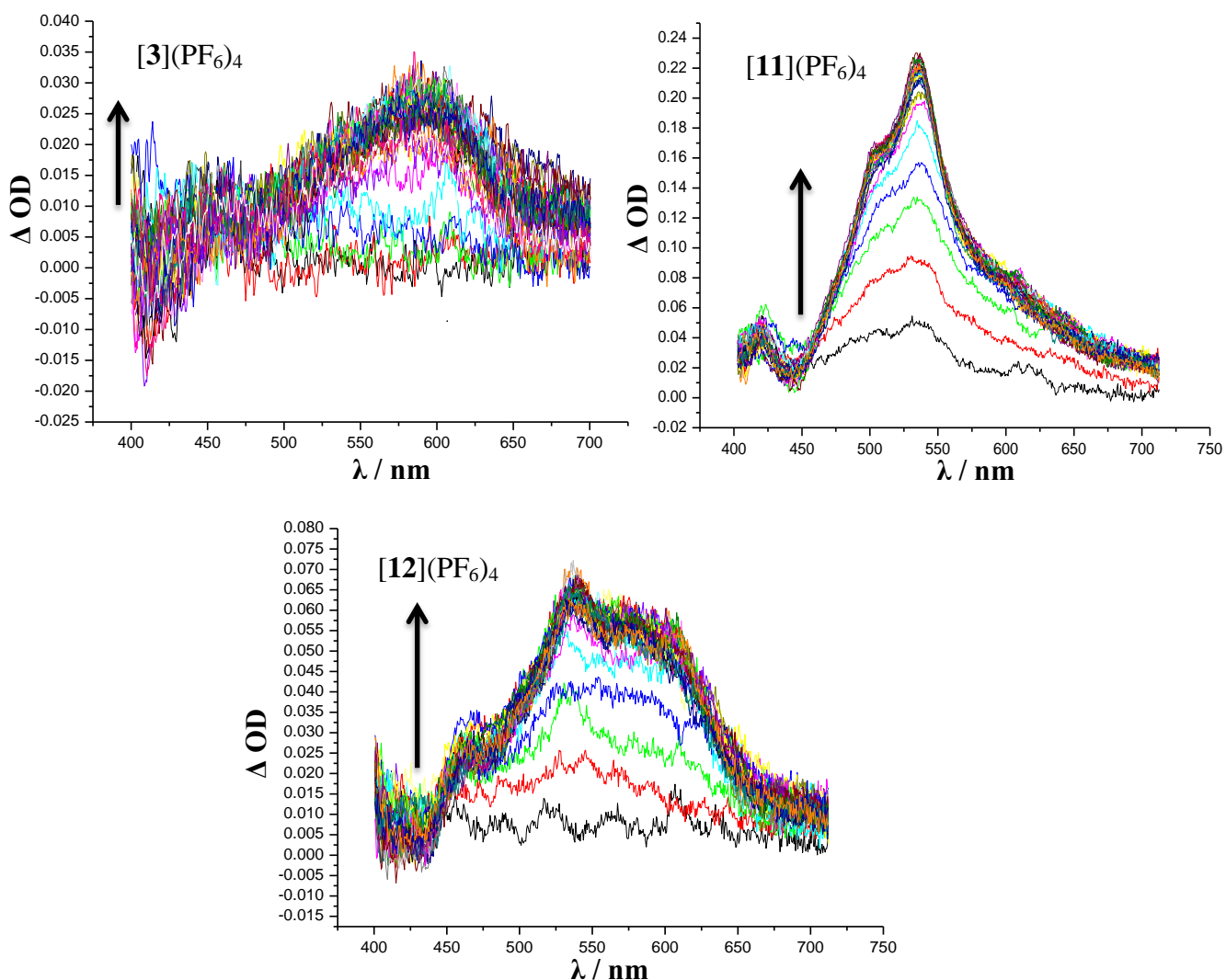


**Figure 5.2.6:** Transient absorption spectra of complexes  $[3]^{4+}$ ,  $[11]^{4+}$  and  $[12]^{4+}$  at different time delays after the laser excitation with a 355 nm in  $\text{CH}_3\text{CN}$ .

Excitation of solutions of all three complexes at 355 nm with a 7 ps laser pulse leads to the formation of several distinctive transients due to bleaching of the absorption bands of the ground state. The transient spectra for  $[3]^{4+}$ ,  $[11]^{4+}$  and  $[12]^{4+}$  are completely unmatched; these data imply that the lowest excited state detected on the picosecond time scale is not the same in all cases. The observed transient spectrum of complex **[3]** are characteristic of dppz-based MLCT absorption, which is in a good agreement with the fact that the lowest triplet excited state in complex **[3]** is  $^3\text{MLCT}$  states with abroad absorption at  $\sim 600$  nm.

However, the transient absorption spectrum of complex [11] differs significantly from that of [3] and [12] due to the fact that the lowest triplet excited state in complex [3] is localized on the  $^3\pi\pi^*$  of the dppn with absorption at ~540 nm rather than  $^3\text{MLCT}$ .

Interestingly, in the presence of both dppz/dppn ligands in the same complex [12], the transient absorption spectrum is the combination of both triplet excited states  $^3\pi\pi^*$  and  $^3\text{MLCT}$ . The  $^3\pi\pi^*$  absorption grows at 540 nm as well as a broad  $^3\text{MLCT}$  absorption around ~600 nm. This study reveals that  $\text{Ru}^{\text{II}}(\text{dppz})$  systems exhibit an  $^3\text{MLCT}$  lowest excited state, however  $^3\pi\pi^*$  is the lowest excited state of all the  $\text{Ru}^{\text{II}}(\text{dppn})$  complexes, which is similar to the previously reported data for related systems.<sup>37</sup> In future work these studies will be extended to longer time window so as to investigate the lifetimes of - and the dynamic interplay between - these states

## 5.2.5 DNA binding studies

### 5.2.5.1 UV-Vis titrations

To measure the interaction of metal complexes with the DNA double helix, changes in their UV-Vis spectra were used. Changes in the UV-Vis spectra of [10], [11] and [12] upon addition of CT-DNA are shown in **Figures 5.2.7, 5.2.8 and 5.2.9** respectively. In all cases, upon addition of DNA, the complexes showed several bands shifting to longer wavelengths; changes that were often accompanied by decreases in intensity until saturation is reached. These hypochromicity and bathchromic effect are typical for the stacking of aromatic ligands in between the base pairs of DNA.<sup>38,6,39,40</sup>

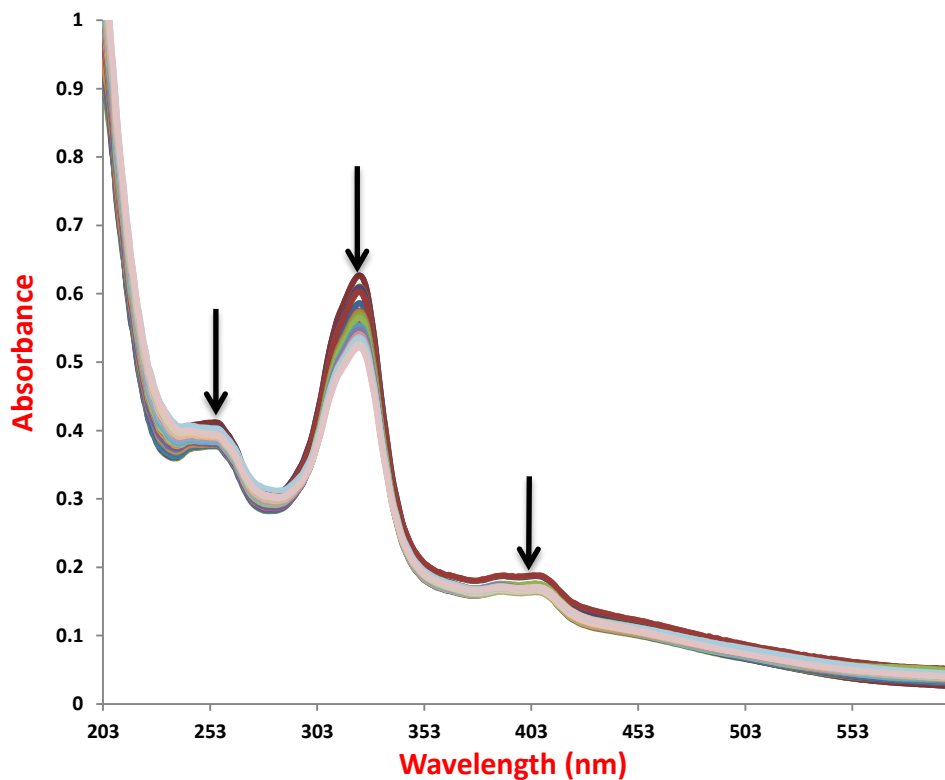


**Figure 5.2.7:** UV-Vis titration of 1.25 mM bp<sup>-1</sup> CT-DNA into a solution of 15 μM [10]Cl<sub>2</sub> in 5 mM tris buffer, 25 Mm NaCl, pH 7.4 at 25 °C.

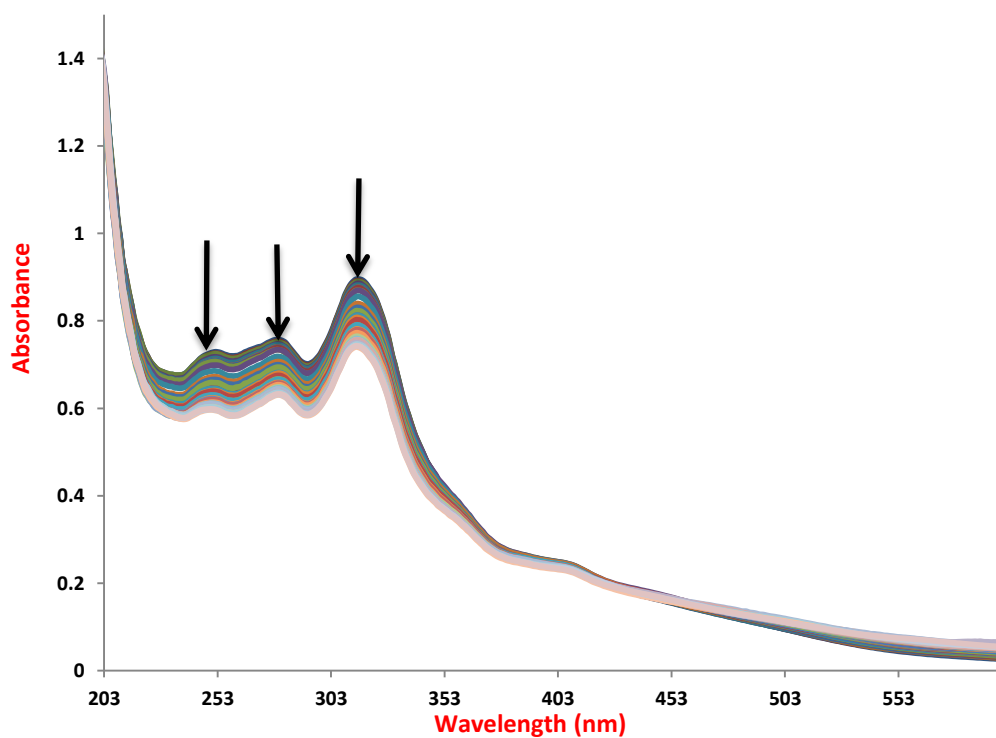


**Figure 5.2.8:** UV-Vis titration of 1.25 mM bp<sup>-1</sup> CT-DNA into a solution of 15 μM [11]Cl<sub>4</sub> in 5 mM tris buffer, 25 Mm NaCl, pH 7.4 at 25 °C.

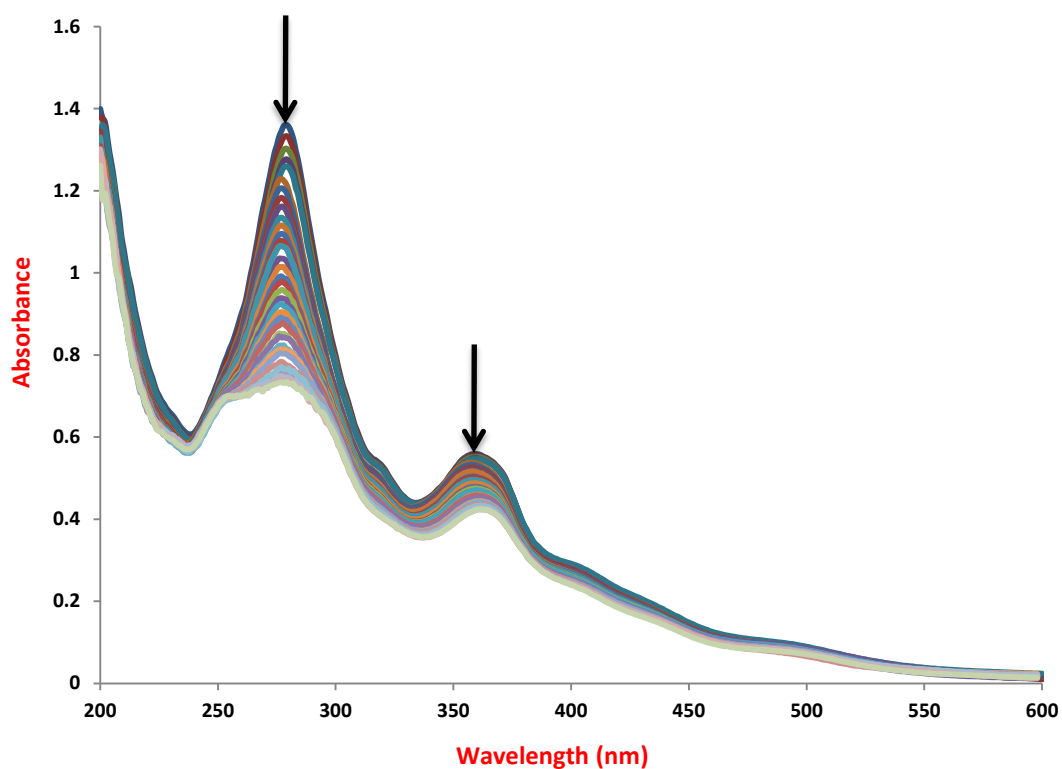


**Figure 5.2.9:** UV-Vis titration of 1.25 mM bp<sup>-1</sup> CT-DNA into a solution of 15 μM [12]Cl<sub>4</sub> in 5 mM tris buffer, 25 Mm NaCl, pH 7.4 at 25 °C.

Binding curves for the interaction of [10], [11] and [12] with CT-DNA, following the changes in the 320 nm and 314 nm bands for both [10] and [11] complexes respectively (**Figure 5.2.10**), and 280 nm of [12] (**Figure 5.2.11**) were constructed. They all showed that saturation binding had taken place.

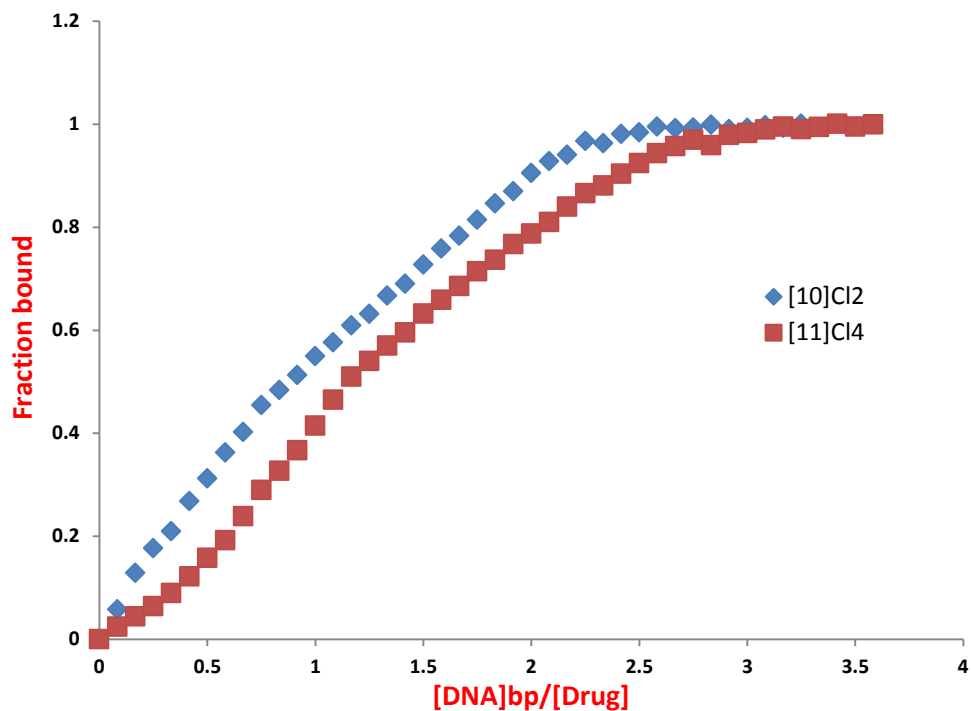


**Figure 5.2.10:** Binding curves obtained by UV-Vis titrations for [10]Cl<sub>2</sub> (blue) and [11]Cl<sub>4</sub> (red) binding to CT-DNA

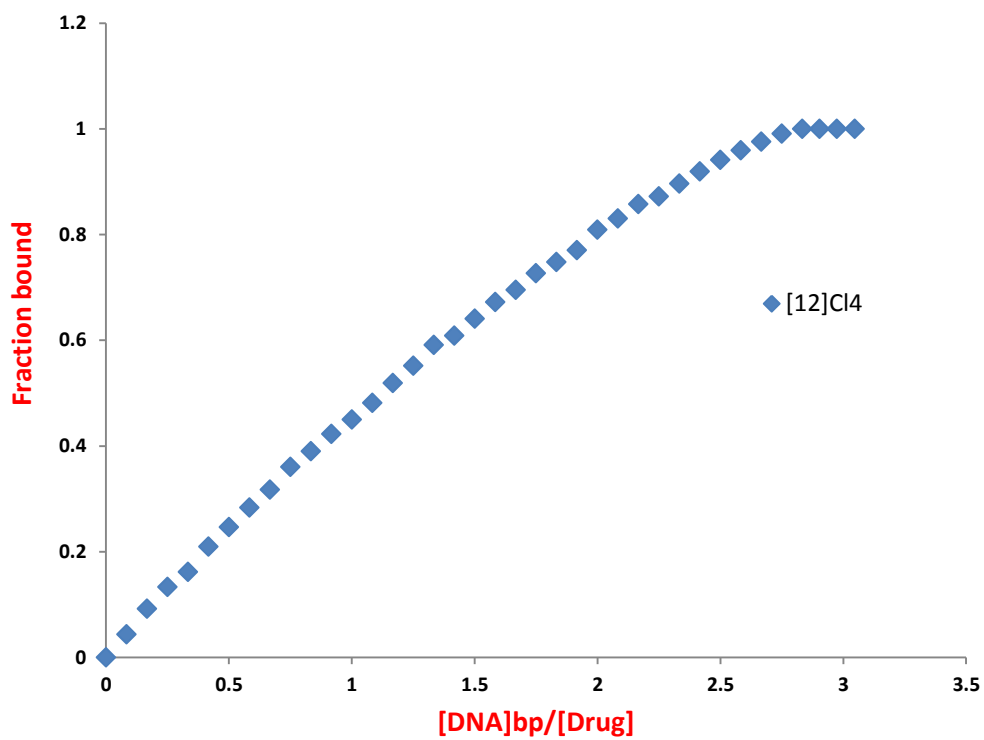


**Figure 5.2.11:** Binding curve obtained by UV-Vis titration for [12]Cl<sub>4</sub> binding to CT-DNA

### 5.2.5.2 Luminescence titrations

As mentioned above, both complexes [10] and [11] showed no emission in acetonitrile and also in aqueous solution upon addition of CT-DNA. These observations agree with previous studies showing that the lowest excited state of the Ru(dppn) moiety is not the MLCT observed in Ru(dppz) systems but a non-emissive dppn-based  $\pi \rightarrow \pi^*$  state. In these previous studies, this state was found to be quenched by O<sub>2</sub>, making these systems highly efficient at sensitising triplet to singlet oxygen conversion. In contrast, the emission spectrum of heteroleptic complex [12] does display a change in emission properties upon addition of CT-DNA. Clearly, due to the presence of the {Ru<sup>II</sup>(dppz)} unit, complex [12] does show a molecular light switch effect (**Figure 5.2.12**) in which Ru(d $\pi$ ) $\rightarrow$ dppz ( $\pi^*$ ) <sup>3</sup>MLCT appears to dominate the excited state of the complex, an observation that is consistent with the TA studies described previously.

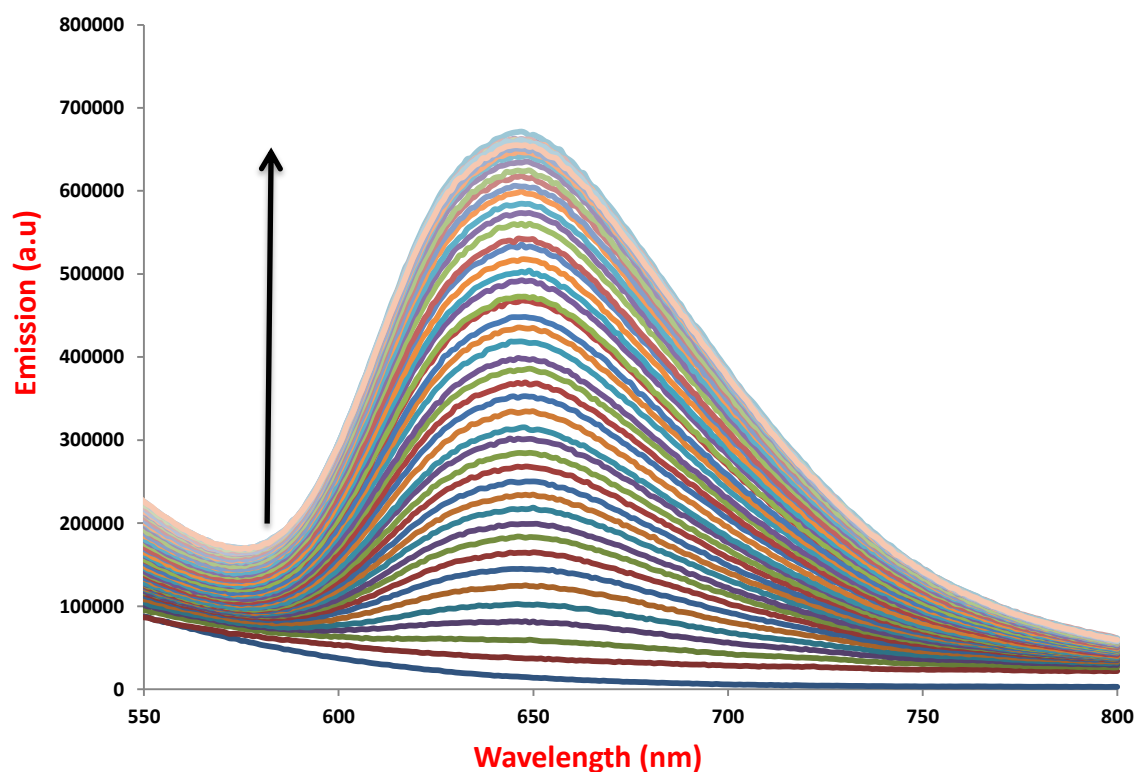


**Figure 5.2.12:** Luminescence titration of complex [12] with CT-DNA. (5 mM Tris buffer, 25 mM NaCl, pH 7.4, 25 °C).

The binding curve for the interaction of  $[^{125}\text{I}]\text{Cl}_4$  with CT-DNA are shown in **Figure 5.2.13**. Once again it shows that saturation binding had taken place.

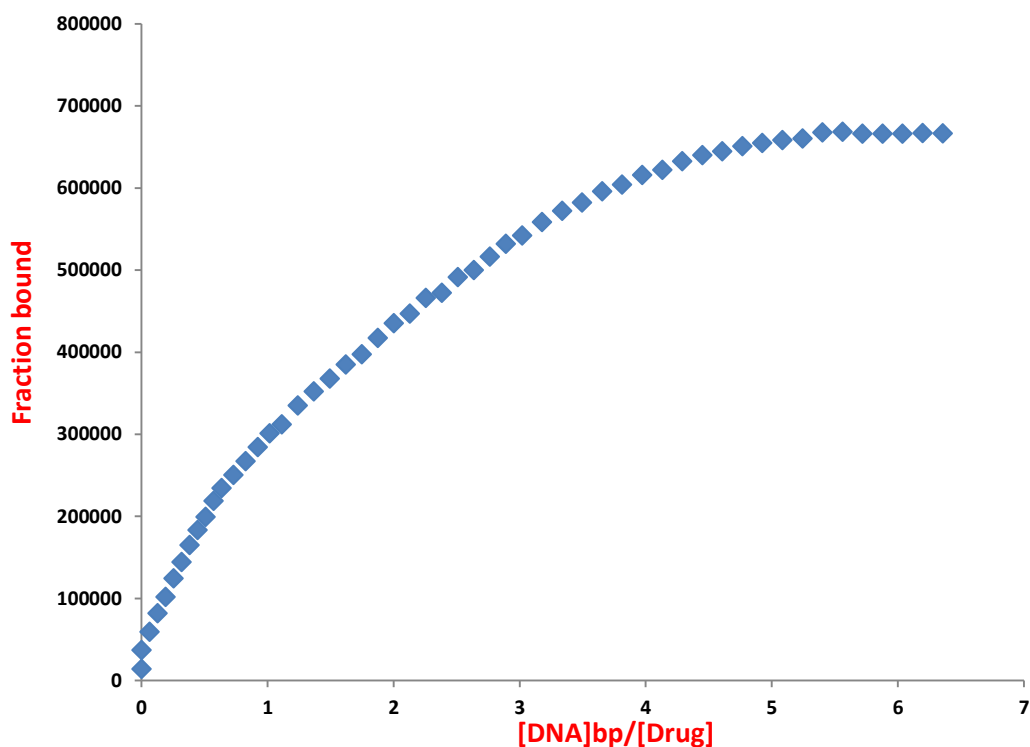


**Figure 5.2.13:** Binding curve obtained by Luminescence titration for  $[^{125}\text{I}]\text{Cl}_4$  binding to CT-DNA

Again, the binding constant for the interaction of these complexes with CT-DNA were calculated by using the simple Wolfe model<sup>9</sup> instead of the Mcghee Von Hippel model as the luminescence and absorption titrations data did not fit to the later model. The binding constant data are summarised in **Table 5.2.3**.

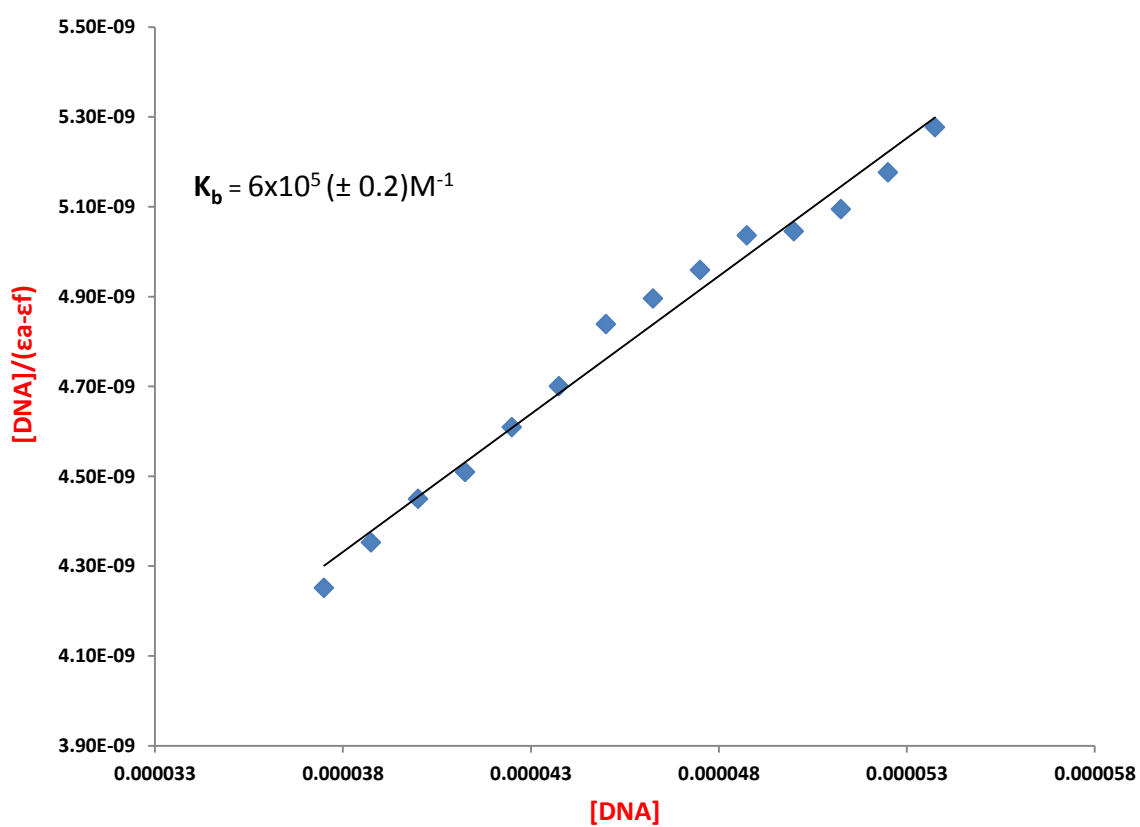
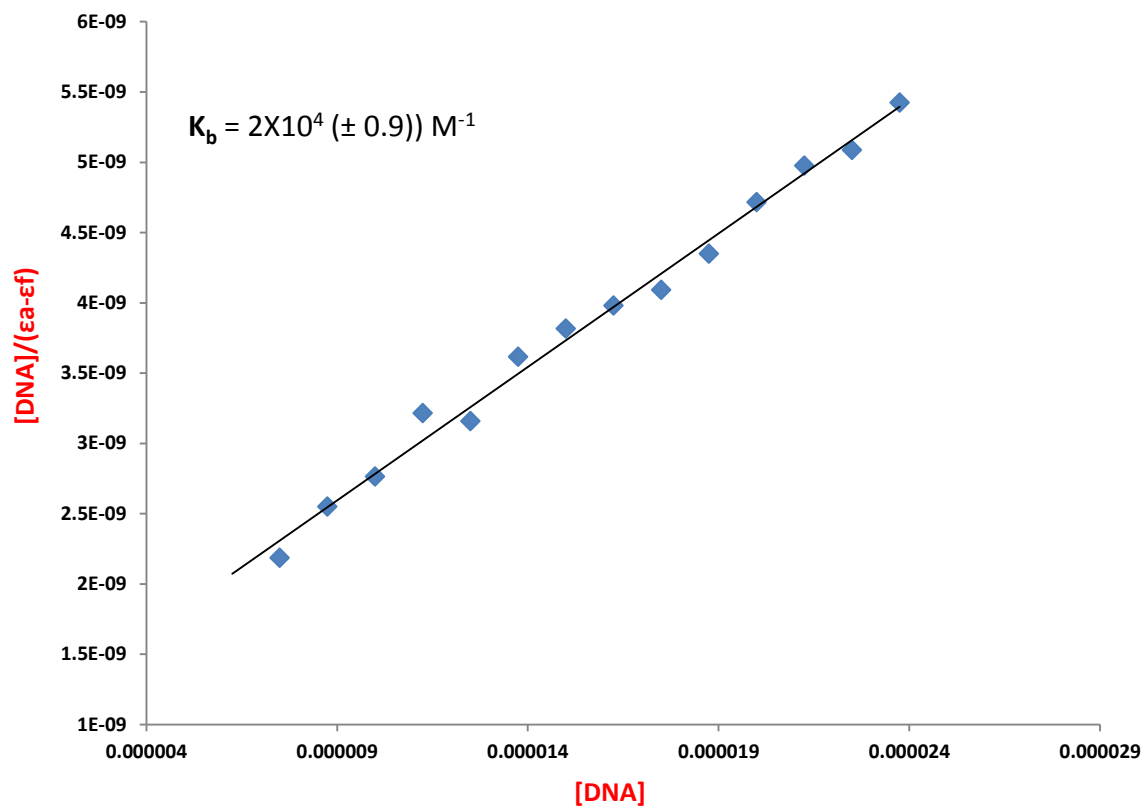


**Figure 5.2.14:** Scatchard plots for the complex **[10]Cl<sub>2</sub>** (top) and complex **[11]Cl<sub>4</sub>** (bottom) obtained from the absorption spectroscopy of CT-DNA. Inserted plot,  $[DNA]/(\epsilon a - \epsilon f)$  versus  $[DNA]$  for the absorption titrations.

Complex	$K_b$ ( $M^{-1}$ )
[10]Cl <sub>2</sub>	$2 \times 10^4$ ( $\pm 0.9$ )
[11]Cl <sub>4</sub>	$6 \times 10^5$ ( $\pm 0.2$ )
[12]Cl <sub>4</sub>	$8 \times 10^6$ ( $\pm 0.7$ )

**Table 5.2.3:** Binding constants and binding site sizes obtained by UV-Visible titrations of CT-DNA with complexes [10]Cl<sub>2</sub>, [11]Cl<sub>4</sub> and [12]Cl<sub>4</sub>.  $K_b$  is the intrinsic binding constant.

Binding constants for the interaction of both complexes [10] and [11] with CT-DNA are similar to other Ru(II)-dppz complexes.<sup>41-43</sup> Increasing the surface area of the intercalator was expected to improve the affinity of complexes for DNA, unfortunately complex [11] shows an affinity for CT-DNA that is very similar to the analogous complex with dppz ( $K_b = 2 \times 10^5 M^{-1}$  for the interaction of  $[(\text{tpm})\text{Ru}(\text{dppz})_2(\text{L1})]^{4+}$  with CT-DNA, see chapter two). In fact, complex [10] actually shows an affinity to DNA that is one order of magnitude lower with respect to the analogous dppz complexes. More interestingly, hetero-intercalator complex [12] has a binding constant around one order of magnitude higher than that obtained for dicationic octahedral complexes of dppz and is the largest observed for any of the dinuclear systems synthesized by the Thomas group.

## 5.2.6 Singlet oxygen quantum yield

Ruthenium (II) polypyridyl complexes with DNA photocleavage activity have received significant attention as potential use as anticancer agents and as DNA structural probes.<sup>12</sup> Many Ru<sup>II</sup> polypyridyl complexes that are active through a <sup>1</sup>O<sub>2</sub> mechanism have been

confirmed to possess DNA photocleavage activities. However, their applications in photodynamic therapy are limited, especially when the absorption maximum of the metal-to-ligand charge-transfer (MLCT) transition is shorter than 500 nm. Ligands can provide Ru complexes with longer MLCT absorption by their delocalized  $\pi$  systems.<sup>44,45</sup> However, as predicted by the energy-gap law,<sup>46</sup> a lower energy gap often leads to a shorter excited-state lifetime, which is unfavourable for  $^1\text{O}_2$  generation.

That said, previous work has shown that complexes with the dppn ligand can cleave DNA. For example, the ability of this ligand to produce sensitised oxygen when coordinated to Ru<sup>II</sup> metal centres has been studied by the Thomas group,<sup>47</sup> these studies showed that oxygen sensitising yields of around 70 - 83% can be achieved. This is due to population of the ligand centred (LC)  $\pi$ - $\pi^*$  transition acting as the sensitiser for singlet oxygen.<sup>25</sup> Such metallo-intercalator systems could possibly be useful in therapeutic systems such as photodynamic therapy. Thus the  $^1\text{O}_2$  quantum yields of [3], [11] and [12] were determined in acetonitrile at 355 nm by a collaborator Luke McKenzie in the Weinstein group. The  $^1\text{O}_2$  quantum yields were measured to be 0.0494 for [3], 0.6721 for [11] and 0.1568 for complex [12]. As expected, the  $^1\text{O}_2$  quantum yield of complex [11] is almost four times larger than that of [12] and thirteen times higher than that of [3], this higher value obtained for complex [11] is assigned to the excited state being dominated by the  $\pi\pi^*$  triplet state of dppn ligand. The  $^1\text{O}_2$  quantum yields data are summarised in **Table 5.2.4**.

Compound	[3]	[11]	[12]
Singlet oxygen yield	0.0494 +/- 0.0104	0.6721 +/- 0.0550	0.1568 +/- 0.0138

**Table 5.2.4:** Quantum yield of singlet oxygen production of [3],[11] and [12] measured in acetonitrile at 355 nm

## 5.2.7 DNA photocleavage and Singlet Oxygen Production

Given the promising singlet oxygen data, the DNA photocleavage properties of [10] and [11] were investigated using supercoiled pUC57 plasmid DNA and analysed by electrophoresis on an agarose gel. Changes in pUC57 plasmid DNA are detected, either when irradiated in the absence of ruthenium complex or when incubated with the sensitizer in the dark. The photocleavage efficiency depends on the structure of the metal complex. After irradiating plasmid DNA in the presence of [10] and [11], the supercoiled native form (**I**) completely disappears. This seems to be because both [10] and [11] complexes cleave the DNA strands into very small, fast moving fragments (**Figure 5.2.15**).

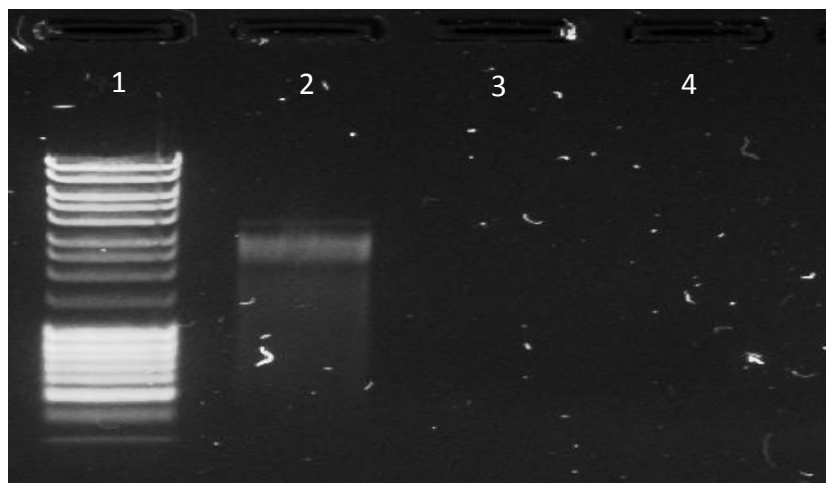


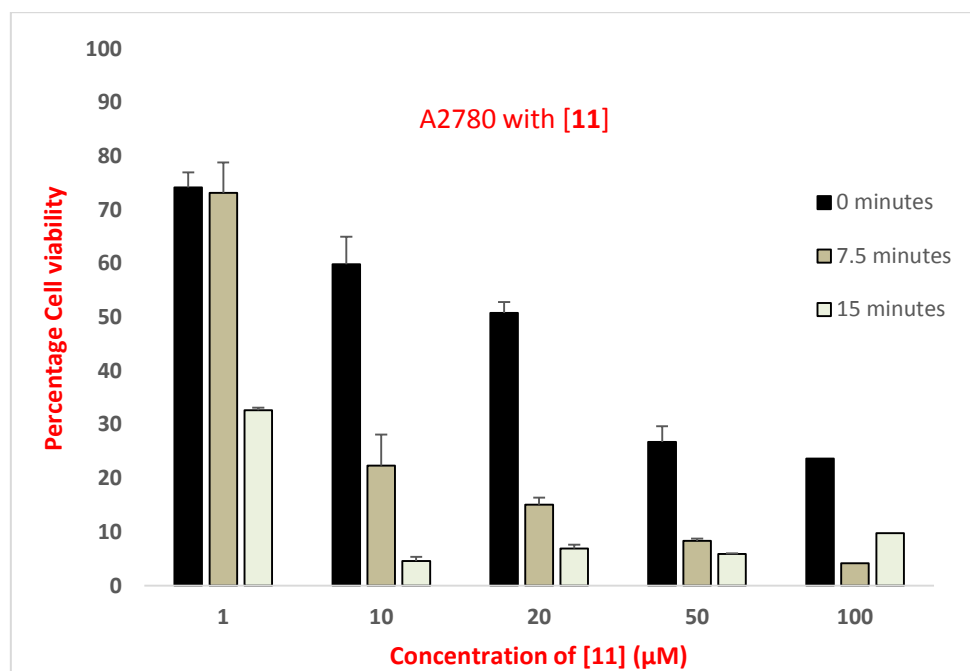
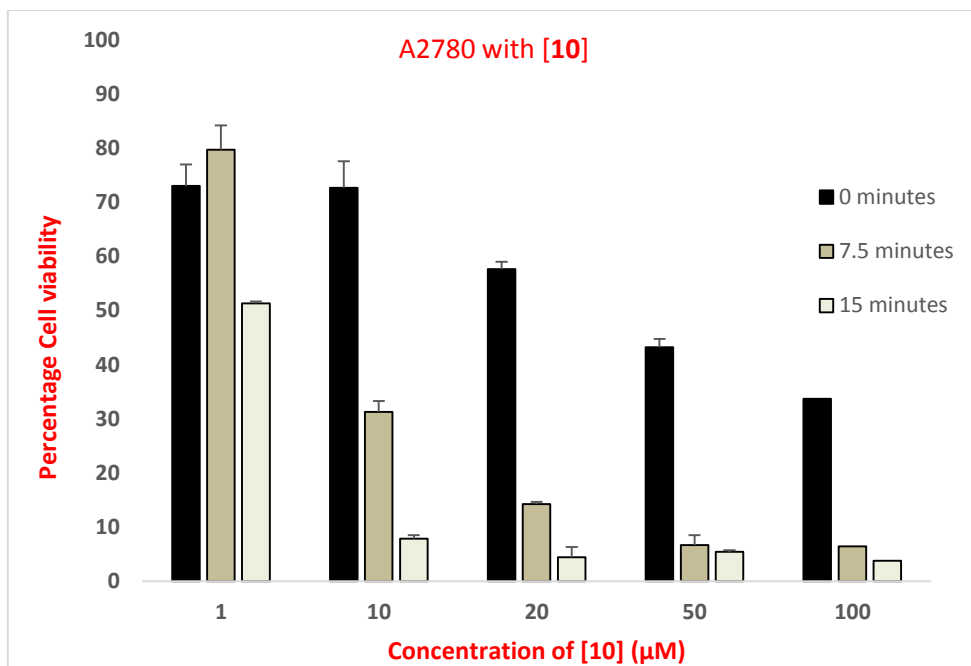
**Figure 5.2.15:** Photocleavage of supercoiled pUC57 DNA ( $0.1 \mu\text{g}/\mu\text{L}$ ) by [10] and [11] under illuminated condition (470 nm, 100 mW, 30 minutes exposure) in 50 mM TAE buffer. Lane 1, DNA marker; lane 2, DNA control; Lane 3, DNA + **10** ( $20 \mu\text{M}$ ); lane 4, DNA + **11** ( $20 \mu\text{M}$ )

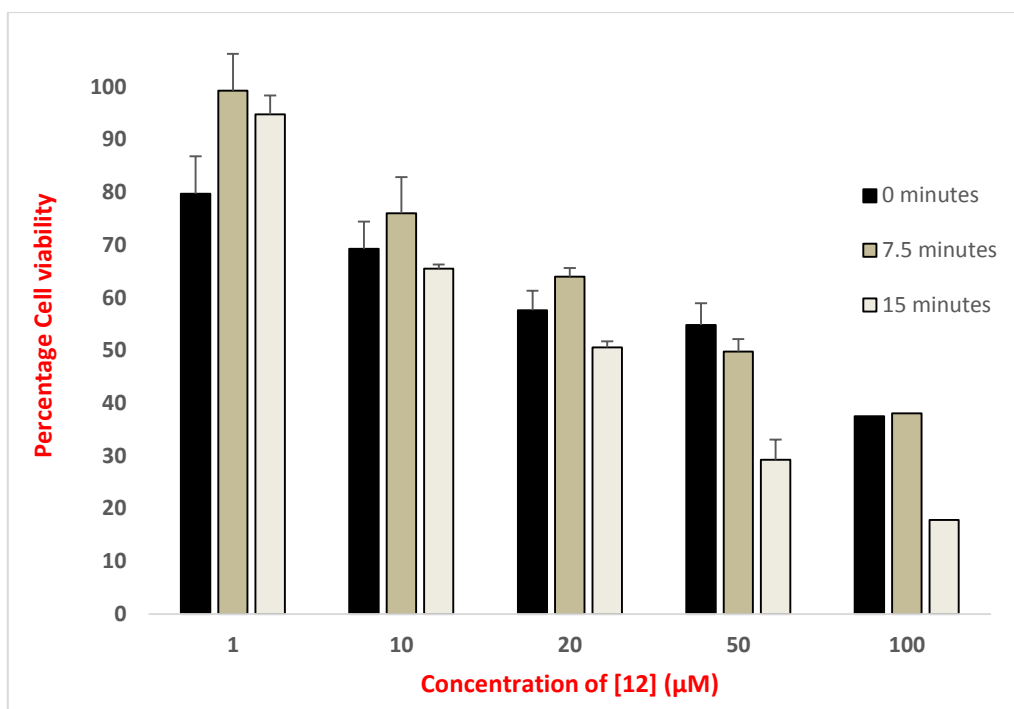
In order to explore how the exposure timing affected photocleavage process, the photocleavage experiment was examined under the same condition except the samples were irradiated for a shorter time 5 minutes. However, the same result was observed.

## 5.2.8 Phototoxicity

To activate a molecule and yield an effective drug with spatial and temporal selectivity by the use of visible light is the aim of photodynamic therapy (**PDT**).<sup>48-50</sup> The general principle of **PDT** is based on a photosensitizer (**PS**), ideally a nontoxic molecule with a higher affinity for cancer cells over healthy cells, that can be excited by irradiation with light and then enter a triplet excited state through intersystem crossing. In this state, the **PS** can react with a substrate or solvent molecule, through hydrogen atom or electron transfer, generating radicals. More significantly the **PS** can also transfer energy to molecular oxygen, forming singlet oxygen ( $^1\text{O}_2$ ).<sup>51,52</sup>

The cellular phototoxicity of complexes **[10]**, **[11]** and **[12]** was evaluated with human ovarian cancer cell lines, A2780 and A2780cis, using laser irradiation at 420 nm. The cells were exposed for 24 h using a concentration range of 1–100  $\mu\text{M}$  for each complex resulting in the phototoxic effects shown in **Figures 5.2.16 and 5.2.17**. This study was done by Dr. Paul Jarman (a fellow member of the Thomas group) using the A2780 cell line. At low concentrations (10  $\mu\text{M}$ ) and exposure to light, both complexes **[10]** and **[11]** produced rapid decreases in cell viability leading to nearly total cell death after an exposure to light intensities above 15  $\text{Jcm}^{-2}$ .  $\text{IC}_{50}$  values (where  $\text{IC}_{50}$  = concentration required to kill half of the cells) for both complexes were calculated. With a decrease in  $\text{IC}_{50}$  values from 32  $\mu\text{M}$  and 20  $\mu\text{M}$  for complexes **[10]** and **[11]** in the dark to 1.8  $\mu\text{M}$  and  $< 0.1 \mu\text{M}$  for both complexes respectively after an exposure of 15  $\text{Jcm}^{-2}$  this cell line showed a considerable phototoxic response. However, somewhat surprisingly, complex **[12]** also induced a dramatic decrease in cell viability with exposure to higher concentrations and longer irradiations. The  $\text{IC}_{50}$  value decreases from 60  $\mu\text{M}$  in the dark to 20  $\mu\text{M}$  after an exposure of 15  $\text{Jcm}^{-2}$ .



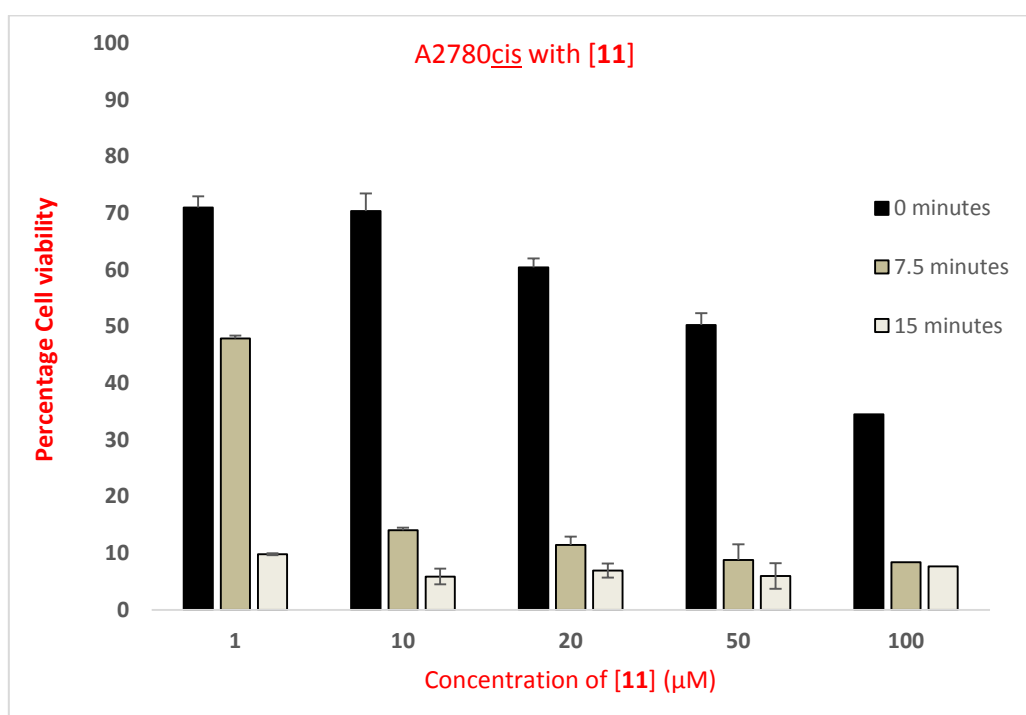
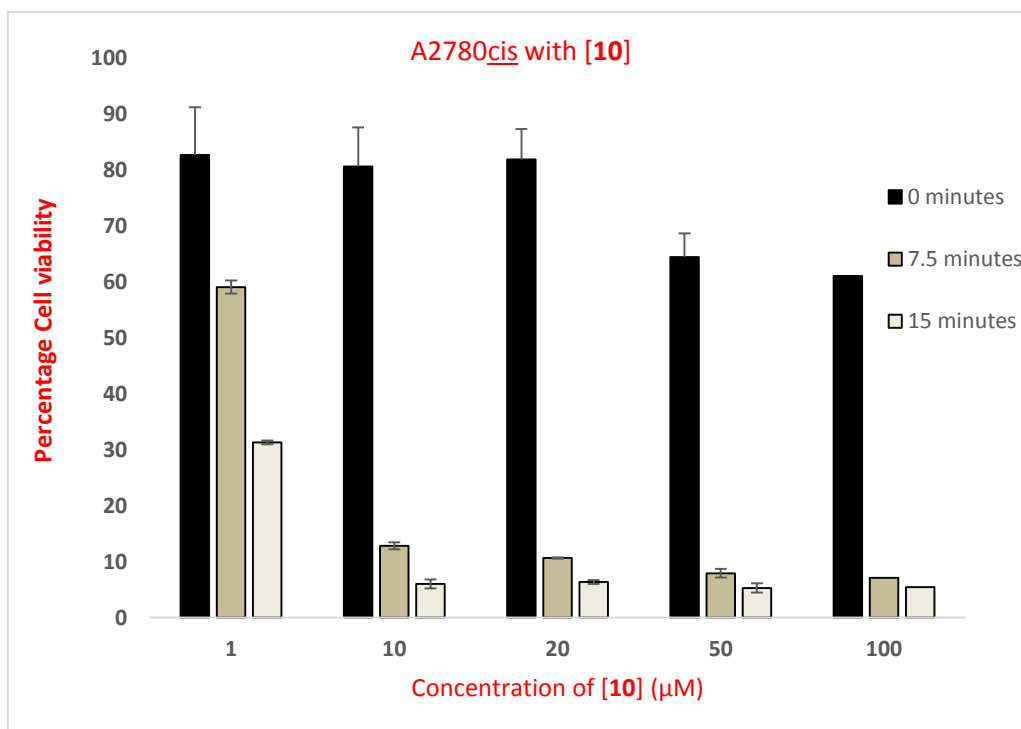


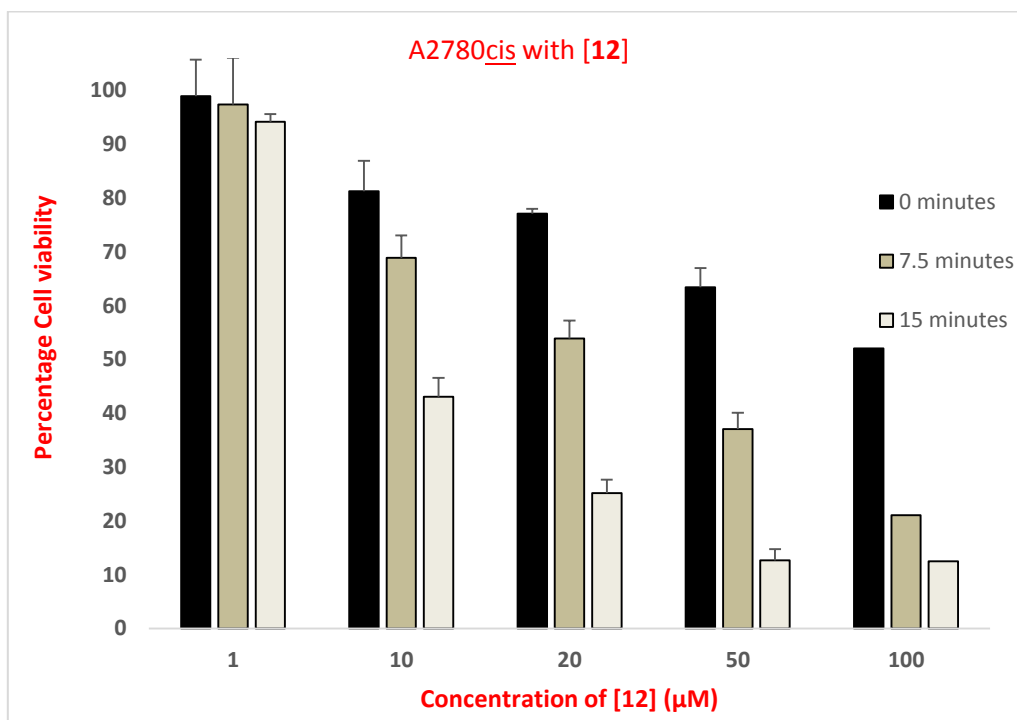
Fluence (J cm <sup>-2</sup> )	[10] IC <sub>50</sub> (μM)	[11] IC <sub>50</sub> (μM)	[12] IC <sub>50</sub> (μM)
0	32	20	60
7.5	4	2.8	50
15	1.8	< 0.1	20

**Figure 5.2.16:** A2780 cell viability data for complexes [10], [11] and [12] upon irradiation

The activity of the complexes [10], [11] and [12] against the cisplatin resistant A2780cis cell-line was also investigated using the same protocol, over a 1–200 μM concentration range. With a decrease in IC<sub>50</sub> values from >100 μM ([10]), 50 μM ([11]) and >100 μM ([12]) in the dark to < 0.1 μM for complexes [10] and [11], and 7.2 μM for complex [12] after an exposure of 15 J cm<sup>-2</sup>.

Significantly, this cisplatin resistant cell line showed a much greater phototoxic response than its cisplatin sensitive analogue. Again, complexes [10] and [11] showed higher phototoxicity effects compared to complex [12] **Figure 5.2.17**.





Fluence (J cm <sup>-2</sup> )	[10] IC <sub>50</sub> (µM)	[11] IC <sub>50</sub> (µM)	[12] IC <sub>50</sub> (µM)
<b>0</b>	>100	50	>100
<b>7.5</b>	1.6	3	25
<b>15</b>	< 0.1	< 0.1	7.2

**Figure 5.2.17:** A2780cis cell viability data for complexes [10], [11] and [12] upon irradiation

In summary, all three complexes have been investigated for phototoxicity show a high phototoxicity indices (PI) against both cell lines A2780 and A2780cis which can be seen in

the table 5.2.5. Mononuclear complex [10] is phototoxic against both cell lines although it displays a better PI against A2780cis. Notably it is not really toxic at all in the dark. In addition, dinuclear complex [11] is phototoxic against both cell lines, but again it displays a better PI against the A2780cis line. Finally, complex [12] is phototoxic against both cell lines but has a much higher PI against A2780cis.

Complex	A2780		PI	A2780cis		PI
	dark IC <sub>50</sub> (μM)	light IC <sub>50</sub> (μM)		dark IC <sub>50</sub> (μM)	light IC <sub>50</sub> (μM)	
[10]	32	<0.1	<b>17.77</b>	>100	<0.1	<b>1000+</b>
[11]	20	<0.1	<b>200+</b>	50	<0.1	<b>500+</b>
[12]	60	20	<b>3</b>	>100	7.2	<b>13.8+</b>

**Table 5.2.5:** Summarising the PI of complexes [10], [11] and [12] after an exposure of 15 J cm<sup>-2</sup>

### 5.2.8.1 Inductively coupled plasma mass spectrometry (ICP-MS)

The differences in cytotoxicities, of the complexes [10-12] could be dependent on both their singlet oxygen quantum yields and their contrasting cellular uptake properties. To accurately quantify intracellular distribution studies of metal content within a population of cells, inductively coupled plasma mass spectrometry can be used.<sup>53</sup> A2780cis cell line was incubated for 1, 3 and 24 hours with 50 μM concentrations of each complex. This analysis confirmed that intracellular concentrations of the dinuclear ruthenium complexes are much higher compared to that of the mononuclear complex, indicating that dinuclear ruthenium complexes [11] and [12] are being taken up better into cells than mononuclear complex [10]. Moreover, these results showed clear evidence that, after 24 hours, the dinuclear dppn-ddpn complex [11] is taken up into cells with a 9.3-fold increase in terms of molarity over a dppn-dppz system such as [12] **Figure 5.2.18**.

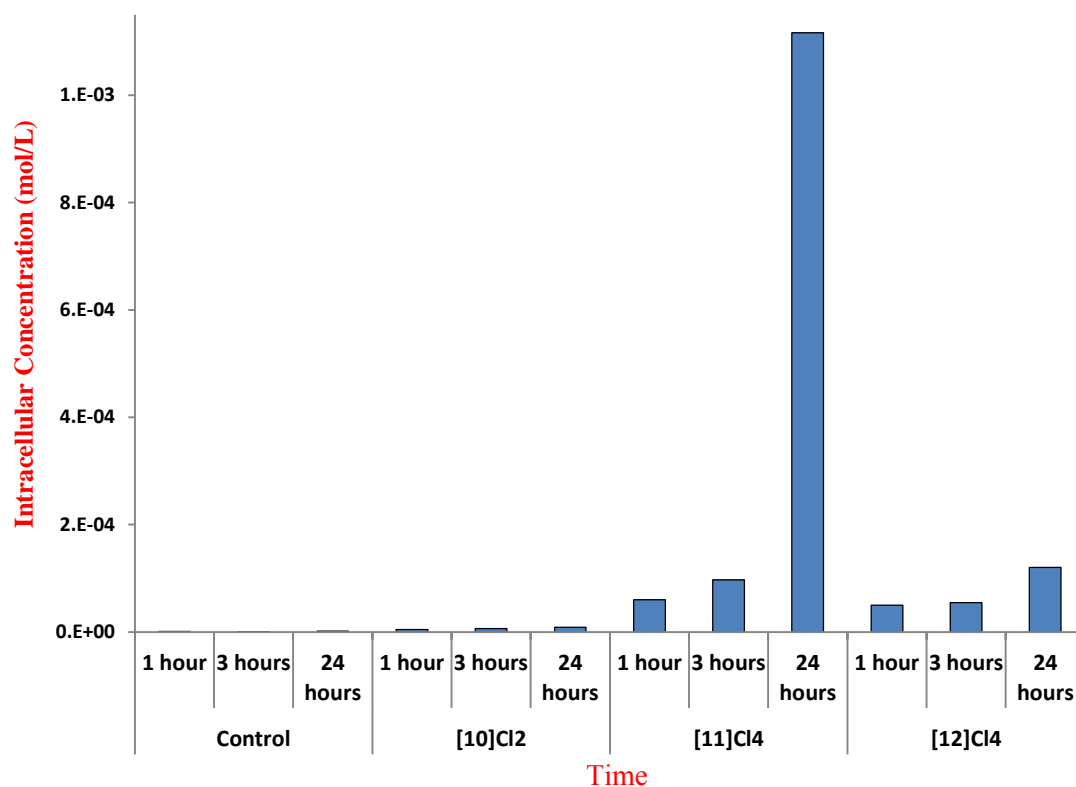


Figure 5.2.18: Intracellular metal content (ruthenium) data from ICP-MS analysis

To sum up, mono and dinuclear ruthenium complexes containing a longer intercalative motif dppn, as well as a dinuclear ruthenium system with mixed-bis-intercalating ligands (dppz-dppn), have been synthesized. The DNA binding properties of these complexes have been investigated. It was found that the mono and dinuclear complexes **[10]** and **[11]** bound to DNA with affinities that are at the same order of magnitude or lower with respect to their analogous dppz complexes. However, hetero-intercalators complex **[12]** had the largest binding constant observed for any of the dinuclear systems synthesized in our group. Complexes **[10]** and **[11]** do not display <sup>3</sup>MLCT based luminescence in both acetonitrile and water. However, complex **[12]** does display a change in emission spectrum around ~640 nm upon addition of CT-DNA. The <sup>1</sup>O<sub>2</sub> quantum yields of these systems revealed that complex **[11]** has a higher quantum yield value compared to complex **[12]**. Furthermore, the DNA photocleavage properties of **[10]** and **[11]** were investigated. The results showed that in the presence of **[10]** and **[11]**, the supercoiled native form (**I**) completely disappears. This

appears to be because both [10] and [11] complexes cleave the DNA strands into very small, fast moving fragments. All three complexes have high phototoxicity indices against both cell lines A2780 and A2780cis.

## References

- (1) De Silva, S. A.; Zavaleta, A.; Baron, D. E.; Allam, O.; Isidor, E. V.; Kashimura, N.; Percarpio, J. M.: *Tetrahedron Letters* **1997**, 38, 2237-2240.
- (2) Meyer, T. J.: *Pure and Applied Chemistry* **1986**, 58, 1193-1206.
- (3) Splan, K. E.; Keefe, M. H.; Massari, A. M.; Walters, K. A.; Hupp, J. T.: *Inorganic Chemistry* **2002**, 41, 619-621.
- (4) Metcalfe, C.; Webb, M.; Thomas, J. A.: *Chemical Communications* **2002**, 2026-2027.
- (5) Erkkila, K. E.; Odom, D. T.; Barton, J. K.: *Chemical Reviews* **1999**, 99, 2777-2796.
- (6) Friedman, A. E.; Chambron, J. C.; Sauvage, J. P.; Turro, N. J.; Barton, J. K.: *Journal of the American Chemical Society* **1990**, 112, 4960-4962.
- (7) Stoeffler, H. D.; Thornton, N. B.; Temkin, S. L.; Schanze, K. S.: *Journal of the American Chemical Society* **1995**, 117, 7119-7128.
- (8) Dyer, J.; Blau, W. J.; Coates, C. G.; Creely, C. M.; Gavey, J. D.; George, M. W.; Grills, D. C.; Hudson, S.; Kelly, J. M.; Matousek, P.: *Photochemical and Photobiological Sciences* **2003**, 2, 542-554.
- (9) Wolfe, A.; Shimer Jr, G. H.; Meehan, T.: *Biochemistry* **1987**, 26, 6392-6396.
- (10) Haq, I.: *Archives of Biochemistry and Biophysics* **2002**, 403, 1-15.
- (11) Foxon, S. P.; Phillips, T.; Gill, M. R.; Towrie, M.; Parker, A. W.; Webb, M.; Thomas, J. A.: *Angewandte Chemie International Edition* **2007**, 46, 3686-3688.
- (12) Armitage, B.: *Chemical Reviews* **1998**, 98, 1171-1200.
- (13) Zeglis, B. M.; Pierre, V. C.; Barton, J. K.: *Chemical Communications* **2007**, 4565-4579.

- (14) TOSSI, A. B.; KELLY, J. M.: *Photochemistry and Photobiology* **1989**, *49*, 545-556.
- (15) Zhou, Q. X.; Lei, W. H.; Chen, J. R.; Li, C.; Hou, Y. J.; Wang, X. S.; Zhang, B. W.: *Chemistry-A European Journal* **2010**, *16*, 3157-3165.
- (16) Juris, A.; Balzani, V.; Barigelletti, F.; Campagna, S.; Belser, P. I.; Von Zelewsky, A.: *Coordination Chemistry Reviews* **1988**, *84*, 85-277.
- (17) Yam, V.-W.; Lo, K.-W.; Kong, R.-C.: *Journal of the Chemical Society, Dalton Transactions* **1997**, 2067-2072.
- (18) Kelly, J. M.; McConnell, D. J.; OhUigin, C.; Tossi, A. B.; Kirsch-De Mesmaeker, A.; Masschelein, A.; Nasielski, J.: *Journal of the Chemical Society, Chemical Communications* **1987**, 1821-1823.
- (19) Sambrook, J.; Fritsch, E. F.; Maniatis, T.: *Molecular Cloning*; Cold spring harbor laboratory press New York, 1989; Vol. 2.
- (20) Barton, J. K.; Raphael, A. L.: *Journal of the American Chemical Society* **1984**, *106*, 2466-2468.
- (21) Levina, A.; Mitra, A.; Lay, P. A.: *Metallomics* **2009**, *1*, 458-470.
- (22) Yam, V.: *J. Chem. Soc., Chemical Communications* **1995**, 1191.
- (23) Foxon, S. P.; Metcalfe, C.; Adams, H.; Webb, M.; Thomas, J. A.: *Inorganic Chemistry* **2007**, *46*, 409-416.
- (24) González González, V.: *DNA Binding of Metal Complexes with Mixed Recognition Motifs: Photophysical and Biophysical Studies*. University of Sheffield, 2006.
- (25) Sun, Y.; Joyce, L. E.; Dickson, N. M.; Turro, C.: *Chemical Communications* **2010**, *46*, 2426-2428.
- (26) Barigelletti, F.; Flamigni, L.; Balzani, V.; Collin, J.-P.; Sauvage, J.-P.; Sour, A.; Constable, E.; Thompson, A. C.: *Coordination Chemistry Reviews* **1994**, *132*, 209-214.
- (27) Balzani, V.; Juris, A.; Venturi, M.; Campagna, S.; Serroni, S.: *Chemical Reviews* **1996**, *96*, 759-834.
- (28) O'regan, B.; Grfitzeli, M.: *Nature* **1991**, *353*, 737-740.

- (29) Nazeeruddin, M. K.; Kay, A.; Rodicio, I.; Humphry-Baker, R.; Müller, E.; Liska, P.; Vlachopoulos, N.; Grätzel, M.: *Journal of the American Chemical Society* **1993**, *115*, 6382-6390.
- (30) Cao, F.; Oskam, G.; Meyer, G. J.; Searson, P. C.: *The Journal of Physical Chemistry* **1996**, *100*, 17021-17027.
- (31) Argazzi, R.; Bignozzi, C. A.; Heimer, T. A.; Castellano, F. N.; Meyer, G. J.: *The Journal of Physical Chemistry B* **1997**, *101*, 2591-2597.
- (32) Bradley, P. G.; Kress, N.; Hornberger, B. A.; Dallinger, R. F.; Woodruff, W. H.: *Journal of the American Chemical Society* **1981**, *103*, 7441-7446.
- (33) McClanahan, S. F.; Dallinger, R. F.; Holler, F. J.; Kincaid, J. R.: *Journal of the American Chemical Society* **1985**, *107*, 4853-4860.
- (34) Cooley, L. F.; Bergquist, P.; Kelley, D. F.: *Journal of the American Chemical Society* **1990**, *112*, 2612-2617.
- (35) Yabe, T.; Orman, L.; Anderson, D.; Yu, S. C.; Xu, X.; Hopkins, J. B.: *Journal of Physical Chemistry* **1990**, *94*, 7128-7132.
- (36) Omberg, K. M.; Schoonover, J. R.; Treadway, J. A.; Leasure, R. M.; Dyer, R. B.; Meyer, T. J.: *Journal of the American Chemical Society* **1997**, *119*, 7013-7018.
- (37) Knoll, J. D.; Albani, B. A.; Turro, C.: *Accounts of Chemical Research* **2015**, *48*, 2280-2287.
- (38) Dougherty, G.; Pilbrow, J. R.: *International Journal of Biochemistry* **1984**, *16*, 1179-1192.
- (39) Maheswari, P. U.; Rajendiran, V.; Palaniandavar, M.; Parthasarathi, R.; Subramanian, V.: *Journal of Inorganic Biochemistry* **2006**, *100*, 3-17.
- (40) Phillips, T.; Haq, I.; Meijer, A. J.; Adams, H.; Soutar, I.; Swanson, L.; Sykes, M. J.; Thomas, J. A.: *Biochemistry* **2004**, *43*, 13657-13665.
- (41) Metcalfe, C.; Adams, H.; Haq, I.; Thomas, J. A.: *Chemical Communications* **2003**, 1152-1153.
- (42) Hiort, C.; Lincoln, P.; Norden, B.: *Journal of the American Chemical Society* **1993**, *115*, 3448-3454.

- (43) Nair, R. B.; Murphy, C. J.: *Journal of Inorganic Biochemistry* **1998**, *69*, 129-133.
- (44) Chouai, A.; Wicke, S. E.; Turro, C.; Bacsá, J.; Dunbar, K. R.; Wang, D.; Thummel, R. P.: *Inorganic Chemistry* **2005**, *44*, 5996-6003.
- (45) Williams, R. L.; Toft, H. N.; Winkel, B.; Brewer, K. J.: *Inorganic chemistry* **2003**, *42*, 4394-4400.
- (46) Englman, R.; Jortner, J.: *Molecular Physics* **1970**, *18*, 145-164.
- (47) Foxon, S. P.; Alamiry, M. A.; Walker, M. G.; Meijer, A. J.; Sazanovich, I. V.; Weinstein, J. A.; Thomas, J. A.: *The Journal of Physical Chemistry A* **2009**, *113*, 12754-12762.
- (48) Juarranz, Á.; Jaén, P.; Sanz-Rodríguez, F.; Cuevas, J.; González, S.: *Clinical and Translational Oncology* **2008**, *10*, 148-154.
- (49) Macdonald, I. J.; Dougherty, T. J.: *Journal of Porphyrins and Phthalocyanines* **2001**, *5*, 105-129.
- (50) Zuluaga, M.-F.; Lange, N.: *Current Medicinal Chemistry* **2008**, *15*, 1655-1673.
- (51) Dolmans, D. E.; Fukumura, D.; Jain, R. K.: *Nature Reviews Cancer* **2003**, *3*, 380-387.
- (52) Foote, C. S.: *Photochemistry and Photobiology* **1991**, *54*, 659-659.
- (53) Gill, M. R.; Thomas, J. A.: *Chemical Society Reviews* **2012**, *41*, 3179-3192

## Chapter 6

### Conclusions

---

6.0 Conclusions.....	175
6.1 Chapter 2: Bimetallic DNA Metallo-intercalators containing the ruthenium (II) tris(1-pyrazolyl)methane Unit. ....	175
6.2 Chapter 3: The effect of the nature and positioning of the functional group on the binding mode and affinity of Ruthenium polypyridyl complexes. ....	175
6.3 Chapter 4: Isothermal Titration Calorimetry (ITC). ....	176
6.4 Chapter 5.1: DNA Binding and Cleavage Properties of a heterobimetallic Ru <sup>II</sup> -Re <sup>I</sup> system. ....	176
6.5 Chapter 5.2: Ru <sup>II</sup> -Ru <sup>II</sup> Polypyridyl complex with mixed-bis-intercalating ligands (dppz-dppn).....	177

## 6.0 Conclusions

### 6.1 Chapter 2: Bimetallic DNA Metallo-intercalators containing the ruthenium (II) tris(1-pyrazolyl)methane Unit.

Four new polypyridyl ruthenium (II) complexes containing a linker group,  $[\text{Ru}(\text{tpm})(\text{dppz})(\mu\text{-L1})](\text{PF}_6)_2$  [**1**],  $[\text{Ru}(\text{tpm})(\text{dppz})(\mu\text{-L2})](\text{PF}_6)_2$  [**2**],  $[\{\text{Ru}(\text{tpm})(\text{dppz})\}_2(\mu\text{-L1})](\text{PF}_6)_4$  [**3**] and  $[\{\text{Ru}(\text{tpm})(\text{dppz})\}_2(\mu\text{-L2})](\text{PF}_6)_4$  [**4**], and their DNA binding properties have been established. The combination of viscometry, fluorescence and absorption spectroscopy data show that these complexes bind to DNA, most likely through intercalation. Complexes [**1**] and [**3**] seem to intercalate more strongly than complexes [**2**] and [**4**]. It seems the more rigid linker group may restrict full insertion of intercalative sites between the DNA base pairs. For the more flexible linker, the complex can sit more comfortably within the minor groove resulting in enhanced the binding compared. Whatever the reason, it is clear that the binding affinity of these complexes towards DNA is affected by the nature of the functional group in a linker.

To further investigate the properties of these complexes with DNA, isothermal titration calorimetry (ITC) was used as this can provide a complete thermodynamic profile on the interaction of metal complexes with biomolecules – *vide infra*.

### 6.2 Chapter 3: The effect of the nature and positioning of the functional group on the binding mode and affinity of Ruthenium polypyridyl complexes.

In this chapter, the synthesis and characterization by UV-visible spectroscopy, luminescence titrations,  $^1\text{H}$  NMR and mass spectrometry of four new ruthenium complexes,  $[\text{Ru}(\text{tpm})(\text{dppz})(\mu\text{-L'1})](\text{PF}_6)_2$  [**5**],  $[\text{Ru}(\text{tpm})(\text{dppz})(\mu\text{-L'2})](\text{PF}_6)_2$  [**6**],  $[\{\text{Ru}(\text{tpm})(\text{dppz})\}_2(\mu\text{-L'1})](\text{PF}_6)_4$  [**7**] and  $[\{\text{Ru}(\text{tpm})(\text{dppz})\}_2(\mu\text{-L'2})](\text{PF}_6)_4$  [**8**], have been investigated and their binding with CT-DNA has been studied. Absorption titrations showed ~10nm bathochromic shift of the absorption band at ~ 278 nm along with significant hypochromicity.

Viscosity measurements confirmed that the complex-DNA interaction is through intercalation. These results confirm that both mono and di complexes are avid binders of CT DNA and that the dipyridophenazine ligand on them is engaged in the intercalative interaction with DNA.

Furthermore, in comparison with complexes [1-4] the interactions of complexes [5-8] with DNA are stronger. Of particular note is the fact that the dinuclear complexes show enhanced binding compared to their mononuclear analogues. Indeed, the viscosity measurement presents clear evidence that [8]Cl<sub>4</sub> is in fact a bis-intercalator. The results described in this study highlight how the nature and positioning of functional groups within the complexes affect binding affinities. Results from the isothermal titration calorimetry for complexes [1-4] and [5-8] are discussed in chapter 4.

### **6.3 Chapter 4: Isothermal Titration Calorimetry (ITC).**

The ITC evidence has been used to obtain complete thermodynamic profiles ( $\Delta G^\circ$ ,  $\Delta H^\circ$ ,  $\Delta S^\circ$ ) for the interaction of both sets of complexes [1-4] and [5-8] with CT-DNA. The results show the binding of these complexes are generally entropically favoured. The binding affinities of these complexes suggest that complexes [5-8] interactively bind to CT-DNA more strongly than complexes [1-4]. Moreover, both ITC and spectroscopic studies show a significant increase in binding affinity for DNA for the monometallic and bimetallic complexes [5-8] containing 3-Py positioned tethers. These results have confirmed that the positioning of the functional group can have a profound effect on the binding affinities of these complexes.

### **6.4 Chapter 5.1: DNA Binding and Cleavage Properties of a heterobimetallic Ru<sup>II</sup>-Re<sup>I</sup> system.**

The new hetero-dinuclear dppz complex is reported. The interaction of complex [9] with double-stranded calf thymus DNA has been studied by absorption and emission titrations. The complex binds to the duplex by intercalation with good affinity and displays a DNA light

switch effect but not DNA cleavage properties. The thermodynamic parameters showed that the complex-DNA interaction is enthalpically unfavourable and entropically favoured. Moreover, although the molecule does not display significant phototoxicity, with a PI of 2, it displays significant dark cytotoxicity.

## **6.5 Chapter 5.2: Ru<sup>II</sup>-Ru<sup>II</sup> Polypyridyl complex with mixed-bis-intercalating ligands (dppz-dppn).**

In this section, mono and dinuclear ruthenium complexes containing a longer intercalative motif dppn, as well as a dinuclear ruthenium system with mixed-bis-intercalating ligands (dppz-dppn), have been synthesized. The DNA binding properties of these complexes have been investigated. It was found that the mono and dinuclear complexes [10] and [11] bound to DNA with affinities that are at the same order of magnitude or lower with respect to their analogous dppz complexes. However, hetero-intercalators complex [12] had the largest binding constant observed for any of the dinuclear systems synthesized in our group. Complexes [10] and [11] do not display <sup>3</sup>MLCT based luminescence in both acetonitrile and water. However, complex [12] does display a change in emission spectrum around ~640 nm upon addition of CT-DNA. The <sup>1</sup>O<sub>2</sub> quantum yields of these systems revealed that complex [11] has a higher quantum yield value compared to complex [12]. Furthermore, the DNA photocleavage properties of [10] and [11] were investigated. The results showed that in the presence of [10] and [11], the supercoiled native form (I) completely disappears. This appears to be because both [10] and [11] complexes cleave the DNA strands into very small, fast moving fragments. All three complexes have high phototoxicity indices against both cell lines A2780 and A2780cis.

## Chapter 7

### Experimental

---

7.0 Experimental .....	178
7.1 Materials and Equipment .....	178
7.1.1 Chemicals .....	178
7.1.2 Nuclear Magnetic Resonance (NMR) Spectra .....	178
7.1.3 Mass Spectrometry .....	178
7.1.4 UV-Visible Absorption Spectroscopy .....	178
7.1.5 Luminescence Spectroscopy .....	179
7.2 DNA Binding Studies .....	179
7.2.1 Buffer Preparation .....	179
7.2.2 Sample Preparation .....	179
7.2.3 DNA Preparation .....	180
7.2.4 Viscometry .....	180
7.2.5 UV-Visible Titrations .....	181
7.2.6 Luminescence Titrations .....	181
7.2.7 Isothermal Titration Calorimetry .....	181
7.2.8 Agarose Gel Electrophoresis of DNA .....	182
7.2.9 Transient Absorption Spectroscopy .....	182
7.3 Cellular phototoxicity Studies .....	183
7.3.1 Light Irradiation Source Apparatus (LISA) .....	183
7.3.2 Photocytotoxicity (phototoxicity) .....	184
7.3.3 Intracellular metal content (ICP-MS) .....	184
7.4 Synthesis .....	186
7.4.1 Preparation of Tris(1-pyrazolyl)methane (tpm) <sup>2</sup> .....	186
7.4.2 Preparation of 1, 10-phenanthroline-5,6-dione (dpq) <sup>3</sup> .....	187
7.4.3 Preparation of dipyrido [3,2-a:2',3'-c] Phenazine (DPPZ) <sup>4</sup> .....	188
7.4.4 Preparation of N,N'-bis(4-pyridylmethyl)-1,6-hexanediamine (L1) .....	188
7.4.5 Preparation of N,N'-bis(4-pyridylmethyl)-1,4-benzene dimethyleneamine (L2) ..	189
7.4.6 Preparation of (tpm)RuCl <sub>3</sub> ·3H <sub>2</sub> O .....	190
7.4.7 Preparation of [(tpm)RuCl(dpz)][(PF <sub>6</sub> )] .....	191
7.4.8 Preparation of [(tpm)Ru(dpz)(μ-L1)][Cl <sub>2</sub> ] .....	192

7.4.9 Preparation of [(tpm)Ru(dppz)( $\mu$ -L2)][Cl <sub>2</sub> ] .....	193
7.4.10 Preparation of [{(tpm)Ru(dppz)} <sub>2</sub> ( $\mu$ -L1)][(PF <sub>6</sub> ) <sub>4</sub> ] .....	194
7.4.11 Preparation of [{(tpm)Ru(dppz)} <sub>2</sub> ( $\mu$ -L2)][(PF <sub>6</sub> ) <sub>4</sub> ] .....	195
7.4.12 Preparation of N,N'-bis(3-pyridylmethyl)-1,6-hexanediamine (L'1) .....	196
7.4.13 Preparation of N,N'-bis(3-pyridylmethyl)-1,4-benzene dimethyleneamine (L'2) .....	197
7.4.14 Preparation of [(tpm)Ru(dppz)( $\mu$ -L'1)][Cl <sub>2</sub> ] .....	198
7.3.15 Preparation of [(tpm)Ru(dppz)( $\mu$ -L'2)][Cl <sub>2</sub> ] .....	199
7.4.16 Preparation of [{(tpm)Ru(dppz)} <sub>2</sub> ( $\mu$ -L'1)][(PF <sub>6</sub> ) <sub>4</sub> ] .....	200
7.4.17 Preparation of [{(tpm)Ru(dppz)} <sub>2</sub> ( $\mu$ -L'2)][(PF <sub>6</sub> ) <sub>4</sub> ] .....	201
7.4.18 Preparation of [Re(CO) <sub>3</sub> dppzCl] .....	202
7.4.19 Preparation of [Ru(tpm)dppz-L1-Re(CO) <sub>3</sub> dppz][Cl <sub>3</sub> ] .....	203
7.4.20 Preparation of Benzo[i]dipyrido[3,2-a:2',3'-c]phenazine (dppn) <sup>5</sup> .....	204
7.4.21 Preparation of [Ru(tpm)dppnCl][PF <sub>6</sub> ] .....	205
7.4.22 Preparation of [Ru(tpm)dppn( $\mu$ -L1)][(PF <sub>6</sub> ) <sub>2</sub> ] .....	206
7.4.23 Preparation of [Ru(tpm)dppn-L1-Ru(tpm)dppn][(PF <sub>6</sub> ) <sub>4</sub> ] .....	207
7.4.24 Preparation of [Ru(tpm)dppz-L1-Ru(tpm)dppn][(PF <sub>6</sub> ) <sub>4</sub> ] .....	208
References .....	209

## **7.0 Experimental**

### **7.1 Materials and Equipment**

#### **7.1.1 Chemicals**

All chemicals and solvents were purchased from commercial sources and were used as supplied unless otherwise stated.

#### **7.1.2 Nuclear Magnetic Resonance (NMR) Spectra**

Standard  $^1\text{H}$  NMR spectra were carried out on a Bruker AV2-400 machine, working in Fourier transform mode.

More complex  $^1\text{H}$  NMR experiments were performed by Sue Bradshaw of the University of Sheffield. The spectra were recorded on a Bruker DRX500 machine.

The following abbreviations are used in the annotation of  $^1\text{H}$  spectra; s - singlet, d - doublet, dd - double doublet, dt - double triplet, t - triplet, q - quartet and m - multiplet.

#### **7.1.3 Mass Spectrometry**

ES mass spectra were recorded on a Micromass LCT ES-TOF machine. All spectra were run by Simon Thorpe or Sharon Spey of the University of Sheffield Mass Spectrometry Service.

#### **7.1.4 UV-Visible Absorption Spectroscopy**

All UV-Visible spectra were recorded on a thermo regulated Varian-Carey 50 UV-Visible spectrometer, using quartz cells of 10 mm path length at 25°C. Spectra were baseline

corrected using Cary Win UV software and were diluted accordingly to give readings between 0.0 and 1.0 absorbance units.

### **7.1.5 Luminescence Spectroscopy**

Luminescence spectra were recorded on a thermo regulated Horiba Jobin-Yvon FluoroMax-3 spectrophotometer operating in luminescence wavelength scan mode at 25°C, with excitation and emission slit widths at 5 nm.

## **7.2 DNA Binding Studies**

### **7.2.1 Buffer Preparation**

Tris buffer (pH 7.4) was prepared using Trizma HCl (Tris(hydroxymethyl)aminomethane) base at 5 mM concentrations in 25 mM NaCl. Trizma HCl and NaCl were measured into a volumetric flask and dissolved in deionised water (Millipore HPLC grade). The pH was adjusting using dilute HCl and additional water added to achieve the correct volume. Buffer solutions were passed through 0.2 micron Millipore filters and autoclaved for 4 hours. The subsequent sterile solution was refrigerated at 4°C.

### **7.2.2 Sample Preparation**

All ruthenium complexes were converted into their water soluble chloride derivatives prior to biological testing. This was done by dissolving the hexafluorophosphate salt of each complex in the minimum volume of acetone and a saturated solution of ammonium chloride in acetone added. The resultant precipitated chloride salt was collected by filtration, washed with acetone and dried *in vacuo*.

### 7.2.3 DNA Preparation

Calf Thymus DNA (CT-DNA) was purchased from Sigma-Chemicals as the lyophilised solid sodium salt and used without further purification. DNA length was averaged to 200-300 base pairs by dissolving ~100 mgs of the solid material in 20 ml of tris buffer (5 mM Tris, 25 mM NaCl) and leaving refrigerated overnight and then subjecting samples to discontinuous sonication using a Sonics Vibra-Cell VCX130, fitted with a 19 mm diameter probe. DNA samples were quantified in terms of quality and concentration by conventional absorbance measurements.<sup>1</sup> Nucleic acids have an absorbance maximum at 260 nm and contaminants such as proteins and single stranded DNA/RNA absorb maximally at 280 nm. The purity of a sample is measured by calculating the ratio of contaminants to DNA, with  $A_{260}/A_{280} > 1.9$  indicating a protein free sample (in reality anything over 1.8 is acceptable for a cuvette sample in a spectrometer). The concentration of the resulting solutions was also determined per base pair (bp) by UV-Visible spectroscopy using  $\epsilon_{260} = 13200 \text{ M}^{-1}\text{cm}^{-1}$  for CT-DNA.

### 7.2.4 Viscometry

Viscosity experiments were carried out in a 1 ml Cannon-Manning semi-micro viscometer (size 50) immersed in a thermostated water bath. The temperature was maintained at  $26 \pm 1$  °C. The concentration of CT-DNA in the viscometer was kept at  $\sim 50 \mu\text{M bp}^{-1}$ . Additions of the analyte were made so that the values of  $1/R$  ( $R = [\text{DNA}]/[\text{ligand}]$ ) were between 0 and 0.3.

Buffer solutions were allowed to stand in the viscometer for 45 minutes before readings were taken. After the addition of CT-DNA the solution were left to equilibrate for 20 minutes. After each addition of the analyte to the system an equilibrium time of 20 minutes was allowed before the flow times were recorded. After each addition the solution was drawn through the viscometer and mixed under vacuum 5 times before being left to equilibrate in order to ensure the solution was homogenous. Times were recorded in triplicate and the average calculated after thermal equilibration.

### **7.2.5 UV-Visible Titrations**

UV-Visible titrations were performed on a thermo regulated Varian-Carey 50 UV-Visible spectrometer at 25°C. 1 ml of buffer was loaded into a 10 mm path length cuvette and allowed to equilibrate inside the spectrometer before a baseline reading was taken. A volume of buffer was removed with a Gilson pipette and replaced with the same volume of a stock solution of complex to give a final concentration of around 10-15  $\mu\text{M}$  complex inside the cuvette. After equilibration the spectrum was recorded between 200-600 nm. 2.5  $\mu\text{L}$  of a concentrated stock solution of CT-DNA was added to the cuvette and mixed 10 times with a pipette to ensure homogeneity. The spectrum was recorded after leaving the sample to equilibrate for 5 minutes, checking no bubbles were present. This procedure was continued until the absorbance became constant indicating saturation binding had occurred or the increase of CT-DNA concentration only caused small changes in the absorption spectra.

### **7.2.6 Luminescence Titrations**

Luminescence titrations were carried out in a thermo regulated Horiba Jobin-Yvon FluoroMax-3 spectrophotometer in a procedure similar to the UV-Visible titrations. 3 mL of buffer was loaded into 10 mm path length luminescence cuvette and allowed to equilibrate inside the spectrophotometer at 25°C before a background reading was taken. A volume of buffer was removed and replaced with the same volume of a stock solution of complex to give a final concentration of around 15  $\mu\text{M}$  complex inside the cuvette. After equilibration, the emission spectrum of the solution was recorded using the excitation wavelength characteristic of the complex. 2.5  $\mu\text{L}$  of a concentrated stock solution of CT-DNA was added to the cuvette and mixed 10 times to ensure homogeneity. After leaving the sample to equilibrate for 3 minutes and checking no bubbles were present, the emission spectrum was recorded, showing an enhancement in emission. The procedure was continued until the emission became constant.

### **7.2.7 Isothermal Titration Calorimetry**

Calorimetric data was obtained in Cardiff University, using a MicroCalorimeter. During interactions the reference cell was filled with distilled water and the sample cell with CT-

DNA (0.25 mM in tris buffer). Aliquots of the interacting complex (1 mM) were then titrated into the DNA solution, which was stirred continuously at 301 rpm and maintained at 25 °C unless is specified. Initial injection of 5  $\mu$ l was made to remove error followed by 15  $\mu$ l throughout the rest of the experiment. Heats of dilution for each compound were determined by titrating the complex into buffer solution. These dilution heats were subtracted from the  $\Delta$ H value for DNA-complex titrations to give a corrected heat effect. Each titration was repeated at least 2 times to give an average value for the thermodynamic parameters in an interaction.

### **7.2.8 Agarose Gel Electrophoresis of DNA**

Photoinduced cleavage of supercoiled pBR322 and pUC57 DNA by the complexes was studied by agarose gel electrophoresis. The reactions were performed under illuminated conditions using 470 nm using FLUOstar OPTIMA microplate reader. The sample was prepared in a dark room at room temperature using supercoiled DNA (0.1  $\mu$ g/ $\mu$ L) in 50 mM Tris-HCL buffer and varying concentrations of the complex. After photoexposure, the sample was incubated followed by the addition of the loading buffer containing 25% bromophenol blue, 0.25% xylene cyanol and 30 % glycerol (2  $\mu$ L), and the solution was finally loaded on an 0.8% agarose gel containing 1.0  $\mu$ g/mL ethidium bromide. Electrophoresis was carried out for an hour at 100 mW in TAE (Tris-acetate-EDTA) buffer. The gel was visualised using a UVP transilluminator and photographed for analysis.

### **7.2.9 Transient Absorption Spectroscopy**

Picosecond transient absorption experiments were performed on a home-built pump-probe setup. The fundamental output ( $\sim$  3 mJ, 20 ps, 10 Hz, 1064 nm) of a ps mode-locked Nd:YAG laser PL2251 (EKSPLA) was passed through a computer-controlled optical delay line (made of IMS600 linear stage from NEWPORT; 60 cm travel range), and focused with a 0.5 m lens into a 10 cm cell with D<sub>2</sub>O to generate a picosecond super-continuum, which served as a probe beam. The broadband super-continuum beam was split with a beam splitter into signal and reference beams of equal intensity. Both signal and reference beams were

passed through the sample one above the other, each focused into a  $\sim 0.5\text{mm}$  spot on the sample. Afterwards the signal and reference beams were focused with an achromatic condenser onto the entrance slit of the spectrograph (a Hilger & Watts 30 cm monochromator home-converted into a spectrograph by replacing the grating, exit flat mirror, removing exit slit, and fitting a CCD mounting adaptor). Both signal and reference beams were detected with a CCD camera (ANDOR iDus, DV420A) operated in the dual-track mode. The excitation beam was focused into 1 mm spot on the sample, with the pulse energy of  $120 \mu\text{J}$  at the sample. The pump and the signal probe beams were overlapped at the sample at small angle. The instrumental response function duration of the setup is estimated to be ca. 27 ps. The operation of the setup and the data acquisition process are controlled by custom-developed software. All the measurements were performed in quartz cells with a 2 mm path length.

## 7.3 Cellular phototoxicity Studies

### 7.3.1 Light Irradiation Source Apparatus (LISA)

The apparatus used to irradiate the samples was a custom made device featuring a broadband illumination source fully contained in an empty computer base unit, referred to as the Light Irradiation Source Apparatus (LISA). The technical specifications of the bulb contained within are as follows (*Table 1*).

Product Code	871691
International Model Number	HC01080i
Description	CFL 80W E40 Integrated Clusterlite
Watts	80W
Cap	E40
Operating Hours	15000
Colour Temp	4000K
Lumens	5400 lm
Dimming	No
Dimensions (length x diameter)	256mm x 80mm

*Table 1* – Specification of the bulb contained within the irradiation apparatus

### **7.3.2 Photocytotoxicity (phototoxicity)**

Cells were maintained in RPMI 1640 medium supplemented with 10% FBS, 100 mg ml<sup>-1</sup> streptomycin, 100 units ml<sup>-1</sup> penicillin, and 2 mM glutamine at 37°C in a humidified atmosphere containing 5% CO<sub>2</sub>. Experimental cultures were grown on 48 well plates at a seeding density of 5 x 10<sup>4</sup> cells per well and incubated for 24 h. The cells were then treated with complex (solubilised in and maintained at 10% PBS/H<sub>2</sub>O: 90% medium throughout all solutions) of a 1 – 100 µM concentration range, in triplicate, and incubated for 24 h. All complex solution (and control medium) was removed from the cells and replaced with regular growth medium 30 min prior to irradiation. Of the four prepared well plates, one remained in the incubator whilst the other three were exposed to the LISA for the duration of 5, 15 or 30 min (corresponding to light doses of 8, 24 or 48 J cm<sup>-2</sup>) before being incubated for a further 24 h after culmination of light treatment. All medium was then removed and cells incubated with MTT (0.5 mg ml<sup>-1</sup> dissolved in PBS) for 30 – 40 min. The MTT was removed and formazan product eluted using 120 µl/well acidified isopropanol, 100 µl of which was transferred to a 96 well plate for the absorbance to be quantified by spectrophotometer (540 nm, referenced at 640 nm). An average absorbance for each concentration was calculated and cell viability was determined as a percentage of the untreated negative control wells (10% PBS/H<sub>2</sub>O: 90% medium, average of triplicate). Data were plotted in a graph of concentration against cell viability to produce a curve from which the IC<sub>50</sub> value could be derived by interpolation.

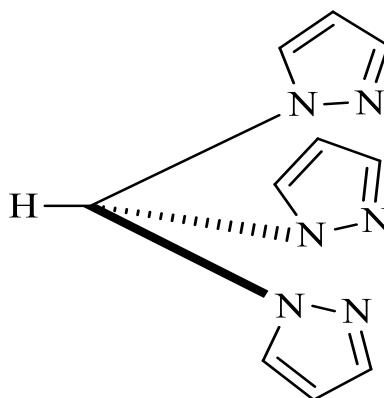
### **7.3.3 Intracellular metal content (ICP-MS)**

Cell cultures were grown on 60 mm dishes at a seeding density of 5 x10<sup>5</sup> cells per dish and incubated for 24 h. Cells were then treated with the complex (solubilised in and maintained at 10% PBS/H<sub>2</sub>O: 90% medium throughout all solutions) at the stated concentration and incubated for 24 h. All complex solution (or control medium) was removed, cells washed with PBS and 1 ml of both serum-free medium and trypsin solution added. Dishes were incubated for 3 min and shaken to remove cells (plus scraped to detach any remaining cells) which were transferred to microcentrifuge tubes and centrifuged (4000 rpm, 3 min). The supernatant was removed, pellet resuspended in 500 µl serum-free medium and cells counted. Each sample was transferred to a glass sample tube, 2 ml concentrated HNO<sub>3</sub> added, heated

to 60°C overnight and then diluted to 10 ml total volume with ultrapure Milli-Q H<sub>2</sub>O before analysis of ruthenium content by inductively coupled plasma mass spectrometry (ICP-MS). Using the obtained ruthenium concentration, the sample volume, number of cells per sample and the assumption of a cell volume of  $2 \times 10^{-12}$  L an estimate of intracellular concentration (mol L<sup>-1</sup>) could be deducted.

## 7.4 Synthesis

### 7.4.1 Preparation of Tris(1-pyrazolyl)methane (tpm)<sup>2</sup>



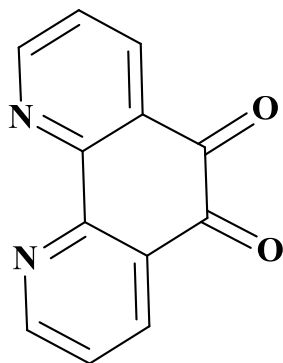
This compound was prepared following a previously reported procedure. A three neck round bottom flask equipped with a reflux condenser and a mechanical overhead stirrer was placed in an oil bath on a stirrer hot plate. Pyrazole (40.0 g, 0.59 mol) and tetra-*n*-butylammoniumbromide (9.4 g, 29.27 mmol) were added to the flask followed by distilled water (500 ml) with vigorous stirring, sodium carbonate (400 g, 3.78 mol) was added gradually to the reaction mixture, constant stirring increase the efficiency of the reaction. After cooling to near room temperature, chloroform (250 ml) was added and the mixture heated at gentle reflux for 3 days with rapid stirring, after which time the organic layer had turned dark yellow in colour the mixture was allowed to cool to room temperature and filtrate. The organic layer was separated and the aqueous layer extracted with dichloromethane (3 x 300 ml). The combined organic layers were then washed with saturated brine solution (500 ml) and dried over magnesium sulphate. Filtration and concentration of the filtrate under reduced pressure yielded a yellow coloured solid. The crude product can be purified by a recrystallization from water and dried under vacuum.

**Mass (Yield):** 24.92 g (60%).

**TOF MS ES<sup>+</sup>, *m/z*:** 147 [M-py]<sup>+</sup>, 215 [MH]<sup>+</sup>.

**<sup>1</sup>H NMR (400 MHz, CDCl<sub>3</sub>):** δ<sub>H</sub> = 8.74 (s, 1H), 7.87 (d, *J* = 1.4 Hz, 3H), 7.63 (d, *J* = 2.5 Hz, 3H), 6.41 (dd, *J* = 2.4 Hz, 1.9 Hz, 3H).

#### 7.4.2 Preparation of 1, 10-phenanthroline-5,6-dione (dpq)<sup>3</sup>



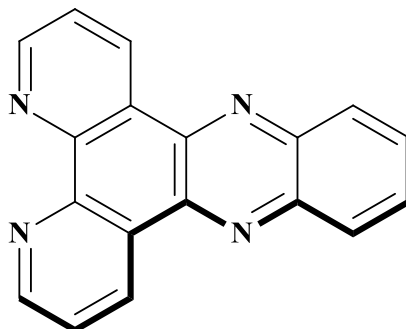
This compound was prepared following a previously reported procedure. 1,10-phenanthroline (5.40 g, 30 mmol) was added into a solution of 60% sulphuric acid (70 ml). After the solid compound was dissolved, potassium bromate (5.510 g, 32 mmol) was added over a period of half an hour. The mixture was stirred at room temperature for 20h. Then, the mixture was poured over ice and was carefully neutralized to pH 7 using a saturated solution of sodium hydroxide. The solution was then filtered, extracted with CH<sub>2</sub>Cl<sub>2</sub> and evaporated to dryness. The crude product was recrystallised from methanol to provide the desired product in 80-90%.

**Mass (Yield):** 4.59 g (85%).

**TOF MS ES+, *m/z*:** 211 [MH]<sup>+</sup>

**<sup>1</sup>H NMR (400 MHz, CDCl<sub>3</sub>):** δ<sub>H</sub> = 8.45 (dd, *J* = 4.7 Hz, 1.8 Hz, 2H), 7.98 (dd, *J* = 7.9 Hz, 1.8 Hz, 2H), 7.65 (dd, *J* = 7.9 Hz, 4.7 Hz, 2H).

### 7.4.3 Preparation of dipyrido [3,2-a:2',3'-c] Phenazine (DPPZ)<sup>4</sup>



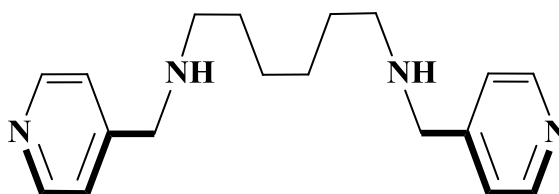
This compound was prepared following a previously reported procedure. 1,10-phenanthroline-5,6-dione (2.0 g, 9.51 mmol) and o-phenylene diamine (1.02 g, 9.43 mmol) were refluxed in ethanol (100 ml) for 2 hours, (solution turned from dark brown to deep red). After cooling the solvent was removed in vacuo and the resulting solid was recrystallized with 1:1 ethanol/water. The recrystallized orange needles were collected by filtration, washed subsequently with ice cold water (30 ml) and ethanol (50 ml) and dried in vacuo.<sup>4</sup>

**Mass (Yield):** 1.11 g (58%).

**TOF MS ES<sup>+</sup>, *m/z*:** 283 [MH]<sup>+</sup>.

**<sup>1</sup>H NMR (250 MHz, CDCl<sub>3</sub>):**  $\delta_{\text{H}}$  = 9.67 (dd, *J* = 8.1, 1.8 Hz, 2H), 9.30 (dd, *J* = 4.5, 1.8 Hz, 2H), 8.46 – 8.28 (m, 4H), 7.28 (dd, *J* = 8.1 Hz, 4.4 Hz, 2H).

### 7.4.4 Preparation of N,N'-bis(4-pyridylmethyl)-1,6-hexanediamine (L1)



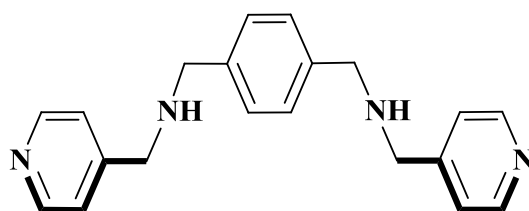
A solution of 4-pyridinecarboxaldehyde (18.5 g, 173 mmol) in ethanol (100 mL) was added to a solution of 1,6-hexanediamine (10.0 g, 86.6 mmol) in ethanol (200 mL) and then heated to reflux for 2 h. The reaction solution was allowed to cool to room temperature. NaBH<sub>4</sub> (8.0 g, 211 mmol) was carefully added in small portions and the mixture was heated to reflux for 2 h and then stirred at room temperature overnight. Aqueous NaOH (2.0 M, 200 mL) was added to the solution. The aqueous solution was extracted with CH<sub>2</sub>Cl<sub>2</sub> (3 × 200 mL), the organic fractions combined and dried over anhydrous MgSO<sub>4</sub>. Filtration and concentration under reduced pressure yielded pale coloured viscous oil. On shaking with diethyl ether a cream coloured solid precipitated, which was collected by filtration, washed with copious amounts of diethyl ether and dried in vacuo.

**Mass (Yield):** 20.2 g (74%).

**TOF MS ES<sup>+</sup>, *m/z*:** 299 (MH<sup>+</sup>).

**<sup>1</sup>H NMR (400 MHz, CDCl<sub>3</sub>):** δ<sub>H</sub> = 8.49 (dd, J = 8.0, 2.8 Hz, 4H), 7.50 (d, J = 8.0 Hz, 4H), 3.82 (s, 4H), 2.64 (t, J = 6.72 Hz, 4H), 1.81 (t, J = 8.4 Hz, 4H), 1.45(m, 4H).

#### 7.4.5 Preparation of N,N'-bis(4-pyridylmethyl)-1,4-benzene dimethyleneamine (L2)



Benzene-1,4-dicarboxaldehyde (5.0 g, 27.3 mmol) and 4-(aminomethyl)pyridine (8.06 g, 74.6 mmol) were placed in CH<sub>2</sub>Cl<sub>2</sub> (100 mL). Anhydrous MgSO<sub>4</sub> (20 g) was added to the solution and the mixture was stirred at room temperature for 24 h. The mixture was filtered and the filtrate concentrated under reduced pressure yielding the Schiff base as golden coloured

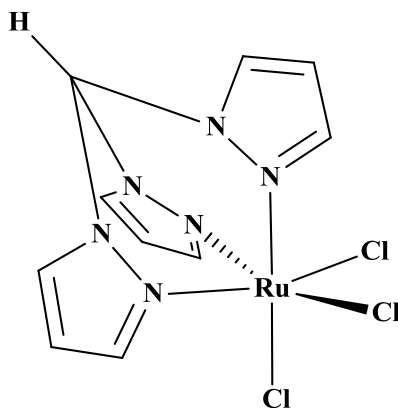
viscous oil which was not isolated. The oil was taken up in ethanol (150 mL), NaBH<sub>4</sub> (4.0 g, 106 mmol) was added in small portions and then the mixture was heated to reflux for 2 h and then stirred at room temperature overnight. Aqueous NaOH (2.0 M, 200 mL) was added to the solution. The aqueous solution was extracted with CH<sub>2</sub>Cl<sub>2</sub> (3×100 mL), the organic fractions combined and dried over anhydrous MgSO<sub>4</sub>. Filtration and concentration under reduced pressure yielded the product as golden coloured viscous oil which solidified into a waxy solid.

**Mass (Yield):** 9.5 g (80%).

**TOF MS ES<sup>+</sup>, *m/z*:** 318 (MH<sup>+</sup>).

**<sup>1</sup>H NMR (400 MHz, CDCl<sub>3</sub>):** δ<sub>H</sub> = 8.47 (dd, J = 6.2, 2.8 Hz, 4H), 7.28–7.22 (m, 8H), 3.78 (s, 4H), 3.72 (s, 4H).

#### 7.4.6 Preparation of (tpm)RuCl<sub>3</sub>.3H<sub>2</sub>O



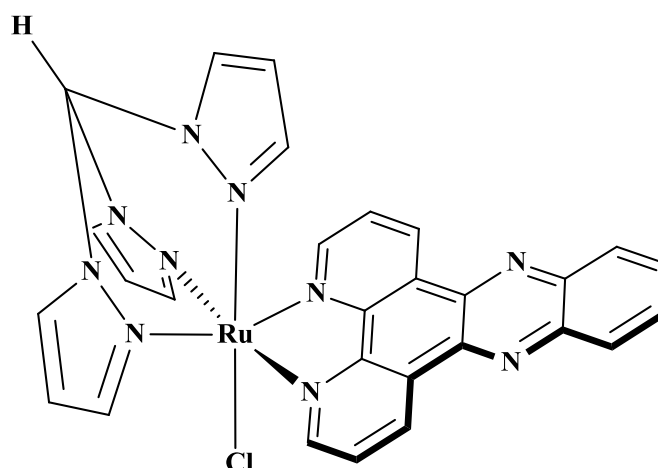
Tris (1-pyrazolyl) methane (0.861 g, 4.02 mmol) and RuCl<sub>3</sub>.3H<sub>2</sub>O (1.051 g, 4.01 mmol) were refluxed in ethanol (200 ml) for three hours. After cooling, the dark precipitate was filtered and washed with cold ethanol (5 ml) and diethyl ether (5 ml) and then dried under vacuum.

**Mass (Yield):** 1.27 g (62%).

**TOF MS ES<sup>+</sup>, *m/z*:** 386 [M-Cl]<sup>+</sup>.

$^1\text{H NMR}$  (400 MHz,  $\text{CDCl}_3$ ):  $\delta_{\text{H}} = 8.87$  (s, 1H), 8.52 (d,  $J = 6.4$  Hz, 3H), 8.11 (d,  $J = 6.5$  Hz, 3H), 6.65 (m, 3H).

#### 7.4.7 Preparation of $[(\text{tpm})\text{RuCl}(\text{dppz})][(\text{PF}_6)]$



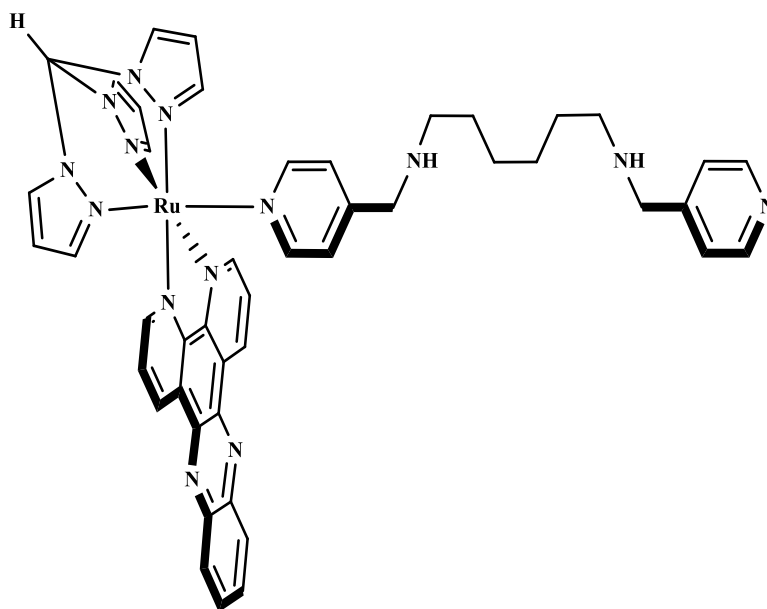
$(\text{tpm})\text{RuCl}_3 \cdot 3\text{H}_2\text{O}$  (0.6 g, 1.42 mmol), dppz (1.1 eq, 0.44g, 1.57 mmol) and LiCl (0.48 g, 0.011 mmol) were heated to reflux in 3:1 ethanol: water (100ml) for 10mins. 12 drops of triethylamine were added and refluxing continued for 3 hours. After cooling the solvent was removed and the black residue was dissolved in methanol (25 ml) and a fine black solid was filtered out. The product was precipitated by addition of aqueous  $\text{NH}_4\text{PF}_6$  and collected by filtration. The crude product was chromatographed on grade one alumina with 1:1 toluene: acetonitrile. The deep brown band was collected and concentrated. Addition of  $\text{Et}_2\text{O}$  precipitated the product as a deep brown solid.

**Mass (Yield):** 0.35 g (42%).

**TOF MS ES+**,  $m/z$ : 319  $[\text{M}-\text{PF}_6]^+$ .

$^1\text{H NMR}$  (400 MHz,  $\text{d}_6$ -acetone):  $\delta_{\text{H}} = 9.71$  (dd,  $J = 8.1$  Hz, 1.2 Hz, 2H), 9.40 (dd,  $J = 5.4$  Hz, 1.2 Hz, 2H), 8.74 (s, 1H), 8.57 (d,  $J = 2.9$  Hz, 2H), 8.43 (d,  $J = 2.1$  Hz, 2H), 8.40 (dd,  $J = 6.6$  Hz, 3.4 Hz, 2H), 8.19 (d,  $J = 2.7$  Hz, 1H), 8.12 (dd,  $J = 6.6$  Hz, 3.4 Hz, 2H), 7.1 (dd,  $J = 8.1$  Hz, 5.4 Hz, 2H), 6.88 – 6.87 (m, 2H), 6.45 (d,  $J = 2.2$  Hz, 1H), 6.22 – 6.20 (m, 1H).

#### 7.4.8 Preparation of [(tpm)Ru(dppz)( $\mu$ -L1)][Cl<sub>2</sub>]



[tpmRuCl<sub>2</sub>dppz]Cl (0.213 g, 0.31 mmol) and AgNO<sub>3</sub> (2.1eq, 0.107 g, 0.62 mmol) were refluxed in 1:1 EtOH / H<sub>2</sub>O (100 ml) under nitrogen for 3 hours. The solution was cooled and filtered through celite to remove AgCl. The filtrate was returned to the flask along with L1(dph) ligand (10 eq, 0.946 g, 3.1 mmol ) and the mixture was refluxed for 10 hours. After cooling the solution was concentrated and NH<sub>4</sub>PF<sub>6</sub> was added until the complex precipitated. After collection by filtration the crude product was dissolved in acetone (10 ml). Bu<sub>4</sub>NCl was added to precipitate the product as a chloride salt which was collected by filtration and copiously washed with acetone to remove excess  $\mu$ -L1. The red solid was dried in vacuo.

A small amount of the product was converted to its PF<sub>6</sub><sup>-</sup> salt for analysis.

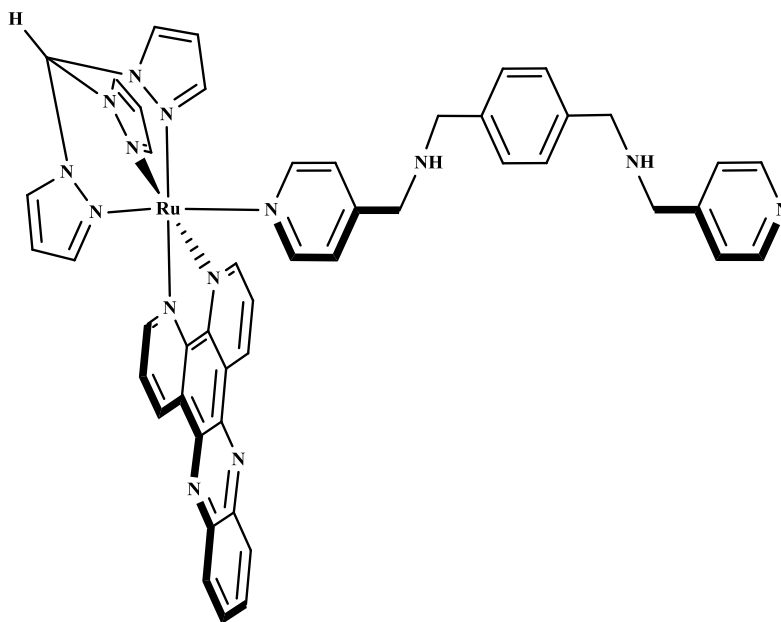
**Mass (Yield):** 0.23 g (75%).

**TOF MS ES<sup>+</sup>, *m/z*:** 1041.2716 [M-PF<sub>6</sub>]<sup>+</sup>.

**<sup>1</sup>H NMR (250 MHz, d<sub>6</sub>-acetone):**  $\delta_{\text{H}}$  = 9.84 (d, *J* = 8.2 Hz, 2H), 9.17 – 9.03 (m, 2H), 8.76 (s, 1H), 8.51 (m, 2H), 8.37 (t, *J* = 11.3 Hz, 2H), 8.23 (dd, *J* = 6.5, 3.4 Hz, 2H), 8.07 (dd, *J* = 8.3, 5.5 Hz, 4H), 7.59 – 7.40 (m, 2H), 7.27 – 7.01 (m, 4H), 6.94 – 6.76 (m, 2H), 6.46 (d, *J* =

2.1 Hz, 1H), 6.33 – 6.16 (m, 2H), 4.14 (s, 2H), 4.05 (s, 2H), 2.99 (t, J = 10 Hz, 2H), 2.94 (t, J = 5 Hz, 2H), 1.93 (m, 4H), 1.59(m, 4H).

#### 7.4.9 Preparation of [(tpm)Ru(dppz)( $\mu$ -L2)][Cl<sub>2</sub>]



This complex was prepared in an identical manner to the previous complex except replacing ligand **L1** with **L2**.

A small amount of the product was converted to its PF<sub>6</sub><sup>-</sup> salt for analysis.

**Mass (Yield):** 0.172 g (56%).

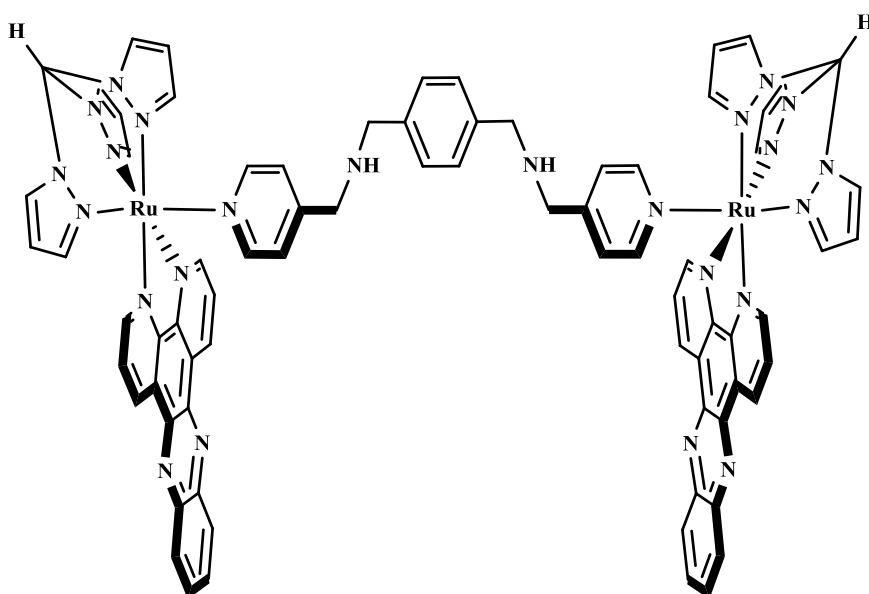
**TOF MS ES<sup>+</sup>, *m/z*:** 1061.2435 [M-PF<sub>6</sub>]<sup>+</sup>.

**<sup>1</sup>H NMR (250 MHz, d<sub>6</sub>-acetone):** δ<sub>H</sub> = 9.84 (d, J = 7.1 Hz, 2H), 9.02 (dd, J = 6.6, 3.3 Hz, 2H), 8.86 (s, 1H), 8.74 – 8.50 (m, 4H), 8.50 – 8.35 (m, 4H), 8.23 (dd, J = 6.5, 3.4 Hz, 4H), 8.12 – 7.94 (m, 2H), 7.73 (dd, J = 3.7, 7.0 Hz, 4H), 7.60 (s, 4H), 7.58 – 7.31 (m, 4H), 6.84 (d, J = 2.4 Hz, 1H), 4.25 (m, 2H), 4.11 (s, 2H), 3.14 – 3.02 (m, 4H).



**$^1\text{H}$  NMR (400 MHz,  $\text{d}_6$ -acetone):**  $\delta_{\text{H}}$  = 10.09 (s, 2H), 9.83 (dd,  $J$  = 3.0, 2.3, Hz, 4H), 9.11 (dd,  $J$  = 1.3, 5.8 Hz, 4H), 8.97 (d,  $J$  = 2.4 Hz, 2H), 8.77 – 8.49 (m, 4H), 8.38 (dd,  $J$  = 4.1, 2.9 Hz, 4H), 8.38 – 8.10 (m, 4H), 8.10 – 7.97 (m, 4H), 7.66 – 7.42 (m, 6H), 7.09 (t,  $J$  = 6.3 Hz, 2H), 6.96 – 6.75 (m, 4H), 6.64 (d,  $J$  = 2.3 Hz, 2H), 6.34 – 6.21 (m, 2H), 4.28 (s, 4H), 3.38 (m, 4H), 1.82 (m, 8H), 1.58 (m, 4H).

#### 7.4.11 Preparation of $\{[(\text{tpm})\text{Ru}(\text{dppz})]_2(\mu\text{-L2})\}[(\text{PF}_6)_4]$



This complex was prepared in an identical manner to that above, except replacing the monomeric complex  $[(\text{tpm})\text{Ru}(\text{dppz})(\text{L1})][(\text{PF}_6)_2]$  with  $[(\text{tpm})\text{Ru}(\text{dppz})(\text{L2})][(\text{PF}_6)_2]$ .

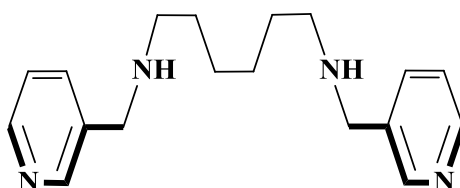
**Mass (Yield):** 0.189 g (45%).

**TOF MS ES<sup>+</sup>,  $m/z$ :** 901.75  $[\text{M}-2\text{PF}_6]^{2+}$ .

**$^1\text{H}$  NMR (400 MHz,  $\text{d}_6$ -acetone):**  $\delta_{\text{H}}$  = 9.96 (s, 2H), 9.90 – 9.74 (m, 4H), 9.64 (d,  $J$  = 8.1 Hz, 4H), 9.30 – 9.00 (m, 4H), 8.59 (dd,  $J$  = 3.7, 2.5 Hz, 4H), 8.39 (t,  $J$  = 2.3 Hz, 2H), 8.28 (d,

J = 4.0 Hz, 4H), 8.19 – 7.99 (m, 4H), 7.68 (d, J = 3.3 Hz, 4H), 7.44 (t, J = 2.1 Hz, 4H), 7.13 (d, J = 5.8 Hz, 4H), 7.13 – 6.92 (m, 4H), 6.87 – 6.57 (m, 4H), 6.57 – 6.37 (m, 2H), 6.19 (t, J = 1.7 Hz, 2H), 4.06 (s, 4H), 3.30 (s, 4H).

#### 7.4.12 Preparation of N,N'-bis(3-pyridylmethyl)-1,6-hexanediamine (L'1)



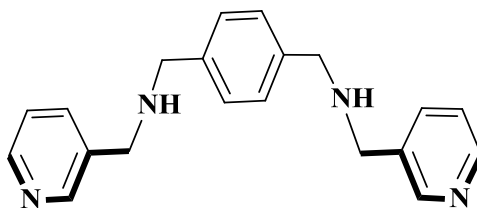
A solution of 3-pyridinecarboxaldehyde (18.5 g, 173 mmol) in ethanol (100 mL) was added to a solution of 1,6-hexanediamine (10.0 g, 86.6 mmol) in ethanol (200 mL) and then heated to reflux for 2 h. The reaction solution was allowed to cool to room temperature. NaBH<sub>4</sub> (8.0 g, 211 mmol) was carefully added in small portions and then the mixture was heated to reflux for 2 h and then stirred at room temperature overnight. Aqueous NaOH (2.0 M, 200 mL) was added to the solution. The aqueous solution was extracted with CH<sub>2</sub>Cl<sub>2</sub> (3 × 200 mL), the organic fractions combined and dried over anhydrous MgSO<sub>4</sub>. Filtration and concentration under reduced pressure yielded a cream coloured viscous oil product.

**Mass (Yield):** 15.72 g (84.9 %).

**TOF MS ES<sup>+</sup>, m/z:** 299 [MH]<sup>+</sup>.

**<sup>1</sup>H NMR (400 MHz, CDCl<sub>3</sub>):** δ<sub>H</sub> = 8.49 (s, 2H), 8.33 (d, J = 6.0 Hz, 2H), 7.38 (m, 2H), 6.99 (m, 2H), 4.42 (s, 4H), 2.79 (m, 4H), 2.05 (s, 2H), 1.51 (m, 4H), 1.07 (m, 4H).

### 7.4.13 Preparation of *N,N'*-bis(3-pyridylmethyl)-1,4-benzene dimethyleneamine (L'2)



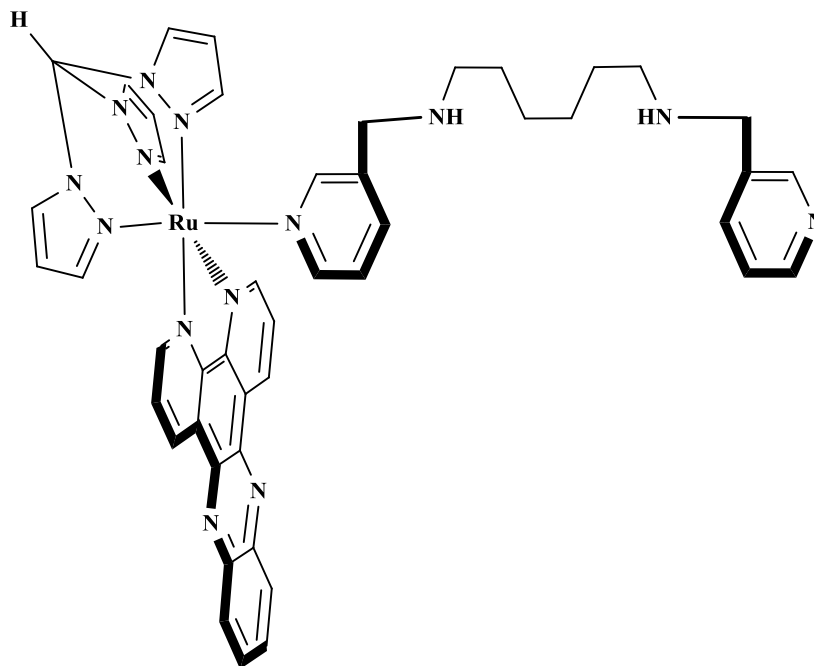
Benzene-1,4-dicarboxaldehyde (5.0 g, 27.3 mmol) and 3-(aminomethyl)pyridine (8.06 g, 74.6 mmol) were placed in  $\text{CH}_2\text{Cl}_2$  (100 mL). Anhydrous  $\text{MgSO}_4$  (20 g) was added to the solution and the mixture was stirred at room temperature for 24 h. The mixture was filtered and the filtrate concentrated under reduced pressure yielding the Schiff base as golden coloured viscous oil which was not isolated. The oil was taken up in ethanol (150 mL),  $\text{NaBH}_4$  (4.0 g, 106 mmol) was added in small portions and then the mixture was heated to reflux for 2 h and then stirred at room temperature overnight. Aqueous  $\text{NaOH}$  (2.0 M, 200 mL) was added to the solution. The aqueous solution was extracted with  $\text{CH}_2\text{Cl}_2$  (3×100 mL), the organic fractions combined and dried over anhydrous  $\text{MgSO}_4$ . Filtration and concentration under reduced pressure yielded the product as golden coloured viscous oil.

**Mass (Yield):** 4.01 g (80%).

**TOF MS ES<sup>+</sup>, *m/z*:** 319  $[\text{MH}]^+$ .

**<sup>1</sup>H NMR (400 MHz,  $\text{CDCl}_3$ ):**  $\delta_{\text{H}}$  = 8.52 (s, 2H), 8.35 (d,  $J$  = 6.0 Hz, 2H), 7.76 (d,  $J$  = 8.0 Hz, 2H), 7.49 (m, 2H), 7.30 (s, 4H), 3.85 (s, 4H), 3.80 (s, 4H),

#### 7.4.14 Preparation of [(tpm)Ru(dppz)( $\mu$ -L'1)][Cl<sub>2</sub>]



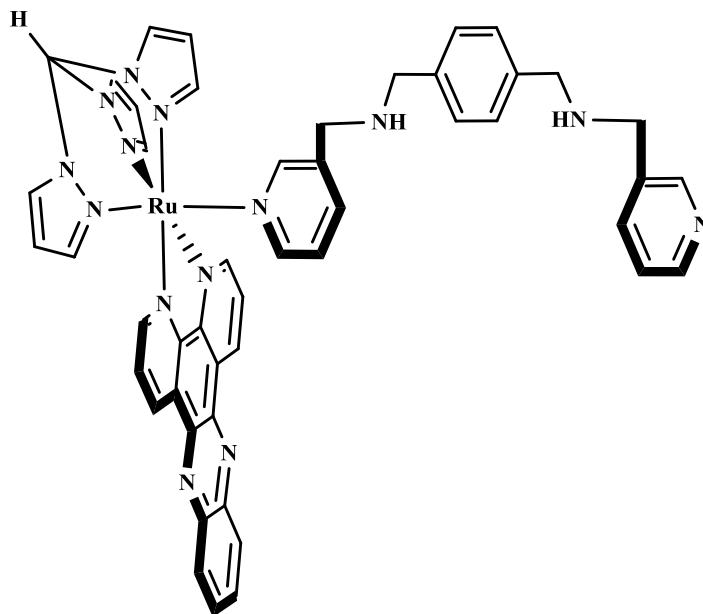
This complex was prepared in an analogous way to (7.4.8) except using **L'1** ligand instead of **L1** ligand.

**Mass (Yield):** 0.095 g (63.3 %).

**TOF MS ES<sup>+</sup>, *m/z*:** 1040 [M-PF<sub>6</sub>]<sup>+</sup>.

**<sup>1</sup>H NMR (400 MHz, CD<sub>3</sub>CN):**  $\delta_{\text{H}}$  = 10.06 (s, 1H), 9.81 (d, *J* = 8.2 Hz, 2H), 9.10 (d, *J* = 5.5 Hz, 2H), 8.67 (d, *J* = 5.3 Hz, 2H), 8.48 (d, *J* = 2.8 Hz, 2H), 8.20 (m, 2H), 7.87 (m, 2H), 7.82 (m, 2H), 7.48 (dd, *J* = 10 Hz, 4 Hz, 2H), 7.38 (m, 2H), 7.06 (dd, *J* = 4.4, 1.4 Hz, 2H), 6.83 (t, *J* = 4 Hz, 2H), 6.79 (m, 2H), 6.44 (d, *J* = 2.2 Hz, 2H), 6.29 – 6.14 (m, 1H), 4.34 (s, 2H), 3.53 (s, 2H), 2.98 (m, 2H), 1.97 (m, 2H), 1.50 (dt, *J* = 4.9, 2.5 Hz, 4H), 1.36 (m, 4H).

#### 7.4.15 Preparation of [(tpm)Ru(dppz)( $\mu$ -L'2)][Cl<sub>2</sub>]



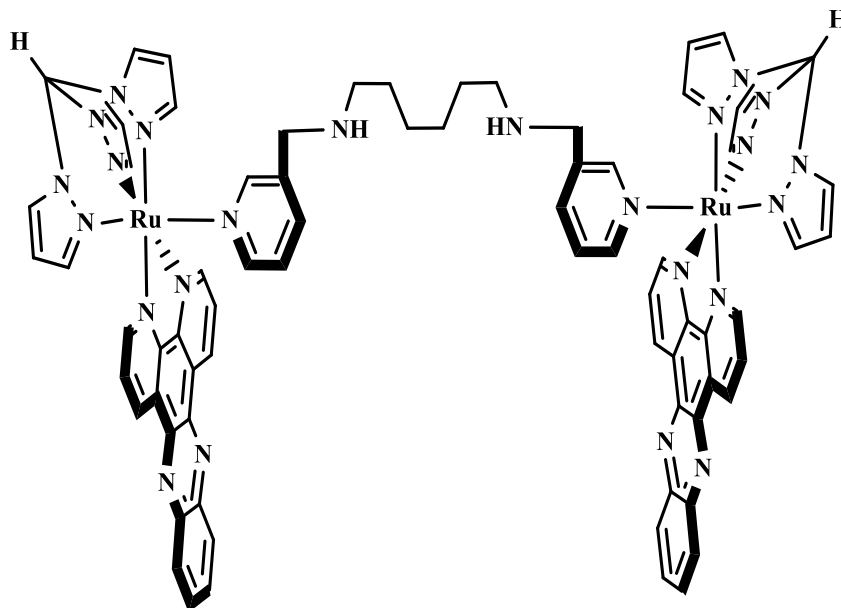
This complex was prepared in an analogous way to (7.4.9) except using L'2 ligand instead of L2 ligand.

**Mass (Yield):** 0.065 g (65%).

**TOF MS ES<sup>+</sup>, *m/z*:** 1061.5 [M-PF<sub>6</sub>]<sup>+</sup>.

**<sup>1</sup>H NMR (400 MHz, CD<sub>3</sub>CN):**  $\delta_{\text{H}}$  = 9.81 (d, *J* = 7.6 Hz, 2H), 9.13 (s, 1H), 9.08 (d, *J* = 4.7 Hz, 2H), 8.63 (t, *J* = 7.8 Hz, 2H), 8.60 (d, *J* = 2.4 Hz, 2H), 8.57 (m, 2H), 8.41 (d, *J* = 2.5 Hz, 2H), 8.21 (m, 2H), 8.06 (d, *J* = 2.8 Hz, 2H), 7.85 (d, *J* = 8 Hz, 2H), 7.56 (m, 4H), 7.36 (d, *J* = 6 Hz, 2H), 7.05 (t, *J* = 8 Hz, 2H), 6.80 (t, *J* = 2.3 Hz, 2H), 6.38 (d, *J* = 2.0 Hz, 2H), 6.17 (t, *J* = 8.4 Hz, 1H), 2.60 (s, 2H), 2.55 (m, 2H), 1.59 (m, 2H), 1.52 (m, 2H),

#### 7.4.16 Preparation of $[\{(tpm)Ru(dppz)\}_2(\mu-L'1)][(PF_6)_4]$



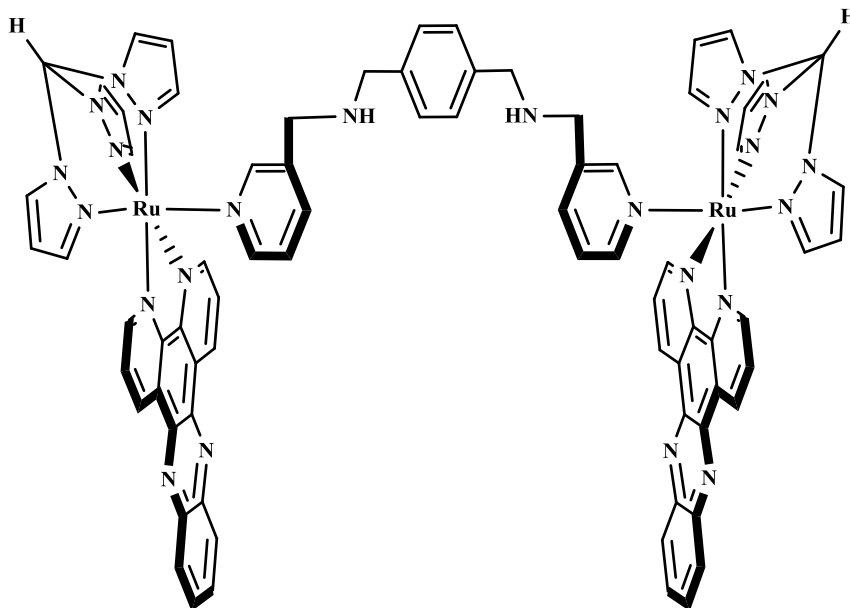
This complex was prepared in an analogous way to (7.4.10) except using  $[\{(tpm)Ru(dppz)\}(\mu-L'1)][(PF_6)_2]$  instead of  $[\{(tpm)Ru(dppz)\}(\mu-L1)][(PF_6)_2]$ .

**Mass (Yield):** 0.060 g (60%).

**TOF MS ES<sup>+</sup>,  $m/z$ :** 892  $[M-2PF_6]^{2+}$ .

**<sup>1</sup>H NMR (400 MHz, CD<sub>3</sub>CN):**  $\delta_H$  = 9.83 (dd,  $J$  = 8.2, 1.2 Hz, 4H), 9.21 (s, 2H), 9.10 (d,  $J$  = 5.6 Hz, 2H), 8.38 (d,  $J$  = 2.8 Hz, 4H), 8.27 (m, 6H), 8.12 (s, 2H), 8.02 (m, 2H), 7.81 (dd,  $J$  = 9.9, 4.2 Hz, 8H), 7.67 (dd,  $J$  = 7.8, 6.0 Hz, 4H), 7.50 (m, 4H), 7.25 (t,  $J$  = 1.6 Hz, 2H), 6.86 (t,  $J$  = 4 Hz, 6H) 6.40 (m, 2H), 3.47 (s, 4H), 2.79 (m, 4H), 1.83 (m, 4H), 1.76 (m, 4H).

#### 7.4.17 Preparation of $[\{(tpm)Ru(dppz)\}_2(\mu-L'2)][(PF_6)_4]$



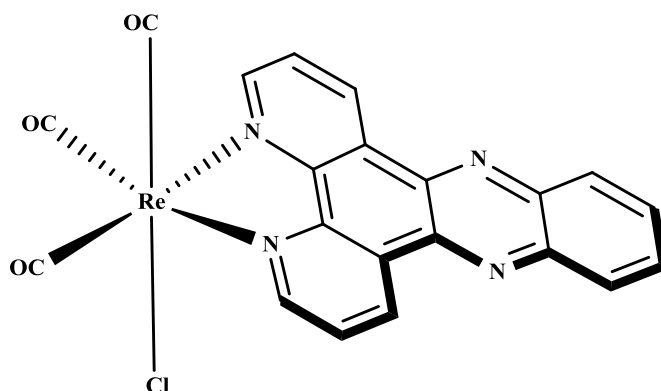
This complex was prepared in an analogous way to (7.4.11) except using  $[\{(tpm)Ru(dppz)\}(\mu-L'2)][(PF_6)_2]$  instead of  $[\{(tpm)Ru(dppz)\}(\mu-L2)][(PF_6)_2]$ .

**Mass (Yield):** 0.073 g (56 %).

**TOF MS ES+,  $m/z$ :** 902  $[M-2PF_6]^{2+}$ .

**$^1H$  NMR (400 MHz,  $CD_3CN$ ):**  $\delta_H =$  9.79 (dd,  $J = 7.9, 2.5$  Hz, 4H), 9.21 (m, 2H), 9.10 (s, 2H), 8.64 (m, 4H), 8.53 (t,  $J = 4.9$  Hz, 4H), 8.36 (t,  $J = 4.9$  Hz, 4H), 8.20 (s, 2H), 8.17 (m, 2H), 7.96 (m, 4H), 7.80 (m, 4H), 7.62 (d,  $J = 2.3$  Hz, 4H), 7.28 (m, 2H), 7.08 (s, 4H), 6.81 (m, 4H), 6.62 (d,  $J = 2.3$  Hz, 4H) 6.28 (m, 2H) 2.97 (s, 4H), 2.73 (m, 4H),

#### 7.4.18 Preparation of [Re(CO)<sub>3</sub>dppzCl]



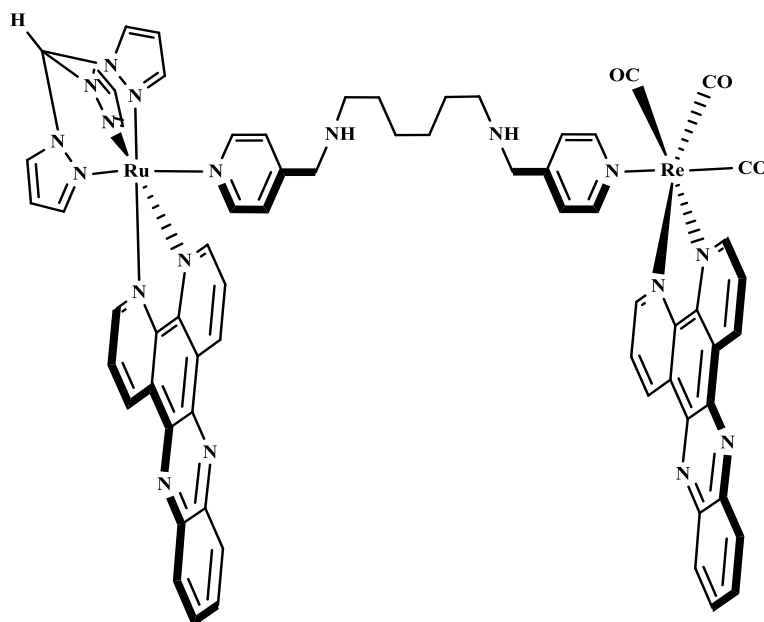
Re(CO)<sub>5</sub>Cl (150 mg, 0.410 mmol) and dppz (130 mg, 0.460 mmol) were refluxed in toluene (50 ml) for 6 hours. After cooling to room temperature a yellow precipitate formed which was collected by filtration, washed with toluene (25 ml) and Et<sub>2</sub>O (25 ml) and dried in vacuo.

**Mass (Yield):** 0.135 g (90 %).

**TOF MS ES<sup>+</sup>, *m/z*:** 588 (15) [M<sup>+</sup>], 560 (90) [M<sup>+</sup>-CO], 524 (100) [M<sup>+</sup>-CO-Cl].

**<sup>1</sup>H NMR (400 MHz, CDCl<sub>3</sub>):** δ<sub>H</sub> = 9.90 (dd, *J* = 8.2, 1.4 Hz, 2H), 9.49 (dd, *J* = 5.2, 1.4 Hz, 2H), 8.49 (dd, *J* = 6.6, 3.4 Hz, 2H), 8.10 (dd, *J* = 10, 3.5 Hz, 2H), 8.04 (dd, *J* = 8.2 Hz, 5.2 Hz, 2H).

#### 7.4.19 Preparation of [Ru(tpm)dppz-L1-Re(CO)<sub>3</sub>dppz][Cl<sub>3</sub>]



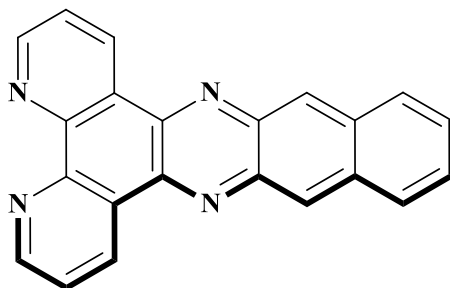
[Re(CO)<sub>3</sub>Cl]dppz] (80 mg, 0.131 mmol) and AgCF<sub>3</sub>SO<sub>3</sub> (2.1eq, 45 mg, 0.175 mmol) were placed in ethanol (50 mL) and heated to reflux overnight. The solution was allowed to cool and filtered through celite to remove the AgCl precipitate. The yellow coloured filtrate was returned to the reaction vessel. [(tpm)Ru(dppz)(L1)]Cl<sub>2</sub> (40 mg, 0.041 mmol) was added and the solution was refluxed overnight again. The solution was allowed to cool to room temperature and then evaporated to get a red-brown precipitate.

**Mass (Yield):** 0.030 g (37.5 %).

**TOF MS ES<sup>+</sup>, *m/z*:** 744.0 [M-2Cl<sub>2</sub>]<sup>2+</sup>.

**<sup>1</sup>H NMR (400 MHz, D<sub>2</sub>O):** δ<sub>H</sub> = 9.79 (s, 1H), 9.59 (d, J = 9.0 Hz, 4H), 9.02 (d, J = 5.3 Hz, 4H), 8.55 (d, 4H), 8.20 (m, J = 2.8 Hz, 4H), 8.08 (m, 4H), 7.85 (dd, J = 8.2, 5.4 Hz, 4H), 7.50 (d, J = 6.2 Hz, 4H), 7.31 (d, J = 5.9 Hz, 4H), 6.92 (d, J = 5.9 Hz, 2H), 6.70 (m, 2H), 6.24 (m, 1H), 3.98 (s, 4H), 3.86 (m, 4H), 2.62 (m, 4H), 1.39 (m, 4H).

#### 7.4.20 Preparation of Benzo[i]dipyrido[3,2-a:2',3'-c]phenazine (dppn)<sup>5</sup>



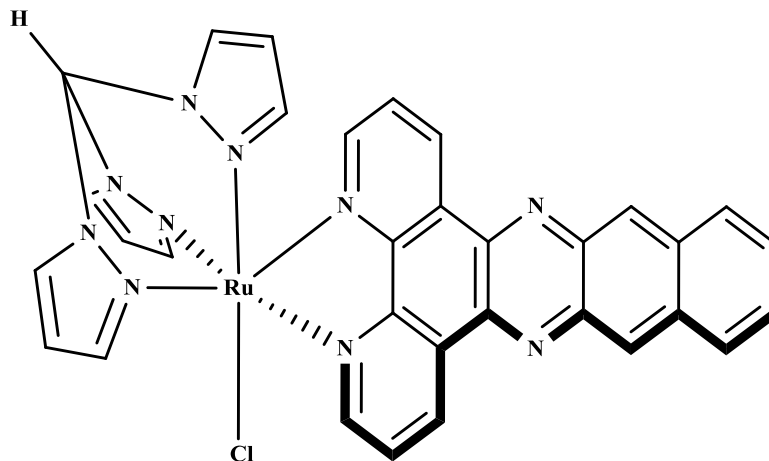
This compound was prepared following a previously reported procedure. 1,10-phenanthroline-5,6-dione (300 mg, 4.76 mmol) and 2,3-diaminonaphthalene (252 mg, 1.59 mmol) were suspended in methanol (60 ml) and heated under reflux for 1 h, during which time a bright-orange coloured precipitate formed. The precipitate was collected, washed subsequently with water (25 ml), methanol (25 ml) and diethyl ether (25 ml) and dried in vacuo.<sup>5</sup>

**Mass (Yield):** 0.273 g (91%).

**TOF MS ES+, *m/z*:** 333.1 [MH]<sup>+</sup>.

**<sup>1</sup>H NMR (400 MHz, CDCl<sub>3</sub>):**  $\delta_{\text{H}}$  = 9.56 (dd, *J* = 8.1, 1.7 Hz, 2H), 9.25 (dd, *J* = 4.4, 1.7 Hz, 2H), 8.86 (s, 2H), 8.16 (dd, *J* = 6.5, 3.2 Hz, 2H), 7.76 (dd, *J* = 8.1, 4.5 Hz, 2H), 7.68 (dd, *J* = 6.6 Hz, 3.1 Hz, 2H).

#### 7.4.21 Preparation of [Ru(tpm)dppnCl][PF<sub>6</sub>]



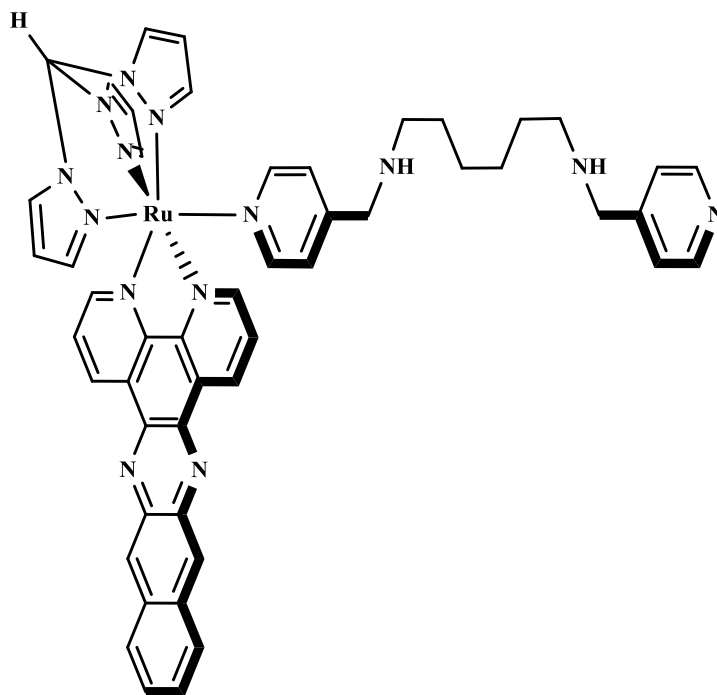
(tpm)RuCl<sub>3</sub>·3H<sub>2</sub>O (125 mg, 0.262 mmol) and dppn (95 mg, 0.286 mmol) were heated to reflux in ethylene glycol (50 ml) at 120 °C for 18 hours. The solution was allowed to cool, poured into methanol (100 ml), and filtered through celite. An excess of aqueous NH<sub>4</sub>PF<sub>6</sub> was added to the solution, causing precipitation of brown coloured solid which was collected with copious amount of water, diethyl ether and dried in vacuo to give a dark-brown coloured solid. The crude product was purified via chromatography through neutral alumina, using acetonitrile:toluene [50:50, V/V] as eluent. The desired brown coloured band containing the product were collected and concentrated then dries in vacuo.

**Mass (Yield):** 0.087 g (70 %).

**TOF MS ES<sup>+</sup>, *m/z*:** 682.9 [M-PF<sub>6</sub>]<sup>+</sup>.

**<sup>1</sup>H NMR (400 MHz, CD<sub>3</sub>CN):** δ<sub>H</sub> = 9.77 (dd, *J* = 8.0, 1.2 Hz, 2H), 9.15 (dd, *J* = 5.2, 1.2 Hz, 2H), 9.01 (s, 1H), 8.62 (m, 4H), 8.41 (d, *J* = 2.9 Hz, 2H), 8.37 (dd, *J* = 6.4, 3.2 Hz, 2H), 8.13 (dd, *J* = 9.4, 4.0 Hz, 2H), 7.92 (m, 2H), 6.83 (d, *J* = 2.5 Hz, 2H), 6.63 (d, *J* = 8.1 Hz, 2H), 6.20 (m, 1H).

#### 7.4.22 Preparation of [Ru(tpm)dppn( $\mu$ -L1)][(PF<sub>6</sub>)<sub>2</sub>]



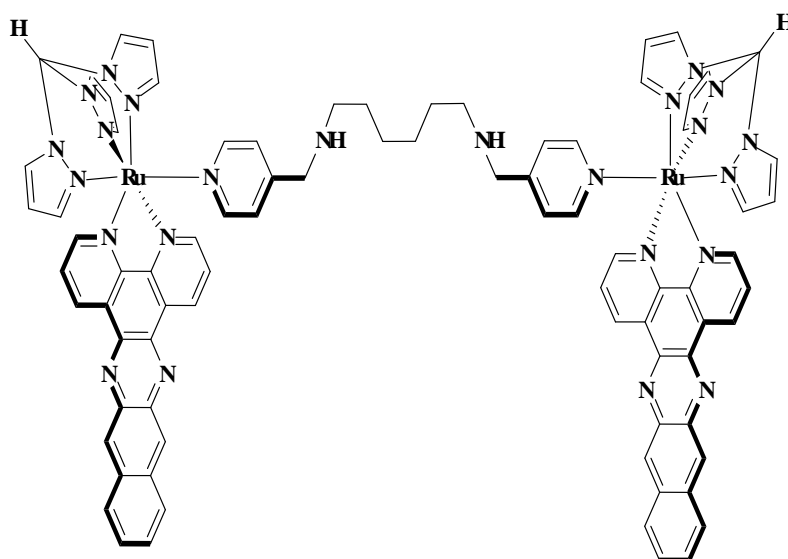
[Ru(tpm)Cl]dppn][PF<sub>6</sub>] (204 mg, 0.186 mmol) and AgNO<sub>3</sub> (2.1eq, 87 mg, 0.512 mmol) were placed in a 1:1 mixture of ethanol and water (100 mL) and heated to reflux for 2 hours. The solution was allowed to cool and filtered through celite to remove the AgCl precipitate. The filtrate was returned to the reaction vessel alongside with (734 mg, 2.46 mmol) L1 ligand and the solution reflux for 72 hours. The solution was allowed to cool, poured into an excess of saturated solution of NH<sub>4</sub>PF<sub>6</sub> then the precipitate was collected by centrifuging and washed with water and diethyl ether before being dried under vacuum.

**Mass (Yield):** 0.130 g (63.7 %).

**TOF MS ES<sup>+</sup>, *m/z*:** 1090.34 [M-PF<sub>6</sub>]<sup>+</sup>.

**<sup>1</sup>H NMR (400 MHz, MeOD):**  $\delta_{\text{H}}$  = 9.90 (d, *J* = 8.0 Hz, 2H), 9.25 (s, 1H), 9.20 (m, 2H), 9.10 (d, *J* = 5.3 Hz, 2H), 8.90 (m, 2H), 8.74 (m, 2H), 8.42 (dd, *J* = 6.5, 3.1 Hz, 4H), 8.10 (d, *J* = 1.9 Hz, 2H), 7.90 (m, 4H), 7.34 (d, *J* = 6.2 Hz, 2H), 6.84 (m, 4H), 6.43 (m, 2H), 6.25 (m, 1H), 3.89 (s, 2H), 3.62 (s, 2H), 2.63 (t, *J* = 4.8 Hz, 2H), 2.40 (m, 4H), 2.13 (m, 4H), 1.53 (m, 2H).

### 7.4.23 Preparation of [Ru(tpm)dppn-L1-Ru(tpm)dppn][(PF<sub>6</sub>)<sub>4</sub>]



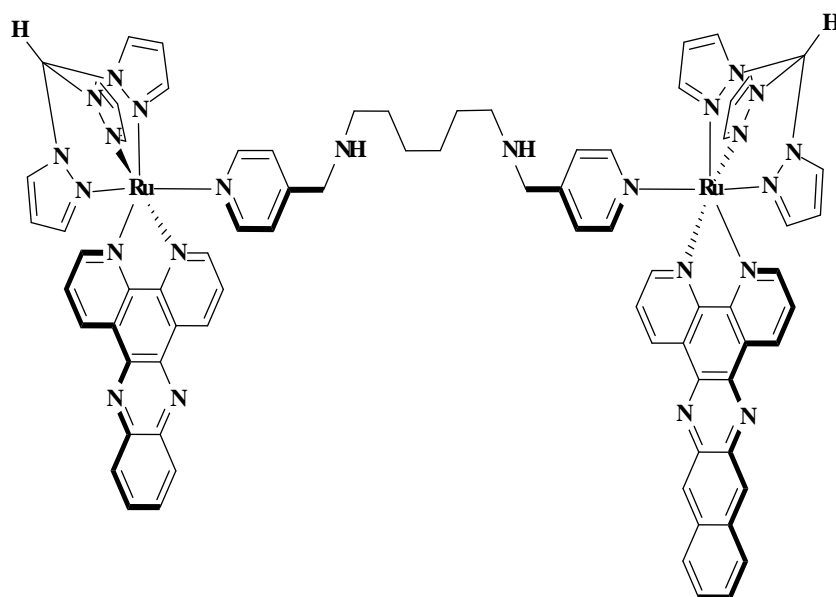
[Ru(tpm)Cl]dppn][PF<sub>6</sub>] (45 mg, 0.054 mmol) and AgNO<sub>3</sub> (2.1eq, 75 mg, 0.441 mmol) were placed in a 1:1 mixture of ethanol and water (80 mL) and heated to reflux for 2 hours. The solution was allowed to cool and filtered through celite to remove the AgCl precipitate. The filtrate was returned to the reaction vessel. [(tpm)Ru(dppn)(L1)][PF<sub>6</sub>]<sub>2</sub> (140 mg, 0.113 mmol) in acetone (20 ml) was added and the solution reflux for 72 hours. The solution was allowed to cool, poured into an excess of saturated solution of NH<sub>4</sub>PF<sub>6</sub> then the precipitate was collected by centrifuging and washed with water and diethyl ether before being dried under vacuum.

**Mass (Yield):** 0.042 g (30 %).

**TOF MS ES<sup>+</sup>, *m/z*:** 942.5 [M-2PF<sub>6</sub>]<sup>2+</sup>.

**<sup>1</sup>H NMR (400 MHz, CD<sub>3</sub>CN):** δ<sub>H</sub> = 9.93 (d, J = 11.9 Hz, 4H), 9.23 (s, 2H), 8.93 (dd, J = 4.36, 3.05 Hz, 4H), 8.63 (m, 6H), 8.46 (dd, J = 12, 7.0 Hz, 4H), 8.16 (m, 4H), 7.96 (m, 6H), 7.89 (m, 4H), 7.24 (d, J = 7.4 Hz, 4H), 6.80 (t, J = 2.5 Hz, 8H), 6.43 (m, 4H), 6.25 (m, 2H), 3.89 (s, 4H), 2.87 (t, J = 4.9 Hz, 4H), 2.13 (m, 4H), 1.53 (m, 4H).

#### 7.4.24 Preparation of [Ru(tpm)dppz-L1-Ru(tpm)dppn][(PF<sub>6</sub>)<sub>4</sub>]



[Ru(tpm)Cl<sub>2</sub>dppn][PF<sub>6</sub>] (45 mg, 0.054 mmol) and AgNO<sub>3</sub> (2.1eq, 75 mg, 0.441 mmol) were placed in a 1:1 mixture of ethanol and water (80 mL) and heated to reflux for 2 hours. The solution was allowed to cool and filtered through celite to remove the AgCl precipitate. The filtrate was returned to the reaction vessel. [(tpm)Ru(dppz)(L1)]Cl<sub>2</sub> (200 mg, 0.206 mmol) in ethanol and water (15 mL) was added and the solution reflux for 72 hours. The solution was allowed to cool, poured into an excess of saturated solution of NH<sub>4</sub>PF<sub>6</sub> then the precipitate was collected by centrifuging and washed with water and diethyl ether before being dried under vacuum.

**Mass (Yield):** 0.110 g (68.7 %).

**TOF MS ES<sup>+</sup>, *m/z*:** 916.5 [M-2PF<sub>6</sub>]<sup>2+</sup>.

**<sup>1</sup>H NMR (400 MHz, CD<sub>3</sub>CN):** δ<sub>H</sub> = 10.08 (s, 2H), 9.92 (dd, J = 7.2, 6.4 Hz, 4H), 9.22 (dd, J = 6.4, 4.6 Hz, 4H), 9.08 (dd, J = 5.4, 1.1 Hz, 4H), 8.62 (t, J = 3.4 Hz, 4H), 8.38 (d, J = 2.7 Hz, 2H), 8.19 (m, 6H), 8.04 (dd, J = 8.2, 5.4 Hz, 4H), 7.45 (dd, J = 6.7 Hz, 4H), 7.39 (m, 6H), 6.92 (t, J = 2.5 Hz, 4H), 6.74 (m, 4H), 6.29 (m, 2H), 4.28 (s, 4H), 3.17 (m, 4H), 2.90 (t, J = 4.9 Hz, 4H), 1.73 (m, 4H).

## References

- (1) Chaires, J. B.; Dattagupta, N.; Crothers, D. M.: *Biochemistry* **1982**, *21*, 3933-3940.
- (2) Reger, D. L.; Wright, T. D.; Little, C. A.; Lamba, J. J.; Smith, M. D.: *Inorganic Chemistry* **2001**, *40*, 3810-3814.
- (3) Zheng, R. H.; Guo, H. C.; Jiang, H. J.; Xu, K. H.; Liu, B. B.; Sun, W. L.; Shen, Z. Q.: *Chinese Chemical Letters* **2010**, *21*, 1270-1272.
- (4) Dickeson, J.; Summers, L.: *Australian Journal of Chemistry* **1970**, *23*, 1023-1027.
- (5) Foxon, S. P.; Green, C.; Walker, M. G.; Wragg, A.; Adams, H.; Weinstein, J. A.; Parker, S. C.; Meijer, A. J.; Thomas, J. A.: *Inorganic Chemistry* **2011**, *51*, 463-471.